MICROSCALE BIOSENSORS FOR HIV DETECTION AND VIRAL LOAD DETERMINATION

BY

GREGORY LAWRENCE DAMHORST

DISSERTATION

Submitted in partial fulfillment of the requirements
for the degree of Doctor of Philosophy in Bioengineering
in the Graduate College of the
University of Illinois at Urbana-Champaign, 2015

Urbana, Illinois

Doctoral Committee:

Professor Rashid Bashir, Chair
Professor Brian Cunningham
Associate Professor Janet Jokela
Assistant Professor Dipanjan Pan

ABSTRACT

The HIV/AIDS pandemic has killed 39 million people worldwide, and nearly as many people are living with HIV infection today. The global response to this disease has come a long way since the emergence of HIV in the early 1980s, including more than 64 billion USD in international spending between 2002 and 2013 alone [1]. Due to the worldwide effort, HIV infection has been transformed from a death sentence into a manageable, chronic illness that can have limited impact on lifespan when treated properly [2]. Antiretroviral therapy, public health campaigns, and other education and prevention efforts have facilitated an age in which no one, regardless of age, gender, sexual orientation, nationality, or socioeconomic status should face despair on account of this infection. However, barriers persist to bringing proper care to millions of people worldwide, including access to testing and the diagnostic tools necessary for proper administration of therapy.

Following serological testing to establish HIV-positive status, the current standard of care requires monitoring of CD4+ T lymphocyte counts and plasma HIV viral load to guide administration of antiretroviral therapy. For many individuals living with HIV worldwide, the expensive and sophisticated laboratory instruments necessary for these measurements are extremely difficult to access due to poor healthcare infrastructure and lack of technical personnel. For those who are capable of bearing the expense and inconvenience of traveling to facilities that can provide one or both of these measurements, continuing care can be hindered by difficulties in patient follow-up. A point-of-care technology capable of performing these essential measurements to HIV therapy, therefore, is a critical need worldwide.

Here we explore solutions rooted in micro- and nanotechnology principles to address this immense challenge in global health. Point-of-care diagnostics which meet the following criteria could improve the way that HIV/AIDS is treated, particularly in remote and resource-limited settings: low-cost assays (approximately $10 or less), small sample volumes (approximately 10 μL or less), rapid measurements (approximately 10 minutes or lesss), as well as technologies that are easy to use and portable. Our expertise in this area began with the development of a lab-on-a-chip micro-cytometer for CD4+ T lymphocyte

enumeration from a drop of whole blood, which was tested on HIV-positive patients in the Champaign-Urbana, IL area and matched results from clinical flow cytometry at Carle Foundation Hospital in Urbana, IL [3]. This thesis describes work on the complementary measurement, viral load detection, aimed at meeting the ideal criteria described above for a point-of-care diagnostic technology.

Our approaches to viral load measurements follow two broad themes. First, we describe an antigen-based approach which leverages immuno-affinity recognition for whole virus particle detection. In this method, the novel component of our sensing system is an ion-filled liposome which, upon stimulation (in this case, by heating), releases ions into low-conductivity media in a microchannel and can be quantitatively measured by a simple impedance measurement. We have termed this technique "ion-release impedance spectroscopy." Employing the liposome in an immunoassay involving a primary capture antibody to HIV surface proteins and a secondary, identical antibody anchored to the exterior of the liposome, we are able to show qualitative detection of HIV virions in a microchannel [4]. We have improved aspects of this approach by performing ion-release impedance spectroscopy with liposomes exhibiting a higher melting temperature, and explored immuno-affinity capture of viruses on magnetic beads in an attempt to perform a concentration or separation step from a whole blood sample.

Our second approach is detection of viral RNA in whole blood. In this technique, we employ loop-mediated isothermal amplification (LAMP) in the detection of viral RNA following a reverse-transcription test. One novel aspect of this approach is in performing the test from unprocessed whole blood, which we introduce into a microfluidic channel, mix with cell lysis buffer, add to RT-LAMP reagents, and distribute into nanoliter-scale droplets on a silicon microchip. Another novel step is to image this reaction with a consumer mobile smartphone device, which we integrate with the microchip setup using a 3-D printed platform. Results from our smartphone-imaged RT-LAMP technique show amplification in reactions containing as few as 3 virus particles per droplet, corresponding to 670 viruses per microliter of whole blood [5]. The true power of this approach, however, can be realized in a quantitative digital detection approach for which we describe a framework and preliminary designs, providing a basis for a highly-practical viral load test based on the proof-of-concept demonstrated in our lab.

These micro- and nanotechnology approaches to HIV viral load measurements give hope for a portable diagnostics platform which could bring the standard of life-saving HIV/AIDS care to people in all parts of the world, no matter how remote or resource-limited.

ACKNOWLEDGEMENTS

I am convinced that my education is the net result of a series of mentors and influencers who have impacted me over the better part of 20 years. These are the people who deserve to be acknowledged for their contributions. Before I even set foot on the University of Illinois campus, I had learned critical thinking and developed a hard work ethic, thanks to the influence of a series of educators who reinforced the notion that there is nothing that cannot be achieved through working hard. Particularly noteworthy are Mr. Liam Keigher and Mr. Patrick Henning. As an undergraduate, Dr. Dave Hertzog always showed confidence in me and convinced me that I could be successful in research, and thanks to him and Dr. Noah Schroeder, my relatively brief adventure in muon physics was a valuable introduction to "detection". Meanwhile, thanks to Dr. George Gollin, I completing a course sequence in intermediate mechanics left me with a sense that academia was the place to pursue my passions. In addition to these educators, few have been as inspiring to me as Dr. Cristina Medrano, who demonstrated compassion in medicine, and whose impact will always be felt on my career as a physician-scientist. The sum of these influences was the notion that through academia, one can strive to embody the ultimate tenet: service to others.

I owe gratitude to Dr. Rashid Bashir for the opportunity to dedicate five years of laboratory research to a project that resonate so well with this idea. Naturally, most of the skills I've acquired through this process are due to his influence, particularly the ability to envision ambitious projects with grand outcomes – a habit which now seems as natural as the micro-pipetting that has been burned into my muscle memory. I am also thankful for a clinician mentor, Dr. Janet Jokela, who has been an endless encouragement and taught me that a physician should be an advocate for his or her patients.

I want to thank Dr. Nicholas Watkins for mentorship and Dr. Umer Hassan for collaboration. Additionally, the journey would have been harder without Carlos Duarte-Guevara, Dr. Eric Salm, Dr. Bobby Reddy, Jr., Tanmay Ghonge, Dr. Larry Millet, and many others who were so helpful in providing feedback, ideas, and advice. The work in this thesis also relied on the expertise of Dr. Hyunjoon Kong, Dr. Cartney Smith, Dr. Brian Cunningham, and Weili Chen who collaborated on all my major projects. Thanks

to Dr. William Rodriguez, Dr. Martina Medkova, and the team at Daktari Diagnostics for their advice and collaboration. Thanks also to my other committee members not mentioned here: Dr. Dipanjan Pan and Dr. Logan Liu.

I was supported by the Roy J. Carver Fellowship, the Illinois Distinguished Fellowship, and the Ruth L. Kirschstein National Research Service Award for Individual Predoctoral MD/PhD Fellows (F30) from the National Institute of Allergy and Infectious Diseases. The NIH AIDS Reagent Program, particularly through Dr. Bruce K. Brown who on several occasions took time for lengthy phone calls, was extremely helpful.

I believe that there are valuable aspects of my graduate education not directly reflected in this document, and I have been thankful for the opportunity to learn and organize through the Global Health Initiative, which I started in 2011 with Dr. Rashid Bashir, Dr. Andiara Schwingel, and several others. In addition to these organizers, I am thankful to have had the opportunity to collaborate and/or travel with Dr. Barry Pittendrigh, Dr. Julia Bello-Bravo, Dr. Yvette Johnson, Dr. Ian Brooks, Dr. Merle Bowen, Dr. Paven Aujla, Dr. Erich Lidstone, Dr. Elise Duwe, Dr. Martina Mustroph, Kenny Long, and many others. At the top of this list is the Center for Global Studies and Dr. Elly Hanauer, Dr. Ed Kolodziej, Karen Hewitt, and Jeremie Smith, who were committed to our efforts and treated me more like a faculty member than a student. Finally, the support of the College of Medicine at Urbana, the Medical Scholars Program staff – Dr. Jim Hall, Dr. Nora Few, and Dr. Jim Slauch – and the O'Morchoe Leadership Fellowship made possible several experiences which added depth and meaning to my exploration of international health.

Finally, I want to thank my family. While my mom insists that my dedication to prioritizing schoolwork was inherent from elementary school, I am convinced that my parents are responsible for the underlying work ethic which has gotten me this far. My parents also taught me that faith is the foundation of everything, and it is because of these priorities they have instilled in me that I have followed a path which is to me an expression of that faith. Meanwhile, I am still trying to comprehend the magnitude of my luck that is getting to be married to Lacie, who has supported me through everything. I am glad for the ways she has complemented me and taught me on this journey, and I look forward to the adventures to come.

TABLE OF CONTENTS

CHAPTER 1: INTRODUCTION

THE HISTORY OF A PANDEMIC

On June 5, 1981, a report appeared on the second page of the Centers for Disease Control (CDC) *Morbidity and Mortality Weekly Report* (MMWR) describing five patients seen at three Los Angeles hospitals presenting with biopsy-confirmed *Pneumocystis carinii* pneumonia (PCP, now called *Pneumocystis jiroveci*), an opportunistic lung infection of fungal origin rarely seen in healthy individuals [6], [7]. One month later, in the mainstream media – the New York Times, on July 3, 1981, and the Washington Post, on July 4, 1981 – unusual instances of Kaposi Sarcoma (KS) were reported in several young homosexual men in New York and Los Angeles [8], [9]. KS, a rare cancer typically seen only in older individuals of Mediterranean, Eastern European, and Middle Eastern heritage [10], was similar to PCP in that it was extremely unusual to be found at such high prevalence a relatively young population. These mysteries were the first reports of a pandemic that would kill more than 39 million people worldwide by 2013 [11].

Two years following that historic MMWR, Dr. Luc Montagnier and Dr. Robert Gallo separately published reports of a virus isolated from patients with Acquired Immune Deficiency Syndrome (AIDS), the name that had been given to the disease characterized by a constellation of symptoms and opportunistic infections associated with depleted CD4+ T lymphocyte counts [12], [13]. That virus, the Human Immunodeficiency Virus (HIV), a 100-nanometer assembly of proteins, lipids, and nucleic acids – the building blocks of all of life – would wreak havoc on our globe in the years to come, and continues to affect humankind in an unprecedented manner nearly four decades later [14].

The early risk groups in the United States: homosexual men, injection drug users, hemophiliacs, and Haitians living in America, gave clues to both the mechanism by which HIV is spread, as well as its origins. Transmission of the virus, which occurs between two individuals through exposure to infected blood and body fluids such as during sexual intercourse, re-use of injection needles, and contaminated blood products,

explains the high prevalence in three of these risk groups. The fourth – Haitians, living in the U.S., is clarified by more recent studies of HIV-1 genetic sequences which indicate that HIV in America can be traced from Africa to Haiti to an emergence in the U.S. in the late 1960s [15].

Clues to the virus's African origins first emerged in 1986 with reports of a novel retrovirus – later called HIV-2 – which vaguely resembled HIV-1 but exhibited striking similarities to a form of simian immunodeficiency virus (SIV) infecting macaque monkeys [16], [17]. The next breakthrough in understanding the virus's zoonotic origins came from the study of chimpanzee feces in Cameroon in which SIV nucleic acid sequences that could be traced to modern HIV-1 were identified in isolated groups of *Pan troglodytes troglodytes*, a subspecies of the common chimpanzee [18]. Ultimately, the prevailing theory behind the beginnings of the modern HIV pandemic came to understand the origin as a single zoonotic transmission event between a chimpanzee and human in the early 1900s [17]. "Patient Zero," therefore, was likely an individual in southeastern Cameroon who was exposed to the virus while hunting or preparing bushmeat [17], [18]. From there, the virus traveled, through the movement of its hosts and human-to-human transmission, to what is now Kinshasa, Democratic Republic of Congo on the shores of the Congo River [17], [18]. Recent studies have identified its likely route from there: early transportation networks – waterways and railroads – and the individuals who traveled them were a mechanism for the spread of the virus through population centers in central Africa in the first half of the Twentieth Century, igniting the global pandemic that we still battle worldwide today [19].

TREATING HIV

Upon its emergence in the United States in the early 1980s, HIV infection was a death sentence. Hope emerged, however, in the form of the first antiretroviral drug, zidovudine (AZT), which was approved for use by the Food and Drug Administration (FDA) in 1987 [14]. Today, 37 drugs appear on the FDA list including six classes (nucleoside reverse transcriptase inhibitors, nonnucleoside reverse transcriptase inhibitors, protease inhibitors, fusion inhibitors, CCR5 co-receptor antagonist entry inhibitors, and integrase

strand transfer inhibitors) as well as three combination products [20]. Activism and international health initiatives have led to dramatic increases in access to and availability of antiretroviral therapy (ART) in the past thirty years, especially in low and middle-income countries. From 2002 to 2012, for example, access to ART has been increased from 300,000 people to 9.7 million people in low and middle-income countries [21]. Much still needs to be done to reach the goal described by World Health Organization (WHO), Joint United Nations Programme on HIV/AIDS (UNAIDS), and the United Nations Children's Fund (UNICEF): to bring ART to 15 million people in 2015 [21]. However, the success of ART in those individuals who can access it has meant that millions of people living with HIV worldwide no longer face a death sentence, but instead live with a life-long chronic illness that ultimately has little effect on life expectancy [21].

As ART is increasingly available in remote and resource-limited settings, a key barrier to successful treatment of HIV-infected individuals is access to diagnostic technologies. Separate clinical care guidelines issued by the WHO, Infectious Diseases Society of America (IDSA), and U.S. Department of Health and Human Services (DHHS) are unanimous on the need for CD4+ T lymphocyte counting ("CD4 count") and quantitative plasma viral RNA measurements ("viral load") at the initiation of care and at regular intervals during life-long administration of ART [22]–[25]. The goals of ART include preventing immunologic and virologic failure, referring to inadequate CD4 counts and unsuppressed viral loads, respectively. While specific benchmarks and frequencies vary depending on the source and scope of the guidelines, all clinical authorities agree on the necessity of both CD4 counts and viral load measurements as diagnostic and prognostic tools for assessing the success of ART [22]–[25]. The consequence of limitations of poor healthcare infrastructure in the world's poorest regions, however, mean that the technologies necessary for performing these essential measurements are not available to everyone living with HIV. It is in addressing this problem that micro- and nanotechnologies hold the power to make a difference in the lives of millions of people worldwide.

MICRO- AND NANOTECHNOLOGIES FOR HIV/AIDS DIAGNOSTICS

This thesis describes efforts to develop a point-of-care HIV viral load test using tools of the micro and nanoscale. Chapter 2 provides a broad overview of these engineering approaches in the context of HIV/AIDS and several other global infectious diseases: particularly the "big three," including tuberculosis and malaria. This chapter also explains the context of the "silicon era," giving brief homage to the fabrication processes of modern computing which have enabled and inspired lab-on-a-chip biomedical device engineering. The second section in Chapter 2 is a thorough review of micro- and nanotechnology approaches in the literature for CD4 counts and viral loads, as well as a brief discussion of the provirus and methods for its detection.

Our approaches to viral load follow two broad themes: antigenic detection and nucleic acid detection. Chapter 3 describes a novel biosensing technique based on ion-filled liposomes which we apply to whole-particle HIV detection. Chapter 4 addresses approaches to improve the liposome-based antigen-recognition technique, including novel approaches to magnetic-bead separation of viruses from sample. Chapter 5 describes a nucleic acid detection approach employing reverse-transcription loop-mediated isothermal amplification (RT-LAMP) in nanoliter-scale droplets where the sample is lysed whole blood. Finally, Chapter 6 builds on the RT-LAMP, describing a digital quantification approach and its potential for a practical point-of-care viral load test.

CHAPTER 2: DIAGNOSTICS IN GLOBAL HEALTH AND HIV/AIDS

MICRO- AND NANOSCALE DIAGNOSTICS FOR GLOBAL INFECTIOUS DISEASES

Introduction

Infectious diseases continue to be a major factor in an increasingly complicated global public health picture. The "Big Three" pathogens span the spectrum of basic microbiology: a virus (HIV), a parasite (Plasmodia spp., which cause malaria), and a bacterium (Mycobacterium tuberculosis). Alongside dozens of other pathogens, these infectious agents represent critical challenges to global public health, including the vision espoused by the Millennium Development Goals for social and economic well-being nearly 15 years ago [26]. Figure 2.1 and Table 2.1 summarize the impact of major infectious diseases worldwide, and indicates the countries bearing the largest burden of HIV, malaria, and tuberculosis (TB), clearly depicting how disproportionally countries among the world's poorest and most resource-limited regions are affected.

The approach to global control of these infectious pathogens, as well as numerous other infectious diseases that are endemic or resurgent, has three battlefronts. First, since most of these conditions have roots in poverty, inequality, and environmental degradation, efforts promoting economic and environmental health and social equality are key to eliminating the risks of acquiring infectious diseases at their source.

Second, the impact of antimicrobial drugs and vaccines targeting global infectious disease has been staggering. Conditions such as smallpox, polio, and dracunculiasis (guinea worm disease) have been nearly eliminated globally by effective vaccines, while measles, mumps, diphtheria, tetanus, yellow fever and a handful of other pathogens have been effectively—though not completely—contained. At the same time, in the nearly century-old antibiotic era, potent drugs have saved countless lives, including in developing countries, 22 million people with TB [27], 5.5 million people with HIV [28], and more than 1 million malaria-infected children under five [29] in the last 15 years alone. New treatments for hepatitis C have raised a glimmer of hope for global control of this scourge, which affects nearly 200 million people [29]. Despite these successes, many challenges remain: antimicrobial drug resistance is at crisis levels; many

This section was previously published as G. L. Damhorst, M. Murtagh, W. R. Rodriguez and R. Bashir, Proc. IEEE, 2015, 103, 150–160. DOI: 10.1109/JPROC.2014.2385078. Reprinted with permission from the copyright owner.

pathogens such as Chagas' disease, dengue, and Ebola lack effective drugs or vaccines altogether; and the delivery of existing, effective interventions remains woefully inadequate.

The third front in the global war on infectious disease is the battle for accurate diagnosis. Accurate diagnostic technologies for use at or near the point of patient care can have a profound impact on the control of global infectious diseases. Yet, in this emerging era of personalized medicine, high-throughput genome sequencing, and laboratory and imaging technologies of unprecedented power and sophistication, most of the world's population has little or no access to basic diagnostic tools, including hematology and chemistry analyzers, electrocardiograms, x-rays, and CT scans [30]. According to a recent study conducted by the RAND Corporation, access to simple, affordable diagnostic tests for just four conditions—bacterial pneumonia, malaria, syphilis, and TB—could save millions of lives each year [31].

Importantly, successful implementation of diagnostic tests for global infectious disease will require technologies—and ultimately, commercial products—with critical attributes: low cost, simple to use, compact and portable, quality-assured, and accurate. The emergence of microfluidics and nanotechnologies suggests that many diagnostic products with these attributes are within reach. Here we examine the ways in which the tools of the sub-millimeter scale may address the shortcomings of what is currently available, and what may be the key to realizing a long held, but not yet fulfilled promise, to meet the needs of people worldwide for simple, accessible diagnostic tests.

The Microfabrication Age

The silicon era, born with the transistor in the 1940s, introduced processes for precise fabrication of sub-micron features. The rapid emergence of silicon-based microelectronics enabled vast computational power to be contained in tiny integrated circuits, which has brought information processing into small-scale devices and instruments. In parallel, the plastics era, heralded by the development of bakelite in the 1910s, has enabled mass production of precise, robust products of increasing complexity and low cost.

One recent outgrowth of the age of microfabrication in silicon and plastic has been the application of these materials and the underlying engineering methods to biomedical problems. Medical devices from

insulin pumps to pacemakers to glucometers have been made possible at mass scale by applying microscale fabrication and processing methods utilizing silicon semiconductor and plastics manufacturing industries to medical problems.

Diagnostics are the most recent biomedical field to make use of advances in silicon and plastics engineering. A new paradigm is emerging in which mass produced, low cost, ultra-portable instrumentation with sophisticated sample and information processing capabilities can provide answers to medical diagnostic questions far from laboratory facilities. New fluid handling and sensing modalities have emerged that enable the manipulation and interrogation of tissues and fluids like blood, urine, and saliva, which can be used to identify major infectious agents, their molecular signatures, and the body's response to them. Synergies with mobile communications infrastructure can also be leveraged for so-called "point-of-care" deployment of portable diagnostic technologies.

As a result, many conditions that have been undiagnosable in hard-to-reach settings will now be diagnosable, alerting patients and health workers to the need for specific, available treatments. The impact of a new generation of diagnostics is beginning to be felt in areas of the world hardest hit by HIV, TB, and malaria [31], [32].

Assessing the Current State of Global Health Diagnostics

The underlying biology of infectious diseases is at the heart of the opportunity and the challenge of developing new diagnostics. The workhorse of current global infectious disease diagnosis: the rapid lateral flow immunoassay and related methods, often termed a "Rapid Diagnostic Test" or RDT, takes advantage of components of the pathogen or host-generated antibodies to diagnose infection. But not every pathogen behaves in a way that allows for RDT-style detection, and the numerous RDTs available have limitations. A closer look at the methods for infection, replication, and reproduction of major pathogens in Figure 2.2 may shed light on the opportunity – and challenge – of identifying effective biomarkers that can be used for development of diagnostic tests.

Rapid lateral flow immunoassays. The first RDTs, with principles of latex agglutination and radioimmunoassay, were developed in the 1950s and 1960s; RDT technology matured to the point of wide commercialization in the 1980s. Today, RDTs for global infectious diseases are supplied by more than 200 manufacturers worldwide, in the form of dipsticks, cards, cassettes, strip tests, or pads, and are generally easy-to-use and inexpensive ($1-$10 per test result). The most familiar RDT is the home pregnancy test; in global health, the HIV antibody test and the malaria RDT are the most widely used, each performed at least 100 million times per year worldwide [33], [34].

Despite their tremendous impact, lateral flow RDTs have fundamental limitations. First, the level of detection is limited to proteins present in high molar concentrations, like antibodies produced in response to chronic viral infections. For instance, malaria RDTs that target the malarial proteins pLDH (Parasite lactate dehydrogenase) or PfHRP2 (Histidine-rich protein 2 of P. falciparum) can reliably detect malaria only when at least 200 pfu/ml are present in the blood, a relatively large infectious burden. As a result, malaria RDTs will misdiagnose most patients with low-level parasitemia. While many of these patients are minimally symptomatic, they remain sources of malaria transmission. Thus, while malaria RDTs remain extremely useful clinically, they are not sensitive enough to support public health programs designed to stop malaria transmission or eliminate malaria entirely—which would require diagnosis and treatment of asymptomatic carriers not currently detectable by RDTs.

Second, lateral flow RDTs are not generally applicable to conditions in which a biomarker does not exist in high concentrations in body fluids. For these conditions, so-called "molecular tests," which can measure protein antigens, RNA, and/or DNA derived from the pathogens themselves, are required. In particular, "viral loads" in the form of viral protein antigen or viral nucleic acid tests for HIV, hepatitis B virus (HBV), hepatitis C virus (HCV), influenza, and dengue have proven to be essential to accurately diagnose these conditions. In addition to the fact that the target biomarkers are present at low molar concentrations, they often are tucked away inside cells, or complexed—meaning, hidden—within agglomerations of host proteins. The challenge of isolating the target molecule for subsequent detection—a fluid processing challenge ill-suited to RDTs—represents the thorny problem of sample preparation.

State-of-the-art technologies: NAT and cell counting. Broadly speaking, the state-of-the-art in infectious disease diagnostics is nucleic acid testing (NAT). NAT is sensitive and can allow for the detection and even quantification of just a few pathogens in a body fluid (e.g. blood plasma, sputum) by amplifying the RNA or DNA sequences that are uniquely contained within the infectious organism. NAT is necessary for the most accurate quantitative assessment of viral loads and drug resistance testing. The challenge for global health applications, however, is that NAT typically involves large instruments, expensive reagents, and trained operators; therefore functioning NAT systems are rarely found in developing countries, even in large hospitals and universities.

A few technologies, however, have emerged to increase the availability of NAT, although still not portable or hand-held. The Xpert MTB/RIF assay (Cepheid Inc., Sunnyvale, CA), for example, was endorsed by the World Health Organization (WHO) in 2011 [35], [36]. Operated on Cepheid's GeneXpert platform, GeneXpert® MTB/RIF performs real-time PCR (Polymerase chain reaction) to detect M. tuberculosis identification at concentrations as low as 131 cfu/ml as well as genetic mutations responsible for 99.5% of rifampicin resistant strains [35]. Reflecting the major gap in the diagnostics portfolio that the GeneXpert® has begun to address, more than 3,000 GeneXpert® instruments and more than 7.5 million GeneXpert® MTB/RIF cartridges have been procured as of June 30, 2014 in the public sector in 108 of 145 countries eligible for concessional pricing pursuant to the TBXpert Project, a three-year UNITAID-funded collaboration executed by the WHO Global TB Programme and the Stop TB Partnership secretariat [37]. As a result of the Programme, individual tests and the instrument itself have been made available to high-burden developing countries at $9.98 and $17,000.00, respectively [38]. The GeneXpert® has been a significant step forward in decentralizing TB testing, but because of the technical requirements for the test, including the need for phlebotomy and electricity, as well as the lack of portability of the platform, it cannot be used at the lowest levels of the healthcare system in resource-limited settings. A point-of-care, hand-held NAT using a finger prick or sub-milliliter volumes is still a technical grand challenge not met, although miniature devices claiming to accomplish this feat are beginning to appear [39].

In addition to NAT, cell counting is a major need in global infectious diseases diagnostics. In particular, the CD4+ T lymphocyte count is critical to the management of HIV disease and the staging of patients infected with HIV. Typically assessed by flow cytometry, the instrumentation for CD4 counting suffers from the same practical limitations as standard NAT systems. However, increasingly portable cell counting technologies like the PimaTM CD4 Test (Alere Inc., Waltham, MA) have emerged. The PimaTM CD4 Test requires 25 μl of whole blood – volume that can be obtained from a finger prick with no need for venipuncture – and it became the first point-of-care CD4 assay to make the list of WHO prequalified diagnostics when it was added in 2012 [40]. Several companies have followed suit with comparable CD4 technologies, including BD's FACSPresto, and products from Daktari Diagnostics and Omega Diagnostics [40].

The role of micro and nanotechnologies. Broadly stated, the challenge in accurate diagnosis can be divided into performing two processes, sample preparation and target detection, simply, quickly, accurately, and inexpensively. Sample preparation is the less glamorous and more challenging problem. Body fluids, especially blood and sputum, are complex, and generally filled with a significant amount of cells, proteins, DNA, and small molecules other than the target biomarker which, from a diagnostic perspective, represent "noise," or background signals that have to be overcome. The first step in diagnostic testing is to remove as much of this noise as possible, while retaining the target of interest. In sophisticated laboratories, this is addressed by repetitive steps of filtering and washing the sample in a variety of buffers and chemicals using manual or robotic pipetting techniques. Miniaturizing sample preparation protocols has proven to be a tremendous challenge for most diagnostic technologies.

Once the target signal has been washed and purified (and in the case of nucleic acids, amplified), the second step is detection. A wide variety of techniques have been developed to detect biological signals at the micro and nanoscale. These include optical sensing methods, ranging from color changes visible to the human eye to single-molecule fluorescence sensors, as well as electrochemical, electromagnetic and mass sensors. Each detection technique has unique advantages and weaknesses; the best serve as general

detection platforms applicable to a variety of biomarkers and infectious disease pathogens. For global health applications, successful detection techniques need to be exquisitely simple, easy to miniaturize, or both.

Collectively, efforts to develop point-of-care systems that can process body fluids, and isolate and detect infectious pathogens or their physiologic signatures at small scale, have coalesced under the broad headings of microfluidics and nanotechnology. Figure 2.3 summarizes the broad categories under which most of these techniques fall.

Microfluidic Sample Preparation

The diverse collection of microfluidic sample preparation approaches include mechanical, magnetic, electrokinetic, immunoaffinity, and chemical techniques. The appropriate choice of approach, or combination of approaches, is determined by the sample source and the analyte of interest. Sputum, whole blood, and other biological fluid samples each exhibit their own set of challenges for microfluidic sample preparation. Sputum is highly viscous and hard to obtain in large volumes, while a few microliters of blood contain millions of cells that have inherent clotting tendencies.

Detecting blood-borne pathogens such as HIV and HCV, bacteria in sputum, or even a single blood cell subtype requires isolating the target and/or clearing a sample of contamination. Detection of viruses from whole blood may require the extraction of blood plasma due to the small size and quantity of viruses compared to cells. Traditionally, whole blood is processed in large volumes (several milliliters) by centrifugation, chemical lysis, or immunoaffinity isolation kits. While microfluidic methods can draw on the basic principles of these laboratory methods, they also offer some opportunities available only at the micro scale.

Physical filtration. Physical filtration in microfluidic sample processing takes advantage of the sizes of sample components to separate cells or contaminants. Microfluidic filters can employ arrays of pillars, porous membranes, or micron-sized holes, and can be useful for size separation, although they are very susceptible to clogging, especially with blood samples [41]–[46]. As an example, in a flow-through

immunoassay capable of detecting 20 ng/ml of pfHRPII, a plasma extraction membrane is used to separate malaria protein from larger blood components [46].

Hydrodynamic methods. Hydrodynamic methods leverage laminar flow – a characteristic behavior of fluids at a small scale – and the forces on sample components in precisely designed fluidic channels with carefully controlled flow rates, usually to focus cells within a sample or to enrich the target by removing as many contaminants as possible [41], [44], [47], [48]. For example, deterministic lateral displacement employs an array of pillars to separate large cells from a blood sample, and is capable of removing nearly 100% of lymphocytes and monocytes, though the flow rate is slow, only 1 μl min-1 [41]. Another recent example adds to the deterministic lateral displacement method with hydrodynamic focusing that enables sorting rare tumor cells by magnetophoresis and is capable of processing 8 ml hour-1 [49]. These techniques are promising, though the repeatability of precise geometries and flow rates – typically controlled by laboratory syringe pumps – is yet to be demonstrated on a mass-production scale.

On the other hand, some microfluidic techniques aim to mix samples with other reagents, often employing channel designs to induce turbulent flow. Several examples have emerged that leverage osmotic forces and precise timing to selectively lyse erythrocytes [3], [50], [51]. In one study to separate white blood cells from red blood cells, for example, a serpentine microfluidic channel patterned with herringbone structures was used to rapidly mix blood at 20 μl min-1 with hypotonic solution and lyse erythrocytes before restoring osmolarity by mixing a second buffer, thus preserving white blood cells which remain largely intact through the brief exposure to hypotonic solution [50]. This approach appears to be an effective method for quickly processing whole blood leading to white blood cell measurements, though it once again relies on precise timing, and to the knowledge of the authors, has not yet been adapted for commercial production.

Immunoaffinity techniques. Immunoaffinity techniques are widely employed in microfluidic sample processing when an antibody with specificity for the target is available. Surface chromatography in which an antibody is immobilized on one or more planes of a microfluidic device have been used for applications, including isolating CD4+ T cells [3], [52], [53] and even whole viruses [54] from blood. A recent report of

CD4+ T cell capture demonstrated up to 98.3% efficiency [3], while a report of microfluidic capture of viruses on a planar surface reported between 60% and 80% capture for different virus subtypes [54]. In a more common approach, micro- or nanoparticles, particularly magnetic particles, functionalized with antibodies are mixed with the sample to bind the analyte and then separated downstream. Recent work demonstrates magnetic particle binding capable of separating 78% of HIV virions from blood plasma [55], and detecting HIV capsid protein p24 as low as 0.1 pg/ml as part of a biobarcode detection system [56], among others.

While immunoaffinity is the basis of separation or recognition components of several established technologies, it can be challenging – antibodies may be the most expensive component of many point-of-care diagnostics. Other recognition elements may be employed as well, such as nucleic acid aptamers specifically designed to bind a target and DNA strands complementary to a sequence of interest. While the cost of aptamers still remains very high, one recent example employs polymer beads and magnetic nanoparticles functionalized with DNA for capture and labelling of nucleic acid from TB, enabling detection of as low as 103 bacteria from 1 ml of sputum with a micro-NMR (Nuclear Magnetic Resonance) barcode sensing method [57].

Microfluidic devices can also be fabricated with electrodes in order to implement electrokinetic methods in the enrichment or concentration of a target in a biological sample. Electrophoresis, the migration of cells or molecules in an externally applied magnetic field, has been applied in microfluidic systems but has limited throughput and may require high voltages [45]. Dielectrophoresis, on the other hand, employs an alternating current (AC) electric field which polarizes particles, resulting in a net force either in the direction or opposite the direction of the electric field. This technique has been reported and applied widely to cells and micro- and nanoparticles, and can be used to concentrate a target in a microfluidic system – in one example, dielectrophoresis was employed in a microfluidic device, resulting in 50- to 200-fold enrichment of malaria-parasitized cells [58]. However, this technique has not yet translated to commercial applications, largely because the forces are very weak in high salt physiologic solutions, while the use of low ionic strength solutions is rather prohibitive in practical applications. In the unique case of red blood

cells, which are susceptible to magnetic forces, magnetism has also been used for sample processing in microfluidic devices, though the results do not suggest this method is suitable for highly-efficient separation of erythrocytes [45], [59].

In the end, the primary goal of microfluidic sample processing techniques like those described above is to enable increased detection sensitivity while keeping input sample volumes low. When coupled with the sensing technologies described below, microfluidics may be able to address many of the pitfalls of currently available technologies: for instance, RDTs which require high molar concentrations of analytes, or other point-of-care diagnostic systems that still require manual sample processing steps and are not fully-automated, sample-to-answer capable.

Micro and Nanoscale Detection Technologies

The ideal detection approach for global health applications for diagnostics should be low-cost, easy-to-use and robust technologies that are as sensitive as those employed in state-of-the-art laboratory instruments. Micro- and nanotechnologies offer a variety of solutions, each with its own advantages and drawbacks. While a major drawback of optical detection methods in point-of-care diagnostics for resource-limited settings has been the cost and size of lasers, photo-detectors and cameras, the latest trend in camera technologies promises to put increasingly capable imaging ability into smartphones, which are already being used for diagnostics applications. Non-optical methods, particularly electrical impedance sensing, are attractive for their simplicity. As discussed here, a number of approaches aim at miniaturizing PCR, flow cytometry, and even microscopy, with micro- and nanoscale technologies, while others leverage sub-micron fabrication techniques to create novel sensing modalities.

Optical methods. Common optical detection methods include fluorescence, absorbance, and chemiluminescence [60]. Fluorescence is highly sensitive and perhaps the most common optical technique in diagnostics, widely employed in microscopy, flow cytometry, and molecular biology measurements like PCR. Fluorescent markers conjugated to antibodies for proteins or other cellular components give this

approach an excellent specificity. Many micro-scale technologies have employed fluorescence detection, often incorporating a laser or LED (Light-emitting diode) for excitation of the tag.

Fluorescence microscopy has for a long time been a standard method for TB detection in sputum samples, but has been difficult to implement in the field. Although recently LED-based microscopy has increased access to microscopy [61], it is still limited by lack of portability and the need for a trained technician. In one microscale technique employing fluorescence for whole-cell TB detection, bacteria from a processed sputum sample are concentrated, captured, and tagged on the surface of a microtip, which is then imaged with a camera, demonstrating a lower limit of detection of 200 CFU ml-1 from spiked sputum and 10 CFU ml-1 in buffer [62]. In another approach, antibody-conjugated magnetic beads are used to separate bacteria from a sample and quantum dots are used as labels for detection, demonstrating sensitivity down to 103 bacteria ml-1 when a spectrofluorometer is used [63].

In addition to imaging approaches, fluorescence is commonly used as an indicator in NAT, either as a DNA intercalating dye or as part of a fluorophore-quencher system conjugated to probe DNA. Numerous nucleic acid amplification on-a-chip approaches incorporate similar methods, including the digital SlipChip device capable of detecting 37 copies/ml of viral RNA with HIV and HCV samples [64]. Many NATs include isothermal alternatives like Loop-Mediated Isothermal Amplification (LAMP), which are common in micro- and nanotechnology approaches, though it remains to be seen whether a test can be made sufficiently low-cost and robust for use in a hand-held, ultra-portable device that could improve upon the capabilities of systems like the GeneXpert®.

Unlike fluorescence, the appeal of absorbance approaches like colorimetry is that the signal is visible to the naked eye, which can eliminate the need for cameras in tests where a qualitative result is desired. Among the drawbacks is that instrument-based analysis of colorimetric signals is not as precise as other methods. Gold nanoparticles are a common component of colorimetric tests for the color-change phenomenon observed when they are concentrated. The previously-mentioned example employing a membrane filter and capable of detecting 20 ng/ml of pfHRPII uses antibody-conjugated gold nanoparticles for colorimetric detection, with quantitative analysis achieved by reading the result with a flatbed scanner

[46]. An example of a nanoparticle-based TB detection strategy is one that employs gold nanoparticles attached to short strands of DNA that are complementary to opposite ends of a target amplicon and produce a visible color change when 0.75 μg or more of DNA is present [65]–[67]. Subsequent reports describe versions of the approach on a portable platform [66] and on paper substrates [67].

Chemiluminescence, the emission of light from a chemical reaction, is also a useful approach for portable diagnostics as it does not require an external light source, though it is limited by the reagents available to produce such a signal [60]. An example is an ELISA-style CD4-counting approach in which CD4 T cells are first separated with antibody-conjugated magnetic beads, tagged with another antibody conjugated to horseradish peroxidase, and the signal measured with a cell phone camera [68]. CD4 counts determined by this method showed an 0.86 R2 compared to flow cytometry for HIV patients with CD4 counts between 237 and 1,446 cells μl-1 [68]. Although this is an interesting approach that leverages a standard mobile phone device, the need for multiple antibodies limits its ability to be low cost.

Other optical detection technologies include the lens-less shadow imaging technique in which diffraction patterns are imaged by a detector behind an illuminated sample. Shadow imaging has been employed for whole cell detection in microfluidic devices, including for point-of-care testing of CD4+ count [69], [70]. Additionally, plasmon resonance has been employed to detect the binding of intact viruses on a gold nanoparticle surface functionalized with antibodies down to 98 +/- 39 virus copies/ml in the best report [71]. Another report from the same group employed photonic crystals to detect viruses from spiked plasma between 104 and 108 copies/ml [72].

Non-optical methods. Non-optical methods exhibit a different set of advantages and drawbacks. Electrical sensing techniques are often simpler and cheaper than optical methods; however, they typically rely heavily on sample processing steps to remove background noise. Impedance spectroscopy measures electrical impedance of an aqueous solution as a function of AC frequency, commonly using microfabricated electrodes. The presence of a cell-sized target obstructing the movement of charge carrying ions in the solution, or changes in ion concentration as a result of cell lysis, or metabolism have been used as the basis for sensors measuring a variety of targets including cells and small molecules.

One technology counts CD4+ T cells after immunoffinity separation from whole blood by a method called lysate impedance spectroscopy, which measures impedance change resulting from the release of intracellular ions and is capable of detecting 20 cells μl-1 [52]. Another is a microfabricated Coulter counter with dual-frequency impedance sensing capable of distinguishing white blood cell populations, and enumerating CD4+ T cells with the addition of a bead attached to the CD4 surface marker, demonstrating 95% correlation with clinical laboratory equipment [73]. A third example draws on both approaches to count CD4 and CD8 T cell cells from whole blood in a differential counting approach in which cells are counted before and after immunoaffinity depletion in a microfluidic chamber, demonstrating an R2 of 0.92 for CD4 counts compared to a clinical laboratory's standard [3]. Similar impedance-based cell counting approaches have also been used to distinguish the intrerythrocytic stages of malaria-infected red blood cells, as well as to distinguish infected from uninfected cells [74], [75]. In our view, the impedance-sensing approach to cell counting is a highly promising approach, and it is already emerging in commercial applications.

Another electrical detection method, voltammetry, measures the current in a sample as a response to varied electrical potential. One example detects IFN-γ (Interferon gamma)s released in the presence of TB antigens, an indicator of latent TB infection, by voltammetry employing micro-patterned half-ring electrodes as the detector component which surround a site for cell attachment, capable of detecting IFN-γ at concentrations between 0.06 and 10 nM [76], [77].

Electrochemical approaches are similarly promising, though they are limited to enzymes and reagents capable of producing an electrochemical signal. One method sandwiches pfHRPII from spiked human serum between two antibodies, one covalently linked to a magnetic nanoparticle and the other bound to a reporter enzyme, horseradish peroxidase [78]. The sandwiches are then drawn magnetically to the surface of an electrode, which is polarized by the enzyme-facilitated chemical reactions, enabling detection of pfHRPII at concentrations as low as 0.36 ng ml-1 [78]. There is some question, however, whether an approach like this provides any advantage over a traditional ELISA as it requires many of the same reagents.

Other approaches may detect mass or mechanical forces. For example, a piezoelectric immunosensor designed to bind pfHRPII in diluted human serum could detect mass changes as a shift in the resonant frequency of an antibody-functionalized quartz crystal microbalance, facilitating detection down to 12 ng ml-1 [79]. However, as is true with many mechanical sensors, there is some concern whether such a sensor exhibits the robustness necessary for a hand-held diagnostic test. Nevertheless, one example which appears promising for its simplicity is a microfluidic system in which red blood cells are passed through a funnel chain with micron-sized constrictions measuring the threshold deformation pressure required to squeeze the cell through, finding that parasitized cells are between 1.5 and 200 times stiffer than healthy red blood cells [80]. It is suggested that this microfluidic approach can be used for detection of the presence of malaria parasites and assessment of treatment efficacy, although there is a question as to whether the throughput would be sufficient to process enough sample in a short time.

But innovations in micro and nanotechnology do not appear to be only within the categories mentioned here. As microfabrication techniques improve, we may find sophisticated measurement techniques increasingly miniaturized for diagnostic applications, and we may be seeing glimpses of this already. For example, consider the previously mentioned report in which amplified DNA from TB was detected with micro NMR [57]. Additionally, mass spectrometry, a highly sensitive technique for measuring the composition of materials based on charge and molecular weight – has been miniaturized and coupled with microfluidic devices [81], and may be among the next generation of detection methods to be adapted for the point-of-care.

It is one thing to demonstrate the enrichment of an analyte from a biological sample, and another to show the sensitive detection of analyte in a debris-free buffer or after the sample has been processed by standard laboratory methods. The integration of these pieces, however, presents a new challenge. The quest for complete sample-to-answer platforms requires coping with the added complexity of loading and metering the biological sample, and tuning microfluidic devices, flow rates, and capillary forces. These are problems often barely examined in research laboratories, but inevitably faced when moving from prototyped devices to plastics and mass manufacturing.

Research Funding and Commercialization of Micro- and Nanotechnology Diagnostics

The road from discovery to delivery of diagnostic products involves many steps, and the process can easily take 5 years or more, even after prototype development, and costs can run from $5 million to $50 million or more. Funding is frequently an early barrier to product development, and can slow the process even more than technical challenges. Mobilizing funding for diagnostic products designed for the developing world is particularly difficult, as financial returns on such products are generally expected to be low relative to products being developed for resource-rich settings.

Seed funding for basic research and proof-of-principle of a new diagnostic technology, including platform development and feasibility studies, is often available from a variety of sources, including the National Science Foundation (NSF), the National Institutes of Health (NIH), National Institute of Allergy and Infectious Diseases (NIAID), the Bill & Melinda Gates Foundation, and Small Business Innovation Research (SBIR) grants. In the next stage of product development, including prototype development, clinical trials and product optimization, funding may be available from angel investors, technology laboratories and SBIR Phase II grants, among others. However, at the subsequent stage of product development, including pre-market validation, manufacturing scale-up, and commercial release and regulatory approval, funding for new diagnostics is very difficult to obtain, and has often been called the 'valley of death' facing new product concepts and start-up companies. Possible sources of funding include venture capital, corporate venture funds, and commercial debt. Some funders, including UNITAID, Children's Investment Fund Foundation, and others may provide funding at the later stages of product development, but only for certain targeted disease areas (e.g., TB, HIV, malaria) or target populations (children).

With respect to microfluidics and nanotechnologies for detection of global infectious diseases, many of which are in the earliest stages of development, additional governmental and non-governmental funding sources are needed to accelerate their path from bench to bedside. Moreover, from the point of design lockdown through market validation and manufacturing scale-up, additional sources of funding and new business models to facilitate commercialization and uptake of new diagnostic technologies are sorely

needed. The business model for commercializing point-of-care devices for global health infectious diseases is unique. The entities purchasing these devices are typically governments of high-burden countries, often using international aid from developed countries and foundations. Meanwhile, manufacturing technologies from the developed world lead to individual tests that are too costly to be sold in the developing world, unless a sufficient volume of demand measured in the millions of units can make the price point financially attractive.

Outlook

Micro- and nanotechnologies have enabled clear progress in HIV diagnostics, with the commercial availability of microfluidics-based CD4+ T cell counting using a drop of blood from a finger prick. The next grand challenge in HIV diagnostics is to reliably measure viral load from a drop of blood at the point-of-care with high sensitivity. Methods based on capture and detection of whole virus particles, may be simpler to implement but less sensitive than approaches involving nucleic acid amplification-based methods. A point-of-care, single-use nucleic acid-based detection of viruses from a finger prick is a technical challenge that still needs to be addressed. In fact, management of TB, malaria, and a host of other infectious diseases would benefit from such a point-of-care, single-use nucleic acid amplification device.

Mobile health care is a trend that is here to stay. Improvements in camera technology allows for unprecedented levels of sensitivity and spatial resolution for detection of optical signals. The use of sensors and adaptors with smartphone cameras and other mobile technologies is likely to increase dramatically. In additional to cell phone-based optical approaches, electronic or electrochemical approaches based on impedance or field effect mechanisms can provide direct interface between the system and the sensors resulting in portable and miniaturized devices.

It should also be noted that as the cost of sequencing continues to approach $1,000 and lower, the full sequencing of genomes of pathogens may be an option that is not far off, providing holistic analysis of a pathogen as well as aiding in the identification of new and unknown strains and mutants. Unconventional approaches such as portable mass spectrometers coupled with microfluidic sample preparation approaches

could allow for determination of peptides, protein fragments and related biomarkers to identify pathogens using fingerprinting and data analytics. However, whether desired sensitivities from small samples can be achieved is an open question.

While the progress in research and feasibility demonstrations of micro and nanotechnology-based diagnostics for HIV, TB, and malaria have been rapid, the commercialization and translation is only beginning to become a reality. Challenges still include the cost of manufacturing, production and scale up itself and the corresponding business models for financial success. Continued philanthropic sources and funding from the developed world would be critically needed to sustain further investments for commercialization of the promising approaches. The potential for impact is limitless as millions of people can benefit if these technologies can be commercialized and brought into the hands of the health care providers in the world's poorest regions that are disproportionately impacted by these infectious diseases

DIAGNOSTICS IN HIV/AIDS

Introduction

Approximately 34 million people worldwide are living with Human Immunodeficiency Virus (HIV), the virus that causes Acquired Immune Deficiency Syndrome (AIDS) [2]. Epidemiological trends reflect recent progress in the expansion of access to prevention, testing, counseling and treatment, including a drop in new HIV infections from 3.1 million annually in 2002 to 2.7 million in 2010 and a decline in AIDS-related deaths from 2.2 million annually in 2006 to 1.8 million in 2010 [2].

These data do not mask the epidemic proportions of the disease, however, and combating HIV/AIDS remains one of eight Millennium Development Goals outlined by the United Nations for reducing extreme poverty [26]. The disease disproportionately affects the world's poorest nations – for example, 68% of all people living with HIV reside in Sub-Saharan Africa, a region that represents only 12% of the global population [2]. Because of the absence of an effective vaccine, the availability of antiretroviral medications

This section was previously published in G. L. Damhorst, N. N. Watkins and R. Bashir, IEEE Trans. Biomed. Eng., 2013, 60, 715–26. DOI: 10.1109/TBME.2013.2244894. Reprinted with permission from the copyright owner.

and accessibility of testing represent the most significant grand challenges in fighting the HIV/AIDS epidemic worldwide. These two challenges do not stand independently, however, as regular and appropriate monitoring is required for effective treatment.

HIV infection is typically diagnosed by serologic tests indicating the presence of anti-HIV antibodies, a test for which rapid point-of-care assays are available including tests of oral fluids and whole blood from a finger prick [23]. Following diagnosis, guidelines issued by the Infectious Disease Society of America (IDSA) recommend immediate evaluation of two core markers of the progress of infection: the CD4+ T lymphocyte count and plasma viral load, in addition to antiretroviral therapy (ART) resistance testing, a complete blood count, and blood chemistry panels [23]. Typical levels of CD4+ T lymphocytes and plasma viral load during the course of HIV infection are depicted in Figure 2.4 [82], [83]. World Health Organization (WHO) guidelines recommend the initiation of ART for people living with HIV upon determination of a CD4 count less than or equal to 350 cells/mm3, while CD4 count monitoring is recommended to be performed at least every six months for individuals not yet eligible for ART [84].

During treatment, the WHO recommends CD4 counting and viral load monitoring in a routine approach [84]. Ultimately, the goal of regular monitoring is to guide treatment strategies toward the prevention of immunological failure (CD4 count below baseline, 50% of on-treatment peak value, or 100 cells/mm3), and virological failure (viral load above 5000 copies/ml) [84].

The CD4 count reflects the health of the immune system and is occasionally paired with the CD8+ T lymphocyte count in assessment of an HIV+ patient, although there are conflicting reports on the utility of CD8 counts or CD4/CD8 ratio [23], [85]. Viral load measurements complement the CD4 count and are a direct assessment of viral number. Viral load is typically assessed by quantifying viral RNA in the blood plasma, although alternative approaches to quantifying plasma load as well as intracellular viral reservoirs have been described. A review of the HIV lifecycle in Figure 2.5 reveals several traditional and alternative biomarkers for monitoring virus levels.

Because of retrovirus integration with the host in the form of a provirus, HIV establishes a long-term reservoir and accomplishes production of new virions in host cells – a process which can be interrogated at

all levels of gene expression inside the cell. Detection of proviral DNA is the most commonly assessed intracellular marker and has established clinical relevance as a method for assessing virus status in newborns in whom mother-to-child transmission of HIV is suspected, since passive transfer of maternal antibodies can produce false-positives on serological tests [23]. However, assessment of levels of cell-associated unspliced and multiply-spliced HIV RNA have also been suggested as clinical markers of disease progression [86]–[88], to have prognostic value [89], or to be useful metrics for assessing ART efficacy [90], [91]. Laboratory-based methods for the detection of cell-associated RNA have been demonstrated [92], [93].

The core principles of micro- and nanotechnology offer opportunities for new approaches to monitoring all of these biomarkers. Modern fabrication techniques have enabled the development of novel optical, mechanical, and electrical biosensor platforms with greater sensitivity for cell and biomolecule sensing, including those which replace or eliminate the need for expensive and bulky components of state-of-the-art clinical diagnostic instruments. Microfluidic systems enable precise manipulation of small volumes of biological fluids, significantly decreasing blood sample size requirements and allowing for less invasive collection techniques. Finally, smaller instrument footprints promise a high degree of portability in sample-to-answer systems.

This review emphasizes approaches toward the implementation of technologies for CD4 T lymphocyte counting, plasma viral load and proviral load determination in resource-limited settings. Approaches vary from adaptations of state-of-the art technologies to novel assays based on innovations in micro- and nanotechnologies. Several technologies discussed here address testing challenges through complete sample-to-answer integrated systems while others demonstrate partial solutions, yet demonstrate potential for application in an integrated system.

In addition to the typical requirements for sensitivity and specificity required of diagnostic technologies, the criteria for effective CD4 counting or viral load determination in resource-limited settings includes: (1) the test must be able to operate at the point-of-care, addressing the need to bring testing to patients with limited ability to travel to a healthcare facility, (2) the test must be rapid, addressing

complications in resource-limited settings associated with healthcare provider follow-up when results cannot be obtained same-day, (3) the test must be low-cost, mitigating the financial burden on individuals, agencies or governments in poor countries, and (4) the test must be easy to use, allowing for implementation in areas where skilled technicians are not available. The end goal is a comprehensive technology capable of taking whole blood input in the form of a finger-prick or heel-prick, and outputting the desired results.

Plasma Viral Load

Current State of the Art. Several challenges complicate the monitoring of HIV plasma viral load, including the diversity of HIV forms and subtypes as the result of high recombination and mutation rates – one of the primary barriers to the development of an effective vaccine [94]. Effective viral load devices must therefore be capable of flexibility among genetic or antigenic variation from infection to infection.

State of the art technology for plasma viral load involves amplification and detection of viral nucleic acid. Tests approved by the U.S. Food and Drug Administration for quantification of plasma viral load by nucleic acid amplification are listed in Table 2.2 [95]–[98]. To date, however, no Reverse-Transcription Polymerase Chain Reaction (RT-PCR), branched DNA (bDNA), or Nucleic Acid Sequence-Based Amplification (NASBA) assay has demonstrated the qualities necessary to become ubiquitous in resource-limited settings.

Multiple studies have also explored the possibility of transporting dried blood or plasma specimens from more primitive sites to a capable laboratory as a global health solution for plasma viral load testing, though this does not address the ultimate need for a rapid, point-of-care test [99]–[102]. Progress toward viral load in resource-limited settings has emerged in the form of assays for other biomolecular components of HIV, including the structural capsid protein p24 and the enzyme reverse transcriptase, platforms aimed at the miniaturization of the amplification and/or detection aspects of nucleic acid quantification, and isolation of whole viruses from blood samples as a processing step toward direct particle counting. Several novel non-quantitative technologies for detection of HIV in plasma have been reported, including a recent report from De la Rica and Stevens on a gold-nanoparticle-based p24 assay that can be analyzed with the

naked eye [103]. Non-quantitative techniques are only presented extensively in this section, however, when considered relevant to the development of a future quantitative technique.

Global Health Solutions

Detection of p24 capsid proteins. The Enzyme-Linked ImmunoSorbent Assay (ELISA) is a standard technique for laboratory detection and quantification of proteins. P24 assays developed by Perkin Elmer Life Sciences (Boston, MA) [104]–[107], NEN Life Science Products (Geneva, Switzerland) [108], and Biocentric (Bandol, France) [109] have been evaluated for use in resource limited settings but sensitivity [105], reliability [105], [108] and false positives [109] have been cited as reasons limiting implementation of these tests in resource-limited settings. Alternative assays have been developed, however, for the detection of p24 as the basis for HIV quantification [56], [110]–[113].

Lee, et al. sought to improve upon the standard ELISA with a nanoarray patterned with anti-p24 antibodies by dip-pen nanolithography [110]. Instead of an enzyme with chemiluminescent product, a gold nanoparticle probe functionalized with anti-p24 antibody was used as a secondary tag and detected with atomic force microscopy and scanning electron microscopy. While this report serves as an interesting proof-of-concept, a more appropriate detection technique is necessary as these microscopy techniques are probably not suited for low-cost, portable applications.

Parpia, et al. described a dipstick assay for p24 designed for rapid detection of HIV in infants [111]. Plasma samples were mixed with heat shock buffer, heated to disrupt immune complexes, and then exposed to the dipstick test. The sample hydrates an antibody-conjugated tag and flows laterally by capillarity to a test line where antigen-bound tags are immobilized. The dipstick is then scanned and analyzed by a computer for semi-quantitative results. This technique makes strides toward the ideal platform for point-of-care viral load determination, although integrated scanning and analysis may be necessary to achieve the desired ease-of-use.

The concept of a biobarcode detection assay was introduced by Nam, Thaxton and Mirkin in Science in 2003 [114]. The technique was later adapted for detection of HIV capsid protein p24 [56], [112], [113] and an overview of the concept is depicted in Figure 2.6 [112]. The biobarcode assay is a modification of

traditional ELISA techniques in which p24 is first captured in microtiter wells coated with anti-p24 antibody and subsequently tagged with a biotinylated anti-p24 [112]. Streptavidin-coated gold nanoparticles are then bound to the secondary antibody, providing a substrate for attachment of biotinylated barcode DNA. Following washing and heating, biobarcode DNA immobilized on gold nanoparticles bound to p24-antibody sandwiches is eluted and hybridized to a sequence complementary to half of the barcode DNA on a glass slide. A DNA-probe labeled gold nanoparticle binds to the other half of the immobilized barcode DNA and silver ions are reduced by hydroquinone on the surface, amplifying the visualization of biobarcode signals. A later version of this assay replaced the microtiter wells with antibody-coated magnetic nanoparticles which facilitated the separation of the antigen-nanoparticle complexes from solution [56]. This biobacode technique has demonstrated promising strides toward the grand challenge of early HIV detection [113] and bears the potential for a quantitative test, yet it has not yet been shown as a suitable replacement for quantitative nucleic acid detection technologies or to have been evaluated for efficacy in resource-limited settings.

Detection of reverse transcriptase activity. Reverse transcriptase (RT) is an essential component of replication-competent HIV and thus a specific marker of HIV infection. The ExaVirTM Load assay (Cavidi Tech AB, Uppsala, Sweden), which is based on the detection of RT activity, was first described by Ekstrand, et al. [115]. This assay requires pre-treatment of blood plasma from HIV-positive blood and isolation of the virus on an immobilization gel column with subsequent washing to remove anti-RT antibodies or RT-inhibiting antiretroviral drugs which are present in many individuals undergoing ART [116], [117]. The sample is eluted from the immobilization column by washing with a viral lysis buffer that frees virus-encapsulated RT for assay. RT activity is quantified based on incorporation of 5-bromodeoxyuridine 5' triphosphate (BrdUTP) in RT DNA product and subsequent BrdUTP tagging with an alkaline phosphate-conjugated antibody. A substrate for AP is then introduced after washing for colorimetric or fluorimetric analysis. The ExaVirTM assays have been evaluated for sensitivity, practicality and flexibility among various HIV subtypes by several clinical studies, including investigations in Burkina Faso [118], Mobmasa, Kenya [109], Botswana [119], Nairobi, Kenya [120], and Johannesburg, South Africa [105]. Evaluations

appear optimistic toward the potential of the ExaVirTM as a less-expensive alternative to PCR [104], [105], [109], [118]–[126].

Miniaturization of PCR, non-quantitative. Several efforts to adapt state-of-the-art testing for resource limited settings has involved simplification or automation of various aspects of PCR. For example, Tang et al. developed an isothermal amplification kit based on a reverse-transcriptase helicase-dependent nucleic acid amplification technique which was integrated with a vertical-flow DNA detection strip [127]. The assay, however, still required rigorous preparation of the sample in a laboratory setting, including the purification of viral RNA. Lee et al. described an isothermal simple amplification-based assay (SAMBA) that could be performed on a table-top point-of-care machine including both amplification and dipstick detection [128].

Lee, Kim, Kang and Ahn developed a microfluidic design for on-chip RT-PCR containing mixture and reaction chambers for reverse transcription and PCR as well as a detection chamber in which amplified product is immobilized on complementary probe DNA [129]. An overview of their microfluidic PCR device is depicted in Figure 2.7 [129]. An infrared lamp serves as the heart source for PCR thermo cycling and immobilized amplified PCR product is tagged with horseradish peroxidase which reacts with substrate solution to produce a chemiluminescent product for optical detection. This lab-on-a-chip design was capable of performing RT-PCR in 35 minutes, but requires further demonstration of sufficient sensitivity and has not been analyzed for quantitative detection.

Miniaturization of PCR, quantitative. Shen, et al. described the application of a SlipChip device to amplification of HIV RNA [64]. RT-PCR mixture containing samples is introduced to 160 wells each of 1 nL, 5 nL, 25 nL and 125 nL allowing for multiplexed analysis. Correct volumes are ensured by dead-end filling facilitated by rotational slipping of a layer of the chip and digital PCR is performed, allowing quantification of viral RNA copies. Digital PCR fluorescence on the SlipChip is demonstrated in Figure 2.8 [64]. Ultimately, the technique was capable of detecting 37 viral copies per ml plasma although additional demonstration of this approach is necessary for consideration as a platform for field testing.

Rohrman, et al. recently described another gold nanoparticle-based technique for the detection of amplified HIV RNA [130]. In their study, NASBA product is placed on a conjugate pad containing gold nanoparticles functionalized with complementary RNA strands which bind the sequence of interest. The sample flows laterally by capillarity down a nitrocellulose membrane strip to a detection zone in which nanoparticle-bound sequences are immobilized. An enhancement solution reduces metallic ions on the surface to increase the colorimetric result, which can be assessed with a common cell phone camera. The assay is paper-based and is easily destroyed by incineration and is reported to cost approximately $0.80 per strip, however it relies on amplified nucleic acid and thus does not present a solution to some of the most fundamental challenges to implementing PCR-based technologies in resource-limited settings.

Tanriverdi, et al. adapted a commercially available HIV assay to fit a portable, fully integrated and automated diagnostic system called Liat Analyzer [131]. 200 µl plasma is loaded into an assay tube and loaded into the analyzer which prepares the sample by performing viral lysis and nucleic acid conjugation with magnetic glass beads. The analyzer elutes the viral RNA and performs reverse transcription and PCR with real-time fluorescence detection, showing good correlation with COBAS TaqMan HIV-1 and Versant HIV-1 RNA (bDNA) assays. The full process is depicted in Figure 2.9 [131]. The fully-integrated test is completed in 88 minutes and exhibits a limit of detection of 1,000 copies/ml, leaving room for improvement to compete with the most rapid and sensitive technologies.

Virus isolation. In strides toward alternative (non-PCR) approaches to HIV quantification, direct capture of HIV in microfluidic flow-through devices has been demonstrated by Demirci, et al. [54], [132], [133]. Briefly, a microfluidic chamber is functionalized with antibodies specific for the HIV envelope-associated protein gp-120 through a variety of surface chemistry techniques and 10 µl [132], [133] or 100 µl [54] of whole blood containing HIV was flowed through the device. Captured viruses were initially visualized with quantum dot tags to verify capture [132], [133], but in a more recent report were lysed on-chip, collected, and interrogated by RT-qPCR for HIV nucleic acid showing 69.7-87.6% capture efficiency for a variety of subtypes and viral loads [54].

In another approach, Chen, et al. mixed virus-containing plasma with superparamagnetic nanoparticles functionalized with anti-CD44, an antibody that binds HIV, and injected the sample onto a microfluidic chip with geometries designed for mixing [55]. Ferromagnetic particles in the fluidic device concentrate an external magnetic field that concentrates virus-bound particles, achieving separation from plasma. Isolated sample is then lysed and interrogated for p24 with an ELISA kit, revealing a maximum capture efficiency of 79% [55]. An overview of this capture device is shown in Figure 2.10 [55]. These platforms, which ultimately could be integrated in a sample-to-answer system, create the opportunity for improved sensitivity by removing the virus from whole blood or plasma and thereby eliminating contaminants which may interfere with detection.

Proviral Load

Current State of the Art. Provirus refers to the genome of a virus directly integrated with the DNA of the host cell. The proviral load is not as ubiquitous as the plasma viral load or CD4+ T lymphocyte count in clinical management of HIV/AIDS, yet it bears certain significance as the standard for early diagnosis of infection in newborns for whom mother-to-child transmission is suspected, since serological testing is inadequate due to the possibility of false positives from the presence of passively acquired maternal antibodies [23], [134]–[140]. Many have also acknowledged that the proviral load may be an opportunity for early detection in adults in the 2-8 week window period [141] before seroconversion [135]–[137], a useful alternative for monitoring of ART when plasma RNA levels are undetectable [135], [142], [143], or a complement to the plasma RNA load for diagnostic or prognostic purposes [135], [142], [144]–[147]. Laboratory techniques for detection of proviral DNA that have been described including non-quantitative PCR approaches [138], [148], quantitative PCR approaches [92], [135], [142], [143], [149], [150], electrochemiluminescence-based detection of PCR products [136], enzyme immunoassay detection of PCR products [137], and one study which performed PCR analysis on dried blood spots [134].

Global Health Solutions. Jangam, et al. presented a solution to the challenges of sample preparation in resource-limited settings when analyzing proviral load with a low-cost extraction technique called

filtration isolation of nucleic acids (FINA) [151]. In this technique, whole blood is introduced on a membrane disk and subsequently washed with NaOH resulting in isolation of genomic DNA on the membrane. The membrane is then placed directly in a PCR reaction mix for quantitative analysis. Recently, the same group has reported integration of this extraction method with a sample-to-answer point-of-care PCR system for proviral DNA detection [152]. In this case, blood collected from a heel prick is lysed in the blood collection device, applied to a separator module for FINA, and inserted into an injection-molded assay card. The assay card contains reagents for PCR prepackaged in a foil laminate reagent reservoir and the entire card it inserted directly into a table-top instrument which performs reagent delivery, thermal cycling and fluorescence detection. The estimated cost of the instrumentation is $3,000.00 while each disposable assay card is expected to cost $50.00 or less, a per-test cost on the higher end of the range of estimates reported in the approaches discussed in this review.

Wang, et al. have also recently described a device capable of proviral DNA detection on a chip [153]. In this proof-of-concept, HIV-infected T cells were loaded onto the chip where they were first heat-lysed and then hybridized with nucleotide probe-conjugated magnetic beads. A permanent magnet was then used to immobilize probes while debris was cleared with a vacuum and the sample was washed. Purified sample was then split between four separate chambers containing unique primer pairs, and PCR amplification was performed and monitored by SYBR Green I fluorescence and integrated optical detection. The whole process was completed in 95 minutes, demonstrating potential for implementation as a point-of-care device in resource-limited settings, although demonstration of this technique from whole-blood input would be necessary for truly point-of-care applications.

CD4+ T Lymphocyte Count

Current State of the Art. The current gold standard for enumeration of CD4+ T lymphocytes involves immune-staining and analysis of cells with a flow cytometer, a technique that not only requires expensive and bulky instrumentation but also highly-trained laboratory technicians. In efforts to bring CD4 enumeration to resource-limited settings, various techniques have been employed. Here we organize

various technologies for CD4 enumeration in resource-limited settings based on the following categories: optical detection methods, electrical detection methods, technologies based on microcytometry employing either optical or electrical techniques, catch-and-release devices, and instrument-free methods.

Global Health Solutions

Optical methods. Many efforts have used fluorescent tagging and subsequent image processing to automatically enumerate CD4+ T lymphocytes in micro chambers. Some designs relied on the even distribution of cells in a plastic chamber to produce accurate counts [154]. Others have used a micro fabricated membrane to filter out erythrocytes, leaving leukocytes, which were fluorescently labeled [155]. Specialized image processing algorithms have been developed for the analysis of images from such devices [156]. Thorslund et al. developed and refined a bio-activated PDMS device for capture of CD4+ cells and subsequent imaging with HOECHST and CD3-FITC [157], [158].

Fluorescence detection was later enhanced by using quantum dots [159], [160], forming the technology behind LabNow, Inc. Another approach used immuno-specific paramagnetic beads to bring fluorescently labeled CD4+ T cells into the focusing plane for analysis, reducing counting error [161]–[163]. Cheng et al. have investigated CD4+ T cell capture by controlling shear stresses at the chamber walls and enumerating cells using a cocktail of fluorescently labeled antibodies [164], [165]. They improved their design by including a monocyte depletion chamber to reduce the positive bias created at lower CD4+ T cell concentrations [166].

Beck et al. have eliminated the off-chip labeling step required by the aforementioned methods by coating capture chambers with hydrogels containing fluorescent antibodies and drying them for storage [167]. During testing, blood enters the capture region, causing the hydrogel to swell and release the antibodies, specifically labeling CD4+ and CD8+ T cells. Subsequent fluorescent image cytometry is used to obtain the CD4+ and CD8+ T cell counts. The Alere Pima CD4 counter uses a similar method to label CD4+ T cells using cartridges containing a lyophilized antibody pellet [167], [168], and has shown some success in field testing including sites in Harare, Zimbabwe [169], Maputo, Mozambique [170], Gauteng

Province, South Africa [171], Kampala, Uganda [172] and London, UK [173]. However, in some situations, it has operational costs similar to or more expensive than standard lab flow cytometric analysis [171], [174].

The aforementioned optical methods require the use of lenses and focusing to analyze samples, but this can increase the cost and decrease the portability of the device and several technologies have made attempts at simplifying the optical component. Gohring et al. quantified the antibody-mediated attachment of T cells by the amount of shift in the whispering gallery mode of an optofluidic ring resonator [175]. Moon et al. counted immobilized helper T cells by their shadows cast over a charge coupled device (CCD) by a white light source [70], [176]. Wang et al. further simplified the optics by not requiring an external light source: immobilized CD4+ T cells were labeled with CD3-conjugated horseradish peroxidase to facilitate a chemiluminescent reaction, which was amplified and quantified by a photodetector [177]. This device was tested using samples from patients at a treatment center in Dar es Salaam, Tanzania [178].

Electrical methods. Electrical methods for enumerating CD4+ T lymphocytes are promising due to the fact that they would not require optical components such as lenses, filters, light sources, photodetectors, and CCDs, which can be expensive, bulky, fragile, and require periodic maintenance. An electrical PoC solution could require only solid state components to electrically interrogate a sensing geometry, process sensor output, and provide input from and results to the user.

Mishra et al. used three-electrode cyclic voltammetry to estimate the number of CD4+ T cells that were selectively captured on a working electrode [179], [180]. Jiang et al. have used this design as a building block to create an array of 200 of these electrochemical sensing regions, or pixels, conjugated with CD4 antibody. A pixel would be considered on when a CD4+ T cell was captured, and a total cell count was the total number of on pixels [181].

Cheng et al. enhanced their CD4+ T cell capture device ([164], [165]) by integrating impedance spectroscopy sensing into the capture channel to monitor cell lysate [52]. T cells from whole blood were captured on-chip and lysed in a low-conductivity buffer, releasing intracellular ions into the bulk solution, thereby changing its conductance, which increased proportionally with cell concentration. Impedance-phase spectra and correlation with cell concentration are shown in Figure 2.11 [52]. The authors were able

to correlate cell concentration with channel conductance with a detection sensitivity of 20 cells/uL, eliminating the need of a microscope and manual cell counting. Daktari Diagnostics, Inc., has developed the Daktari CD4 counting platform based on this technology.

The lysate impedance method has shown to be an extremely promising technology to penetrate into resource poor regions, as it requires no off-chip sample preparation, employs an electrical interrogation method, and is simple to operate. However, inherent drawbacks from measuring lysate impedance may reduce its efficacy. This technology assumes that T cells from various individuals contain similar ion concentrations, which may not be true, resulting in counting error. In addition, since the technology is sensitive to the concentration of ions, contamination from the sensor chip's materials and failure to wash away excess ions may reduce the system's counting resolution and dynamic range.

Microcytometer approach. Kiesel et al. worked toward the goal of a compact flow cytometer with a spatial modulation technique for CD4 identification [182]. Wang et al. have developed a microfluidic chip which first labels CD4+ and CD8+ T lymphocytes (from buffy coat samples) on-chip using pneumatic vortexing before hydrodynamically focusing and laser-induced fluorescence (LIF) counting [183]. They were able to produce CD4/CD8 T cell ratios similar to that found using standard flow cytometry. Yun et al. developed a microfluidic flow cytometer enhanced by FITC-doped silica nanoparticles that required only a single detector [184]. Mao et al. designed a microfluidic flow cytometer with three-dimensional hydrodynamic focusing of CD4+ T lymphocytes and LIF detection [185].

Wang et al. integrated a commercial metal oxide semiconductor field effect transistor (MOSFET) with optical fluorescence detection to determine the percent of CD4+ T cells among a total population of lymphocytes [186]. They have also created a similar system replacing the MOSFET with a two-stage differential amplification system [187], [188]. However, the added complexity of integrating both electrical and optical measurement systems may be prohibitive for PoC applications.

Holmes et al. have developed an electrical microcytometer that can differentiate between different leukocyte subtypes, such as lymphocytes, monocytes, and neutrophils, solely on their impedance characteristics at two different frequencies, as depicted in Figure 2.12 [73], [189].They were subsequently

able to enhance electrical differentiation of CD4+ T cells from other leukocytes by specifically attaching 2.2 μm CD4 antibody conjugated latex beads to the T cells to modify their high and low frequency characteristics [190]. They showed good correlation between their electrical chip-based method and the flow cytometry standard for the percentages of CD4+ T cells in white blood cell populations. However, the off-chip bead labeling steps they used would need to be integrated into the chip itself for this technology to be practical in resource-poor applications – a task that is difficult to perform in the laminar flow regime found at the microscale.

Watkins, et al. developed an impedance-based microcytometer for determining CD4 T cell counts employing a resistive pulse technique [47]. Cells were initially focused in a three-dimensional flow sheath for one-by-one flow past a pair of coplanar electrodes and subsequent analysis of AC impedance indicated cell passage by a impedance pulse. A coplanar three-electrode configuration was implemented in a later device which incorporated entrance and exit counting as white blood cells were passed through an anti-CD4 antibody-functionalized capture chamber as illustrated in Figure 2.13 [53]. CD4+ T cells were depleted from the sample by immobilization in the capture chamber and the absolute CD4 count was provided by the difference between entrance and exit counts.

Catch-and-release. Chemical release of CD4+ T cells post capture has proven to be more difficult, as the cells may further bond to the substrate nonspecifically through membrane adhesion molecules. Zhu et al. have shown the capture and release of CD4+ T cells using electrochemical reactions on microfabricated electrodes; however some drawbacks are that some cell death occurs after T cell release (~10%) and agitation is needed to assist in electrochemical desorption, which is more difficult in the laminar flow regime found in a closed microfluidic chamber [191], [192]. In addition, mass production may be hindered by the fact that the capture region is limited to the area defined by the electrodes, requiring a PEG gel passivation layer elsewhere to prevent non-specific cell capture.

Gurkan et al. used a temperature responsive polymer to capture and release CD4+ T cells [193]. A capture chamber coated with poly(N-isopropylacrylamide) (PNIPAAm) was immobilized with CD4 antibody-Neutravidin complexes at 37 degrees C – when the polymer is hydrophobic and prefers

interactions with the Neutravidin. CD4+ T cells are captured at the same temperature before washing away unbound cells and lysing erythrocytes. The CD4+ T cells are released by decreasing the chip's temperature below 32 degrees C, when the PNIPAAm layer becomes hydrophilic, releasing the antibody-Neutravidin complexes and thereby releasing the CD4+ T cells. They were able to release 59% of captured CD4+ T cells with high viability (94%). This method needs to address a few challenges before being a practical PoC device. This includes ensuring surface chemistry is preserved from manufacture to test (i.e., storing the chips at ~37 deg C) and improving the release efficiency for accurate CD4+ T cell enumeration.

Instrument-free methods. Since 2005, the Bill and Melinda Gates Foundation has been funding a CD4 initiative (centered at Imperial College London) to create simple, power-free CD4+ T cell counting technologies that would lessen costs and increase penetration into resource-poor regions [194]. A semiquantitative immunochromatographic strip (ICS) being developed by The Burnet Institute compares the intensity of gold particles that are specifically attached to CD4+ T cells at a CD4 capture strip to a reference strip which has a similar intensity to a known concentration of CD4+ T cells [195]. Zyomyx has developed a device that uses the sedimentation of high density CD4 antibody-conjugated beads to estimate the concentration of CD4+ T cells from whole blood samples [195], [196]. These beads specifically attach to the CD4+ T cells and are sedimented with the help of a manually powered centrifuge. The height of sedimentation in the column is proportional to the concentration of CD4+ T cells, and is viewed through a window and compared to calibrated markings to give the CD4+ T cell count. The device also contains a chamber which used CD14-conjugated magnetic particles and a magnetic collar to deplete monocytes before the sedimentation step. These semi-quantitative instrument-free methods may be viewed as short-term solutions, but fully-quantitative micro- and nanotechnology solutions promise more precise and user-friendly approaches.

Conclusion

The United Nations reports that recent progress toward grand challenges in HIV/AIDS has primarily taken the form of record increases in accessibility of treatment worldwide [26], leading to decreased HIV

prevalence and mortality. The global state of AIDS, however, is far from the target highlighted by the United Nations of zero new HIV infections [197]. Until a vaccine or a cure can be developed, point-of-care testing will be a critical factor in controlling the epidemic and reversing the spread of HIV. Key studies have shown that viral load is a chief determinant of risk of transmission [198]. With viral load suppression a primary goal of ART, it follows that regular testing which enables effective management of HIV in people currently living with the disease must be an essential component of the global strategy.

The emergence of biomicro- and bionanotechnology in the past few decades has introduced new techniques for fluid handling and cell and biomolecule manipulation and identification, enabling highly-sensitive interrogation of small sample volumes and setting the foundation for innovation in point-of-care diagnostics. Most encouraging is the development of techniques capable of performing analysis from whole blood input without any requirement for manual preparation or pretreatment. Furthermore, technologies which couple automated sample processing with electrical biosensor techniques impart hope that a holistic solution to practical point-of-care needs is being realized.

The Millennium Development Goals have set a target to not only halt the spread of HIV/AIDS but to reverse its spread by 2015 [26]. If this milestone is to be realized, it will involve a concerted effort requiring the collaboration of world leaders, policymakers, community leaders, health care providers, and many others. But it is certain that these goals will not be reached if those at the forefront of combating the HIV/AIDS epidemic are not equipped with the proper tools for their mission. It is here that we look to these recent innovations in cell counting and virus quantification to rise to this grand challenge in global health.

TABLES

TABLE 2.1
2012 Global Mortality

Cause of death	Global burden
Lower respiratory infections	3,051,318
HIV/AIDS	1,533,760
Diarrhoeal diseases	1,497,674
Tuberculosis	934,838
Malaria	618,248
Meningitis	395,225
Acute hepatitis B	149,162
Measles	130,461
Syphilis	78,910
Encephalitis	77,870
Whooping cough	67,061
Tetanus	66,131
Leishmaniasis	48,405
Acute hepatitis C	38,913

TABLE 2.2
FDA-approved tests for plasma viral load quantification

Test name [95]–[97]	Manufacturer	FDA Approval [96], [98]	Type
Roche Amplicor HIV-1 Monitor Test	Rochem Molecular Systems, Inc.	3/2/1999	RT-PCR
NucliSens HIV-1 QT	bioMerieux, Inc.	11/19/2001	NASBA
VERSANT HIV-1 RNA 3.0 Assay (bDNA)	Bayer Corporation, Berkeley, CA	9/11/2002	bDNA
Abbott RealTime HIV-1 Amplification Kit	Abbott Molecular, Inc.	5/11/2007	RT-PCR
COBAS TaqMan HIV-1 Test	Roche Molecular Systems, Inc.	5/11/2007	RT-PCR

FIGURES

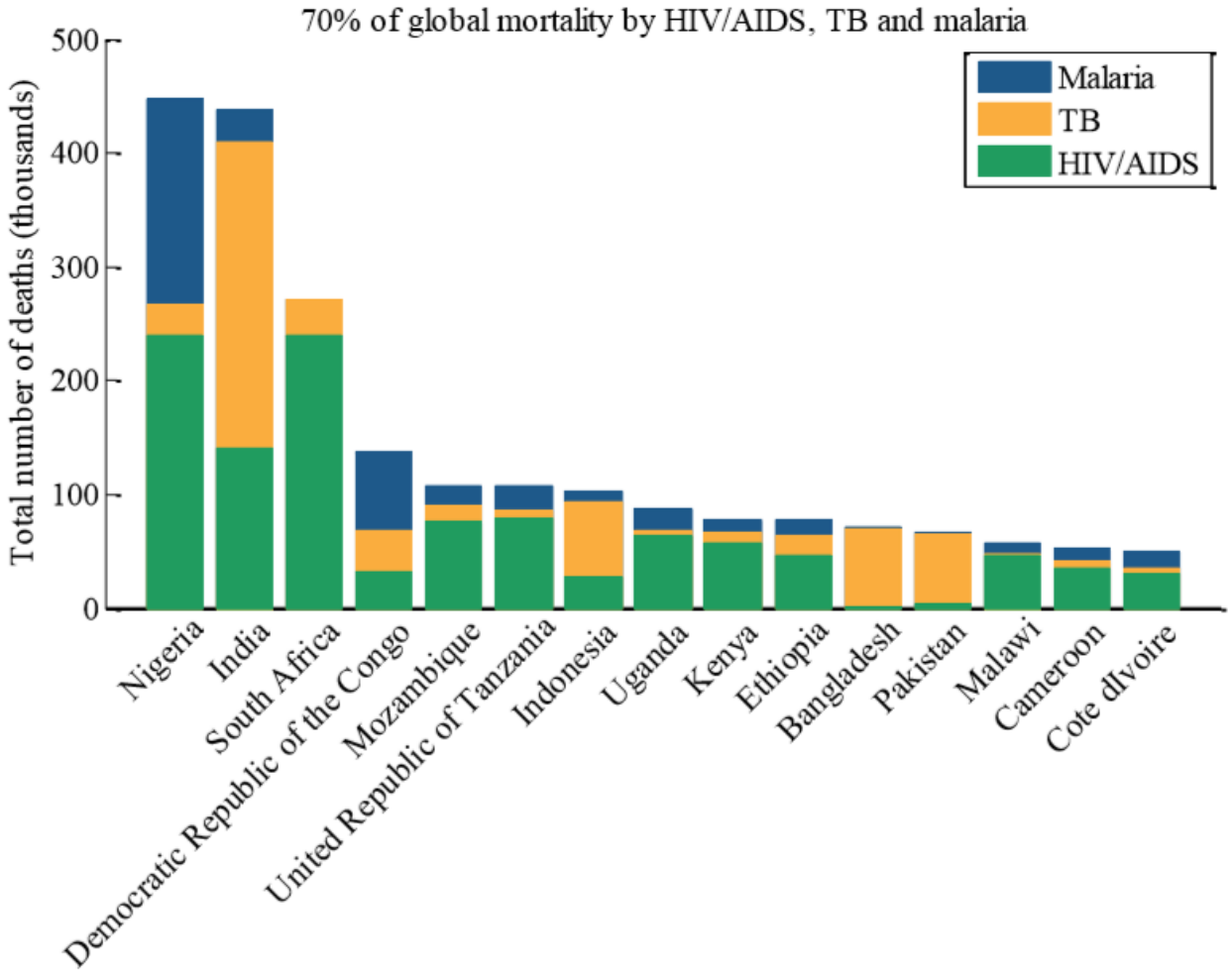

Figure 2.1. The impact and burden of major infectious diseases. Based on 2012 causes-of-death data available from the WHO, the bar chart depicts country-specific mortality data only for HIV, TB and malaria. These 15 countries bear more than 70% of the global mortality associated with these three pathogens. Source: [199].

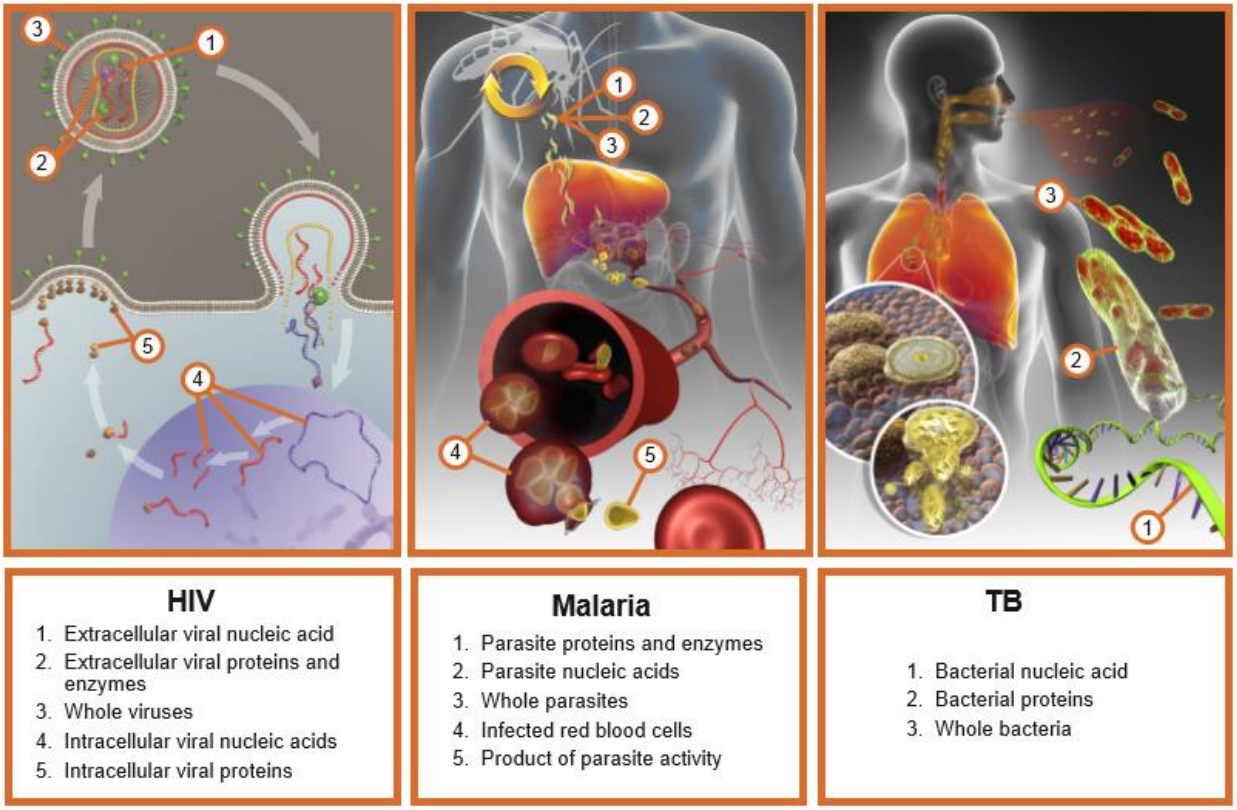

Figure 2.2. Methods of infection, replication, and production of HIV, malaria and TB. An understanding of the underlying mechanisms of pathogen replication and activity reveals specific biomarkers that may be leveraged for diagnostic purposes.

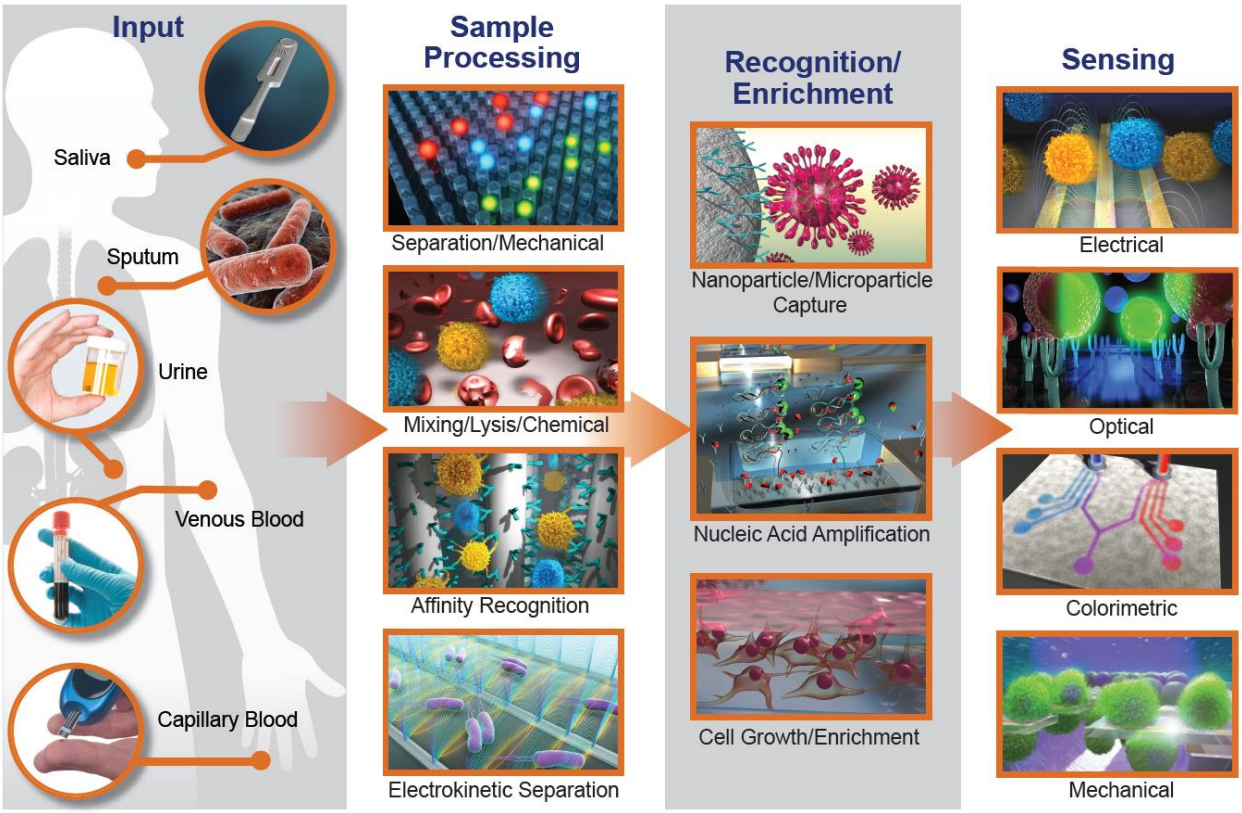

Figure 2.3. A broad overview of micro- and nanoscale technologies that can be applied to common body fluid samples to address the two challenges of point-of-care diagnostics: sample processing and sensing.

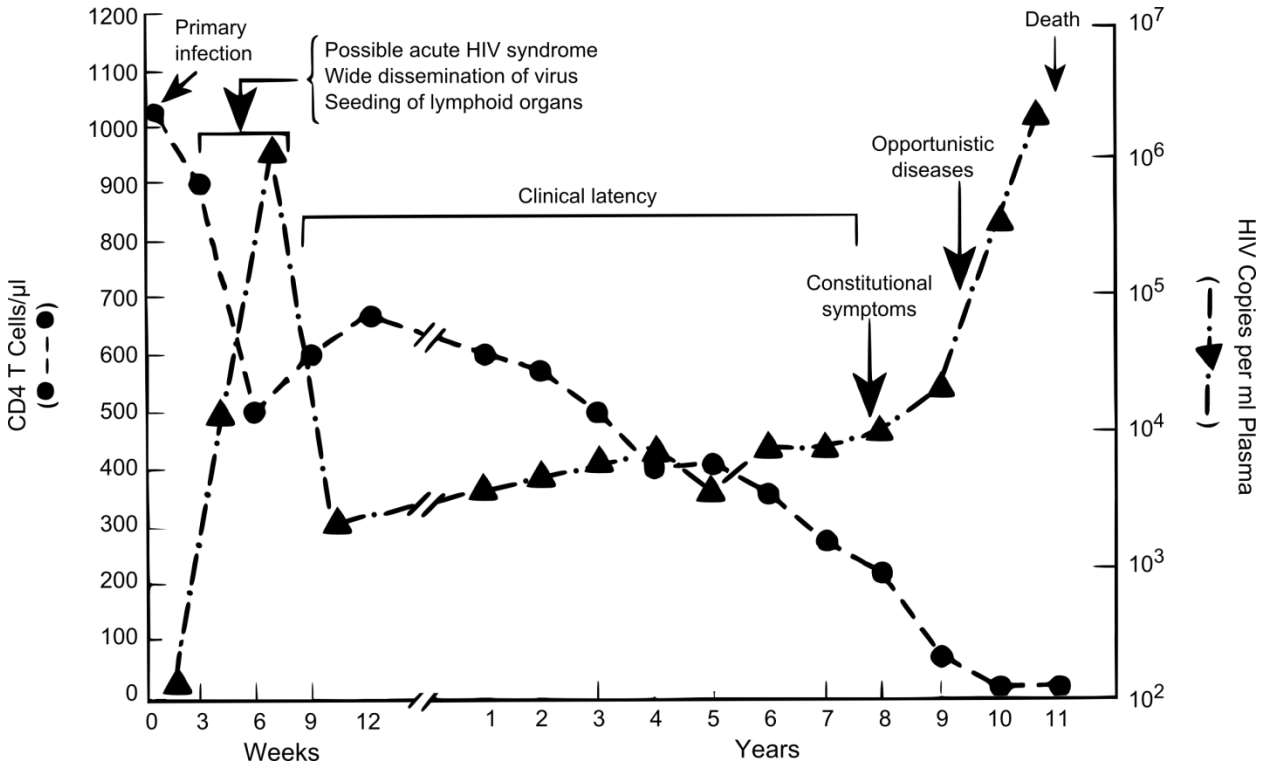

Figure 2.4. Typical course of infection. Typical CD4 counts and plasma viral load during the course of an HIV infection. Adapted from [82], [83].

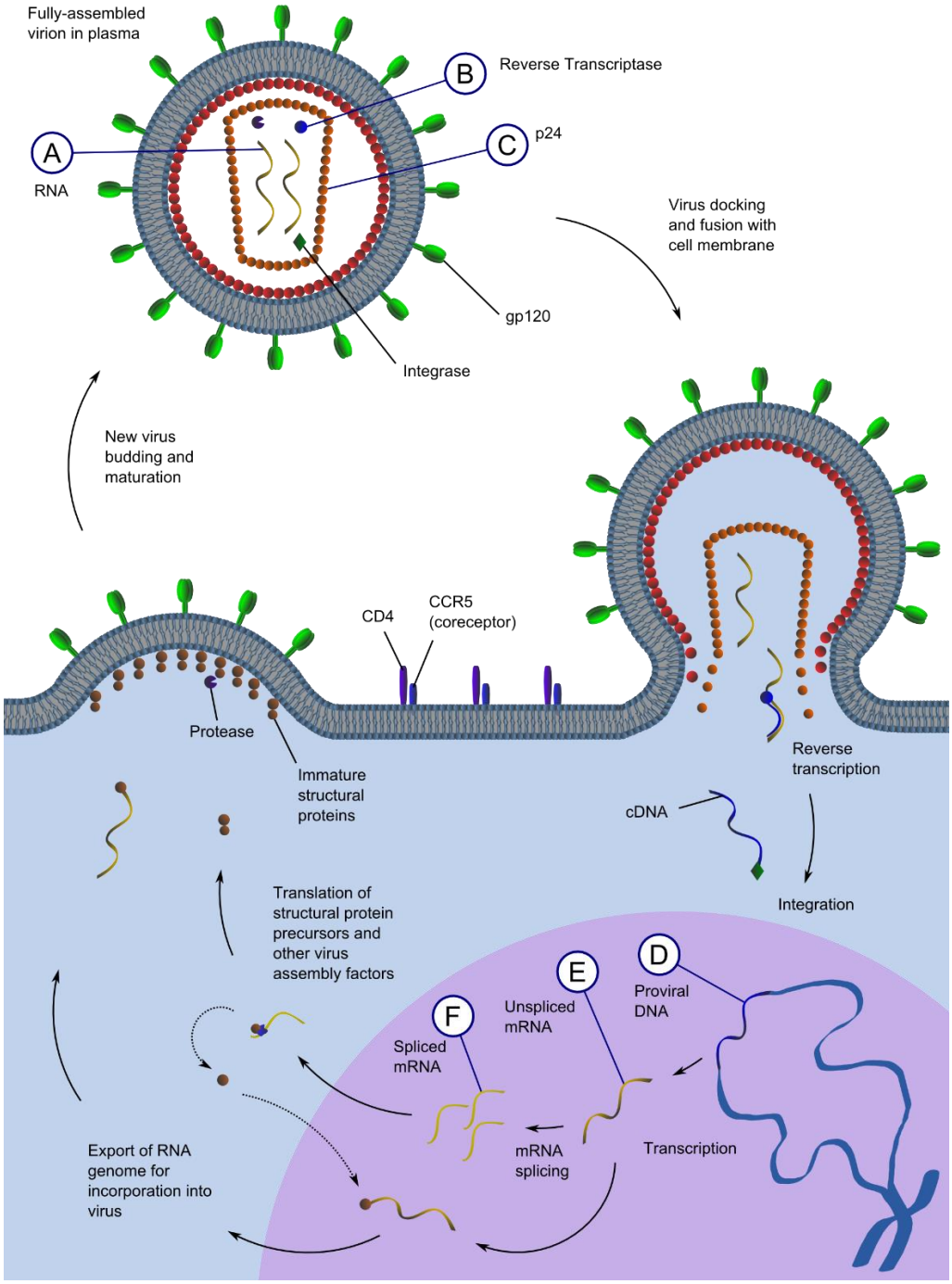

Figure 2.5. HIV lifecycle showing critical points for virus detection. Virions in plasma infect CD4+ T lymphocytes via the high-affinity interaction between the viral surface protein gp120 and the host cell CD4 receptor and CCR5 co-receptor. This docking facilitates fusion of the viral and cell membranes and injection the protein capsid into the cytoplasm which dissociates to release viral RNA. Highly error-prone reverse transcriptase makes a cDNA copy of the viral genome which is targeted to the host cell nucleus and integrated with the host genome by viral protein integrase. Host cell gene expression including mRNA alternative splicing ensues, resulting in expression of both viral structural protein precursors and those involved in the facilitation of viral gene expression. Genomic RNA and structural proteins are targeted to the cell surface where budding occurs. Maturation facilitated by protease action takes place after budding. Labels indicate biomarkers for viral diagnostics, including (A) Viral RNA in plasma (B) Reverse Transcriptase in plasma (C) Capsid protein p24 in plasma (D) Proviral DNA (E) Cell-associated unspliced RNA (F) Cell-associated spliced RNA

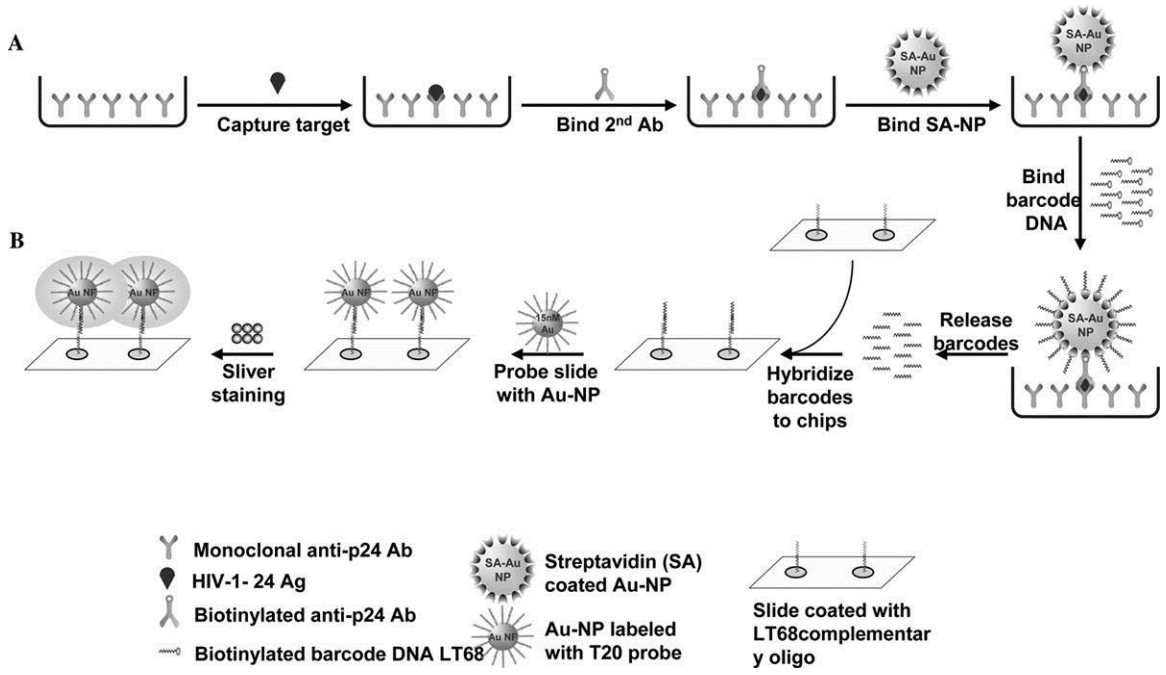

Figure 2.6. Biobarcode assay for the detection of HIV p24 antigen. Reprinted from Ref. [112] with permission from Lippincott Williams & Wilkins, Inc.

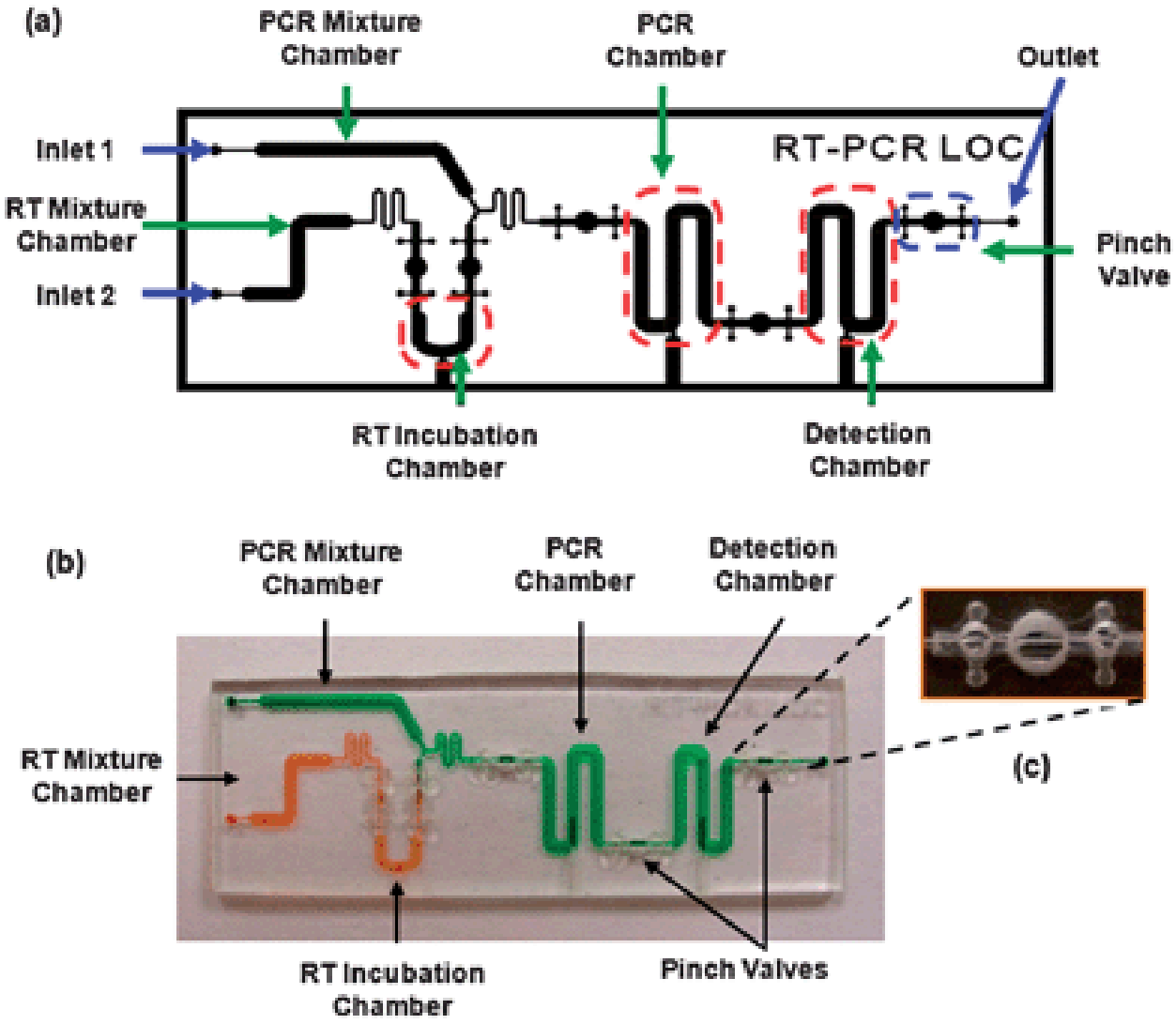

Figure 2.7. Polymer-based device for on-chip PCR. Reproduced from Ref. [129] with permission from The Royal Society of Chemistry.

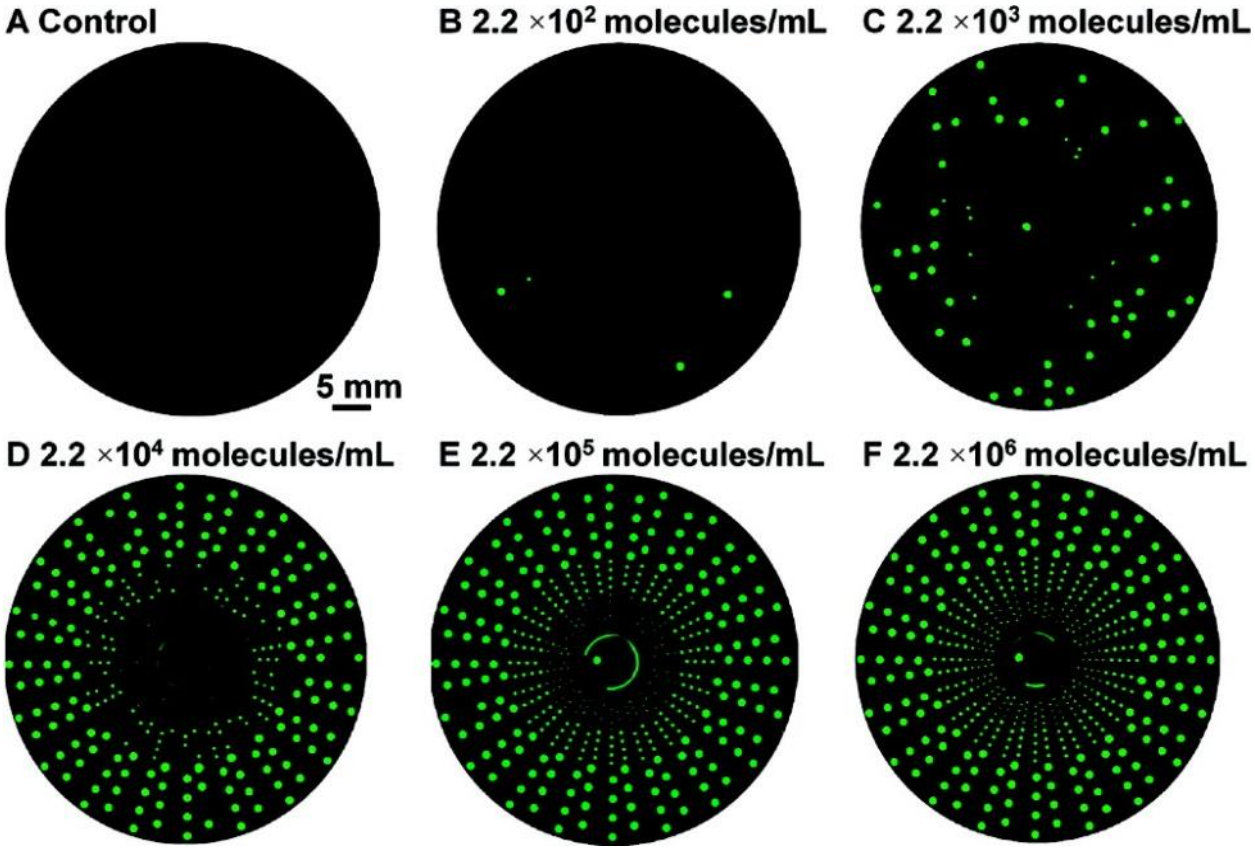

Figure 2.8. Digital RT-PCR results on a rotational SlipChip. Reprinted with permission from Ref.. [64] Copyright 2011 American Chemical Society.

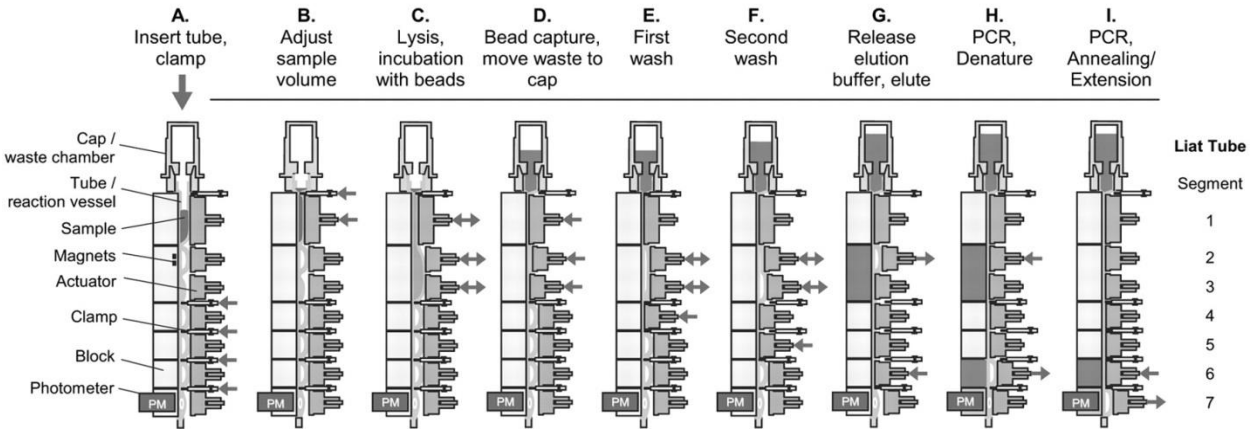

Figure 2.9. Overview of Liat analyzer. Reprinted from Ref. [131] with permission from Oxford University Press.

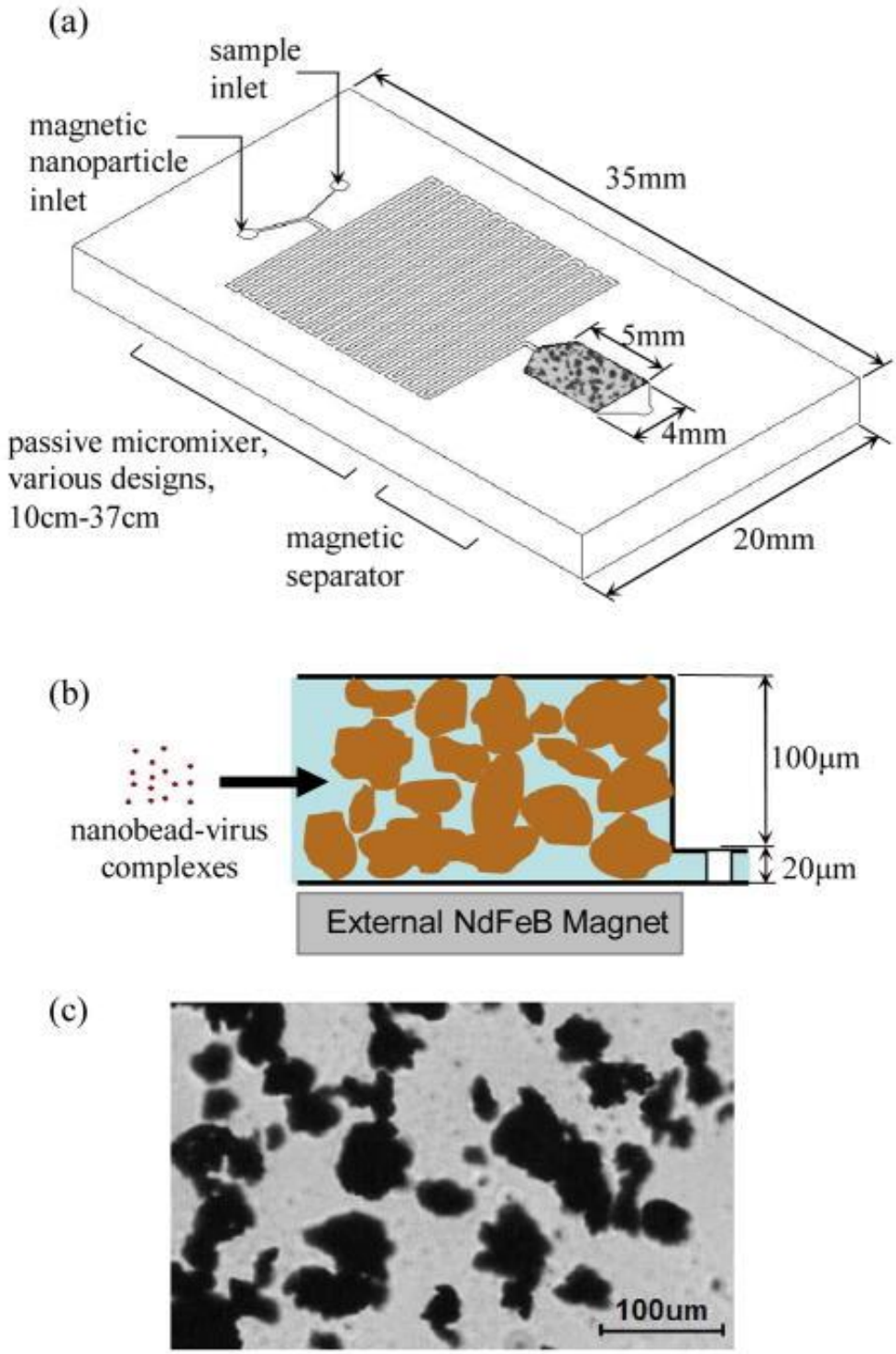

Figure2.10. Superparamagnetic nanoparticle capture device. Reprinted with permission from Ref. [55]. Copyright 2009 American Chemical Society.

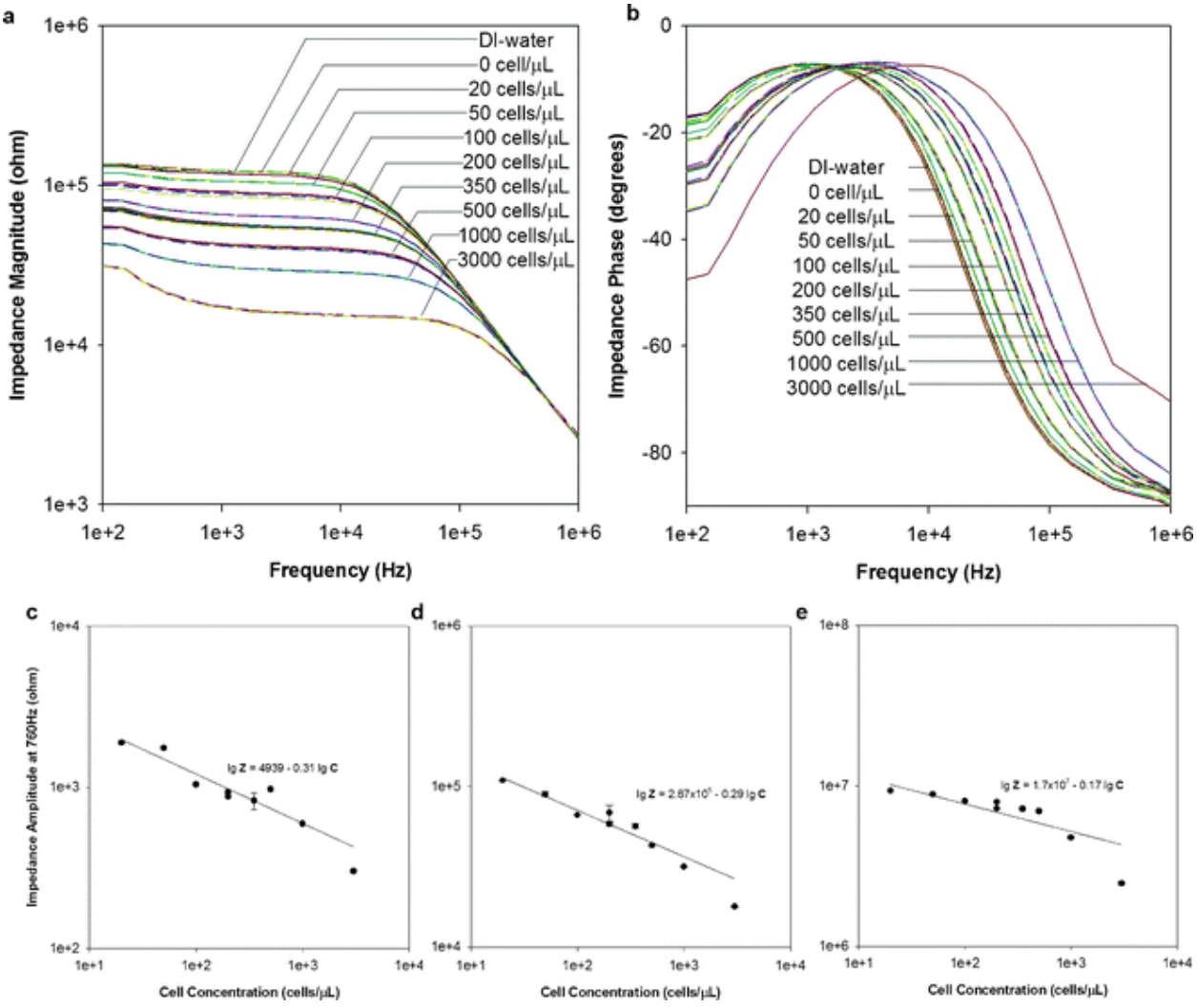

Figure 2.11. Cell lysate impedance spectroscopy for enumeration of CD4 T lymphocytes. Reprinted from Ref. [52] with permission from The Royal Society of Chemistry.

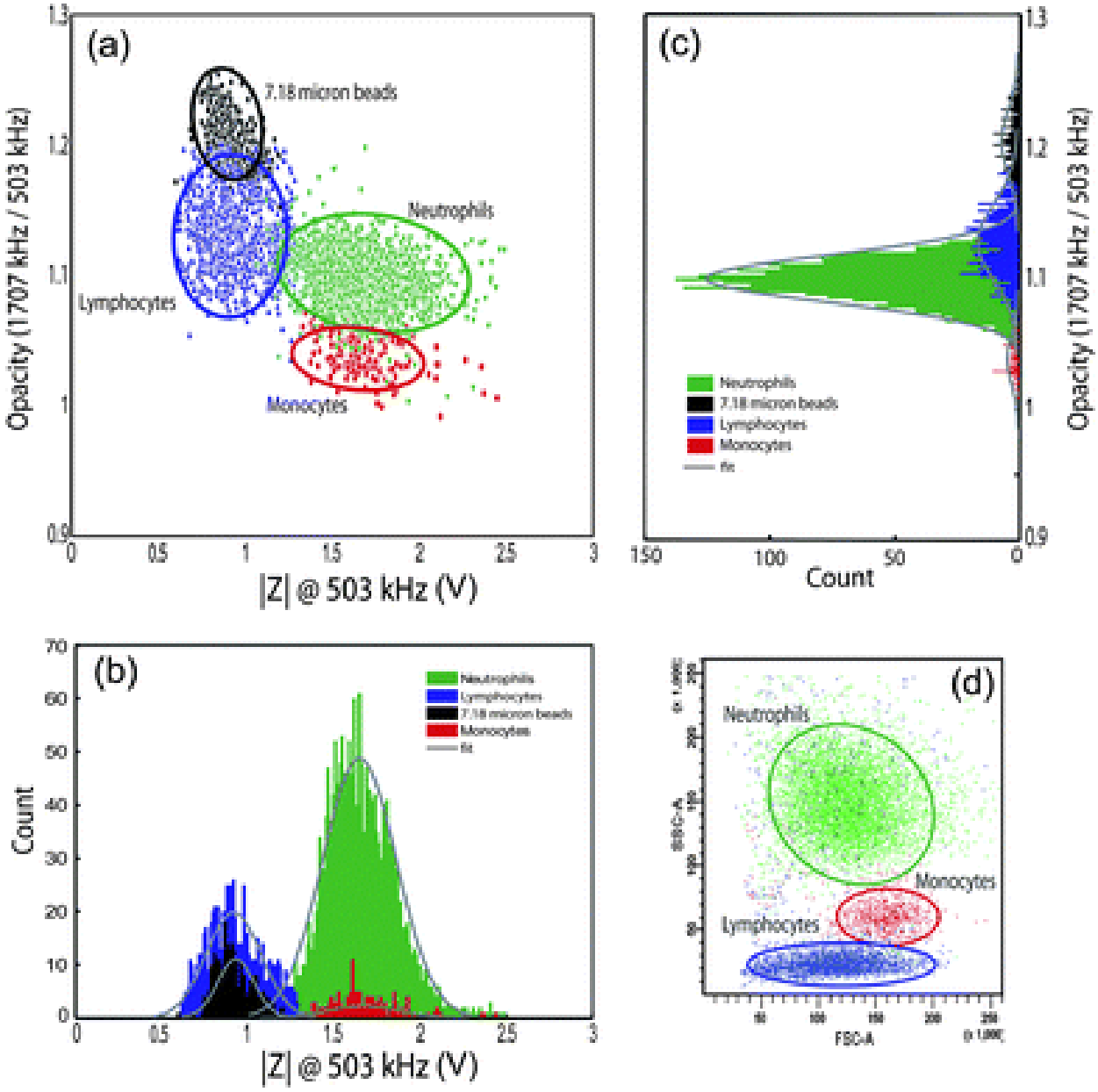

Figure 2.12. Leukocyte type differentiation by dual-frequency impedance characteristics. Reprinted from Ref. [73] with permission from The Royal Society of Chemistry.

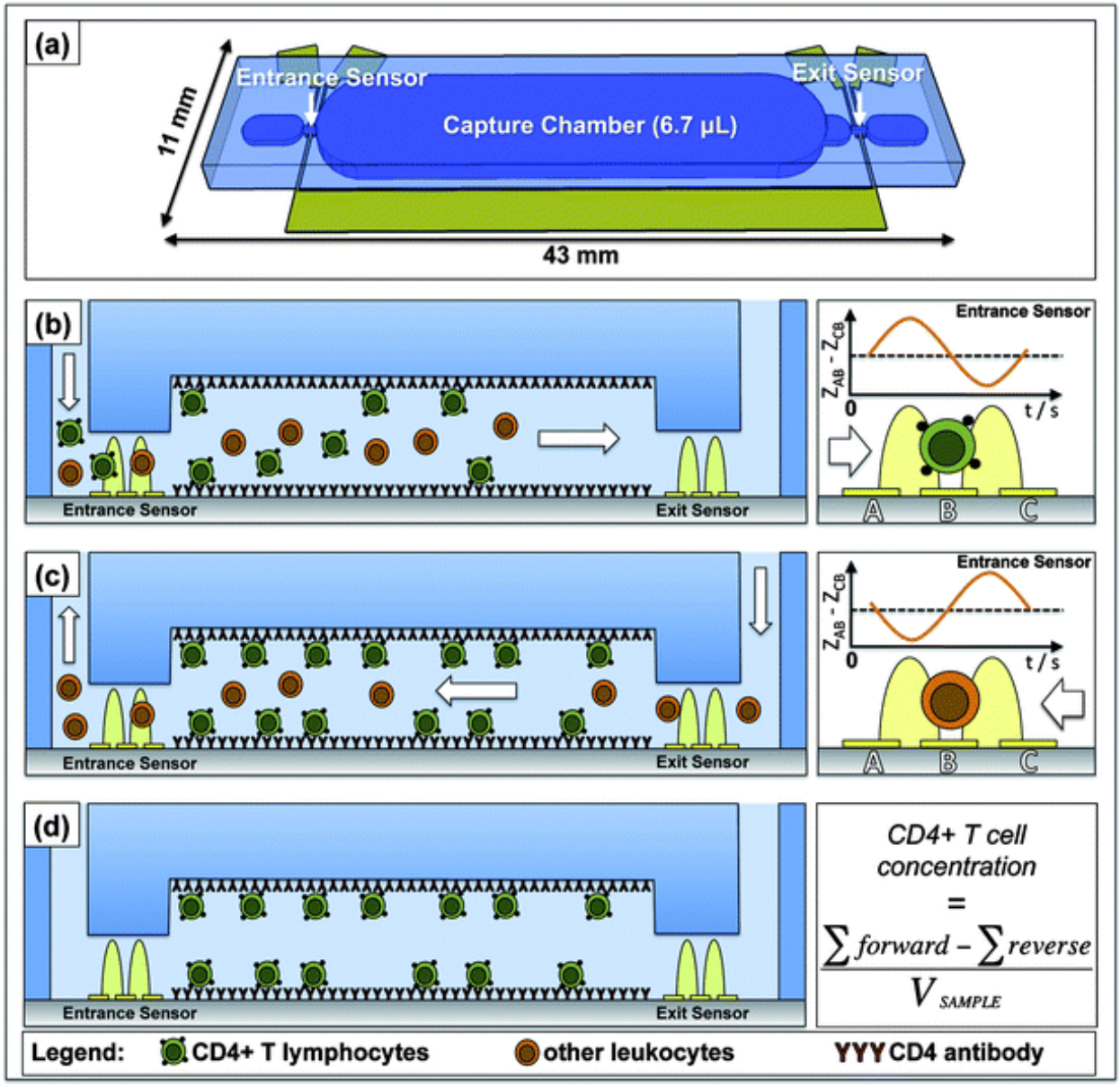

Figure 2.13. Differential counter technique for CD4+ T cell enumeration. Reprinted from Ref. [53] with permission from The Royal Society of Chemistry.

CHAPTER 3: LIPOSOME ION-RELEASE IMPEDANCE SPECTROSCOPY

INTRODUCTION

The point-of-care detection of biological entities will play an essential role in the changing face of health care delivery by making the detection of disease and monitoring of treatment more ubiquitous in developed nations and more accessible in developing nations. Sensing platforms for biomolecular entities such as cardiac enzymes, cancer biomarkers, toxins, bacteria and viruses can dramatically improve clinical outcomes by enabling earlier diagnosis and personalized monitoring. In particular, populations residing in remote and resource-limited settings stand to benefit significantly from low-cost portable technologies capable of detecting the mediators of major communicable diseases.

As an example, 34 million people worldwide are living with human immunodeficiency virus (HIV), the virus that causes acquired immune deficiency syndrome (AIDS), and many face barriers to accessing diagnostic testing necessary for effective treatment. A critical need exists for a low-cost HIV detection assay for the point-of-care which could provide (i) a qualitative assessment of plasma viremia, especially during the early weeks of infection prior to seroconversion, and (ii) a quantitative assessment of plasma viral load as a tool for informing treatment strategies in individuals with established HIV-positive status, especially during initial viremia when antibodies are undetectable but plasma viral load is in the range of 10^6 copies/ml [200].

Several micro- and nanotechnology solutions have been described in attempts toward point-of-care platforms for HIV/AIDS diagnostic applications [201]. These approaches have often included assays for the p24 viral capsid protein [56], [110]–[113] and viral enzyme reverse transcriptase activity [115]. Others have attempted isothermal amplification of viral nucleic acid on point-of-care platforms [127], [128] or miniaturized polymerase chain reaction (PCR) [64], [129], [131]. Few approaches have attempted detection of whole virus particles for a point-of-care measurement, although strategies for the separation of HIV from whole blood or plasma for diagnostic assays by microfluidic immunoaffinity chromatography [54], [132],

This chapter was previously published as G. L. Damhorst, C. E. Smith, E. M. Salm, M. M. Sobieraj, H. Ni, H. Kong and R. Bashir, Biomed. Microdevices, 2013, 15, 895–905. DOI: 10.1007/s10544-013-9778-4. Reprinted with permission from the copyright owner.

[133] and superparamagnetic nanoparticles [55] have been reported and may lend themselves well to a whole particle detection approach. Many of the approaches reported to date, however, are not fully portable and automated, rely on expensive detection instrumentation, or do not demonstrate the sensitivity necessary to rival state-of-the-art nucleic acid amplification assays, thus a ubiquitous platform for point-of-care HIV viral load detection is yet to emerge.

The concept of lysate impedance spectroscopy was introduced by Cheng, *et al.* for the detection of human CD4+ T lymphocytes [52]. Cells were captured in a microfluidic channel and lysed by the addition of low-conductivity hypotonic solution and impedance changes detected by surface electrodes were showed to be indicative of cell number down to just 20 cells μl^{-1}. Others have applied impedance spectroscopy more broadly for the detection of bacterial growth [202], [203], binding of an analyte to a recognition site on electrodes [204], and, recently, the qualitative detection of HIV from viral lysis at high concentrations [205].

The concept of releasing liposome contents as a biosensor component has been reported in the past; however, the materials encapsulated by the liposomes in these cases were either fluorescent molecules or redox couples [206]–[212]. Our ion-encapsulating liposomes represent a simpler approach which would better accommodate the requirements for portable sensing platforms.

Here we report an ELISA-inspired approach to biological detection consisting entirely of on-chip electrical impedance sensing and apply to HIV detection. At the core of this detection strategy is a micron-sized, antibody-functionalized liposome particle encapsulating concentrated phosphate buffered saline (PBS). These liposome tags can be quantified by impedance spectroscopy upon ion release in low conductivity media and are also shown to specifically bind surface-immobilized virus particles captured in a microfluidic channel. Here we characterize dipalmitoylphosphatidylcholine (DPPC) liposome particles, show quantification by this electrical sensing method, and demonstrate an ELISA-like approach to virus capture, liposome tagging and sensing.

MODELLING OF IMPEDANCE SPECTROSCOPY

Conductivity changes from liposome ion release

The change in impedance sensed by our system is the result of ion release into the surrounding media from the permeabilization of liposomes. The average diameter of liposomes used in this report (see Figure 3.1) was determined to be 3.7 μm, which corresponds to an average volume of 26.5 fL per liposome. Each liposome encapsulated 10X PBS containing 1.37 M NaCl and 0.027 M KCl. Each liposome therefore contributes approximately 3.6×10^{-14} moles of NaCl to the surrounding media upon complete release of its contents. Assuming that the beginning solution is true deionized water (conductivity of 0.055 $M\Omega^{-1}$ cm^{-1}) [213], 33,000 liposomes (~5,000 liposomes per μl) would produce a 0.18 mM change in NaCl in the 6.628 μl volume fluidic channel. Assuming the effects on conductivity of NaCl in 10X PBS dominates over the effects of KCl, this change in ion concentration can be calculated to produce a change per liposome per microliter of approximately 4.27 $G\Omega^{-1}$ cm^{-1} [213], [214]. It has been shown previously that change in capacitance from ion release into solution is several orders of magnitude lower than the change in bulk conductance, thus the effect on conductance dominates [52].

Modelling impedance spectra

Electrodes in solution can be modelled by the equivalent circuit in Figure 3.4d. In this simplified model, C_{di} is the dielectric capacitance resulting from all materials surrounding the electrodes, R_{sol} is the solution resistance, R_{ser} is the series resistance of the electrodes and wires, and Z_{para} is the parasitic impedance, which is measured from the open circuit [52], [202], [203]. $Z_{dl,}$ the interfacial or Warburg resistance, is described by

$$Z_{dl} = [(j\omega)^n B]^{-1} \quad (1)$$

Where $j = \sqrt{(-1)}$, and the parameters n and B depend on the properties of the electrolytes and electrodes [52], [202], [203]. This model will be used to fit the impedance spectra of liposome ion release in the interdigitated electrode device described here.

MATERIALS AND METHODS

Reagents

1,2-dipalmitoyl-*sn*-glycero-3-phosphocholine (DPPC) and 1-palmitoyl-2-{12-[(7-nitro-2-1,3-benzoxadiazol-4-yl)amino]dodecanoyl}-*sn*-glycero-3-phosphocholine (NBD PC) were purchased from Avanti Polar Lipids (Alabaster, AL, USA). Protein A was purchased from ProSpec (East Brunswick, NJ, USA). Phosphate buffered saline (10X solution) was purchased from Fisher Scientific (Hampton, NH, USA) and Lonza (Basel, Switzerland). Sucrose, dextrose and Triton X-100, deoxycholic acid, sodium azide palmitic acid N-hydroxysuccinimide (pal-NHS), and rhodamine B isothiocyanate were purchased from Sigma-Aldrich (St. Louis, MO, USA). Calcein was purchased from Fisher Scientific (Hampton, NH, USA). Anit-gp120 goat IgG was purchased from Abcam (Cambridge, MA, USA). Virus buffer consisted of Tris, NaCl, and EDTA purchased from Sigma-Aldrich (St. Louis, MO, USA). HIV-1 strain IIIB was purchased from Advanced Biotechnologies Inc. (Columbia, MD, USA).

Preparation of liposomes

DPPC was dissolved in chloroform and dried in a round bottom flask by rotary evaporation. The lipid film was hydrated with 10X PBS at 50 degrees C to create liposomes at a lipid concentration of 1 mg/ml. This mixture was then sonicated for 15 minutes in an ice bath.

To create fluorescent NBD-liposomes, NBD-PC lipids were dissolved with DPPC at 1 mol%. Liposomes were then formed by the same hydration and sonication processes described above.

Devices

Planar interdigitated electrode chips were fabricated on glass with standard photolithography and gold lift-off technique. A polydimethylsiloxane (PDMS) cover 4 mm x 34 mm x 50 μm (6.628 μl total volume)

was cured on a master mold of SU-8 photoresist patterned on a 4" silicon wafer using standard photolithography technique. Inlet and outlet ports were punched in each PDMS cover, which were then aligned with the electrodes and bonded after oxygen plasma activation in a barrel etcher. A schematic and photograph of the device are provided in Figure 3.1.

Liposome stability characterization

NBD-liposomes were prepared in 10X PBS as described above. Initially, four samples were each added to deionized (DI) water, centrifuged at 3220 rcf for 10 minutes to pellet the liposomes, and the supernatant was aspirated. The pellet was then re-suspended in DI water and the process was repeated to achieve thorough washing. After the second aspiration of supernatant, each pellet was re-suspended in 10X PBS, 1X PBS, sugar solution, or DI water. Each sample was well-mixed by pipetting up and down to ensure even re-suspension of the pellet and placed on a sample rotisserie to prevent settling. Liposome number was assessed regularly for each sample by a Guava EasyCyt Plus flow cytometer (EMD Millipore, Billerica, MA, USA) over the course of several hours.

To consider the effects of detergent on liposome stability, NBD-liposomes were washed as described above and re-suspended in DI water or DI water containing 1% v/v Triton X-100. Samples were placed on a sample rotisserie and analysed by flow cytometry over the course of several hours.

To consider the effects of heating on similar samples, NBD-liposomes were washed and re-suspended in DI water or 1% v/v Triton X. Each sample was aliquoted into several vials which were independently heated to temperatures ranging from 30 degrees C to 99 degrees C. After heating and cooling to room temperature, liposomes were analysed in a flow cytometer to determine liposome number.

Liposome permeability characterization

Liposomes were prepared in 10X PBS containing 50 mM calcein and washed twice by adding an equal volume of DI water, centrifugation and aspiration of supernatant. After the second wash, liposomes were re-suspended in 10X PBS, 1X PBS, sugar solution, or DI water and added as eight replicates of each sample

in 0.2 ml PCR reaction tubes. This reaction strip was placed in a Mastercycler ep realplex real time PCR system (Eppendorf, Hauppauge, NY, USA) for temperature analysis. The sample temperature was increased from 25 degrees C to 95 degrees C over 30 minutes and at 520 nm emission was monitored throughout. Control samples containing 10X PBS without calcein were also analysed in the same assay.

Heat-induced liposome permeabilization for impedance spectroscopy

NBD-liposomes were washed and re-suspended in DI water in four different concentrations. Serial dilutions of each of these liposome suspensions were performed in DI water to achieve the desired range of liposome number. A dilution within the range of the flow cytometer was analysed to determine liposome concentration for each of the four sample sets. Samples were heated to 50 degrees C for 15 minutes and allowed to cool to room temperature. Each sample was then injected into the interdigitated electrode chip for impedance spectroscopy analysis.

Impedance spectroscopy measurements

Impedance magnitude and phase angle were determined using an Agilent 4284 LCR meter (Agilent Technologies Inc., Palo Alto, CA, USA). Micromanipulator probes were used to connect the microfabricated device to the LCR meter and the measurement process was automated by MATLAB (MathWorks, Natick, MA, USA). Impedance spectra were measured for frequencies between 100 Hz and 1 MHz with an increase factor of 1.5 and amplitude of 250 mV.

Real-time impedance monitoring of ion release from liposomes

NBD-liposomes were prepared and washed as described previously. However, to ensure complete elimination of ionic contamination from liposome samples, each wash was performed in a 50 ml centrifuge tube and repeated twice for a total of three washes. Liposomes were then suspended at various solutions and a portion of the sample was immediately analysed by flow cytometry to determine liposome number. Within one minute of re-suspension in DI water, the liposome sample was injected into the interdigitated

electrode device. The device was set on a heating stage and held at 23 degrees C for 30 seconds before being heated to 50 degrees C and held for several minutes. Impedance was monitored throughout at 2 kHz and 10 kHz.

Preparation of antibody-functionalized liposomes

Protein A was hydrophobically modified with hexadecyl chains for anchoring on the liposome surface. Briefly, 1mg of protein A was reacted with 0.1 mg of pal-NHS in a solution of 0.3% deoxycholic acid and 0.1% sodium azide in 1X PBS according to the procedure described by Kim and Peacock [215]. After reacting for 24 hours at room temperature, palmitated protein A was purified by centrifuge filter (MWCO 3kDa, Millipore).

Protein A was adsorbed to liposomes by mixing 5 μg of palmitate-modified protein A for every 1 mg of lipid. The mixture was incubated for 12 hours at room temperature, followed by addition of DI water to pellet the liposomes upon centrifugation for 10 minutes at 3220 rcf to remove protein A that was not adsorbed.

To verify adsorption of protein A, the protein was fluorescently labeled with the amine-reactive rhodamine B isothiocyanate, followed by purification by centrifugal filtration and dialysis to remove unreacted rhodamine. This fluorescent palmitated protein A was incubated with liposomes, which were then purified by centrifugation as described. Fluorescent intensity of the supernatant and re-suspended liposomes was recorded with a Tecan Infinite 200 PRO (Tecan AG, Switzerland), indicating that 40% of the protein A initially added remained adsorbed to the liposomes.

Liposomes with protein A were then mixed with 18 μg/ml anti-gp120 IgG for four hours on a sample rotisserie.

Virus detection by heat-induced liposome permeabilization

Interdigitated electrode devices were infused with 25 μl of 0.3 mg/ml anti-gp120 IgG in PBS and incubated at 4 degrees C overnight. Excess antibody was rinsed from the fluidic chamber with 100 μl PBS

flowing at 10 µl min^{-1}. Following this rinse, 50 µl buffer containing 6.7e11 virus particles per µl or buffer without viruses was infused into each device at 5 µl min^{-1} and incubated for approximately four hours. Following incubation, each device was rinsed with 100 µl PBS at 10 µl min^{-1} to remove the buffer and unbound viruses. Subsequently, 100 µl of 6,537±70 μl^{-1} liposomes functionalized with anti-gp120 IgG were injected at a rate of 10 µl min^{-1} followed immediately by rinsing with 200 µl DI water at 20 µl min^{-1} to rinse away unbound liposomes and lower the conductivity of the bulk solution. Each device was then placed on a heating stage and real-time impedance was measured during heating as described above.

RESULTS

Liposome stability characterization

To determine the stability of liposomes in various media, flow cytometry measurements were recorded over several hours with NBD-liposomes. Three replicates each of liposomes suspended in isotonic (10X PBS) and hypotonic (1X PBS, sugar solution, DI water) media were measured to assess the effects of various osmotic forces. Sugar solution was chosen because it has been used in the past as an approach to maintaining lymphocyte stability when a low-conductivity medium is desired for impedance measurements of cell lysate [52]. The 8.5% sucrose/0.3% dextrose solution used in these measurements would have approximately the same osmolarity as cytosol or 1X PBS. A sugar solution which matches the osmolarity of 10X PBS is not practical (too viscous) and therefore was not investigated.

Flow cytometry analysis of liposomes in the four media considered showed little to no decrease in both PBS samples and some depletion in both sugar and DI water over approximately fourteen hours. To analyse the counting data for each sample, each replicate was fitted separately and the three fits were averaged. This averaged fit is presented in Figure 3.2a. The slope of the fits showed depletion rates of approximately 0.0905% min^{-1}, 0.0569% min^{-1}, 0.0089% min^{-1}, and 0.0125% min^{-1} for DI water, sugar solution, 1X PBS and 10X PBS respectively (Figure 3.2a, inset).

In order to compare the stability of liposomes in DI water with a common liposome permeabilization/lysis reagent, Triton X-100, a separate flow-cytometry measurement was performed with liposomes in DI water and 1% Triton X. In this case, liposomes with and without membrane-integrated protein A were also compared to determine if liposome functionalization would compromise stability. The results, presented in Figure 3.2b, show that liposomes are compromised in the presence of detergent, showing rapid depletion in the first hour and nearly 100% depletion of liposomes after five hours. The presence of adsorbed protein A showed little effect.

Upon initial consideration of heating as a chemical-free permeabilization technique for liposome impedance sensing, liposomes in DI water and 1% Triton X were also analysed by flow cytometry after heating to various temperatures. Counting data in Figure 3.2c shows that the destabilizing effects on the liposomes of detergent were accelerated by the addition of heat to the solution. A proposed mechanism explaining the behaviour of liposomes upon heating and in the presence of detergent is provided in the Discussion section of this paper.

Effects of heat on liposome stability

A DNA melting curve assay proved to be the ideal measurement for characterizing the effects of heating on liposome stability and to determine the critical temperature, which we define as the temperature at which the lipid bilayer is partially compromised and encapsulated contents are released into the surrounding media. An ideal reporter molecule for this measurement was calcein, a fluorescent dye which self-quenches at millimolar concentrations [216], [217].

Liposomes were prepared in concentrated calcein and removed from free calcein in surrounding media by centrifugation and re-suspension of the liposome pellet. Calcein encapsulated within liposomes exhibited very little emission at 520 nm. Upon heating in the thermocycler, however, a sharp increase in fluorescence is observed in the range of 40-43 degrees C, indicating the release of liposome contents as calcein dissociates and self-quenching subsides. A plot of raw fluorescence is presented in Figure 3.3a, with the

first derivative with respect to temperature, dI/dT, presented in Figure 3.3b as reported by the instrument's data analysis software.

Liposome quantification by ion-release impedance spectroscopy

The quantification of liposomes by impedance spectroscopy was demonstrated by suspension of liposomes at various concentrations in DI water and off-chip heating to promote release of encapsulated ions. After cooling to room temperature, each sample was injected into the fluidic chamber and impedance spectra were measured. The measured impedance depends on the concentration of ions in the fluid. We assume the average liposome size is consistent between measurements and that all liposomes encapsulate 10X PBS, which allows for impedance to be directly related to liposome number. Figs. 4a-b show the impedance magnitude and phase angle versus AC frequency for each sample. In Figure 3.4c, the impedance recorded at 2.6 kHz is plotted versus liposome concentration as measured by a flow cytometer. A lower limit of detection was determined to be at a liposome concentration of approximately 10^3 μl^{-1} and impedance values measured at concentrations above this were fitted with a straight line on log-log axes.

Impedance modelling

The simplified circuit model in Figure 3.4d was used to fit measurements displayed in Figs. 4a-b. The parasitic impedance Z_{para} was determined by fitting the impedance data measured with the device prior to adding any fluid and was then held constant for the other fits. Examples of fits with the measured data are provided in Figs. 4e-f. The bulk conductance $G_{sol} = 1/R_{sol}$ can be determined from the parameters extracted for each measurement and are plotted in Figure 3.4g versus liposome concentration [52]. The slope of the fit to conductivity data gives the sensitivity of the interdigitated electrode chip, determined in this case to be 16.022 $G\Omega^{-1}$ (liposomes per $\mu l)^{-1}$ [52].

Real-time impedance monitoring and quantification

Ion release from liposomes was monitored in real time and the resulting impedance trace could be used to determine liposome concentration as described above. 10X PBS-containing liposomes in DI water were injected into the interdigitated electrode device which was placed on a small heating stage. The temperature was held constant near room temperature for 30 seconds and quickly increased to 50 degrees C where it was held constant until the measurement completed. Because conductivity increases with temperature, the impedance trace shows an initial steady decrease as a result of heating of the device; however, a second, sharper decrease is observed as the device reaches critical temperature and the encapsulated ions are released. Sample traces of this behaviour are presented as the normalized impedance over time in Figure 3.5a and the time derivative of normalized impedance in Figure 3.5c. Figs. 5b and 5d show two methods for quantifying liposomes from this data: by fitting the normalized impedance after 200 seconds (Figure 3.5b) and by determining the maximum rate of change (Figure 3.5d). Once again, the signals produced by samples below concentrations of 10^3 ml^{-1} appear commensurate with measurements of DI water and are not included in fitting of the data.

Virus detection

As a proof-of-concept toward liposome ion-release impedance spectroscopy for virus detection, several devices were functionalized with anti-gp120 antibody and exposed to 6.7e11 μl^{-1} HIV to be compared with controls. After prolonged exposure to the virus, the devices were rinsed and 100 µl of IgG-functionalized liposomes (6,537±70 μl^{-1}) in PBS were injected through the device, followed immediately by rinsing with 200 µl DI water. A schematic of this ELISA-like assay is depicted in Figure 3.6a. The same heating and real-time impedance monitoring protocols as described above were followed for analysis of these devices, and the normalized impedance after 200 seconds for devices prepared with immobilized viruses is compared with a control treated with virus-free buffer. Figure 3.6b shows the normalized impedance data and Figure 3.6c summarizes data from four separate devices for each case, showing a significantly larger change in impedance after 200 seconds for virus-containing devices, representing specific capture of liposomes on immobilized HIV.

DISCUSSION

This paper describes progress toward an ELISA-like liposome-based impedance sensing device for biological sensing at the point-of-care. We begin with the characterization of liposome particles containing 10X PBS which are the basis for electrical sensing, providing a simple and low-cost solution to detection of submicron particles. Liposome stability over time is compared in four different media, demonstrating that although liposome depletion rate is greatest in DI water as the result of osmotic forces, the loss of particles is still minimal over a short time span. In our assay, the exposure of liposomes to pure DI water is anticipated to be 10 minutes or less, thus this minimal depletion rate is inconsequential. This is a marked difference from the effects of DI water on human T lymphocytes where it was used by Cheng, *et al*. to promote rapid lysis of human cells [52].

Liposome stability in DI water was also compared to stability in the presence of the detergent Triton X, a reagent which is used ubiquitously to restructure lipid membranes. We believe that the detergent disrupts the liposomes by inserting itself into the lipid bilayers, thus increasing permeability. At a constant temperature, rupture of the entire liposome population appears to occur over several hours and appears to be accelerated by heating the sample.

While heating characterization described in Figure 3.3 demonstrates that liposomes release encapsulated materials above a temperature of approximately 41 degrees, consistent with the lipid phase transition temperature of DPPC, the counting of liposomes in DI water as shown in Figure 3.2c indicates that even upon heating the sample near boiling point (99 degrees C), the liposome population is not significantly decreased upon cooling and counting in the flow cytometer. This phenomenon can likely be explained by the self-repair properties of the lipids. Above the transition temperature, the kinetic energy of these molecules is enough to overcome the hydrophobic interactions which stabilize the bilayer structure, thus explaining the release of encapsulated ions. Flow cytometry analysis, however, is performed after the sample has been cooled again. The data in Figure 3.2c is explained by the presence or absence of detergent – without Triton X, DPPC lipids are free to re-stabilize their ordered bilayer structures, while reformation

of liposomes is inhibited by Triton X, which favours the formation of micelles and may sequester or destabilize DPPC lipids.

In the quantification of human T lymphocytes by lysate impedance spectroscopy [52], the introduction of DI water is used to trigger lysis of cells and release of contents for interrogation. In this measurement, liposomes are more stable in DI water, likely as a result of the absence of membrane proteins, particularly aquaporins, which would allow for the diffusion of water molecules into the cell driven by the osmostic gradient.

DI water is therefore not a suitable technique for triggering liposome permeabilization. Furthermore, chemical-based permeabilization is not preferred for this platform because the introduction of a reagent by flow necessarily results in the displacement of an equal volume of fluid from the microfluidic chamber and thus may result in the loss of lipids or ions and complication of the impedance measurement. Heating is therefore an ideal technique for stimulating the release of encapsulated ions from liposomes in the fluidic chamber as it allows for interrogation of the chamber without displacing its contents.

Liposomes were initially prepared containing 1X PBS, however, 10X PBS was later employed as a means of amplifying the signal produced by liposome permeabilization and is used in all the data presented here. The lower limit of detection determined by the data in Figure 3.4 shows the same signal as the deionized water we obtained for our experiments. It is evident that the DI water that was available to us did contain some small amount of ionic contamination and we anticipate that a higher sensitivity would be possible if DI water containing fewer ions were available. We believe that this was the case for the similar measurements performed with human T lymphocytes in [52] where a lower limit of detection is demonstrated.

We have demonstrated that the sensing device used in these measurements can be modelled with a simple circuit consisting of a capacitor, C_{di}, in parallel with parasitic impedance Z_{para} and the series combination of solution resistance R_{sol} and interfacial impedance Z_{dl}. From this model, the value R_{sol} is used to determine the bulk solution conductance, G_{sol}, which is related to the solution conductivity σ by the equation:

$$G = \sigma mA/L \quad (2)$$

Where A is the solution cross-sectional areas between electrodes, L is the spacing between electrodes, and m is the number of electrodes [52]. For our device, the value of mA/L is 133.7 cm and this value can be used to determine a measured conductivity change of 0.12 $G\Omega^{-1}$ cm^{-1} (liposomes per μl)$^{-1}$. This differs by one order of magnitude from our predicted conductivity change of 4.27 $G\Omega^{-1}$ cm^{-1} (liposomes per μl)$^{-1}$, but can be attributed to the behaviour of ions in bulk as described by Chen, *et al.* [52].

During real-time monitoring of liposome permeabilization, two methods for quantification are demonstrated (Figure 3.5): normalized impedance after 200 seconds and max –dZ/dt. It is still to be determined which method is a more consistent and sensitive method for detection. An improved technique which minimizes the fluctuation of device temperature during heating and heats the device more slowly may result in a lower baseline in the time derivative and thus allow for a lower limit of detection. This technique is to be optimized in future studies.

Additionally, the liposomes described in this report exhibited significant variation in diameter. We anticipate that the decrease in impedance magnitude and –dZ/dt would correlate better if liposome size was uniform. Several microfluidic techniques which produce highly uniform liposome particles have been described [218], [219]. These formation methods can be pursued in future work for a more accurate liposome-based measurement.

The accuracy and sensitivity of this device may also be improved by employing larger liposomes. We found that the lower limit of detection was approximately 1,000 liposomes/μl in our current measurements (average liposome diameter = 3.7 μm). Because the impedance change detected depends on the total volume of 10X PBS released from all liposomes on the device, larger liposomes would enable the sensing of fewer total particles. Furthermore, because the volume of a sphere scales with the radius cubed, a liposome with twice the radius of those used in our measurements would have eight times the volume. In other words, only one eighth of the number of liposomes per microliter would be needed to produce the same impedance

change and fewer liposomes per microliter could be detected. As an example, a 10 μm diameter liposome has 19.7 times the volume of a 3.7 μm diameter liposome. We would expect, therefore, to be able to detect approximately 50 liposomes/μl if 10 μm liposomes were used.

Finally, the qualitative sensing of viruses based on impedance change that we demonstrated is only a proof-of-concept. The time of incubation with virus sample was prolonged in our current study to ensure ample time for virus immobilization. We believe, however, that efficient and rapid capture of viruses can be achieved with optimized device geometry, antibody immobilization methods, and improved protocols for virus capture. We are now pursuing the quantitative detection of viruses after high-efficiency immunocapture from whole blood or plasma from HIV-positive individuals.

CONCLUSIONS

In conclusion, we have developed an electrical sensing technique for the detection of biological entities after tagging with ion-encapsulating liposome particles and ion-release impedance spectroscopy measurements. Our sensing approach eliminates the need for bulky and expensive optical equipment and, because liposome permeabilization occurs rapidly above the critical temperature and only small volumes of reagents are required, is well-suited to become a point-of-care diagnostic tool. Additionally, because the strategy for specific recognition is based exclusively on antigen-antibody interaction, the platform can be easily adapted for the detection of a variety of pathogens, proteins and other biomolecules from biological fluids.

FIGURES

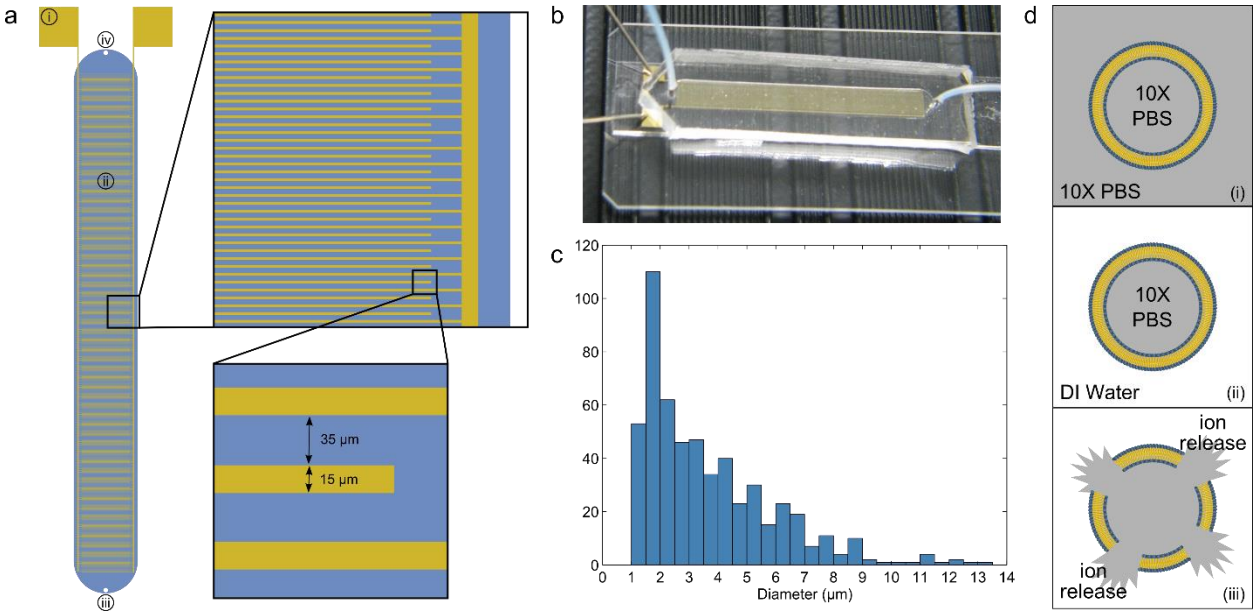

Figure 3.1 (a) Schematic of interdigitated electrode impedance sensing device. Each electrode finger is 15 µm wide with a 35 µm gap between electrodes. Labeled components are (i) gold contact pads where micromanipulator probes contact the device, (ii) sensing region/fluidic chamber, (iii) fluidic inlet port, (iv) fluidic outlet port. The blue region represents the fluidic chamber defined by the PDMS cover. (b) Photograph of device with PDMS cover mounted on a microscope slide. Micromanipulator probes can be seen in contact with the device. (c) Histogram of liposome diameters as determined by optical microscopy (mean diameter = 3.682 µm, standard deviation = 2.262 µm) and analysis with ImageJ software. (d) Illustration of liposome sensing concept: (i) liposomes are hydrated in 10X PBS, producing ion-encapsulating particles, (ii) the external media is replaced with low-conductivity DI water, (iii) ion release is triggered and impedance change is measured in order to quantify liposomes present in the sensing device.

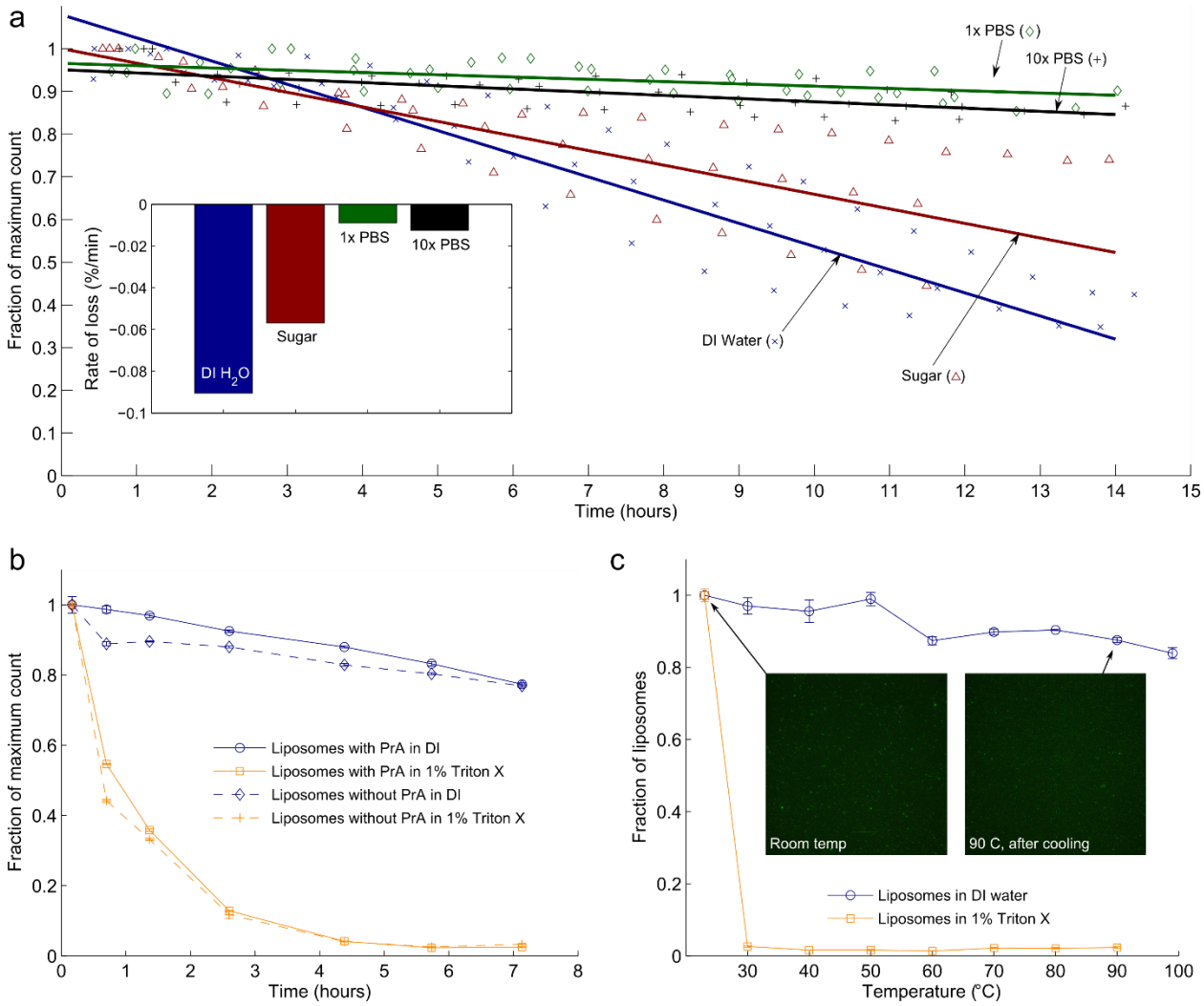

Figure 3.2 Liposomes in various conditions were counted by flow cytometry to characterize stability. (a) Liposome count was measured over several hours in DI water, sugar solution, 1X PBS, and 10X PBS. The measurement was repeated for each condition for a total of three samples. Each repeat was fitted with a linear best fit. The average of the three fits is shown. (inset) Bar chart of slopes determined from averaged fits of three repeats of each condition. (b) Liposomes with and without protein A were suspended in DI water and 1% Triton X. Counting over time shows that detergent accelerates liposome depletion. (c) Similarly, liposomes were suspended in DI water and 1% Triton X, heated to various temperatures and counted with a flow cytometer after cooling to room temperature. This data suggests that heating accelerates the effects of detergent but does not compromise the overall structure of liposomes in DI, although additional data presented in this paper indicates that heating above ~41 degrees C promotes the release of liposome contents. Fluorescence microscopy images of samples at room temperature and after cooling from 90 degrees confirm flow cytometry measurements by demonstrating that liposome particles are still present after extreme heating.

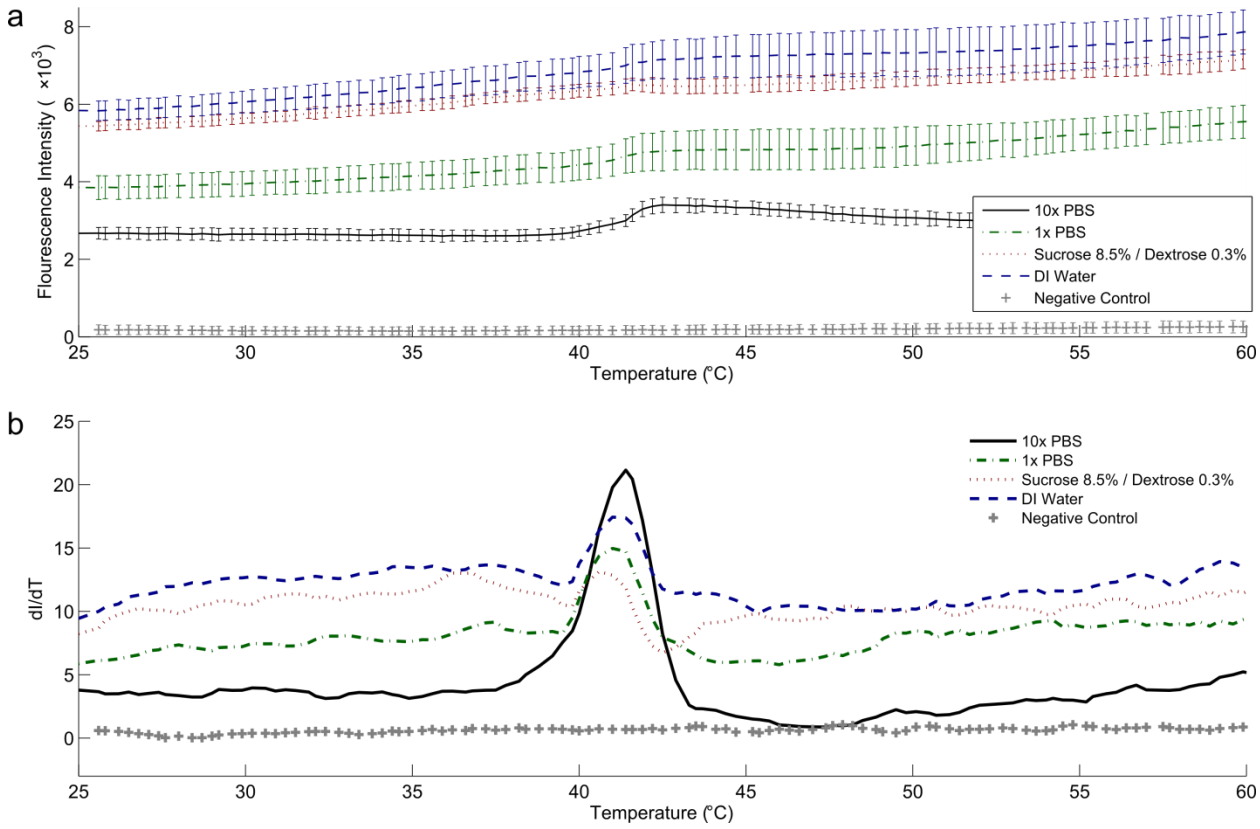

Figure 3.3 Liposomes encapsulating calcein were prepared, re-suspended in various media and analyzed with a melting curve program in a realtime PCR instrument. The sample temperature was increased from 25 degrees C to 95 degrees C over 30 minutes and at 520 nm emission was monitored throughout. (a) Raw fluorescence intensity and (b) the rate of change dI/dT versus temperature show that a dramatic increase in fluorescence intensity occurs at approximately 41 degrees, indicating the release of calcein from within liposomes. This agrees with the lipid transition temperature cited by the product literature.

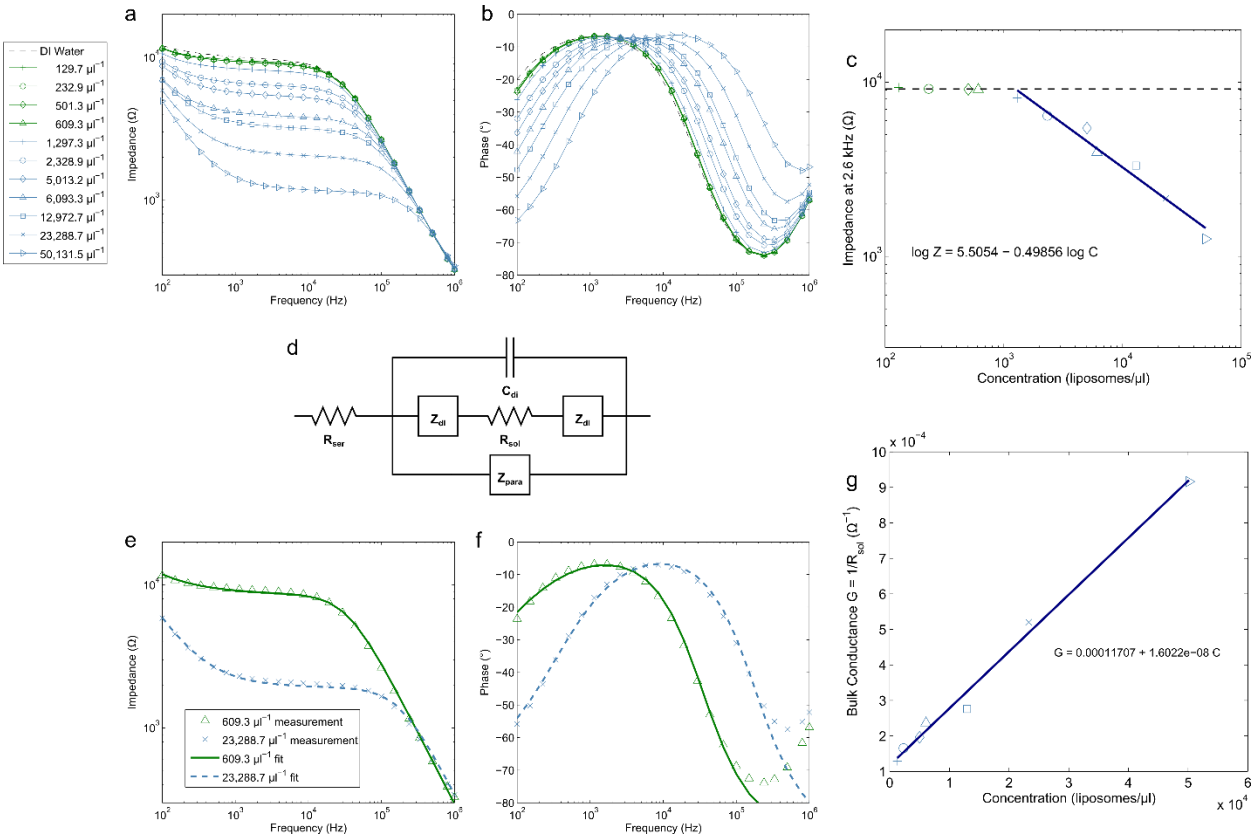

Figure 3.4 (a-b) Ion-release impedance spectroscopy measurements from several heat-permeabilized liposome samples at concentrations ranging from 129.7 µl-1 to 50,131.5 µl-1 and (c) impedance measured at 2.6 kHz versus liposome concentration with fits to measurements above the limit of detection, approximately 1000 µl-1. (d) Simplified circuit model of electrodes in solution which is fitted to experimental data, accounting for the dielectric capacitance Cdi, solution resistance Rsol, series resistance Rser, parasitic impedance Zpara, and interfacial impedance Zdl. (e-f) Sample fits of the simplified circuit model to measured data for high and low concentrations. (g) Bulk conductance calculated from values for Rsol extracted from fitting the experimental data are plotted versus liposome concentration and fitted with a straight line. The slope of this line represents the sensitivity of the device.

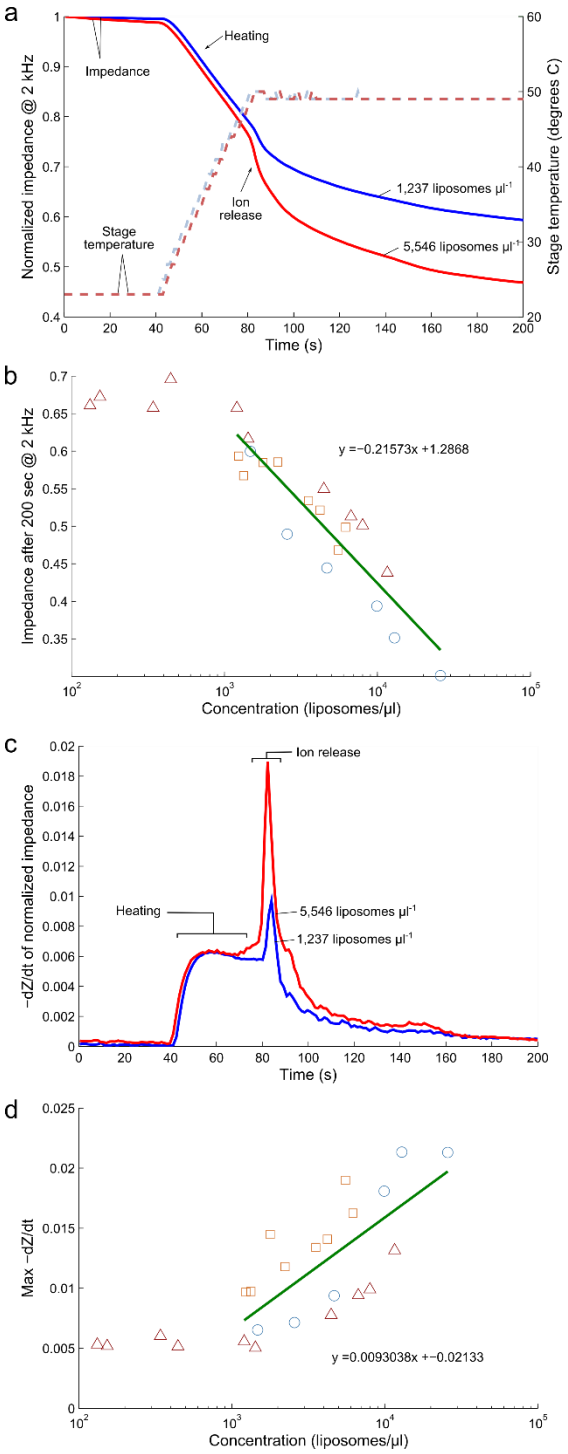

Figure 3.5 Real-time impedance detection of ion release from liposomes by heating of interdigitated electrode device. (a) Sample data for liposomes at two different concentrations is shown, including the normalized impedance and the stage temperature for 1,237 µl-1 and 5,546 µl-1 samples. The actual device temperature lags behind the stage temperature by a few seconds because it is insulated by a glass microscope slide. (b) Shows the normalized impedance value at 200 seconds for all samples versus liposome concentration with linear best fit (on a semilog axis). Measurements indicated by each unique symbol/color combination were recorded from the same batch of liposomes. Three different batches of liposomes were prepared and measured in total. (c) The rate of normalized impedance decrease, –dZ/dt, is plotted for the same two representative samples. (d) Summarizes all measurements with the same symbol/color scheme and linear best fit (on a semilog axis). Only liposome concentrations above the lower limit of detection (103 µl-1) are fitted.

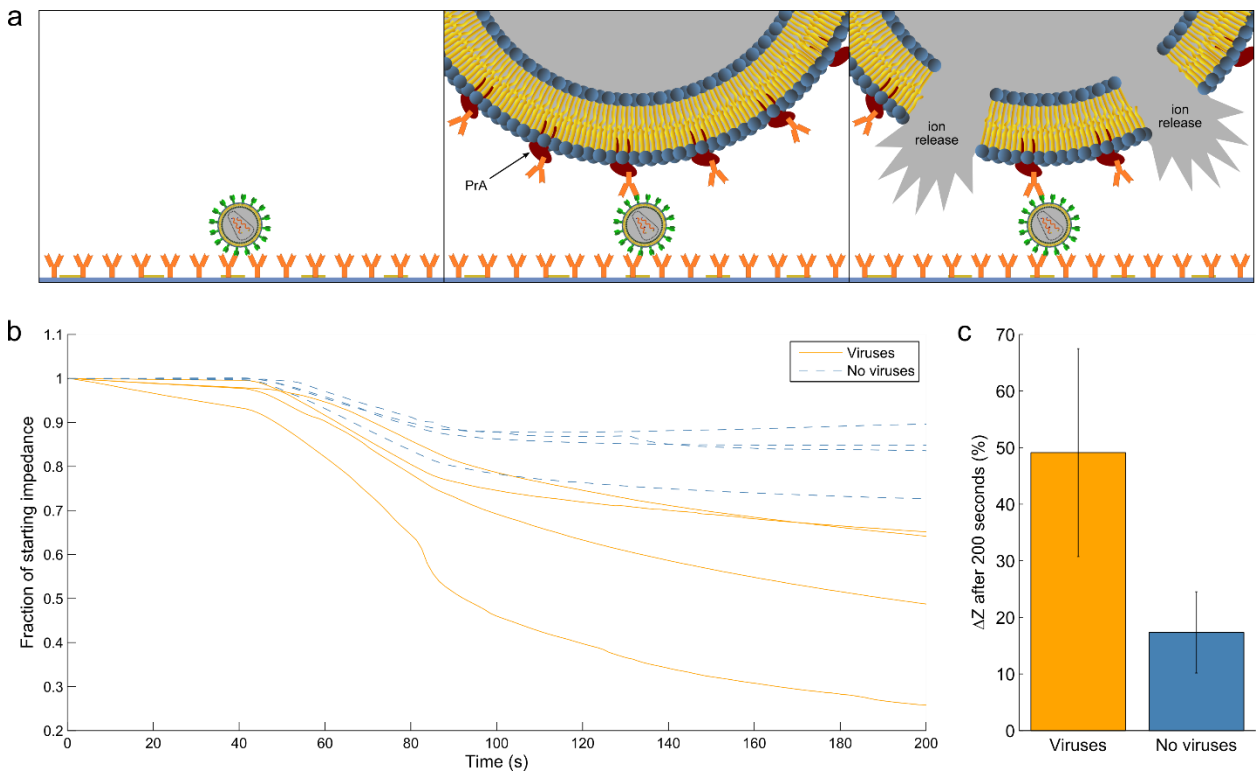

Figure 3.6 Virus sensing by liposome tagging and ion-release impedance spectroscopy. (a) Concept of detection: (1) Virus is immobilized by antibody binding on the surface of the microfluidic channel. (2) Liposomes, functionalized with protein A (PrA) which binds the Fc region of IgG, bind specifically to immobilized viruses and background media is replaced by DI water. (3) Device is heated to trigger the release of encapsulated ions. (b) Normalized impedance data measured at 2 kHz for four repeats of virus-containing devices and controls. (c) Summary of average impedance change after 200 seconds for virus-containing devices (mean = 49.11%, standard deviation = 18.37%, n = 4) versus control (mean = 17.34%, standard deviation = 7.18%, n = 4). The averages are confirmed by two-tailed t-test to be significantly different with 95% confidence (t = 3.22).

CHAPTER 4: ADVANCING ANTIGEN-BASED HIV DETECTION

INTRODUCTION

The method described in the previous chapter is an immuno-affinity biosensing approach that incorporates liposomes as the novel component in an electrical measurement. Continuing with the antigen-recognition and electrical biosensing approach, this chapter explores improvements to various aspects of that approach. First, we characterize a new liposome with higher melting temperature motivated by a specification for point-of-care tests that reagents must be able to withstand temperature spikes of up to 50 degrees C. Next, we briefly test our ion-release sensing approach with liposomes produced by a novel microfluidic droplet generation technique. We then discuss efforts to characterize magnetic micro-particle affinity capture of HIV virions, introducing a novel virus-binding component not known to be used in immunoassay-styled sensors for HIV. Finally, we discuss an inertial microfluidic blood plasma separation technique which could be employed as a sample processing step prior to antigen-based capture of viruses by removing cells and other interfering components from the sample.

ION-RELEASE IMPEDANCE SPECTROSCOPY OF DSPC LIPOSOMES

The key and novel component of our antigen recognition approach is sensing in which the signal is based on electrical detection of ion release from liposomes, which we have originally described in 2013 [4]. The concept involves quantifying liposomes that contain high concentrations of ions (in this case, 10X PBS) when the liposomes are in a low-conductivity medium (such as deionized water). Because the liposome membranes are not as permeable to water as a cell membrane, they do not lyse rapidly in hypo-osmotic conditions and ion release must be stimulated by heating to the point in which the liposome membranes are no longer stable. We have published the initial characterization of this method using DPPC lipids with a transition temperature (T_m) around 41 C [4]. However, reagents that are stable up to 50 C are

desirable for point-of-care tests to withstand potential exposure to high temperatures while in the field. For this reason, we have employed 1,2-dioctadecanoyl-sn-glycero-3-phosphocholine (DSPC) lipids (T_m = 55 C) in the same fashion.

Methods

Liposome characterization. DSPC liposomes containing 10X PBS were characterized based on size and stability in a hypo-osmotic environment (i.e. deionized water). Size distribution was determined by diluting liposomes and placing a small volume on a hemocytometer. Images were captured and analyzed to determine diameter of each particle by comparing to features of known size on the hemocytometer.

Stability characterization was performed by diluting DSPC liposomes in DI water and centrifuging the mixture for 10 minutes at 3220 rcf. Supernatant was aspirated and liposomes were re-suspended in deionized water at an approximate concentration within the range of the flow cytometer. Several aliquots of this liposome suspension were placed in a Guava EasyCyt Plus flow cytometer for serial counts over the course of approximately one hour.

Impedance spectroscopy. For initial impedance spectroscopy analysis, DSPC liposomes were washed several times as described earlier, suspended in DI water, and then disrupted by heating to 95 C and vortexing briefly. Liposome concentrations were obtained before disruption by flow cytometry. Solutions were then cooled to room temperature and infused into the same microfluidic chip with micro-fabricated interdigitated electrodes on the surface described in [4], and impedance spectra were recorded. The impedance magnitude at 2.6 kHz was plotted versus liposome concentration in the solution.

Real-time ion-release impedance analysis was performed by washing liposomes several times with DI, suspending liposomes in deionized water at various concentrations, and measuring impedance while heating the chip to 65 C on a heating stage. After suspension in DI water, a portion of the sample was used to determine liposome counts from a flow cytometer. The remainder of the solution was injected into the microfluidic chamber for impedance analysis. Impedance was measured at 2.6 kHz while a heating stage was used to heat the entire chip to 65 C to stimulate ion release.

To determine the best time following initiation of heating at which liposomes could be quantified, impedance values were systematically assessed by determining the R^2 value for a fit to the plot of impedance change versus concentration for samples containing more than 1,000 liposomes μL^{-1}. The maximum value of R^2 was observed at 211 seconds following heating. This is believed to be approximately the time were ion-release and diffusion is fully realized while evaporation and other sources of noise are still minimal.

Results

Liposome characterization. DSPC liposomes containing 10X PBS exhibited a similar size distribution to DPPC liposomes produced by the same crude method described in [4], with a mean droplet diameter of 3.4917 μm and a standard deviation of 2.2598 μm. A comparison is shown in Figure 4.1b-c.

DSPC liposomes containing 10X PBS placed in deionized water exhibited little decrease (<10%) in count over the course of one hour, suggesting that the higher T_m lipid behavior in the hypo-tonic environment is similar to what was characterized with DPPC in [4].

Impedance Spectroscopy. Results from initial impedance spectroscopy are shown in Figure 4.1d-e. The 2.6 kHz measurements are plotted in Figure 4.1a alongside analogous results from [4]. A trend is observed in samples containing liposomes at concentrations approximately 1,000 liposomes μL^{-1} and higher.

Examples of the impedance profiles measured during real-time ion-release impedance analysis are shown in Figure 4.2. The best fit to the impedance change as a fraction of starting impedance versus liposome concentration was at 211 seconds after heating was initiated. These data are shown in Figure 4.3, exhibiting the trend between impedance change and liposome number.

Discussion. These measurements demonstrate the potential of the 1,2-dioctadecanoyl-sn-glycero-3-phosphocholine (DSPC) lipids for the ion-release impedance spectroscopy method we have developed and described in [4]. The advantage of a higher melting temperature lipid is that liposome particles may be more robust and resistant to temperature fluctuations, which is particularly necessary for a field test in remote

settings which may include hot climates. Disadvantages are also observed, however, including an increase in noise in the real-time measurement which is believed to be due to the higher temperature at which the measurement is performed.

Several improvements can be considered for further developing the liposome-based ion-release impedance spectroscopy technique we have described. First, the size distribution of the liposomes produced by the crude method is undesirable and a greater accuracy measurement could likely be achieved by improving the uniformity of liposome size. More novel methods exist for liposome production which we will explore in future work. Additionally, increasing the size of liposomes would result in increased signal from each liposome. Finally, while preliminary work was done to explore alternative methods to stimulate ion-release, a non-heating approach such as using low concentrations of detergent may result in an improved measurement and requires more rigorous investigation.

LIPOSOMES PRODUCED BY MICROFLUIDIC DROPLET GENERATION

In preliminary work toward an improvement of the ion-release impedance spectroscopy technique, we have collaborated with the Lee group to examine liposomes produced by a microfluidic droplet generation technique [218]. For this preliminary work, DPPC liposomes are used because they were found to be more amenable to the microfluidic generation technique. These microfluidically-produced DPPC liposomes were analyzed with the impedance spectroscopy described previously.

Methods. DPPC liposomes containing 5X PBS produced in a microfluidic device were received from Lee, *et al.* and washed several times as described several times previously. After the final wash, liposomes were suspended in DI water, and then disrupted by heating to 95 C and vortexing briefly. Liposome concentrations were obtained prior to heating/disruption by analyzing a portion of the sample in a flow cytometer. Heated solutions were cooled to room temperature and then infused into the same microfluidic chip with micro-fabricated interdigitated electrodes on the surface described in [4], and impedance spectra

were recorded. The impedance magnitude at 2.6 kHz was plotted versus liposome concentration in the solution.

Results. Impedance spectra measured from the liposomes produced by the novel microfluidic methods are show in Figure 4.4. The expected trend is observed, though the sample containing 1,176 liposomes μL^{-1} overlaps with the sample containing 11,760 liposomes μL^{-1}, suggesting that background contamination was high. The expected trend of decreasing impedance with increasing liposome concentration was observed as expected.

Discussion. The data presented here represents preliminary analysis of DPPC liposomes produced by the novel microfluidic method. Several challenges need to be addressed, including how to make the microfluidic production method compatible with higher ion concentrations and higher melting temperature liposomes. The Lee group has been successful in achieving 5X-PBS encapsulating DPPC liposomes with their microfluidic droplet generation methods [218], which exhibit generally the expected result in our ion-release impedance analysis. Future work will explore the implementation of these liposomes using the microfluidic production method. Ultimately, the approach is promising for a portable diagnostic device, suggesting the liposome component of an electrical biosensor could be produced from raw materials on-chip, simplifying storage of reagents and reducing concerns surrounding consistency of reagents stored in different conditions.

MAGNETIC MICROBEAD IMMUNOAFFINITY CAPTURE OF HIV

It is clear that an increased lower limit of detection and greater sensitivity (ability to discriminate between samples of different concentrations) could be achieved with the ion-release impedance spectroscopy method initially described in [4] by enrichment or concentration of the virus particles. Working toward our goal of a sample-to-answer detection assay, we sought a concentration approach compatible with whole blood. Early on, capture experiments in planar microfluidic channels were performed using Vesicular Stomatitis Virus G (VSV-G)-Pseudotyped Lentivirus (see Appendix B) as a

model for infectious HIV and used an anti-VSV-G antibody. Subsequently, we identified a source for HIV-1 and turned from planar surfaces to capture in suspension. Our chosen approach involved functionalized magnetic micro-particles which offer increased likelihood of interaction with viruses in solution or sample compared to a functionalized plane.

Methods. Magnetic micro-particles (Bangs Labs) were functionalized with various proteins according to the manufacturer's instructions and mixed for one hour with virus-spiked whole blood diluted 1:10 in buffer. A magnetic stand containing a strong permanent magnet was used to separate the micro-particles which were then rinsed several times with clean saline (PBS) buffer. Micro-particles were then exposed to a lysis buffer with proteinase K to lyse captured viruses and removed from solution with a magnet. Viral RNA was purified using the PureLink® Viral RNA/DNA Mini Kit (Life Technologies) and quantified with the RNA UltraSense™ One-Step Quantitative RT-PCR System (Life Technologies). This process is summarized in Figure 4.5.

The same spiked blood sample was assayed for virus concentration as a reference by centrifuging the blood to separate cells, treating cell-free plasma with lysis buffer, purifying viral RNA, and quantifying viral RNA in the same RT-PCR assay as the bead-separated samples. Virus capture efficiency was calculated as the ratio of the quantity of viral RNA detected by the bead separation method (captured virus) to the quantity of viral RNA detected in the reference sample (total virus). Binding components that were tested included two antibodies provided by the AIDS Reagent Program: 4E10 (anti-gp41) and VRC01 (anti-gp120), a commercially purchased antibody (anti-gp120 from AbCam), and two proteins provided by the NIH AIDS Reagent Program: soluble human CD4 (sCD4) and Enfuvirtide (T-20, an antiretroviral infusion inhibitor).

Results. Results of tests with HIV-1 IIIB showed that the protein-functionalized beads (sCD4 or T-20) performed better than the antibody-functionalized beads at affinity capture and pulldown of HIV-1 IIIB particles. T-20 capture was then characterized further to optimize the protein coating of the micro-particle and improve capture efficiency of 42.7%. These results are shown in Figure 4.6.

Discussion. The application of T-20 in an assay for HIV detection is a novel technique and shows some promise as a component of a "recognition and isolation" system. However, the immunoaffinity approach broadly speaking is problematic for HIV. Antibodies available for recognition of epitopes on the exterior of whole virus particles are considered to be neither high-affinity nor universally applicable. Diversity in viral clades and subtypes has made the outlook for any sort of envelope recognition by antibodies bleak, and is in fact a key explanation behind the lack of a vaccine for the virus today. Broadly neutralizing antibodies are available, though their recognition is relatively weak. Beyond epitope recognition challenges, phenomena such as gp120 shedding and aggregation suggest that the sandwich assay approach to HIV may ultimately be impossible. While our analysis demonstrates some potential for CD4 or T-20 as a viral envelope recognition component, we have not yet addressed these issues such as budding or aggregation of receptors on the viral envelope.

One possibility is to employ the imunnoassay approach to HIV core antigen, p24. Virus separation (either by affinity, mechanical filtration, or hydrodynamic mechanisms) followed by viral lysis and downstream detection of p24 as the analyte contains some promise. In the context of existing HIV immunoassays, p24 is the common analyte in ELISAs and other techniques. Future work will explore this approach in conjunction with our liposome ion-release method.

INERTIAL MICROFLUIDICS FOR BLOOD PLASMA SEPARATION

Common perceptions in the field include the notion that detection of small analytes in whole blood requires separation from most other blood components, particularly cells. We therefore have explored methods for automated microfluidic blood plasma separation which would enable magnetic micro-particle, liposome-to-virus, or other binding events in a cell-free matrix. The optimal method in the literature for our application was a serpentine microchannel which leverages inertial physics for dynamic separation of cells from whole blood [220].

Methods. We have adapted and fabricated microfluidic devices based on the design presented in [220] for the removal of cells from whole blood through inertial microfluidics. The basic design is shown in Figure 4.7 and includes a sample and buffer inlet region, a cell focusing region, and an output region. The lengths and diameters of the output channels and the tubing connected in series with each output channel determines their relative fluidic resistance and dictates the fraction of the flow that exits the chip through each channel. Due to inertial phenomena that occurs in a straight channel but it accelerated in the serpentine design, cells are focused to the edges of the fluid stream [220]–[223]. Therefore we are interested in recovering fluid from the center of the channel which would contain cell-free blood plasma. In preliminary work toward utilization of this chip, buffer was flowed at 336 μL/min and whole blood (or buffer in the case of volume analysis) was flowed at 14 μL/min.

Output of the device was analyzed by flowing buffer into both inlets in lieu of blood and collecting fluid from the three output channels (V_A, V_B, and V_C from channels A, B, and C). Volume was determined by weighing the output and assuming the fluid had a density approximately the same as water.

Analysis with blood was performed to measure the cell concentration in the center output channel (B) versus the ratio of the lengths of the output channels (L_B/L_A). An Orflo Moxi Flow cytometer was used to analyze samples collected from the output channel of the chip.

A virus recovery test was also performed with the inertial microfluidic device in which healthy whole blood was spiked with HIV-1 IIIB virions and flowed through a device with a 21-period focusing region and approximate output ratio of $L_B/L_A = 3.9$. Buffer was flowed at 336 μL/min and whole blood was flowed at 14 μL/min, output flowed from channel B at approximately 39.8 μL/min. Approximately 28.4 μL of cell-free plasma and buffer was recovered from 10 μL whole blood input. The test was run with a blood sample of measured hematocrit 43.8%. Sample recovered from channel B was treated with lysis buffer and viral RNA was purified using the PureLink® Viral RNA/DNA Mini Kit (Life Technologies) and quantified with the iTaq™ Universal Probes One-Step Kit (Bio-Rad).

Results. Results of the volume analysis experiments match the expected ratios as dictated by the ratio of fluidic resistances, which are primarily determined by the length of the channels, as shown in Figure 4.8.

Blood cell analysis shows that a configuration in which the ratio is 3.5 results in a negligible concentration of cells (~ 10/μL) in the center channel. These data are shown in Figure 4.8.

Having measured the volume of output of channel B and verifying it was cell-free, we could calculate that the expected virus recovery in the case where blood had completely diffused with the saline buffer was 11.49%. In the actual test, we measured an actual virus recovery of 20.44%, suggesting that, although the cells had been sufficiently removed from the center channel by the inertial focusing method, the blood plasma had not fully diffused with the saline buffer by the time the output fluid was collected. This indicates is may be possible to further optimize the design of the inertial microfluidic cell removal chip to recover an even higher fraction of viruses from whole blood.

Discussion. Inertial microfluidic methods are attractive for their simplicity in that their behavior is a result only of the geometry of the device and is not dependent of biochemical or other potentially complicated components. Here we have performed some preliminary characterization of an inertial microfluidic method for blood plasma (and therefore virus) separation from whole blood. The motivation for exploring this idea is that several of the detection or recognition events we have explored in the context of HIV viral load could benefit from a cell-free matrix, particularly affinity capture with magnetic micro-particles. One simple but novel aspect of the data we have presented here is that our design takes an un-processed whole blood input whereas all of the descriptions in the literature of blood analysis by this method pre-mix the blood and buffer before infusing it into the chip. We have considered whether laminar flow phenomena which minimize the mixing of fluids can be leveraged in this approach to recover blood plasma that is not fully diluted yet still cell-free. The hypothesis here is that by employing the appropriate mixing length, inertial effects may have taken place to migrate cells out of the recovery channel, while diffusion of blood plasma and its components may not yet have completely taken place. Future work will characterize this in increased detail.

CONCLUSION

The liposome-based approach to biosensing termed "ion-release impedance spectroscopy" incorporated novel low-cost components in a format inspired by a traditional immunoassay. Whereas the classic enzyme-linked immunoassay (ELISA) typically incorporates a primary antibody on a solid substrate for capture of antigen, a secondary antibody for specific tagging of the analyte, and an enzyme conjugated by one of several methods to the secondary antibody for conversion of substrate to signal, the liposome-based approach replaced that enzyme with a liposome that would be cheaper to manufacture and more robust. Furthermore, the signal-generating component – ions within the liposome – were also low-cost and since it could be measured with simple impedance measurements, optical components were not required. Further replacement of the solid substrate for primary capture with antibody- or protein-functionalized micro-particles also promised more rapid mixing and efficient analyte capture compared to the traditional approach. Implementation of the integrated test, however, with microfluidic magnetic separation and ion-release measurements proved difficult and was complicated by factors which are not yet clearly understood.

Several opportunities still exist to build upon the liposome-based ion-release impedance spectroscopy technique. First, a simple re-design of the microfluidic chamber for a lower sensing volume could increase the absolute lower limit of the device. This could offer significant utility in the case where a concentration step (e.g. magnetic-microparticle capture) is incorporated. Second, an improvement in the uniformity and size of liposomes could provide a more consistent and sensitive signal. Signal change can be related to the volume and concentration of ions within liposomes which contribute to conductivity changes upon release into the low-conductivity medium. Larger liposomes, as well as liposomes containing more concentrated ions, would lead to increased signal.

A third opportunity for improvement of HIV detection by this technique is to perform a primary capture step of whole virions in sample followed by an isolation step, viral lysis, and an additional capture step targeting p24 protein as the analyte. Mature HIV contains approximately 2,000 p24 molecules per virion [224], and would therefore provide three orders of magnitude increase in analyte concentration. This addresses a challenge to antigen-based detection of HIV because antibodies to the surface proteins of HIV are not considered "good" due to viral diversity (and broadly-neutralizing antibodies are relatively weak).

Antibodies to p24, however, are considered much more effective. Should this approach be implemented, antibodies recognizing two distinct and not overlapping epitopes of the p24 protein should be used for primary and secondary p24 binding.

Finally, replacing the heating to stimulate ion-release by another mechanism would reduce the noise in the device. Early on, detergents were examined instead of heating, though it appeared these reagents introduced ionic contamination into the device. Detergents may be worth revisiting in this technique. Alternatively, novel approaches could be imagined – for example, incorporation of a light-sensitive ion channel such as Channelrhodopsins which could be stimulated with an LED or laser to release ions from liposomes.

Could the challenges faced here be addressed and understood, one could imagine the potential for a fully-integrated device based on ion-release impedance spectroscopy. Beginning with whole blood, the series of inertial microfluidic cell separation and magnetic micro-particle capture could be followed with virus lysis and p24 capture on magnetic micro-particles. Incorporating the techniques described by the Lee group [218], the signal-generating liposome component could be generated from raw reagents on-chip in a portable format, reducing the risk of component degradation in the field.

Ultimately, despite the opportunities described here for improvement of the antigen-based technique incorporating liposome ion-release impedance spectroscopy, the decision was made to pivot from an antigen-based approach to nucleic acid detection. Attractive for its potential to be amplified, nucleic acid detection proved to harness much more potential than expected in the context of whole blood detection.

FIGURES

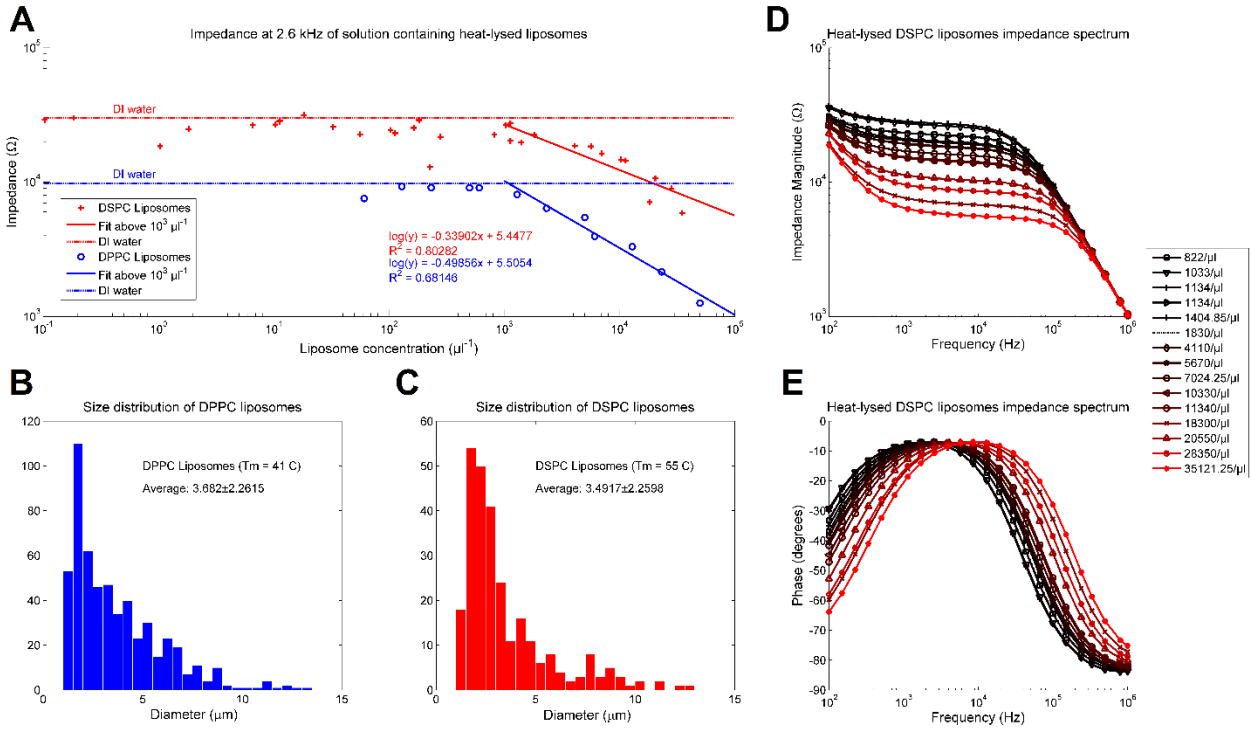

Figure 4.1. (A) Basic impedance spectroscopy analysis of DSPC and DPPC liposomes produced by heating solutions of liposomes in DI water followed by analysis on a microfluidic chip. A similar trend is observed in DSPC lipids when compared to DPPC lipids. Histograms of diameters for (B) DPPC and (C) DSPC show similar distributions for liposomes produced by the crude method described in [4]. (D) and (E) show complete impedance spectroscopy (magnitude and phase) analysis of DSPC as described in the text.

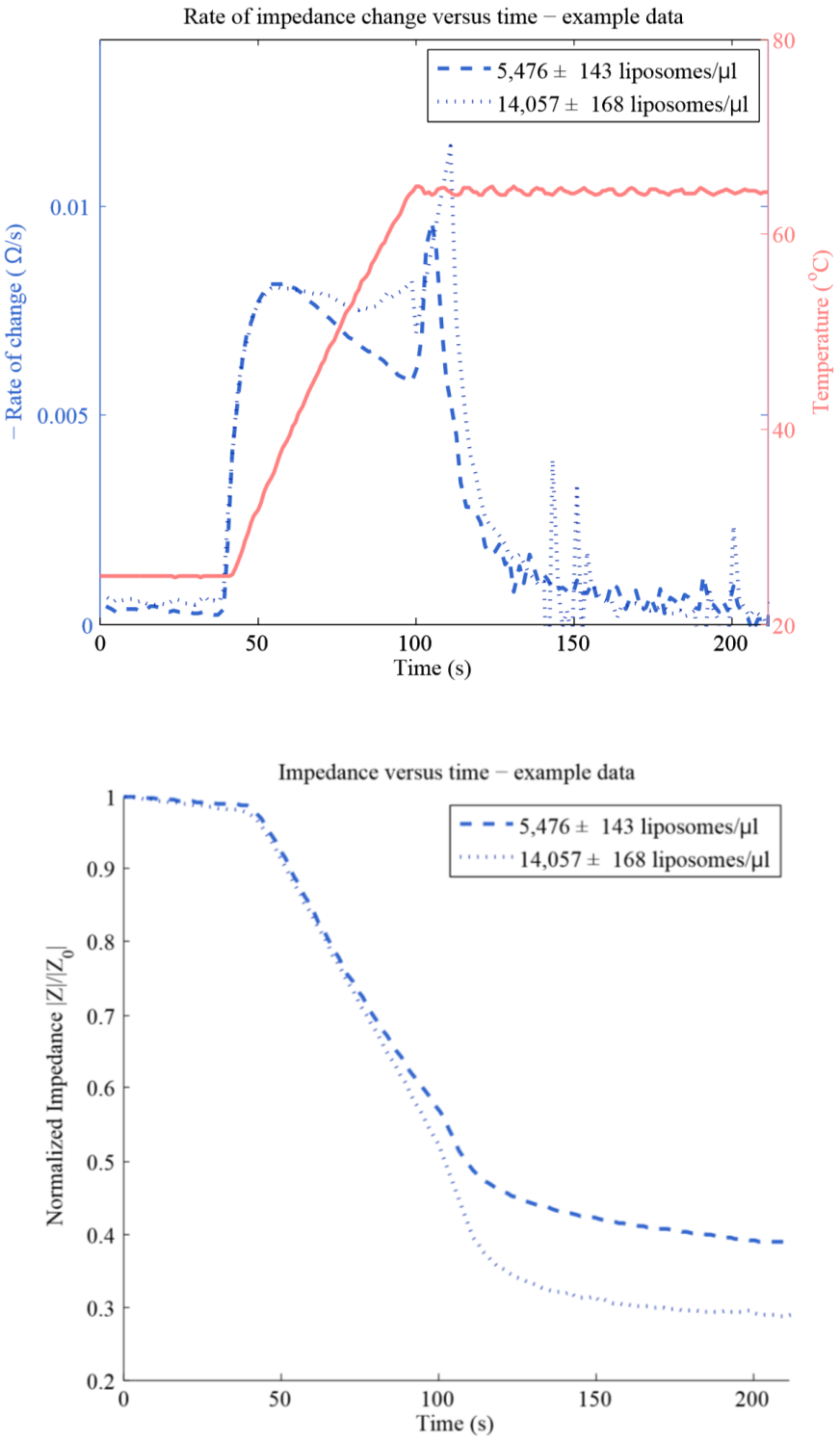

Figure 4.2. Real-time ion-release impedance measurements for DSPC liposomes. Decrease in impedance is initially due to the increased temperature of the fluid; however, around 100 seconds when the critical temperature is reached, a dramatic decrease in impedance is observed, corresponding to ion release from the liposome.

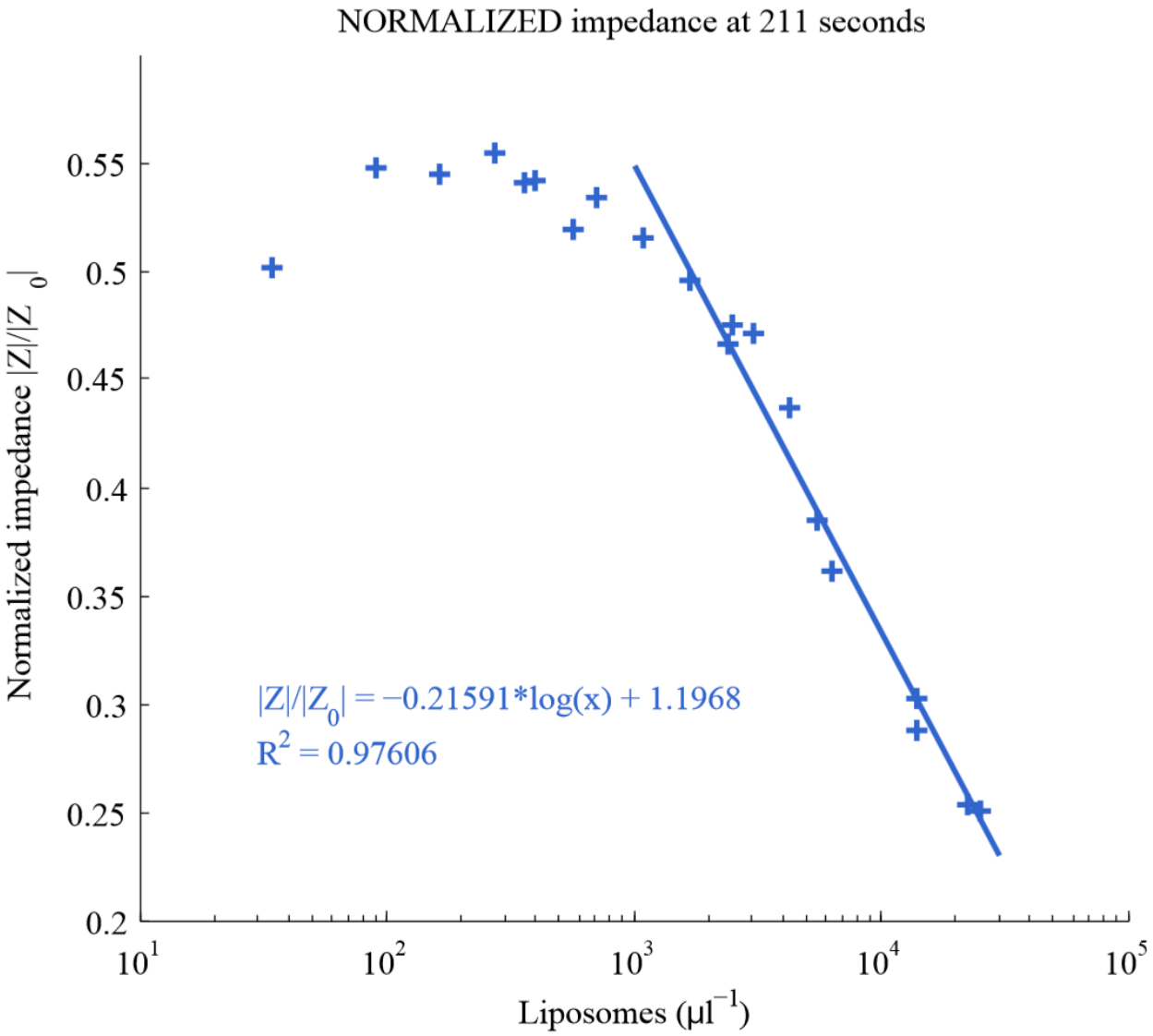

Figure 4.3. Impedance change after 211 seconds versus liposome concentration as determined by real-time ion-release impedance measurements in the microfluidic chip.

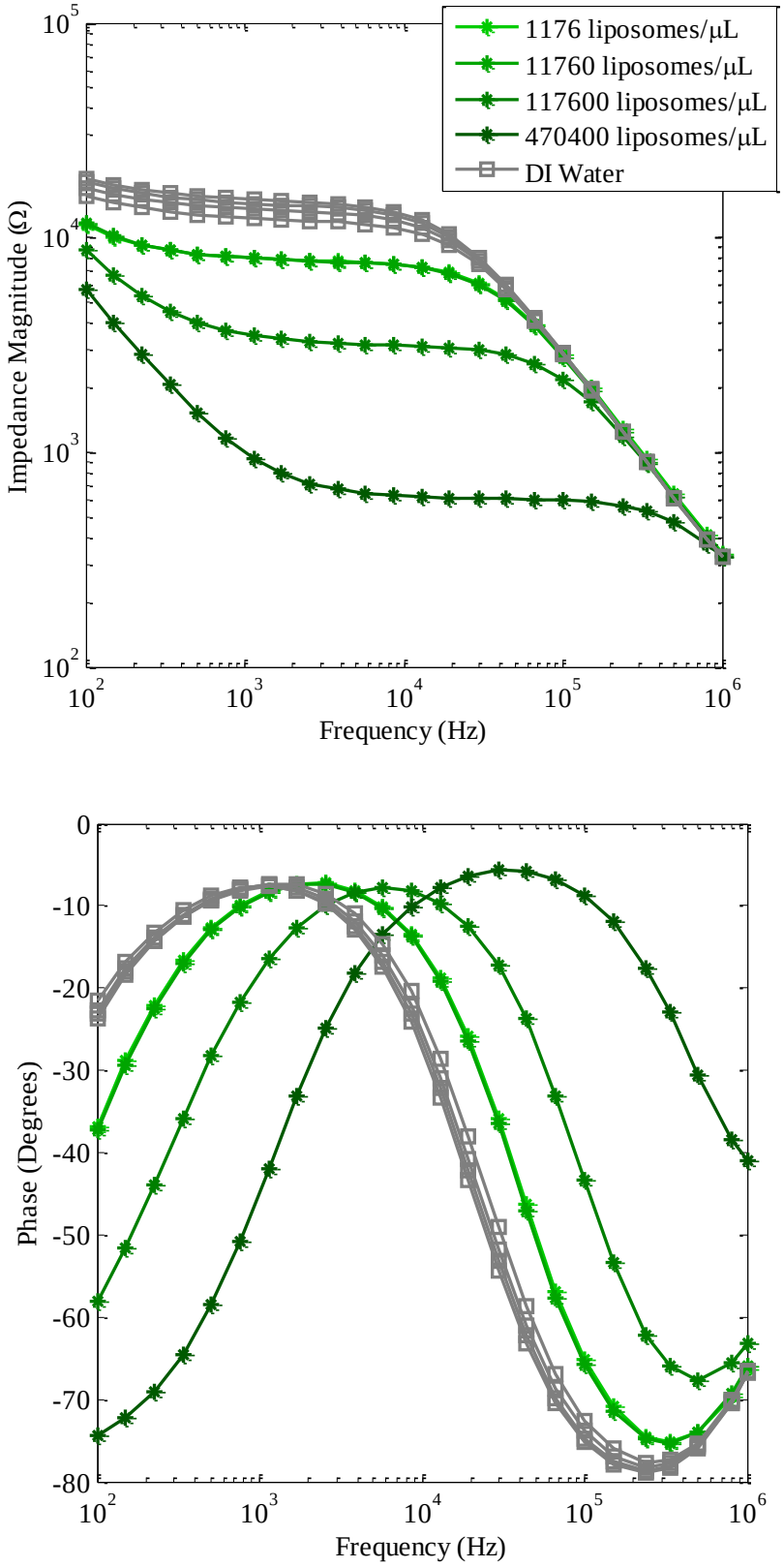

Figure 4.4. Impedance spectroscopy analysis of DPPC liposomes containing 5X-PBS generated on a microfluidic substrate.

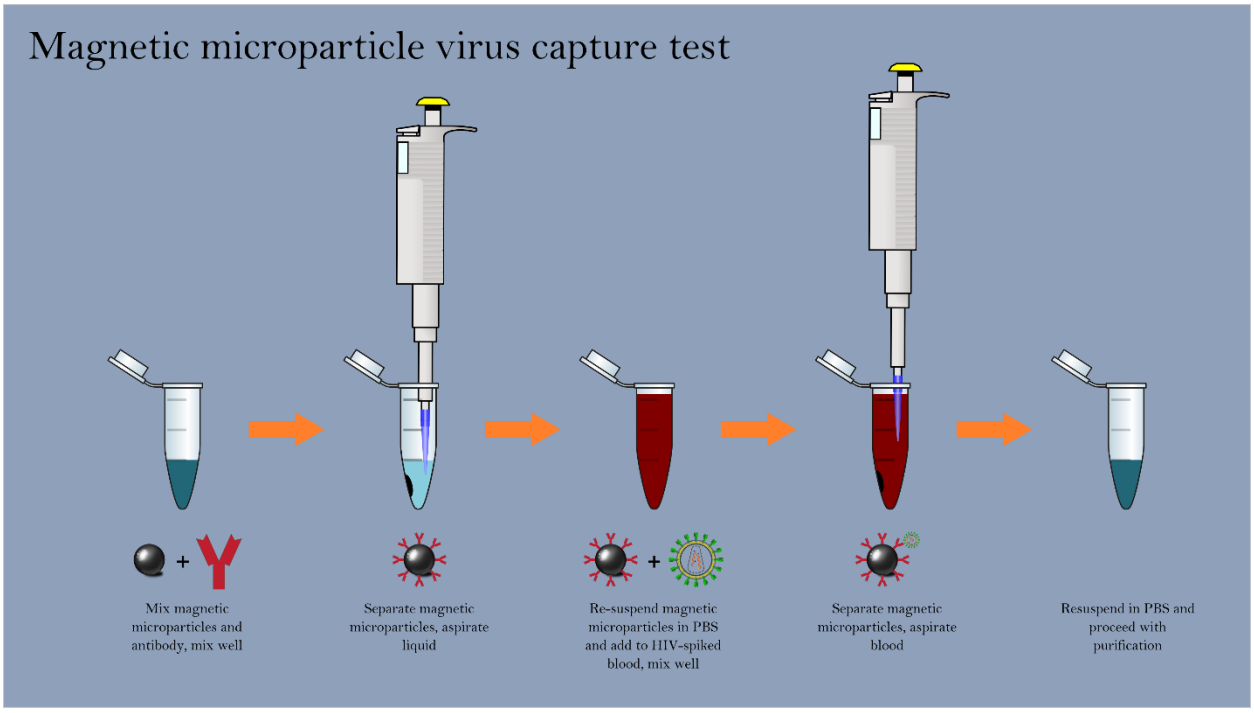

Figure 4.5. Overview of magnetic micro-particle capture test with HIV-1 IIIB and a variety of antibodies and proteins as described in the text.

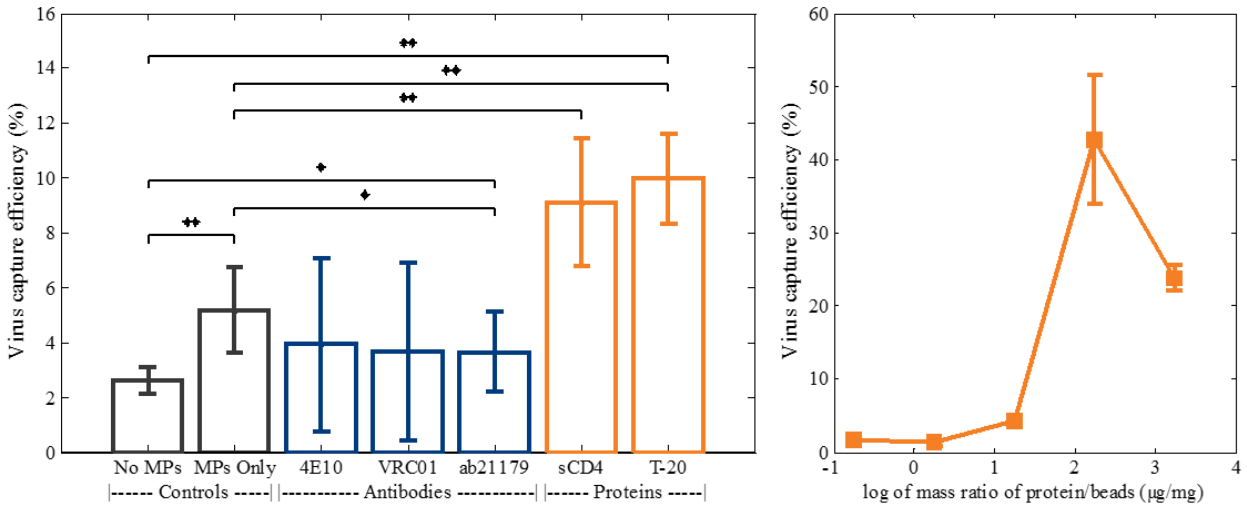

Figure 4.6. Results of magnetic microparticle capture of HIV-1 IIIB in diluted spiked whole blood. (a) Comparison of antibodies and proteins for binding viruses showing the superior performance of sCD4 and T-20. (b) Further characterization of T-20 capture in which a range of protein concentrations was used to functionalize beads.

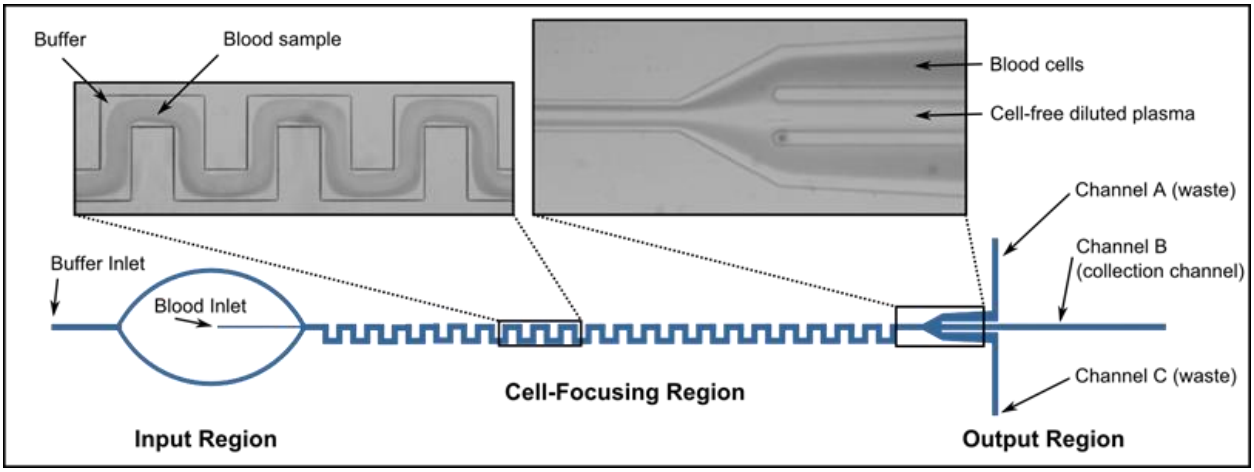

Figure 4.7. Overview of inertial microfluidic cell separation device. Blood is flowed into the chip with a buffer sheath and large objects (i.e. cells) are focused to the edges of the fluid stream in the cell-focusing region, allowing cell-free plasma to be collected from the output channel. Bright field microscopy images show effects on whole blood in each region.

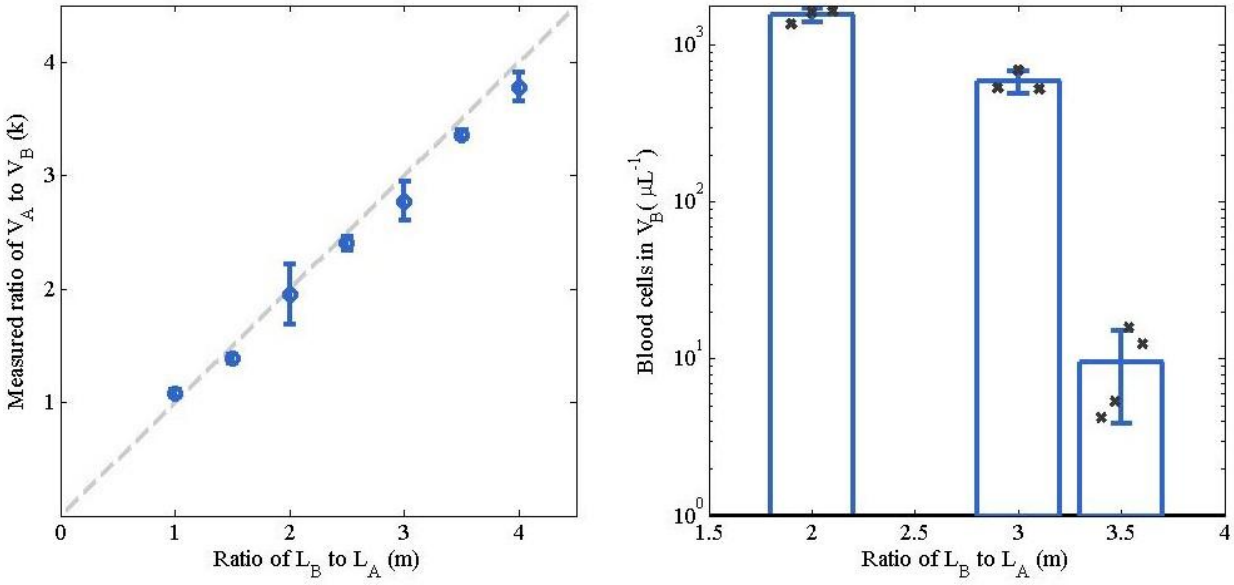

Figure 4.8. Preliminary characterization of the inertial cell removal device. (a) Measured ratio of the output volume of channel A (VA) to output volume of channel B (VB) versus the ratio of the length of output channel B (LB) to the length of output channel A (LA) verifies the 1:1 trend as expected from the design parameters. (b) The blood cell concentrations measured in the output of channel B versus the ratio of LB to LA shows that cell content becomes negligible for the design in which the ratio of the length of B to the length of A is 3.5.

CHAPTER 5: RT-LAMP IN LYSED WHOLE BLOOD

INTRODUCTION

Human Immunodeficiency Virus (HIV) affects 36.9 million people worldwide [11]. During the course of nearly four decades since the emergence of HIV on a pandemic scale, advances in antiretroviral therapy have transformed HIV infection from a death sentence into a chronic illness which can have little impact on life expectancy for those in whom the infection is properly managed [21]. At the population level, rates of new infections, mother-to-child transmission, and deaths from HIV-related causes are declining [21]. However, the availability of the appropriate diagnostic technologies essential to informing treatment in routine HIV care is still among the chief barriers preventing access to the standard of care for millions of HIV-positive individuals worldwide, particularly in resource-limited settings.

CD4+ T lymphocyte counts and blood plasma viral load are the two core diagnostic measurements broadly considered essential to HIV care, as they both guide the initiation of therapy and indicate the efficacy of each individual's treatment regimen [22]. CD4 counts, traditionally performed by flow cytometry, are increasingly available in remote settings due to the introduction of new portable platforms [32], [201], [225], [226]. Viral load platforms, on the other hand, trail CD4 technologies in penetrating the developing world. Viral load instruments are traditionally reverse-transcription polymerase chain reaction (RT-PCR), nucleic acid sequence-based amplification (NASBA), or branched DNA (bDNA) assays which, though they can be capable of detecting fewer than 10 viral RNA copies per mL of blood plasma, require a laboratory setting, extensive sample handling, and sophisticated processing [95]–[97], [201].

One promising solution that can help address this issue is loop-mediated isothermal amplification (LAMP) [227]. LAMP emerged in the early 2000's as an alternative to PCR for nucleic acid detection [228]. LAMP is attractive for point-of-care applications because it does not require temperature cycling like PCR (isothermal at 60–65 C), and because it is typically less sensitive than PCR to amplification inhibitors. RT-LAMP assays for HIV were first described quickly after the introduction of the initial

concept [229], [230], and there have been several reports since then for variations of the assay, including efforts toward point-of-care applications [43], [231]–[236]. Among the novel LAMP approaches applied to HIV that are presented in these reports are a battery-powered handheld microfluidic system which was demonstrated with purified DNA [235], a SlipChip device for digital LAMP [236], and an electricity-free heating container which facilitates a qualitative RT-LAMP assay on minimally processed whole blood [233], [234]. To date, however, an approach capable of performing a quantitative RT-LAMP assay from a drop of whole blood on a platform compatible with a fully-automated, portable device has not been presented.

Traditionally, it is believed that nucleic acid amplification requires complete purification of the RNA or DNA target to be compatible with the amplification reaction. The robustness of LAMP, however, has disrupted this thinking and whole blood treated only with cell lysis buffer has been employed by Curtis, et al. for HIV LAMP in a qualitative measurement in an electricity-free heating device [233]. We present here RT-LAMP with minimally-processed lysed whole blood for a quantitative measurement of HIV viral load capable of detecting as few as 3 whole virus particles per ~60 nL reaction droplet.

Our approach to RT-LAMP HIV viral load measurements begins with a drop of whole blood. The data presented here demonstrates the potential of the approach to be developed into a fully-automated mobile device that does not require manual processing. First, we compare and contrast the performance of the RT-LAMP reaction on a standard laboratory thermocycler both with purified viral RNA in water and whole virus particles in whole blood which has only been treated with cell lysis buffer. Next, we implement a simple microfluidic mixing module to show the whole blood lysis step can be performed on a chip without loss of analyte or interference with the detection assay. We then move to a microchip platform and characterize the RT-LAMP reaction with purified RNA and lysed whole blood spiked with viral RNA, imaging with both a standard fluorescence microscope and a consumer smartphone without hardware modifications in order to compare and contrast standard and novel techniques. To demonstrate the robustness of the assay, we show the compatibility of the on-chip reaction with the presence of viral RNA from Hepatitis C virus (HCV) and viral DNA from Hepatitis B virus (HBV) which do not cross-react. We

then combine the microfluidic lysis, microchip reaction platform, and smartphone imaging to demonstrate the capability of our platform to quantitatively determine HIV viral load from a drop of blood. Finally, we discuss merits and drawbacks, as well as the potential for this approach to address the need for point-of-care viral load technology.

MATERIALS AND METHODS

Samples

Whole blood. Whole venous blood samples were drawn from HIV-negative donors with a syringe and transferred to 4 mL BD Vacutainer K2 EDTA collection tubes. Tubes were stored at room temperature on a sample rotisserie until used for experiments.

Viruses. HIV-1, strain IIIB propagated in the H9 human T lymphocyte cell line was purchased from Advanced Biotechnologies Inc. Virus stock was provided in purified form at a concentration of 6.7E10 vp/mL in storage buffer containing 10 mM Tris, 150 mM NaCl, and 1 mM EDTA at a pH of 7.5. Viruses used for experiments in whole particle form were diluted from aliquots of the stock either in additional storage buffer prepared in-house or in PBS from Fisher Scientific.

Viral nucleic acids. Synthetic Hepatitis B virus DNA (ATCC® VR-3232SD™) and Synthetic Hepatitis C virus RNA (ATCC® VR-3233SD™) were purchased from ATCC. HIV-1 RNA was purified from HIV-1 IIIB whole particles using the PureLink® Viral RNA/DNA Mini Kit from Life Technologies. Two methods were used to produce dilutions of HIV-1 RNA for thermocycler characterization of the RT-LAMP reaction with purified RNA. First, whole virus particles were diluted in PBS and each dilution was separately purified in the PureLink® kit. In the second method, 10 µL of 6.7E10 vp/ml was added to 190 µL PBS to meet kit specifications, purified, and eluted in 150 µL RNase free water for a final concentration

of 4.47E9 vp/mL (or 8.93E9 RNA copies/mL). This purified RNA was then aliquoted and stored at -80 C until use.

Microchip RT-LAMP experiments with the exception of the integrated experiment were performed with this viral RNA. The experiments performed with purified RNA in water are performed because purified RNA is the standard analyte in reverse-transcription nucleic acid amplification assays and these experiments serve as a basis for comparison to lysed whole blood. The ideal analyte in whole blood is whole virus particles, however the preliminary microchip experiments were performed with viral RNA spiked in whole blood for biosafety reasons while the technique was being developed. Preliminary "macroscale" amplification experiments with whole blood in a thermocycler (not on a microchip) did include whole virus particles because the technique was compatible with biosafety practices. To perform the final, integrated experiment on-chip, an apparatus was constructed in a biosafety cabinet to accommodate microchip experiments with whole virus particles.

Blood cell lysis. Whole blood lysis buffer was based on Curtis, *et al.* [233] and contained 2.5 mM KHCO3, 37.5 mM NH4Cl, and 0.025 mM EDTA. A 1:4 ratio of blood to lysis buffer was used for all lysed blood experiments. Blood and lysis buffer in preliminary experiments were metered and mixed with a manual pippettor, while the final integrated experiment and the preliminary experiment to characterize microfluidic mixing employed on-chip lysis in a microfluidic channel. For microfluidic mixing, the ratio of volumes mixed was fixed to 1:4 by setting relative flow rates from two syringe pumps driving each component.

RT-LAMP

Reaction components. The RT-LAMP assay was adapted from Curtis, *et al*. [233]. Reaction concentrations of buffers were 1X Isothermal Amplification Buffer, 1.4 mM dNTPs, and 10 mM $MgSO_4$ from New England Biolabs, and 0.4 M betaine from Sigma-Aldrich. In some cases where indicated, 0.8 M betaine was used. These reaction buffer components were prepared in appropriate ratios in bulk and stored at -20 C between experiments. Enzymes and DNA intercalating dye were added separately to this buffer

mix for a complete mastermix freshly prepared for each experiment. RT-LAMP enzymes used in the reaction were 0.64 U/μL *Bst* 2.0 DNA polymerase and 0.08 U/μL AMV Reverse Transcriptase from New England Biolabs. 1X EvaGreen from Biotium, a double-stranded DNA intercalating dye, was included in the reaction for detection of reaction products.

Primers. Six LAMP primers were based on Curtis, *et al*. [233] and included a six primer set containing 0.2 μM each of F3 (5'-AGTTCCCTTAGATAAAGACTT-3') and B3 (5'-CCTACATACAAATC-ATCCATGT-3') primers, 1.6 μM each of FIP (5'-GTGGAAGCACATTGTACTGATATCTTTTTGGAA-GTATACTGCATTTACCAT-3') and BIP (5'-GGAAAGGATCACCAGCAATATTCCTCTGGATTTT-GTTTTCTAAAAGGC-3') primers, and 0.8 μM each of LoopF (5'-GGTGTCTCATTGTTTATACTA-3') and LoopB (5'-GCATGACAAAAATCTTAGA-3') primers.

Negative controls. All amplification experiments either in the thermocycler or microchip included negative controls which consisted either of water without RNA or lysed blood without viruses/viral RNA according to the nature of the positive samples being tested. Amplification of the negative control within the reaction timeframe would be considered a contaminated test. Fluorescence curves are not presented for these negative controls, though they were included in every experiment.

Reaction platforms. RT-LAMP reactions were performed on two different platforms at various stages of this study. For the purpose of establishing the RT-LAMP reaction and comparing and contrasting purified RNA in water with lysed whole blood, standard 25 μL reactions were performed in 0.2 mL reaction tubes in an Eppendorf Mastercycler® ep *realplex* Real-time PCR System. The thermocycler was also used for RT-LAMP reactions characterizing the microfluidic mixing module to eliminate possible noise introduced by the microchip system.

To develop the microchip amplification, several microchip experiments were performed beginning with RNA in water and RNA-spiked lysed whole blood (RNA was used for biosafety reasons in these preliminary experiments as explained above). Each individual droplet (reaction) on the microchip contained approximately 60 nL and the entire microchip was placed in a copper bowl as described below and heated on an INSTEC STC200 heating stage. Imaging was initially performed with a Nikon Eclipse FN1

fluorescence microscope to employ a standard imaging method. Later, a Samsung Galaxy Note 4 smartphone was introduced. Both the fluorescent microscope and smartphone are used in order to compare the imaging capabilities of the smartphone with standard laboratory imaging equipment. The reactions were incubated initially at 60 C in the commercial thermocycler and later at 65 C for the on-chip experiments. Fluorescence measurements were performed every 60 seconds with the thermocycler and fluorescence microscope, but increased to every 30 seconds with the smartphone platform.

Data are presented in this paper for microchip reactions with purified RNA in water imaged with a microscope and RNA-spiked lysed whole blood imaged with a smartphone. The intermediate experiment, RNA-spiked lysed whole blood reactions imaged with a microscope, is provided in Supplementary Information.

Microfluidic Lysis Module

Fabrication. The microfluidic lysis module is based on an earlier design previously reported [3]. The PDMS-on-glass microfluidic channel was made from an SU-8 master mold fabricated using standard cleanroom photolithography techniques. Uncured PDMS was poured over the SU-8 master, degassed in a desiccator, and cured on a hotplate at 60 C. Holes for tubing connections were punched in the PDMS with a 1.5 mm biopsy punch prior to solvent degrease and oxygen plasma surface activation of both the PDMS and a glass microscope slide in a Diener Pico plasma system. Activated surfaces of PDMS and glass were brought into contact following surface activation and heated at 60-70 C on a hot plate, producing covalent bonds between the two pieces.

Fluidic Apparatus. The microfluidic lysis experiments involving whole HIV particles were performed with a fluidic apparatus which interfaced with the PDMS microfluidic chips and consisted of syringe pumps and HPLC valves built within a biosafety cabinet. Biosafety level 2+ protocols were followed.

2.4 On-chip RT-LAMP

Chip fabrication. Microchip RT-LAMP experiments employed a microfabricated silicon substrate [237]. Briefly, a silicon wafer was thermally oxidized to create a silicon oxide layer of ~150 nm. The oxide

is then patterned with photolithography and hydrofluoric acid etch step, exposing the silicon where the wells will be etched. The wafer was then immersed in a heated Tetramethylammonium hydroxide (TMAH) bath for 18 hours that anisotropically etch the silicon, creating inverted square pyramids that will be later used as reaction wells. An approximation of the dimensions of the inverted square pyramids is provided in Supplementary Information.

Chip preparation. Chips for all microchip RT-LAMP experiments were prepared in the following manner: First, the microchip was cleaned in a piranha solution containing 1:3 30% hydrogen peroxide and sulphuric acid for 10 minutes and then rinsed in deionized water. Each chip was then degreased with acetone, methanol, and isopropanol and dried by blowing with nitrogen gas. To produce a hydrophobic surface to promote stability of droplets, the chip was rinsed with Sigmacote® from Sigma-Aldrich by pipetting the solution repeatedly over the surface of the chip. The chip was then rinsed briefly with isopropanol, dried by blowing with nitrogen, and placed in a copper bowl.

Microinjection. A Narishige IM-300 Microinjector with Eppendorf VacuTip microinjection holding capillary (15 μm inner diameter, 100 μm outer diameter) was used both to spot primers and place reaction droplets. A 20 ms injection pulse was used resulting in a droplet of approximately 60 nL. The microinjection procedure was performed after chip cleaning and preparation as follows: LAMP DNA primers in TE buffer were diluted in water to the final reaction concentration. Droplets were placed in all 36 wells of the microchip array using the microinjection system and a 3D micromanipulator (MCL-D331) from World Precision Systems. The process was visualized with a Leica MZFLIII microscope. Droplets containing primers were allowed to dry completely, leaving dehydrated DNA LAMP primers in the reaction wells. Following visual confirmation that all droplets had dehydrated, the chip was submerged in heavy mineral oil (Fisher) and placed in a desiccator to remove air bubbles. The primary function of the mineral oil is to protect the reaction droplets from evaporation during heating at 65 C.

During degassing, the primer-less RT-LAMP reaction was prepared and transferred to the microinjection capillary. Reaction droplets were then placed in each well by lightly contacting the bottom of each reaction well, injecting a droplet of approximately 60 nL, and lifting the capillary out of the oil. The

chip containing all 36 droplets submerged in oil in the copper bowl was then transferred to the heating stage and imaging apparatus (fluorescence microscope or smartphone apparatus).

Primer spotting and reaction droplet placement for the integrated experiment was performed in the same manner but within a biosafety cabinet under a Leica EZ4D microscope with built-in camera providing a live video feed to a PC.

Fluorescence Microscopy

Fluorescence microscopy images were captured with a Nikon Eclipse FN1 fluorescence microscope with a 2X objective and Nikon 96311 B-2E/C FITC fluorescence filter. NIS Elements software was used to capture fluorescence images for RT-LAMP reactions containing purified RNA in water with 6.3x gain and 1 second exposure time. Additional measurements (presented in Supplementary Information) with lysed whole blood spiked with viral RNA imaged with the microscope required 8x gain and 2 second exposure times to compensate for decreased overall fluorescence intensity.

Smartphone Imaging

Apparatus. A Samsung Galaxy Note 4 smartphone was purchased for imaging of the RT-LAMP reaction on the microchip substrate. The smartphone hardware was not modified from its factory conditions. A Thorlabs 530 nm Longpass Colored Glass Filter was placed between the camera and the chip to isolate the fluorophore emission wavelengths. A 3D-printed cradle (**Figure 5.1**) was designed to position the smartphone horizontally with the camera directly above the microchip. A mounting cylinder was also 3-D printed to hold an Opto Diode Corp high-output blue LED and Thorlabs Shortpass Filter with 500 nm cut-off wavelength, which fit within the cradle and illuminated the microchip from an angle. The LED was powered with 3 volts from an Agilent E364xA DC power supply with automated on/off function controlled with a MATLAB script. It was also determined that the Blue LED could be adequately powered by a standard 3V lithium coin battery, but the DC power supply was used for the purpose of PC control.

Software. Due to biosafety considerations, the entire smartphone imaging apparatus was placed inside a biosafety cabinet for performing integrated measurements. For this reason, remote control of the imaging function was desired. The Android application IP Webcam [238] was downloaded from the Google Play store and installed on the smartphone. This application transmits a live image over the network which can be viewed in real-time in a web browser. The browser interface allowed for control of the smartphone camera's focus, exposure, and gain. Imaging of the RT-LAMP reaction was performed with the following parameters set in the IP Webcam web browser interface: 8X zoom, 99% stream quality, exposure compensation of 4, and "Night vision" function with a gain of 10.00 X and exposure 10.

A MATLAB script was written to automate the image capture process. The script was initialized simultaneously with the activation of the heating stage. The MATLAB script imaged the reaction in the following manner: blue LED was switched on, delay 3 seconds, capture image from IP Webcam web browser interface, delay 2 seconds, and finally switch off blue LED. This process was repeated every 30 seconds while each reaction was imaged.

Data Analysis

Image analysis. Images recorded with fluorescence microscopy or the smartphone imaging apparatus were saved as TIFF (microscope) or JPEG (smartphone) files and fluorescence intensity was analysed. For this analysis, the physical location of each droplet was identified manually in a MATLAB script by importing and displaying the image in a MATLAB figure and adjusting the position of square boxes outlining each droplet. Grayscale TIFF images were imported as a matrix of 16-bit unsigned integers (range 0-65,535) representing each pixel in the image. Grayscale JPEG images were imported as an array of 8-bit unsigned integers (range 0-255) representing each pixel in the image.

Following manual identification of droplet positions, a MATLAB script automated the analysis of each droplet by averaging the numerical value of all pixels within the region defined by the box outlining each droplet. Absolute numerical values are a function of the range of integer values (8-bit or 16-bit), as well as the exposure time and gain of the camera, ambient light in the laboratory, and other factors. For this reason,

the baseline is subtracted from each measurement as described below, and fluorescence measurements in this paper are presented in arbitrary units (AU).

Threshold time analysis. Threshold time was determined from raw fluorescence data on all platforms. First, the baseline was removed by subtracting an early fluorescence measurement from all subsequent measurements. For all thermocycler measurements and the microscope measurements with purified RNA in water, this was the first fluorescence value or image recorded. For smartphone measurements, auto fluorescence of whole blood at room temperature was observed to decrease quickly upon initial heating of the chip. Thus, the baseline was defined to be 90 seconds after initialization of the heating, or the third image recorded by the smartphone.

Threshold time for each individual reaction was approximated from baseline-subtracted fluorescence curves by determining the measurement n at which the signal exceeded 20% of the maximum fluorescence value it achieved during the course of the entire measurement. After determining n, a linear fit was determined by the fluorescence values I_n and I_{n-1} in the form $I(x) = mx+b$ and the threshold time $T_t = (0.2*I_{max}-b)/m$ was determined.

RESULTS

Characterization of RT-LAMP in a benchtop thermocycler

Purified viral RNA in water. The first experiment, presented in **Figure 5.2a-b**, was performed to characterize the RT-LAMP reaction with purified analyte in a standard thermocycler apparatus. HIV-1 IIIB RNA was purified by two different methods as described in the experimental section. RT-LAMP fluorescence curves for the first method are shown in **Figure 5.2a**, and the calculated threshold time versus average number of viruses in each reaction is shown in **Figure 5.2b**. Linear fits to threshold time vs. log of

viruses showed a difference in slope of less than 1.3%, but a vertical offset of more than 4 minutes in the in the y-intercept.

Comparison with lysed whole blood. The next experiment compared threshold time and fluorescence intensity of RT-LAMP containing 9,380 whole virus particles of HIV-1 IIIB in lysed blood to the corresponding amount of purified HIV-1 RNA in water as an initial test of the feasibility of RT-LAMP in lysed whole blood. Fluorescence measurements are shown in **Figure 5.2c** and bar charts comparing threshold time and maximum fluorescence value are in **Figure 5.2d**. Six replicates were performed of each of the two conditions, and the average threshold time in lysed blood varied by less than 2.3% compared to RNA in water and gave a p-value of 0.0755 in a standard two-sample t test. The maximum overall fluorescence intensity (determined from raw fluorescence measurements with baseline subtracted) showed a decrease in fluorescence signal of 88.93% in lysed whole blood compared to purified RNA in water.

Standard curve in lysed whole blood. An experiment with whole virus particles at a range of concentrations was then performed to characterize the RT-LAMP reaction on an ideal platform but with minimally-processed sample. **Figure 5.2e** (fluorescence curves) and **Figure 5.2f** (threshold time vs. virus number) show that even with ten-fold reduced overall fluorescence intensity, amplification curves could still be observed and threshold times analysed. A linear fit to the threshold time vs. log of virus number gives a slope comparable to purified RNA curves (10.3% difference compared to method 1 and 9.1% difference compared to method 2 in **Figure 5.2b**). Due to inconsistent amplification of all replicates, the 9.4 vp/RXN sample is not included in the threshold time curve. Further characterization of the lysed whole blood RT-LAMP reaction was performed by examining variations on the ratio of blood sample to lysis buffer. Results are provided in Supplementary Information.

Microfluidic blood lysis module

On-chip lysis in a microfluidic channel was independently characterized to determine the potential for automated sample handling and characterize any impact of the microfluidic mixing on the overall method. Whole blood samples spiked with three different concentrations of HIV-1 IIIB were each mixed with lysis

buffer in the PDMS mixing chip driven by the fluidics apparatus in a biosafety cabinet described in the Methods section. Output from the microfluidic chip was collected on three separate instances from each sample and analysed separately with RT-LAMP in a thermocycler. Triplicate RT-LAMP reactions were performed for each of the three collections, resulting in nine total RT-LAMP reactions for each virus concentration investigated. As a control, the same spiked blood samples were added to lysis buffer, mixed with a pipette, and analysed with RT-LAMP in triplicate (i.e. three control reactions total for each virus concentration). Results are shown in **Figure 5.3b**. Mean threshold times differed from the manually-pipetted control by 0.85%, 3.88%, and 8.21% for post-lysis virus concentrations of 1,349, 135, and 13 vp/μL respectively.

On-chip RT-LAMP

Next, the RT-LAMP reaction was demonstrated on the microchip. This included experiments with purified RNA in water (**Figure 5.4a-b**) and RNA in lysed whole blood (Supplementary Information) imaged with a fluorescence microscope before the introduction of the smartphone (**Figure 5.4c-d**). This sequence of experiments was performed to establish a basis for comparison and to limit the introduction of new variables and sources of noise in each step in the progression of the experiments. All on-chip RT-LAMP measurements were prepared as described in the Methods section with DNA LAMP primers pre-spotted and dehydrated on the chip prior to oil immersion, degassing, and reaction droplet placement.

Purified RNA in water was first characterized on the chip. **Figure 5.4a** displays fluorescence curves measured with a fluorescence microscope, while **Figure 5.4b** shows the threshold time analysis. In this measurement, data from two droplets were removed due to outlying behavior believed to be due to contamination with inhibitors or experimenter error. This includes one of six reactions in each of the 75 vp/RXN and 7.5E2 vp/RXN samples. Only two of six 7.5 vp/RXN samples amplified and as a result threshold times for this sample were omitted from the curve in **Figure 5.4b**. In **Figure 5.4c-f**, lysed whole blood spiked with viral RNA was imaged with the smartphone apparatus as described in the experimental section. Whole virus particles were not used in this measurement as the apparatus had not yet been

converted to be contained within a biosafety cabinet. **Figure 5.4c** shows fluorescence curves gleaned from the smartphone images, **Figure 5.4d** shows the threshold time analysis, and **Figure 5.4e** shows examples of the smartphone fluorescence images every minute for minutes 7-11. The 11 vp/RXN (green) and 1.1 vp/RXN (blue) samples are omitted from the threshold time curve because of insufficient amplification before 30 minutes.

Figure 5.4f shows an endpoint measurement obtained following termination of the real-time monitoring at 30 minutes. Four additional droplets (three of the 11 vp/RXN samples, one 1.1 vp/RXN sample) in the array had reacted before the image in **Figure 5.4f-i** was captured with the fluorescence microscope. **Figure 5.4f-ii** is an additional smartphone image captured shortly after the microscopy image was obtained. **Figure 5.4f-iii** is identical to **Figure 5.4f-ii** with an additional overlay color-coded consistent with the color-concentration convention used throughout this paper. The sixth column on the far right is a negative control containing blood sample and reaction mix without viral RNA.

Finally, Figure 5.4**f-iv** is a colormap rendering of **Figure 5.4f-ii** produced in MATLAB as an example of the image analysis process.

Compatibility with other viral nucleic acids

Due to the common occurrence of co-infections of HIV and viral hepatitis (HBV and/or HCV), we sought to demonstrate the compatibility of this on-chip RT-LAMP assay with such cases. Because whole virus particles were not available to us for hepatitis viruses, synthetic viral genomes of DNA (HBV) and RNA (HCV) were obtained and tested. Since limited quantities of the synthetic viral genomes were available to us, this experiment was performed in water and not lysed whole blood to avoid the ten-fold dilution of nucleic acids which would result from spiking lysed blood with viral nucleic acids and to perform the test at the highest concentration of viral nucleic acids possible.

Figure 5.5a shows fluorescence data obtained with the fluorescence microscope measurement system for on-chip RT-LAMP of three samples: HIV with and without hepatitis virus nucleic acids, and hepatitis virus nucleic acids without HIV. All twenty-four of the droplets containing HIV RNA successfully

amplified (twelve with hepatitis virus nucleic acid, twelve without), regardless of the presence of other nucleic acids. The twelve HIV-negative droplets, all containing hepatitis virus nucleic acids, did not amplify.

Figure 5.5b shows a comparison of threshold time between the two HIV RNA-containing conditions. The average threshold time for HIV-positive droplets containing hepatitis nucleic acid differed from the droplets which did not by 8.90%. A standard t-test comparing the two gives a p-value of 1.8718E-6.

Integrated experiments

Integrated experiments were designed to demonstrate the full capacity of this approach for a sample-to-answer solution to point-of-care HIV viral load quantification. The complete flow of the experiment is depicted in **Figure 5.6a**. These experiments differed from other measurements presented in this paper in that whole blood samples were spiked with whole HIV-1 IIIB virus particles (not viral RNA) at a range of concentrations and each individual sample was analysed on a separate chip. Of the 36 wells on the micro-chip array, six were used for negative controls and up to thirty were used to test the sample.

Five samples were tested (named A-E), containing approximately 32,000, 3,200, 320, 32, and 3.2 whole virus particles per reaction, respectively. Since each reaction droplet contains approximately 4.8 nl of whole blood, this corresponds to viremias in the range of $6.7 \times 10^5 – 6.7 \times 10^9$ viruses per mL of blood, or $1.3 \times 10^6 – 1.3 \times 10^{10}$ RNA copies per mL of blood plasma (assuming 45% haematocrit).

Due to biosafety considerations, the entire process was adapted as described in the experimental section to be contained within a biosafety cabinet. This introduced challenges to droplet placement, which was performed with a motorized micromanipulator controlled with a joystick and guided by a video feed from a small table top microscope. Decreased control over droplet placement led to a decreased success rate in droplet placement. As a result, not all of the thirty wells designated for a virus-positive reaction droplet were used in every measurement. The number of successfully placed droplets for samples A through E were as follows: 29, 28, 30, 22, and 22.

Figure 5.6b shows the fluorescence curves, measured with the smartphone system, for all droplets which amplified within 30 minutes. **Figure 5.6c** shows the threshold time vs. virus number. The slope of the fit to threshold time vs. virus number is -1.9993, which differs in magnitude by 57.6% compared to on-chip RNA in lysed whole blood, 34.9% compared to on-chip RNA in water, 18.5% compared to whole virus particles in whole blood in the thermocycler, and 25.9% compared to purified RNA in water (method 2) analysed in the thermocycler. A t-test was performed to compare the threshold time and significance was determined by a $p < 0.05$.

In **Figure 5.6d**, we consider a new metric, which is amplification efficiency, and observe a trend between virus number and the fraction of droplets which amplified. A framework for understanding this phenomenon in the context of digital LAMP measurements is described in the Supplementary Information.

DISCUSSION

Characterization of RT-LAMP in a benchtop thermocycler

Purified viral RNA in water. In the initial thermocycler characterization of this RT-LAMP reaction, we have presented a comparison of two methods of viral RNA purification in order to 1) establish a baseline for a "clean" reaction signal, and 2) highlight possible factors which may contribute to variations in RT-LAMP results in subsequent analyses.

While the two independent experiments measuring purified RNA in water differ in the manner in which dilutions were performed (before RNA purification in method 1 and after RNA purification in method 2), they also differ in betaine content (0.8 M in method 1, 0.4 M in method 2). After initial measurements, betaine concentration was decreased in order to allow for a larger fraction of the reaction volume to consist of sample. One initial hypothesis was that betaine, which contains a cation and reduces secondary structure formation in DNA, may explain the difference in the two standard curves. However, a careful comparison was performed in which RNA at various low concentrations was added to a common mastermix containing

0.4 M betaine and, in half of the reactions, additional betaine was added to achieve 0.8 M concentration. The results of this control experiment (see Supplementary Information) indicated no difference in the threshold time nor the amplification efficiency at lower concentrations. Therefore, other factors likely explain the vertical offset in the purified RNA experiment in the thermocycler.

We suspect that these differences may include variations in enzyme concentration due to inherent variation in the pipetting process when preparing mastermixes, time-related decrease in enzyme activity (the two experiments were performed several weeks apart and enzyme activity may have decreased with freeze-thaw cycles of the reagent, or variations in ambient temperature and other factors. Additionally, degradation of RNA over time during storage may have decreased the yield of the samples used in method 2 and variations due to manual pipetting may contribute to discrepancies between the actual RNA concentrations gleaned from the two independent purification procedures.

While these factors are important considerations, we chose at this time to acknowledge their potential effects and the need to minimize variation and establish rigorous controls in future experimental or manufacturing processes. Viral RNA stability or yield from the RNA purification process would not affect the results of experiments using whole virus particles. Subsequent analysis involving purified viral RNA or viral RNA spiked in whole blood employed RNA from a third, "fresh" purification identical in protocol to purification method #2. The purified RNA from this process was aliquoted and frozen at -80 C and thawed only immediately before using in an experiment to minimize degradation of the sample between experiments.

Comparison with lysed whole blood. To our knowledge, a quantitative RT-LAMP measurement of HIV concentration in whole blood processed only by mixing with a cell lysis buffer has not been described previously in literature. These thermocycler results with whole virus particles spiked in whole blood and mixed with cell lysis buffer suggest the possibility of quantifying virus concentration simply based on reaction kinetics.

The decrease in overall fluorescence intensity indicates that there are fluorescence-quenching components in the lysed whole blood sample. However, because the threshold time is identical for purified

RNA compared to whole blood, we can conclude the whole blood does not affect the amplification efficiency. This is a very promising development, given that a major challenge to most point-of-care diagnostics is the process of isolating analyte from complex biological samples in the absence of controlled environments, skilled technicians, or laboratory instruments [239]. In this case, blood cell lysis is an extremely simple processing step compared to more complicated techniques that have been described [201].

Microfluidic blood lysis module

One goal of this paper is to demonstrate the potential for a fully-automated RT-LAMP viral load test from a drop (i.e. finger prick) of whole blood. This requires complete on-chip sample processing from that whole blood drop, which has traditionally been a major barrier for many point-of-care diagnostics approaches. Despite the popularity of PDMS prototyping in this field, many microfluidic and lab-on-a-chip techniques suffer from the ability to translate PDMS devices to commercially viable forms compatible with injection molding and other mass-manufacturing techniques [240]. The converse is also true: that designs compatible with manufacturing may be difficult to prototype in PDMS when some properties (e.g. surface-fluid contact angle) are not comparable. Here we demonstrate valve-assisted sample metering and microfluidic mixing which resembles a method we are aware to be employed in commercial-grade platforms for blood sample handling.

Volumetric metering begins with a drop of blood of unspecified size from which 10 μL is precisely metered in a holding coil with an inner diameter of 203.2 μm, reminiscent of commercial microfluidic cartridges which employ volumetric metering. Viable methods have also been employed for fluid mixing in commercial microfluidic designs, making our simple serpentine channel prototyped in PDMS a reasonable design [168].

Data in **Figure 5.3b** demonstrate that this simple approach of volumetric metering with serpentine channel mixing of blood with lysis buffer is compatible with the downstream RT-LAMP analysis. The results from three separate collections show that the method produces an accurate mixing ratio, and that the on-chip mixing is at least as consistent as manual pipetting.

On-chip RT-LAMP

Purified RNA with fluorescence microscope imaging. It is unclear what absolute conclusions can be gleaned from comparison of the fit to threshold time vs. log of virus number in **Figures 2b and 4b**. The slope of the fit is smaller in magnitude for the on-chip measurement, suggesting that there may be some chip-related factors leading to decrease in sensitivity for quantification of virus number by threshold time analysis. This observation prompted increasing the frequency of images from 60 seconds (used in thermocycler and microscope measurements) to 30 seconds (used in smartphone measurements).

The y-intercept of the fit in **Figure 5.4b** is also significantly smaller compared to those in **Figure 5.2b** (14.68 min vs. 29.1 and 33.3 min), suggesting that the smaller droplet size may contribute to a more rapid RT-LAMP reaction, a phenomenon that has been discussed elsewhere [241]. This may be leveraged toward achieving the end goal of a rapid viral load test.

Lysed whole blood with smartphone imaging. Data from lysed blood measurements imaged with the smartphone demonstrate two significant steps toward the goals of this paper. The replacement of laboratory hardware (e.g. thermocycler fluorescence detection or fluorescence microscope) with a common smartphone is a core aspect of the novelty of this paper. First, it demonstrates that the lysed blood RT-LAMP measurement can be performed with existing mobile technology that is at least as affordable as a high-end smartphone. Furthermore, trends suggest that mobile communications technologies will continue to improve in capabilities and decrease in cost, an exciting outlook for fluorescence and other optics-based point-of-care diagnostics. Second, our platform, consisting of a 3-D printed platform, LED light source, emission filter, and small form-factor heating stage suggests that, if adequately robust, an add-on component may be developed as an attachment to existing smartphones, shifting the computation and imaging burden from components integrated with the diagnostic platform to a consumer item that is becoming ubiquitous, even in resource-limited settings [242]. This could significantly reduce the production and deployment costs of such a technology.

Compatibility with other viral nucleic acids

Anticipating co-infection with other bloodborne viruses may be important for practical HIV nucleic acid tests, since the incidence of co-infection with HIV and one or more other viruses is high, particularly in populations of intravenous drug users [21], [243]. We have demonstrated, most significantly, that the hepatitis viral nucleic acids at high concentrations (equivalent of approximately 1.6×10^3 of each virus per 60 nL reaction) in purified form do not amplify in the RT-LAMP assay designed for HIV.

More detailed analysis gives a p-value of 1.8718E-6 from a standard t-test, indicating a significant decrease in threshold time for the sample containing nucleic acid from all three viruses versus the sample containing only RNA from HIV. This indicates a need for more rigorous characterization of this phenomenon in future work. One explanation for a decreased threshold time is the presence of hepatitis B genome, which is a circular, partially double-stranded DNA, at a relatively high concentration (approximately 1,600 copies/RXN). This may produce an effect not seen in whole blood, since mature erythrocytes do not contain DNA, and our simulated co-infected sample would contain a new source for signal from dsDNA intercalating dye. Leukocytes in the lysed whole blood sample would be very rare (a few per nanoliter of blood), and genomic DNA from these sources may be packaged and largely inaccessible to the dsDNA dye. Because no amplification was observed in the HIV-negative, HBV/HCV-positive samples, we consider it unlikely that HCV RNA or HBV DNA is acting as a non-specific template for LAMP and producing incorrect reaction products.

Integrated experiments

Our integrated experiments demonstrate the capacity of the test for quantitative viral load measurements based on reaction kinetics or digital statistical methods. The slope of the fit to the threshold time plot in **Figure 5.6c** is comparable to the original characterization performed in **Figure 5.2**, suggesting that the integrated approach has the capacity to be quantitative – and perhaps can be demonstrated to have greater sensitivity upon optimization of reaction chemistry, incubation temperature, and other factors. Bars showing differences that are statistically significant between concentrations indicate the resolution of the integrated test performed here at a 95% confidence level.

Clearly several factors need to be improved and addressed to move toward a fully-automated platform. The experiment flow described in **Figure 5.6a** consists of several components compatible with a point-of-care, microfluidic cartridge-based *in vitro* diagnostic platform: volumetric metering of 10 μL of whole blood, microfluidic sample processing, nanoliter-size reaction droplets, silicon chip substrate, and smartphone fluorescence imaging. The process described here does, however, includes a manual step transferring lysed blood from the microfluidic module, mixing with primer-less RT-LAMP mastermix, and placing droplets onto the chip.

We believe the issues requiring this handling step can be addressed by common industry methods not easily demonstrated in the research lab, such as sample distribution into nanoliter-scale reaction well. [244]. The issue of the addition of reaction components to the sample could be addressed by lyophilisation or freeze-drying reagents which are then re-hydrated by the sample. Lyophilized LAMP mastermixes have been described [245], [246]. Additionally, we have observed that while air-drying reaction components other than primers was problematic on our current platform, the RT-LAMP mastermix used here can be lyophilized in a commercial freeze-drier in 0.2 mL reaction tubes (see Supplementary Information), and that amplification capabilities are retained. We did not have the equipment available to attempt this on-chip.

Quantification by threshold time

The measurements presented here exhibit a trend in threshold time vs. virus number which suggests that a kinetic measurement based on the time it takes an array of droplets to react may be a suitable method to quantify viral load, though the limits of the resolution are still to be determined in an improved platform. For this approach, the sensitivity of the reaction, determined by the slope of the fit to threshold time vs. virus number, may need to be increased by optimizing the reaction, including enzyme and buffer concentrations or incubation temperature. Additional optimization would need to be performed to improve (lower) the lower limit of detection of the reaction.

While these improvements may be made, a lysed whole blood approach will be inherently limited in its capabilities by the reaction volume and dilution factor in lysis buffer. For this reason, an variation on the approach involving digital LAMP may be considered.

Quantification by digital LAMP

Digital LAMP and PCR approaches have been widely described in the literature [236], [247]–[252]. The primary advantage of a digital approach is that it relies only on an endpoint measurement – whether a reaction of small volume amplifies or not – from which concentration can be approximated by measuring hundreds, thousands, or millions of droplets. The approach we describe here could be scaled-up for digital LAMP by constructing large arrays of droplets with an automated distribution method.

The upper and lower limits of viral load detection in a digital approach are defined by the number of individual reaction droplets and the total volume of the sample tested. Since the distribution of viruses in reaction droplets is governed by Poisson statistics, we have briefly reviewed these principles in the Supplementary Information for this paper to demonstrate the theoretical utility in clinical HIV management of a scaled-up platform which tests a finger prick of whole blood. For example, a digital LAMP approach requiring just 9 μL of whole blood would be capable of indicating viral loads lower than 500 mL^{-1} of whole blood, with much greater accuracy in the range of 10^4–10^6 mL^{-1} (see Supplementary Information). While this cannot compete with the technical specifications of state-of-the-art systems (lower limit < 10 mL^{-1}), it would be of practical value, such as showing declines in viremia following a drug regimen change or identifying cases of viral rebound in settings where the gold standard is inaccessible [253]. The capacity of this platform as a digital LAMP test increases with larger sample sizes and increased number of reaction droplets.

CONCLUSIONS

In performing these experiments and the preparation of this manuscript, the challenge of finding a sample-to-answer point-of-care HIV viral load quantification solution was viewed as two parallel objectives: (1) sample processing, which traditionally involves isolating or enriching the analyte from its complex matrix, and (2) analyte detection. We broadly considered various approaches to sample processing which might be integrated with a microchip LAMP approach, many of which were guided by the notion that the presence of cellular material is not compatible with nucleic acid amplification methods. Many of these approaches resulted in dilution of the analyte by a factor of ten or more, while our approach results in a dilution by only a factor of five prior to the addition of LAMP reagents with one simple and easily-implemented processing step that neither purifies nor enriches. This is a key merit of this approach which can significantly reduce complexity and cost for a point-of-care device.

The measurements presented here demonstrate that an RT-LAMP quantification approach is indeed compatible with minimally-processed whole blood. To our knowledge, RT-LAMP in lysed whole blood has only been employed by one group, which performs a non-quantitative measurement in a reaction tube on a portable heating device [233]. We demonstrate quantitative detection with the ability to resolve 10-fold changes in concentration above 6.7E4 μL^{-1} and 100-fold changes in concentrations above 670 μL^{-1}. We observed 60 nL droplets with as few as 3 viruses per reaction amplify, which corresponds to a whole blood virus concentration of 670 μL^{-1}. We also discuss that the true power of this approach may be in a quantitative digital LAMP format rather than a kinetic measurement. Our implementation of the lysed whole blood approach in a microchip format with mobile phone imaging represents a significant stride toward a practical solution to viral load measurements in resource-limited settings.

SUPPLEMENTARY INFORMATION

Cell lysis buffer ratio

Methods. For measurements comparing the ratio of blood to lysis buffer, RT-LAMP was performed in the thermocycler with identical mastermixes containing reaction buffers, enzymes, and primers, but where the sample portion consisted of various ratios by volume of whole blood to lysis buffer: 1:4, 1:2, 1:1 or 1:0. Viruses were spiked into lysed blood following the mixing to keep the virus concentration identical between samples.

Results. Threshold time is shown in Figure 5.8a with the 1:0 case omitted (which did not exhibit amplification). Results showed differences in threshold time compared to 1:4 of 0.59% and 1.03% for 1:2 and 1:1, respectively, at 670 vp/RXN and a difference in threshold time compared to 1:4 of 0.97% and 3.09% for 1:2 and 1:1, respectively, at 67,000 vp/RXN. A standard t-test produces p-values compared to 1:4 for 1:2 and 1:1, respectively, of 0.9247 and 0.8444 at 670 vp/RXN, and 0.1604 and 0.0138 at 67,000 vp/RXN.

Figure 5.8b compares the average maximum baseline-subtracted fluorescence intensity of each condition, demonstrating the trend of increased quenching of fluorescence as absolute blood content increases. In this case, the bar for 1:0 (no lysis) condition represents merely the fluctuation of noise, as no amplification was observed in these samples.

Following this characterization, tests were performed to determine if samples prepared at 1:2 or 1:1 ratios of blood to lysis buffer could be adequately imaged on-chip with the fluorescence microscope imaging apparatus. This proved problematic, however, and subsequent lysed blood measurements were performed at the 1:4 ratio.

Discussion. The characterization of blood to lysis buffer ratios confirms that the reduction of fluorescence signal seen in lysed blood versus purified RNA is related to a blood component and not a component of the lysis buffer, and demonstrates a trend of increasing fluorescence quenching with increasing blood content. Initially, it was thought that decreasing the volume of lysis buffer relative to whole blood sample may allow for larger volumes of sample to be employed in the 25 μL or 60 nL reactions, and therefore increase the detection limit of our platform with respect to the viremia of the original sample.

Deviating from the lysis buffer ratio described in Curtis, *et al*. [233], however, proved to be problematic on-chip due to inadequate fluorescence intensity in the microscopy imaging and we decided to maintain the 1:4 ratio for subsequent experiments.

The observation that blood concentration affects the fluorescence intensity suggests that one or more components of the lysed blood has a diminishing effect but does not completely quench the fluorescence signal except for when no lysis is performed, while the lack of effect on threshold time suggests that blood components do not interfere with reaction kinetics. This is a critical result for quantification of the sample based on reaction kinetics to be possible.

Betaine concentration in RT-LAMP reaction

Initial experiments were performed with 0.8 M betaine based on the concentration in Curtis, et al.[233] However, at a stock concentration of 5 M, the betaine reagent occupied 4 μL of the 25 μL reaction – more than any other single reagent. In order to include a greater volume of sample in each reaction, we cut the betaine concentration to 0.4 M, a reaction concentration also seen in the literature [254]. We performed a control experiment to determine if the change in betaine concentration would have any significant effect on the lower limit of detection. Figure 5.9 shows the raw fluorescence curves from this test, which was performed with low concentrations of purified viral RNA in water. In this test, faster threshold times are observed in 0.4 M betaine compared to 0.8 M betaine. For the smaller concentration (average of 4 viruses per reaction), 1/3 reactions amplified in the 0.4 M betaine condition while 2/3 reactions amplified in the 0.8 M condition. While this is not a thorough characterization of the effects of betaine, we consider it adequate indication that the effect of betaine is not significant.

Lysed-blood microchip LAMP with microscope imaging

A microchip RT-LAMP experiment with lysed whole blood spiked with viral RNA was performed and imaged with the fluorescence microscope as described in the main text. Fluorescence curves and threshold time curve are shown in Figure 5.10. This experiment was an intermediate step between microchip LAMP

with purified RNA in water imaged with a microscope and RNA-spiked lysed whole blood imaged with the smartphone. The data is provided here for thoroughness.

Lyophilization of RT-LAMP reagents

To determine whether RT-LAMP reagents could be prepared with a freeze-drying method, we prepared RT-LAMP mastermix containing buffers, enzymes, primers, and intercalating dye. The mastermix was aliquoted into 0.2 mL reaction tubes and frozen at -20 C overnight. Four of the frozen reactions were left in the freezer, while 8 were kept on ice and transferred to a 2L Labconco Freeze Dry System. The samples were left in the freeze drier for 5 minutes after the chamber reached full vacuum, after which the system was vented and the samples were kept slightly below ambient temperature for several hours. Fresh RT-LAMP reactions were then prepared and compared to the frozen mastermixes (kept at -20 C throughout) and the freeze-dried reagents. Results are depicted in Figure 5.11. Of 8 freeze-dried mastermixes, one did not amplify while another showed delayed amplification. Six of eight reactions amplified in a reasonable time, though threshold time was delayed and less consistent compared to fresh or frozen mastermixes.

We consider this a promising initial test demonstrating the feasibility of freeze-drying RT-LAMP reagents. This protocol was not compatible with on-chip reactions, in which 60 nL droplets evaporated rapidly when exposed to air.

Statistical model for digital droplet LAMP

The distribution of viruses in small droplets as performed in our method and any digital PCR or LAMP process is a binomial distribution in which the probability of a "success" is defined by Poisson statistics [249], [255], [256]. Determining the virus concentration from the number of positive droplets in the assay can therefore be calculated by Equation 1 [249], [257]:

$$N\lambda = N \ln\left(\frac{N}{N-x}\right) \quad (1)$$

Where N is the total number of droplets, λ is the average number of viruses in a droplet, and x is the number of positive droplets. The concentration of viruses, therefore, is determined by dividing both sides of Equation 1 by the volume of the sample.

$$c = \frac{N \ln\left(\frac{N}{N-x}\right)}{v} \quad (2)$$

The uncertainty of this measurement can be determined by calculating a 95% confidence interval ($\alpha = 1.96$), the classic form of which is:[252], [257]

$$CI = p \pm \alpha \times \sqrt{\frac{p \times (1-p)}{N}} \quad (3)$$

where p is the proportion of PCR reaction which amplified (x/N).

However, Shen, et al. employ a more sophisticated calculation of confidence intervals based on the so-called "Wilson" method:[252]

$$CI = \frac{p + \frac{\alpha^2}{2 \times N} \pm \alpha \times \sqrt{\left(\frac{p \times (1-p)}{N} + \frac{\alpha^2}{4 \times N}\right)\Big/_N}}{1 + \frac{\alpha^2}{n}} \quad (4)$$

To illustrate this, we will consider a practical "finger prick" test scenario, where a 10 µL sample is obtained and assume 90% of the sample is distributed into our RT-LAMP droplets (60 nL total volume, of which 4.8 nL comes from blood), while 10% is lost to dead volume in the microfluidics.

$$v = 0.9 * 10\ \mu\text{L} = 9\ \mu\text{L}$$

$$N = \frac{9\ \mu\text{L}}{4.8\ \text{nL}} = 1{,}875$$

As an example, if 19 of the 1,875 amplify, Equation 4 produces a confidence interval:

$$\left(\frac{x_{high}}{N}, \frac{x_{low}}{N}\right) = (0.0065, 0.0158)$$

Solving Equation 2 for high and low values of x gives us the range of viral loads that this result (19 positive droplets) represents: 1.36 x 10^3 vp/mL to 3.31 x 10^3 vp/mL.

Examining low values for p (Figure 5.12) demonstrates the increasing uncertainty of the digital method as extremes are approached. The 95% confidence interval calculated by the Wilson method indicates an upper limit of 426 mL^{-1} in the case that no droplets amplify in a valid test. One positive droplet of 1,875 corresponds to viral loads in the range 20 – 629 mL^{-1}.

While digital LAMP from a finger prick of blood cannot rival state-of-the-art tests (lower limit of detection of 10 mL^{-1} in plasma, about 5 mL^{-1} in whole blood), it does offer a working range which would be useful in remote settings where no alternative viral load measurement method is available.

FIGURES

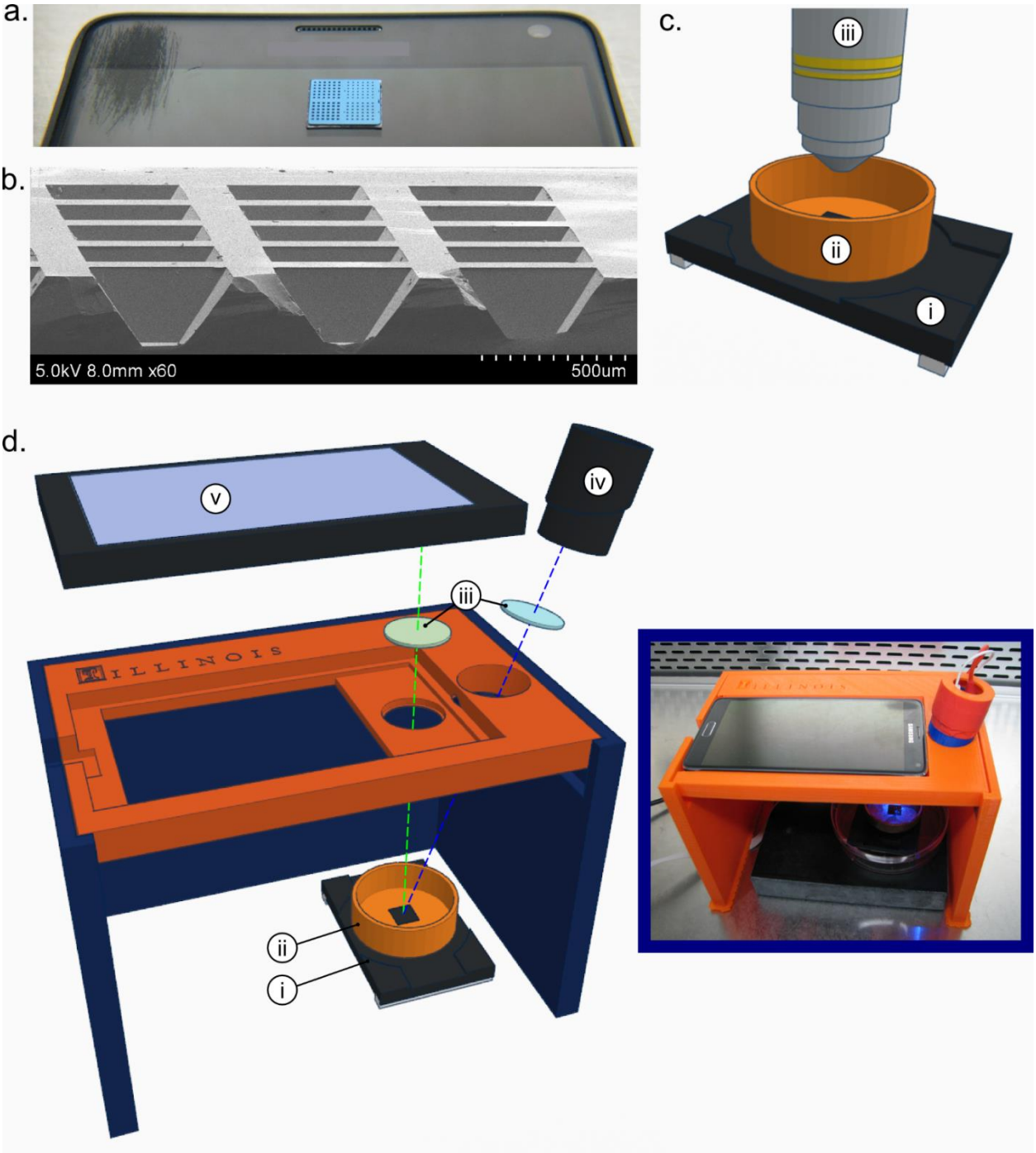

Figure 5.1. RT-LAMP substrate and smartphone apparatus. (a) Image of 1 cm x 1 cm silicon microchip substrate sitting on Samsung smartphone. (b) Scanning electron microscopy cross-section of 160 µm-deep reaction wells. (c) Schematic of microchip and heating stage in fluorescence microscope apparatus, including (i.) Heating stage, (ii.) Copper base containing mineral oil, (iii.) Fluorescence microscope objective. (d) Expanded diagram of smartphone LAMP apparatus including: (i.) Heating stage, (ii.) Copper base containing mineral oil, (iii.) Wavelength filters placed in front of LED and smartphone camera (iv.) Blue LED light source, (v.) Smartphone. (d-inset) Image of apparatus assembled in biosafety cabinet.

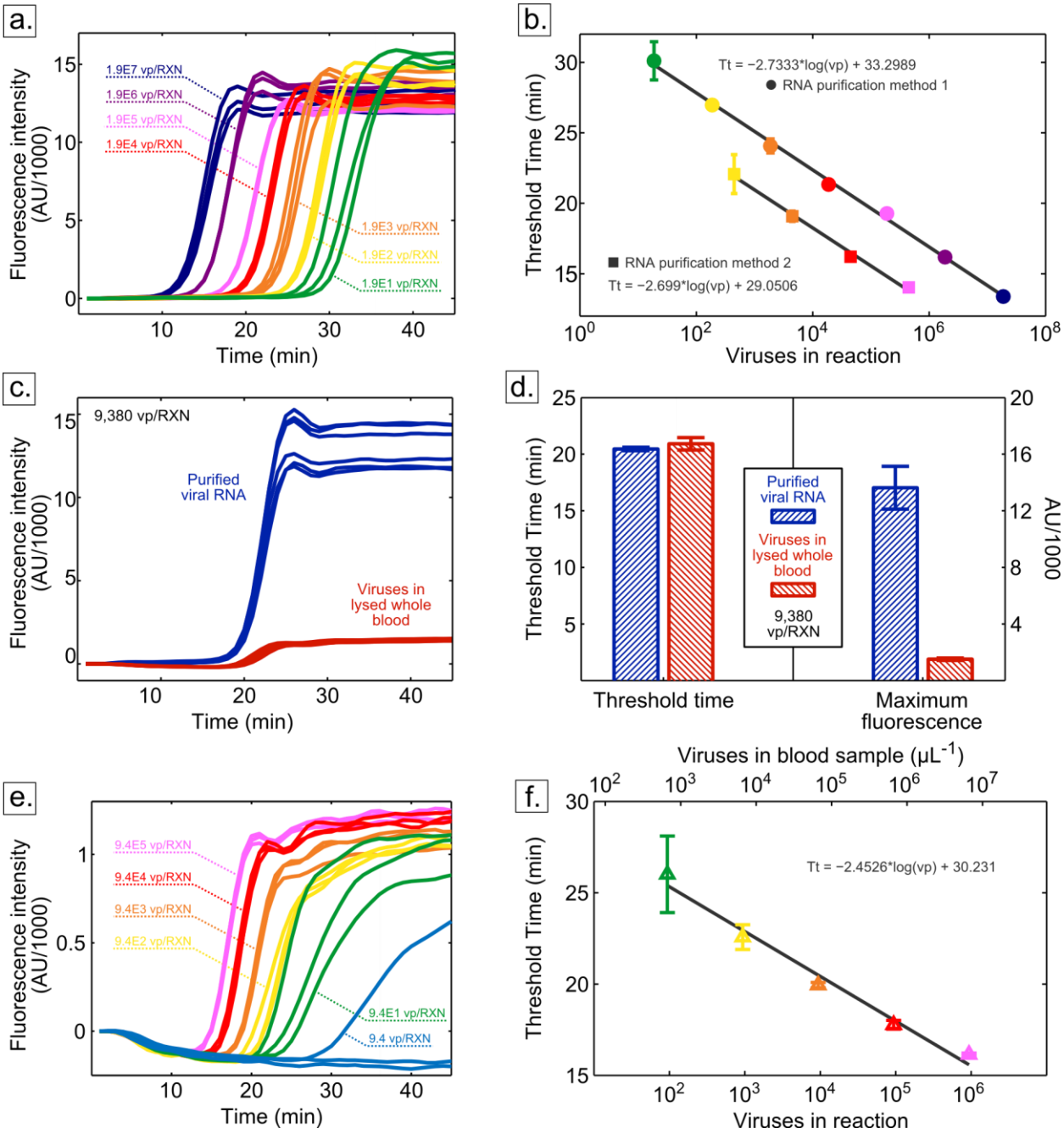

Figure 5.2. Reverse transcription loop-mediated isothermal amplification (RT-LAMP) performed in a standard benchtop thermocycler. (a) Raw fluorescence data for RT-LAMP of viral RNA diluted and purified from dilutions of whole HIV-1 IIIB virus particles (RNA purification method 1). (b) Threshold time curves determined by calculating the time at which fluorescence curves exceed 20% of their maximum value. Data are included for both methods of producing purified viral RNA. (c) Fluorescence curves from six replicates of each condition comparing RT-LAMP in virus-spiked whole blood versus purified RNA. All reactions contained the equivalent of 9,380 virus particles. (d) Comparisons of threshold time and overall fluorescence intensity for both conditions. (e) Fluorescence curves and (f) standard curve for RT-LAMP with HIV-1 IIIB whole viruses spiked in whole blood. The 9.4 vp/RXN sample is not included in (f) due to inconsistent amplification of all replicates.

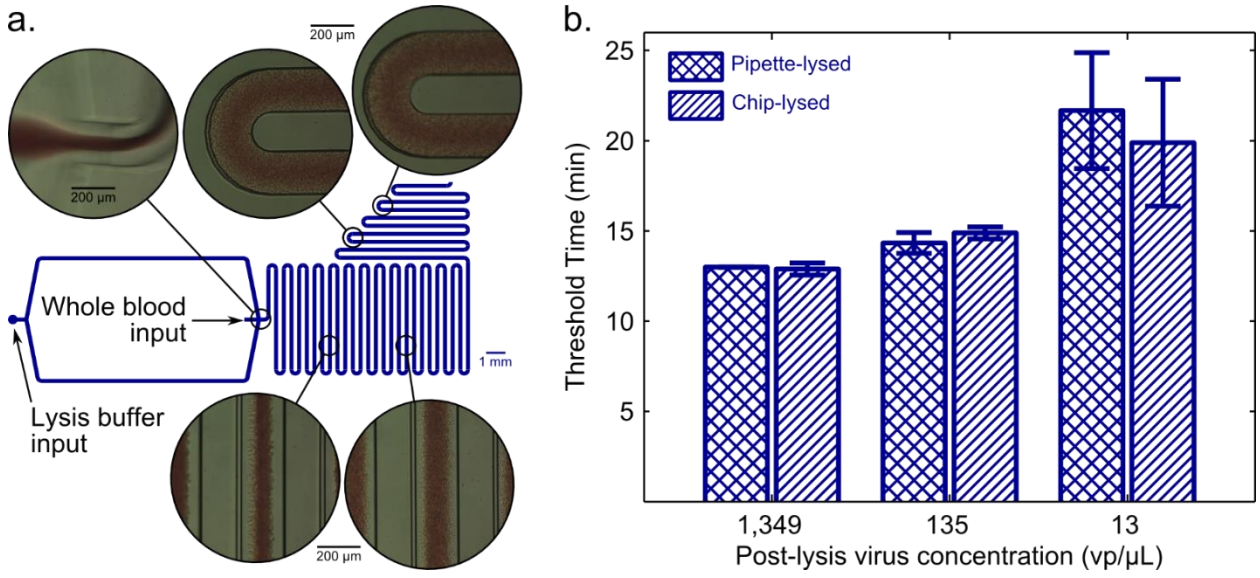

Figure 5.3. Microfluidic lysis of whole blood samples. (a) Diagram of microfluidic device with bright-field microscopy at various points in the channel and their approximate locations indicated. (b) Comparison of threshold time at three virus concentrations for chip-lysed vs. pipette-lysed samples containing whole virus particles. These data verify that the microfluidic lysis method does not result in significant differences in signal compared to the manual method.

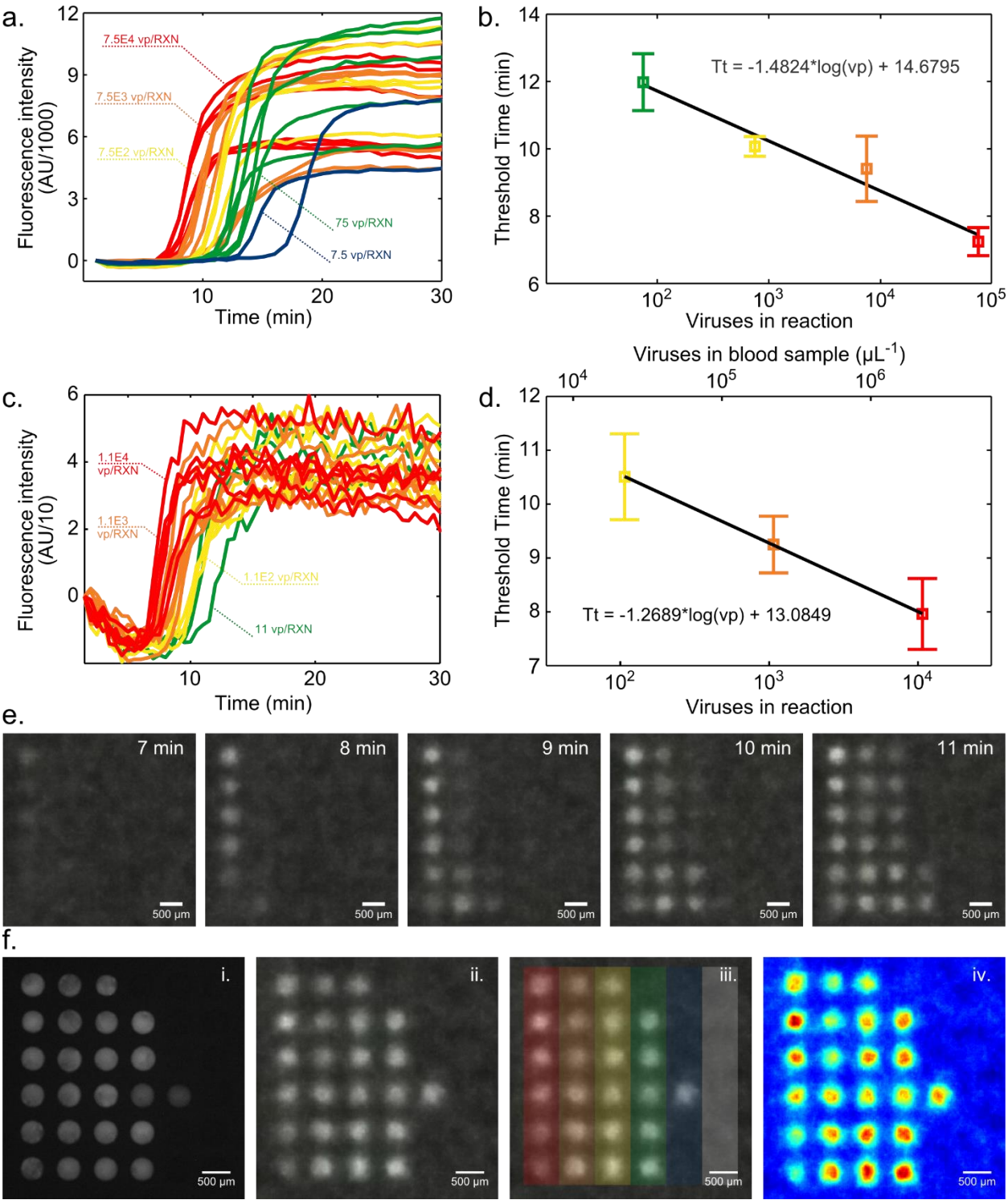

Figure 5.4. On-chip RT-LAMP for HIV-1 IIIB. (a) Baseline-subtracted fluorescence intensity and (b) threshold time versus virus concentration for purified RNA in water on the micro-well substrate imaged with fluorescence microscope. (c) Baseline-subtracted fluorescence intensity and (d) threshold time versus virus concentration for RNA-spiked lysed whole blood on the micro-well substrate imaged with the smartphone camera. (e) Fluorescence images captured by the smartphone showing the amplification of four RNA concentrations. (f) Endpoint measurements of the same chip in (c-e) showing (i.) fluorescence microscopy, (ii.) smartphone image, (iii.) color overlay indicating concentrations (gray bar indicated negative controls). (iv.) Fluorescence intensity colormap created in MATLAB in process for quantifying intensity in images.

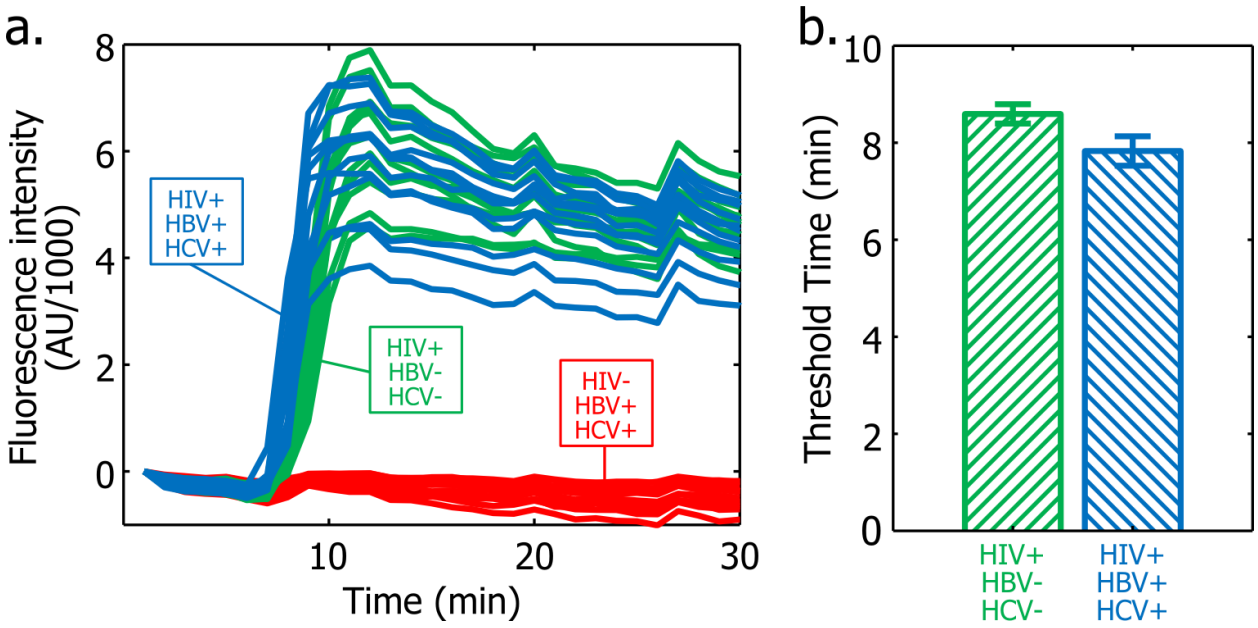

Figure 5.5. Demonstration of compatibility with common co-infections. The HIV-1 on-chip RT-LAMP reaction was tested in the presence of Hepatitis B and C viral nucleic acids at concentrations equivalent to 1.6 x 10^3 of each virus per 60 nL reaction. LAMP primers for HIV-1 detection were dehydrated in each well of the microchip array and purified nucleic acids in water were prepared in various combinations with primer-less RT-LAMP mastermix. The chip was immersed in mineral oil and placed under a fluorescent microscope on a heating stage at 65 C. (a) Fluorescence measurements from fluorescence microscopy chip of three combinations: HIV+HBV-HCV-, HIV+HBV+HCV+, and HIV-HBV+HCV+. (b) Bar chart comparing threshold time for HIV RNA-positive samples with and without hepatitis virus nucleic acid present.

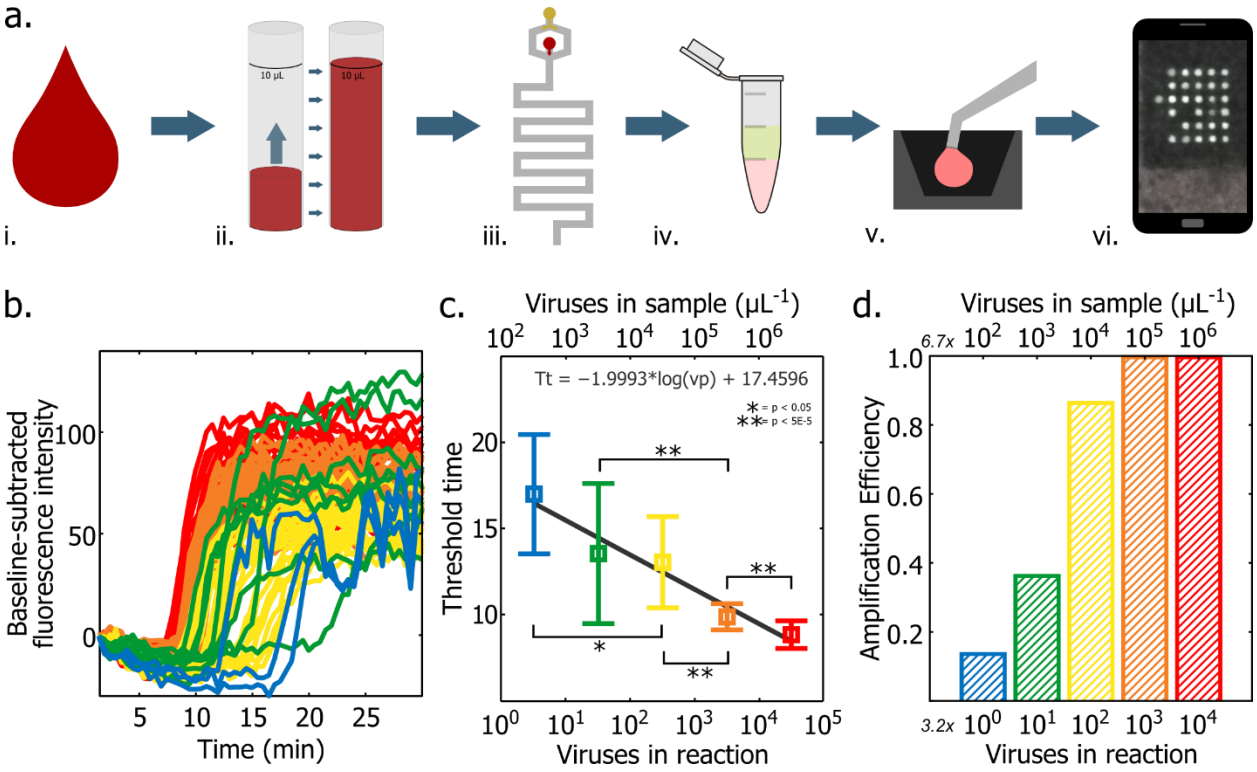

Figure 5.6. Sample-to-answer RT-LAMP detection of HIV-1 IIIB in lysed whole blood. (a) Schematic of integrated process: i. Whole blood spiked with HIV-1 IIIB was infused into a microfluidic apparatus. ii. 10 µL of sample was metered based on the volume of the holding coil. iii. The sample was flowed into a microfluidic mixing module at 10 µL/min with cell lysis buffer at 40 µL/min. iv. Output from the mixing module was added to RT-LAMP mastermix without primers. v. Lysed sample with mastermix was microinjected onto the microwell substrate prepared with dehydrated primers. vi. The chip was heat to 65 C in a copper base with a heating stage and the RT-LAMP reaction was monitored by recording a fluorescent image every 30 seconds using a smartphone. (b) Real-time fluorescence curves as measured by smartphone imaging system. (c) Threshold time values determined by the time at which baseline-subtracted fluorescence intensity exceeds 20% of its maximum value. (d) Amplification efficiency, defined as the fraction of droplets which amplified in the array for each tested concentration.

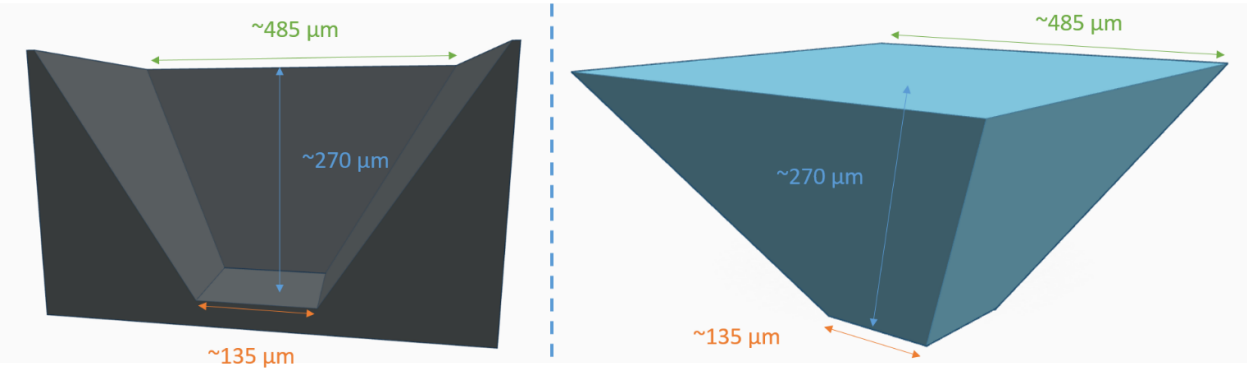

Figure 5.7. (left) Cross-section of pyramidal well with dimensions indicated. (right) Mold of pyramidal well with dimensions indicated.

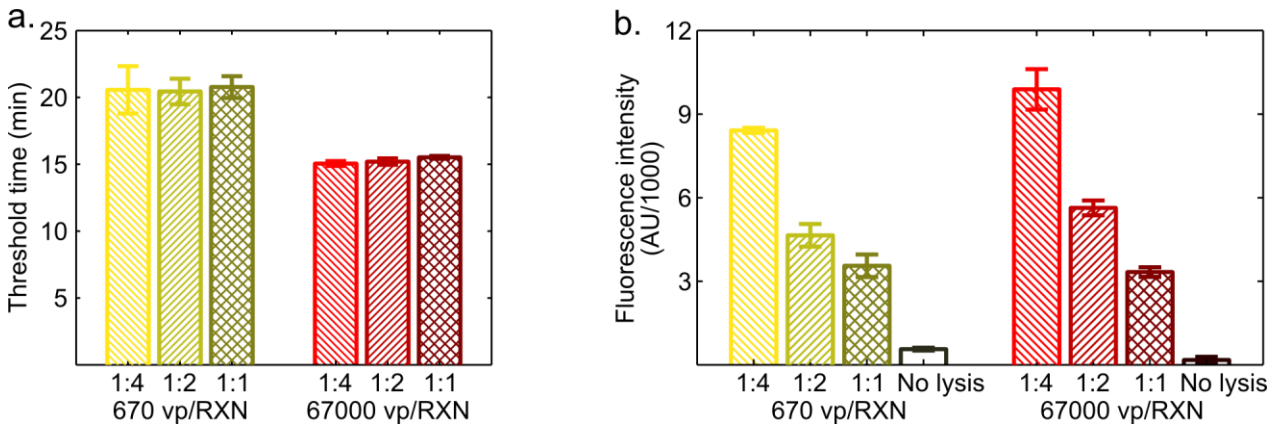

Figure 5.8. (a) Comparison of threshold time as the ratio of blood to lysis buffer is varied, showing that threshold time does not vary significantly with blood lysis ratio. (b) Plot of maximum value of baseline-subtracted fluorescence intensity, which decreases as the fraction of blood in the reaction increases. No amplification was observed in un-lysed blood samples.

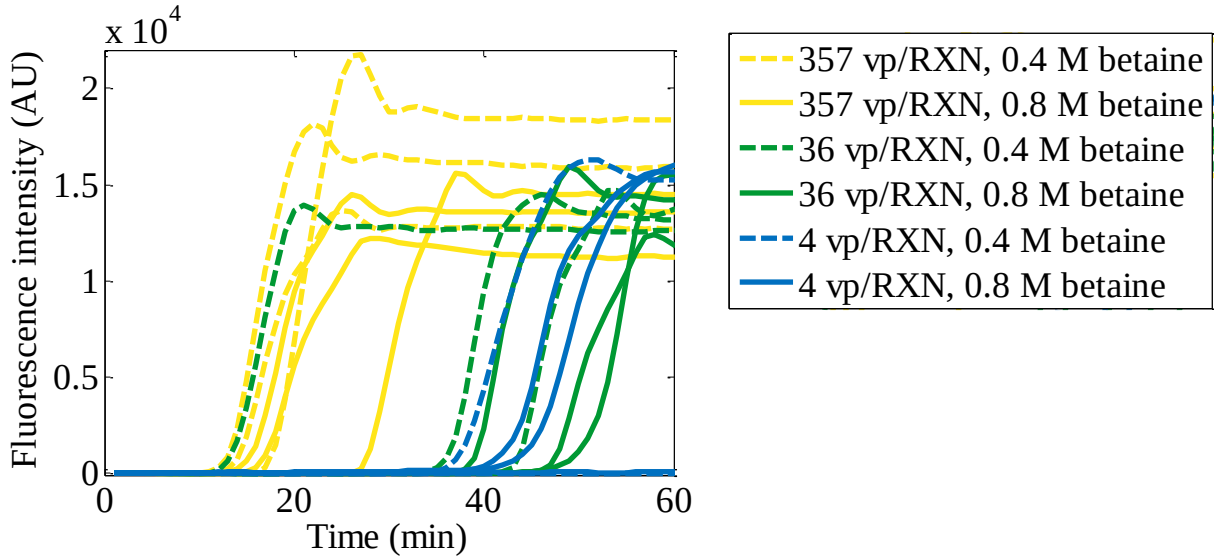

Figure 5.9. Reaction curves from comparison of 0.4 M and 0.8 M betaine in the RT-LAMP reaction.

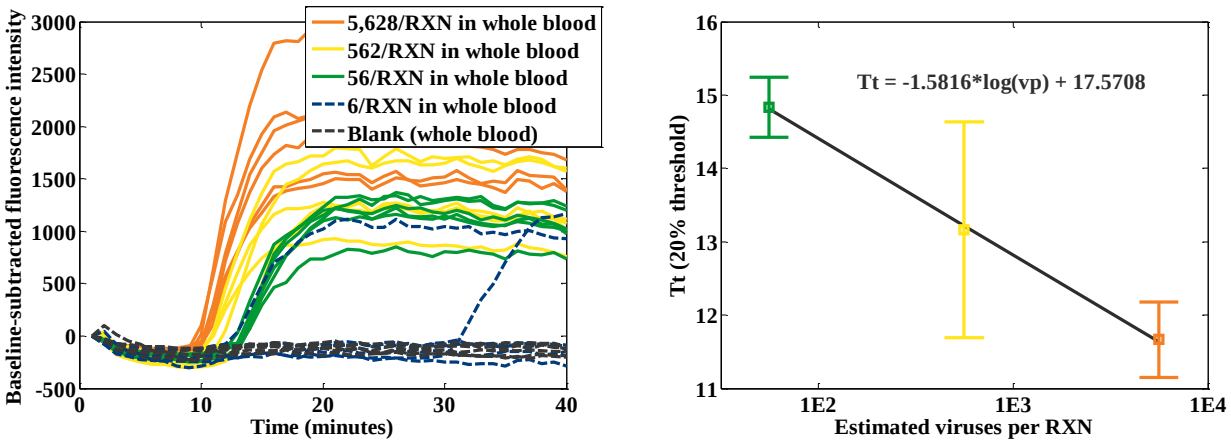

Figure 5.10. Microchip RT-LAMP of lysed whole blood spiked with RNA viruses. (left) Fluorescence curves and (right) threshold time curve.

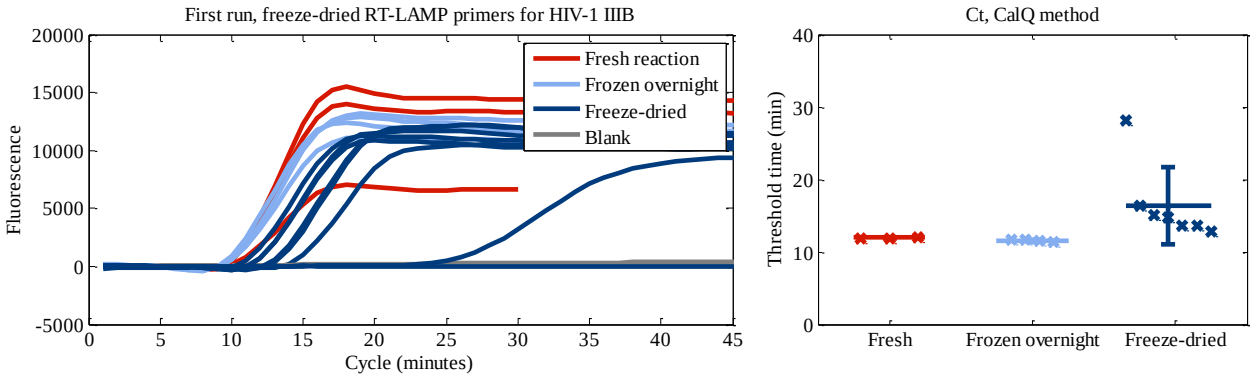

Figure 5.11. Lyophilization of RT-LAMP mastermix. Left: Fluorescence curves from three different conditions: reactions prepared fresh immediately before testing, reactions for which mastermix was frozen overnight and kept at -20 C until immediately before testing, and reactions for which mastermix was frozen at -20 C prior to freeze-drying. Right: threshold times determined by the Eppendorf thermocycler using CalQ curve-fitting method.

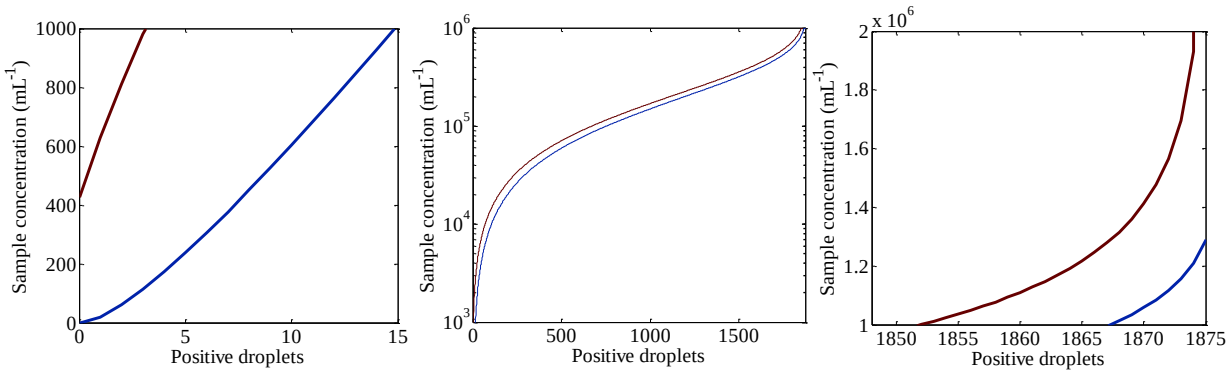

Figure 5.12. Theoretical limits of a 1,875 droplet digital RT-LAMP test utilizing 9 µL of whole blood. Upper and lower bounds determined by 95% confidence interval are indicated.

CHAPTER 6: DROPLET MICROFLUIDICS AND DIGITAL AMPLIFICATION

INTRODUCTION

The methods described in the previous chapter demonstrate a proof-of-concept for a sample-to-answer approach to HIV viral load detection involving the formation of nanoliter-scale droplets of lysed whole blood and RT-LAMP reaction mix. Following this demonstration, we have sought to further the technique by establishing a framework for a digital measurement of viral load employing the lysed blood and RT-LAMP technique. Digital nucleic acid amplification is a widely employed method that has been discussed extensively in the literature [244], [248]–[252]. Fewer examples exist of LAMP or RT-LAMP employed in a digital format, though the underlying principles are the same [236].

The chief advantage of digital nucleic acid amplification is that quantification of the analyte is not sensitive to the time of amplification in the same manner as the traditional reaction kinetics-based measurements. In traditional PCR or LAMP, a DNA intercalating dye is included in the reaction which fluoresces when it binds double-stranded DNA (dsDNA) or (in PCR) a quencher-fluorophore probe construct is included which binds a specific sequence of the target and is cleaved by the exonuclease activity of the DNA polymerase, separating the fluorophore from the quencher and generating fluorescent signal [258], [259]. In both cases, the fluorescence intensity measured in the reaction increases with amplification of the target until a saturation point is reached. A threshold cycle (PCR) or threshold time (LAMP) is determined from the fluorescence measurement by analyzing the raw data for a threshold time or cycle. Threshold time or cycle is defined by the point at which the fluorescence exceeds a threshold value – typically a certain percentage of noise or a percentage of the maximum fluorescence intensity. A standard curve is built by characterizing known quantities of the target and correlating threshold cycle or time to the quantity of target. There is typically a linear relationship between the log of the target copy number and the threshold cycle or time. Problems arise, therefore, when the reaction is inhibited by external factors such as

variations in ambient temperature, reagent degradation as a result of aging or freeze-thaw cycles, and undesired contaminants.

Digital amplification techniques, on the other hand, rely only on an analysis of whether or not a droplet has amplified, removing the variability in quantification that can result from such external factors. In a digital approach, the sample is divided into hundreds, thousands, or even millions of individual reactions which are then discretely analyzed for amplification. Quantification of the analyte concentration in the sample is then determined based on Poisson statistics.

THEORY: STATISTICAL FRAMEWORK FOR DIGITAL AMPLIFICATION

Poisson distribution of viruses in droplets

The classic Poisson distribution describes the probability of a relatively rare event being observed in a certain interval of time, and takes the following form [260]:

$$P(X = i) = \frac{\lambda^i e^{-\lambda}}{i!} \tag{6.1}$$

Where P is the probability function describing the random variable X, observed i times per unit time or space. Luo, *et al.* provides a useful discussion of the Poisson distribution in the context of viral load assays, expressing the probability mass function in terms of virus concentration, c, volume of the sample (in our discussion, this will be the volume of blood sample in a droplet), v, and number of viruses observed in a small sample, i [256].

$$P(i|c) = \frac{(c \times v)^i}{i!} e^{-(c \times v)} \tag{6.2}$$

This probability function provides the framework for understanding the detection limits of digital LAMP, which we subsequently apply to the design of a microfluidic device for digital droplet LAMP measurements.

Binomial distribution of droplet amplification

When applying the framework for understanding digital LAMP measurements, two assumptions are necessary [255]. First, we assume that a droplet containing a single virus will amplify (i.e. a partition containing one or more viruses will always amplify) and that a partition without a virus will not amplify (no false positive partitions). Second, we assume that the Poisson distribution is followed which requires that there is no interaction of the target (i.e. viruses) with the device or any other process which would influence the distribution of viruses into partitions. Under these assumptions, the probability that a droplet contains more than one virus, i.e. $P(i > 0)$, is [249], [255]:

$$P(i > 0) = 1 - P(i = 0) = 1 - e^{-c \times v}$$

We may then model of the array of droplets in a digital LAMP reaction as a binomial distribution in which the probability of success (a positive droplet) comes from the Poisson-based understanding of virus distribution into droplets. The mean (μ) and variance (σ^2) can therefore be determined as [249], [255]:

$$\mu = Np = N\left(1 - e^{-(c \times v)}\right) \tag{6.3}$$

and

$$\sigma^2 = Np(1 - p) = N\left(e^{-(c \times v)} - e^{-2(c \times v)}\right) \tag{6.4}$$

The mean of the binomial distribution (μ) is the expected value for positive partitions in the array, which we will call x. Here the conclusion is worked out in detail for the sake of clarity [249], [257]:

$$x = N\left(1 - e^{-(c \times v)}\right) \rightarrow e^{-(c \times v)} = 1 - \frac{x}{N}$$

Taking the natural log:

$$-(c \times v) = \ln\left(\frac{N - x}{N}\right) \rightarrow (c \times v) = \ln\left(\frac{N}{N - x}\right)$$

We can therefore relate the virus concentration in the sample (i.e. viral load) to the number of positive partitions in a digital amplification array:

$$c = \frac{1}{v}\ln\left(\frac{N}{N - x}\right) \tag{6.5}$$

Uncertainty limits by the Wilson method

As a statistical process, the binomial distribution has an inherent degree of uncertainty for which a confidence interval can be calculated, which in its classic form is [252], [257]:

$$\eta \pm \alpha \times \sqrt{\frac{\eta \times (1 - \eta)}{N}} \tag{6.6}$$

Where $\eta = x/N$, the fraction of droplets in which amplification is observed. In this discussion we will use $\alpha = 1.96$, corresponding to the 95% confidence interval [257]. In these calculations, we prefer a more precise form of the uncertainty calculation as described by Shen, *et al.* using the Wilson method:

$$\frac{\eta + \frac{\alpha^2}{2 \times N} \pm \alpha \times \sqrt{\left(\frac{\eta \times (1-\eta)}{N} + \frac{\alpha^2}{4 \times N}\right)/_N}}{1 + \frac{\alpha^2}{N}} \tag{6.7}$$

In practical implementation, we consider the 95% confidence interval according to the observed fraction of positive partitions (η).

$$x_{high} = N\left(\frac{\eta + \frac{\alpha^2}{2 \times N} + \alpha \times \sqrt{\left(\frac{\eta \times (1-\eta)}{N} + \frac{\alpha^2}{4 \times N}\right)/_N}}{1 + \frac{\alpha^2}{N}}\right) \tag{6.8}$$

$$x_{low} = N\left(\frac{\eta + \frac{\alpha^2}{2 \times N} - \alpha \times \sqrt{\left(\frac{\eta \times (1-\eta)}{N} + \frac{\alpha^2}{4 \times N}\right)/_N}}{1 + \frac{\alpha^2}{N}}\right) \tag{6.9}$$

The upper and lower limits of the virus concentration indicated by the observed number of positive partitions can therefore be determined by solving for concentration c (high and low) in equation 6.5 [252], [255], [257], [261], [262].

Droplet device design parameters

We now apply our understanding of the statistical framework and the upper and lower bounds of the 95% confidence interval to a consideration of the design parameters for a microfluidic device for digital droplet LAMP applied to HIV viral load, and an understanding of its capabilities relative to classical RT-LAMP in which quantification is based on the reaction kinetics. We will consider parameters such as: total volume of blood sample analyzed and the number and size of droplets formed.

First we must define the metrics which we'll consider to guide device design parameters. This discussion will be based on terminology that agrees with a useful and thorough discussion of digital amplification design parameters available from Kreutz, *et al*. in [255].

Keeping the assumptions described previously, the lower limit of detection (LLD) of the digital amplification assay will be defined simply as the concentration of virus in a blood sample which will produce a signal 95% of the time. This is straightforward and based on the Poisson probability mass function in equation 6.2. Figure 6.1. provides examples of curves at four different sample volumes (5 μL, 10 μL, 15 μL, and 20 μL) and their corresponding LLD (600 mL^{-1}, 300 mL^{-1}, 200 mL^{-1} and 150 mL^{-1}, respectively). It should be pointed out that the LLD, the minimum concentration at which at least one partition amplifies 95% of the time, is independent of N, the total number of partitions, and holds true in traditional or quantitative RT-LAMP (qRT-LAMP) as well.

A more useful metric, the lower limit of quantification (LLQ), however, is not as straightforward. In this discussion, we again draw on Kreutz, *et al*. and define the LLQ as the smallest concentration at which a sample of that concentration can be distinguished 95% of the time from a sample with X-fold greater concentration where the desired resolution is X [255]. For a qRT-LAMP reaction, this must be determined experimentally and would be impacted by several factors influencing the ability of the measurement system and the biochemical reaction to resolve these differences in a kinetic measurement. Kreutz, *et al*. provides a theoretical determination of LLQ in [255] which involves a similar statistical framework for multi-volume digital LAMP and applies a common Z-test to determine the minimum number of total droplets and minimum number of amplified droplets required to achieve such a resolution. That analysis is not repeated here, however, the conclusion from [255] is applied: that a 3-fold resolution requires 13 positive wells with a minimum of 131 total wells in the digital amplification assay.

In similar fashion, upper limit of detection (ULD) can be defined as the viral load corresponding to $N - 1$ amplified partitions in a digital assay, as 100% of partition amplification provides no upper limit to the sample virus concentration. Upper limit of quantification (ULQ) as defined by Kreutz, et al., is the

concentration at which one or more wells would be negative 95% of the time and corresponds to the condition in which 3 wells are negative [255].

Volume of sample analyzed. Applying these definitions, we can examine the effects of the volume of sample on the capabilities of the digital amplification assay. To examine this parameter, we pick a reasonable value for the number of droplets: 1,000. Solving equations 6.8 and 6.9 for the full range of integer possibilities of x such that $x/N = \eta$ and solving equation 6.5 for the corresponding virus concentrations (with varying values of v), we get the solutions depicted in Figure 6.2a-b.

Applying the definition for LLQ defined above, we can examine these graphs for an understanding of the effect of sample volume on LLQ. We have already descrived the effect of sample volume on LLD in Figure 6.1. To further examine the relationship between LLOD and sample volume, we recognize that (for a fixed N and x) the relationship is simply determined by equation 6.5, i.e. that there is an inverse relationship between the lowest theoretically detectable virus concentration and the volume of sample analyzed. This is intuitive at its core, though using x_{high} from the $N = 1000$ calculations, we are able to visualize the decrease in LLQ as volume is increased in Figure 6.2c.

The next logical question is if the total sample volume is fixed, how the total number of droplets will affect the dynamic range (LLQ and ULQ). To examine this, we plotted upper and lower bounds of the 95% confidence interval versus number of positive partitions for 10 μL assays of 10^3, 10^4, and 10^5 partitions each in Figure 6.3. Vertical lines indicate the lower and upper limits of quantification based on 13 and N-3 positive partitions, consistent with Kreutz, *et al*. [255].

The conclusion we glean from this examination of the statistical framework for quantification by digital amplification is the ideal quantification range from a 10 μL blood sample is achieved with approximately 10,000 partitions. The lower limit of quantification (LLQ) and lower limit of detection (LLD) could both be improved (i.e. lowered) with increased sample volume. However, 10 μL has long been considered the practical limit for a finger-prick point-of-care diagnostic device. Next we consider briefly the effects on this theoretical framework of an assay which is not capable of single-virus detection.

Binomial distribution of amplified droplets assuming more-than single-virus sensitivity

The nanoliter-scale RT-LAMP which we have demonstrated to this point has exhibited amplification, though inconsistent, in samples containing as few as three viruses per reaction, on average. In order to determine the importance of improving the reaction for consistent amplification of single viruses in a partition, we consider the effect of employing an assay in which the minimum virus-per-reaction required for amplification is either two or three.

He we work through the equations for the case in which three viruses are required for successful amplification. Assuming the array once again follows a binomial distribution, the probability of successful amplification in a droplet is now given by the Poisson distribution in the case that three or more viruses are in the droplet, i.e.:

$$P(i > 2) = 1 - P(i = 0) - P(i = 1) - P(i = 2)$$

From Equation 6.2:

$$P(i > 2) = 1 - e^{-(cv)} - (cv)e^{-(cv)} - \frac{(cv)^2}{2}e^{-(cv)}$$

$$P(i > 2) = 1 - e^{-(cv)}\left(1 + (cv) + \frac{(cv)^2}{2}\right)$$

Once again employing the binomial distribution as a model for amplification success, we get can simplify the expression for x (number of successful partitions) in terms of c, N, and v.

$$x = N\left[1 - e^{-(cv)}\left(1 + (cv) + \frac{(cv)^2}{2}\right)\right]$$

This results in an expression relating c to x that is not easy to solve for c. However, choosing $N = 10{,}000$ and total sample of 10 μL ($v = 1\ nL$) based on our previous analysis for single-droplet we find the plot of x versus c enlightening (Figure 6.4). This shows that for the given parameters, the amplification of a single virus per partition is critical.

Conclusions from theoretical framework

This exercise could be extended infinitely to examine the requirements for number of partitions, total volume of sample, and size of droplet. However, we can glean from our discussion of this framework for digital droplet amplification that lower limit of the dynamic range is improved (lowered) by analyzing more blood and by employing an assay which requires the fewest viruses possible to amplify successfully (i.e. one virus per partition will reliably amplify). On the other hand, upper limit of the dynamic range is influenced strongly by (a) the total number of droplets and (b) volume of blood analyzed, but less significantly by the minimum number of viruses required to see amplification in a single partition.

METHODS

Microfluidic device

Multiple approaches for the partitioning of a fluid sample exist [241], but few are as simple as microfluidic droplet generation methods which generate droplets by flowing two immiscible fluids through a T-junction channel [263]. We have employed standard PDMS prototyping techniques to produce a droplet-generating T-junction. The microchannel design consists of a 400 μm-wide channel in which the continuous phase (heavy mineral oil) is flowed and a smaller orthogonal channel 100 μm in width in which the aqueous phase is introduced. The 400 μm channel containing continuous-phase oil into which the droplets are introduced continues in a serpentine reaction channel allowing for hundreds or thousands of droplets to be produced in series and kept within the device for subsequent incubation and imaging.

Droplet evaporation in microchannel

Evaporation has often been problematic in microscale nucleic acid amplification techniques, particularly in PDMS which is permeable to gases, and several methods have been employed to minimize or eliminate this issue [264]. Glass, acrylic, and PDMS were considered as materials for the serpentine reaction channel in our microfluidic device, however, PDMS was deemed preferable despite is gas-permeable properties. To minimize the effects of evaporation in the PDMS device, we considered modifications which were expected to reduce the permeability of the material. First, the ratio of curing agent and elastomer was varied to see if permeability could be reduced. Then, a glass vapor barrier was added to the channel by pouring a thin layer of PDMS in the mold, degassing, and allowing it to cure, then placing glass microscope slide cover slips over the channels and pouring additional PDMS to embed the glass into the PDMS layer.

To examine the effects of these modifications, we filled a test channel with aqueous droplets in heavy mineral oil continuous phase and placed the channel on a heating stage under a microscope. The stage was heated to 65 C and images were captured periodically beginning when the stage controller indicated the stage had reached 65 C. Images were analyzed in ImageJ image analysis software by converting the image to a binary format and using the "Analyze Particles" function to determine the surface area. The height of the droplet which cannot be determined from the 2-dimensional image is assumed to be uniform and the same as the height of the channel. This assumption makes comparisons of surface areas an adequate approximation of relative droplet volume.

Droplet formation in classic T-junction

A PDMS microfluidic channel with a T-junction for aqueous droplet formation in a mineral oil continuous phase was fabricated via standard soft lithography techniques. The final chip was molded PDMS on glass, and the glass surface was made hydrophobic by flushing the channels with Sigmacote prior to use. To characterize droplet formation, oil was flowed into the 400 μm channel and DI water containing dye was flowed into the 100 μm channel using syringe pumps. Flow rates of the high-viscosity continuous phase

were kept low (5-15 μl/min) due to the high fluidic resistance of the serpentine reaction channel. Flow rates for the aqueous phase were generally kept higher than the continuous phase to maximize the reaction volume in the microfluidic chip.

Short videos were captured with a Nikon microscope for each combination of flow rates and snapshots of six droplets from each video were analyzed in ImageJ to determine the 2-dimensional area of each droplet. Volumes were estimated by assuming the 2-dimensional image has a uniform height of 100 μm, the same as the height of the microchannel.

PRELIMINARY RESULTS

Droplet evaporation in microchannel

Results of the droplet evaporation are show in Figure 6.6. Varied ratios of elastomer and curing agent did not show a significant effect on evaporation in the microchannel. The slowest evaporation rate was observed in the microchannel with added glass coverslip, with an average of 90.25% of the droplet area still present after 28.5 minutes.

Droplet formation in classic T-junction

Droplets formed via continuous flow in the PDMS T-junction are depicted in Figure 6.7. The expected trend of increasing droplet size with increasing dispersed phase flow rate when continuous phase is held constant was observed. Two separate microfluidic chips were tested, and droplet sizes were not consistent between the two devices at the same flow rates. This highlights challenges that will be addressed in continued work.

DISCUSSION

In this chapter, we have provided a theoretical discussion which justifies a digital RT-LAMP approach to HIV viral load measurements as well as preliminary data investigating options for a microfluidic droplet generation and LAMP reaction chip. The statistical framework for droplet LAMP demonstrates the need for single-virus sensitivity in each partition of the digital LAMP reaction. The framework also conveys the need for sample volume and partitioning (i.e. the number of partitions per sample) that will be required to achieve a clinically-relevant measurement.

We have shown preliminary data characterizing the evaporation of aqueous droplets in a PDMS microchannel, as well as droplet formation in a classic T-junction consisting of continuous phase flow in a 400 μm channel and introduction of the dispersed phase through a 100 μm channel. Following formation in this structure, droplets flow into a serpentine channel intended for their imaging under static conditions following incubation of the RT-LAMP reaction. However, we have identified several problematic aspects of the PDMS approach which may result in adjusting the approach.

CONCLUSIONS

Our analysis of the statistical framework for digital nucleic acid amplification testing provides a promising outlook for a point-of-care viral load test which follows this approach. In the case where a single virus can be reliably amplified in a single partition and in which 5 μl of blood or more can be analyzed in at least 1,000 partitions, measurements capable of informing clinical decisions about HIV/AIDS treatment could be provided.

The default approach to prototyping this test in the laboratory would be to fabricate microchannels in PDMS and demonstrate the concept. However, two practical issues have been observed in our preliminary data: evaporation of the aqueous droplet during the incubation phase of the measurement, and handling of the high pressures resulting from a serpentine channel with the capacity for handling adequate reaction volume. While we have shown a temporary fix which reduces but does not eliminate the evaporation issue, we have also observed that incorporating glass slides or coverslips in the PDMS structure results in

increased stresses on the results which compromise resistance to pressures. Alternative channel designs may be considered in which fluidic resistance could be reduced, including a "reaction chamber" in which the droplets are flowed into a large micro-chamber for incubation rather than a serpentine channel, or a design which utilizes parallel channels to reduce overall hydrodynamic resistance. A major potential pitfall of this approach, however, is that it provides less control over the behavior of the droplets in the channel and reaction volume may be lost under flow conditions.

A pragmatic solution is to move to glass, silicon, or plastic components which are professionally produced for microfluidic handling and more rigid and tolerant of the high pressures that result from the microchannel approach. Future work will investigate these options and develop a chip which receives four inputs: whole blood, cell lysis buffer, reaction reagents, and oil (continuous phase) and through a series of serpentine channels: (1) mixes whole blood with lysis buffer at a 1:4 ratio, (2) mixes lysed blood with RT-LAMP reagents, and (3) generates droplets which are stored in a microchannel, incubated, and imaged with a smartphone device. Following thorough characterization of such an apparatus, spike blood samples could be tested for comparison to the theoretical framework and clinical samples could be tested for comparison to the gold standard nucleic acid amplification instruments.

FIGURES

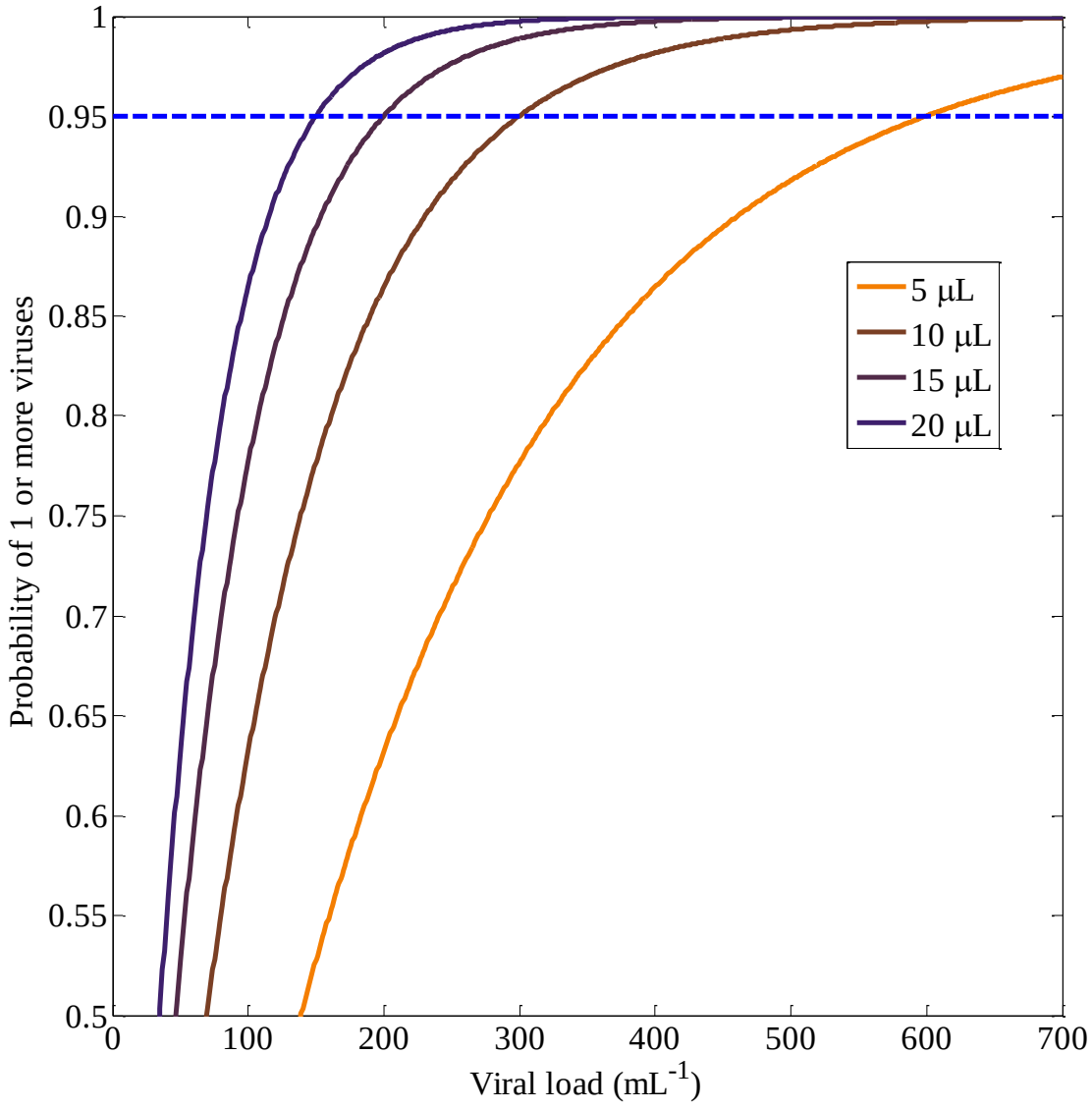

Figure 6.1. Probability of finding one or more viruses in samples of various sizes at low viral loads. The intersection of each curve with 95% (i.e. 0.95) corresponds to our definition of lower limit of detection (LLD) for both classical RT-LAMP (qRT-LAMP) and digital RT-LAMP (dRT-LAMP), based on the same definition discussed in [255].

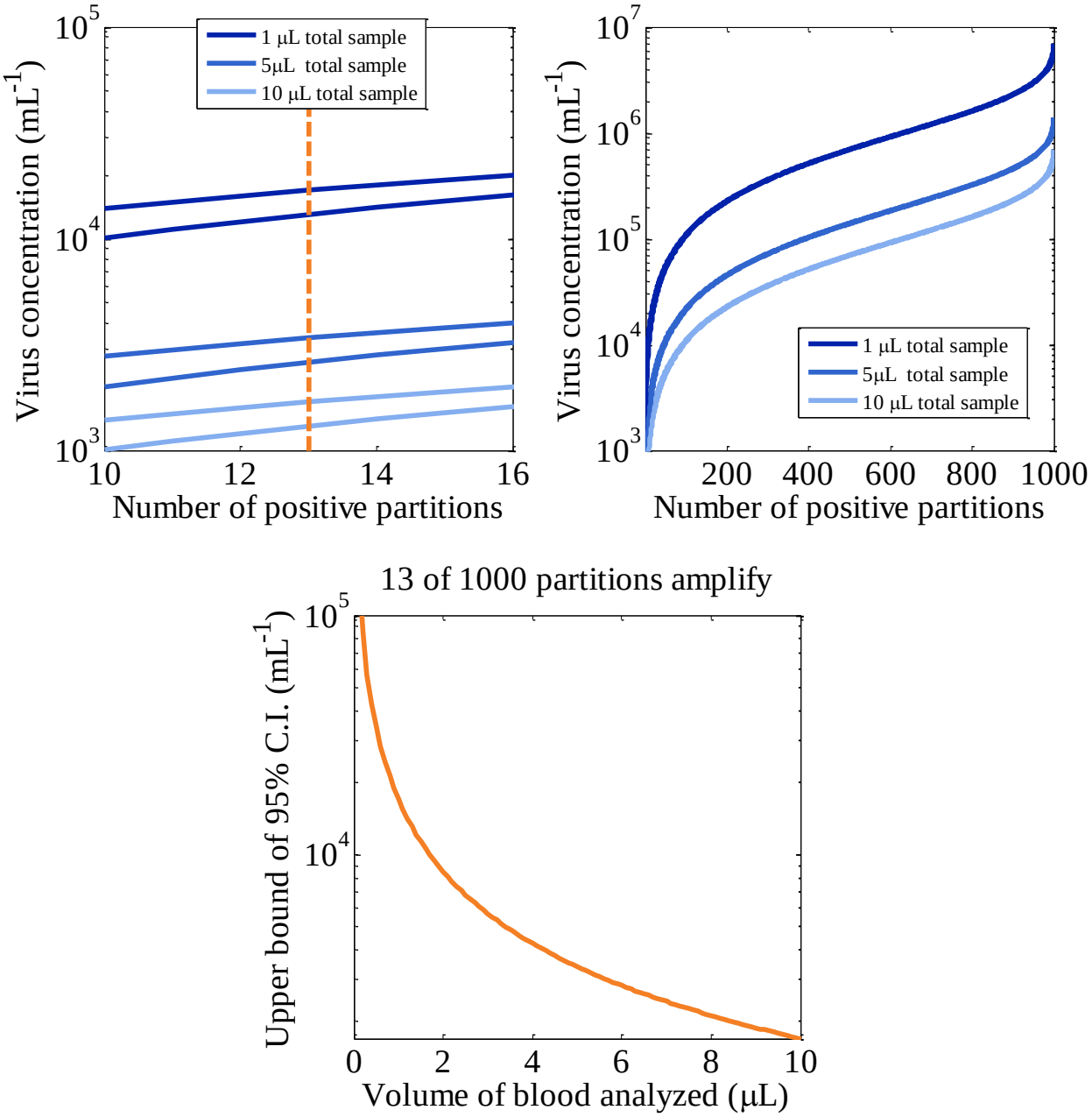

Figure 6.2. Analysis of droplet LAMP design parameters based on statistical framework for virus quantification from digital amplification and definitions of LLD and LLQ in Kreutz, *et al*. [255]. (A) Upper and lower bounds of viral load versus number of amplified droplets in the range of 10-16 droplets amplified. The vertical line indicates 13 droplets, which we define from [255] as the lower limit of quantification (LLQ). (B) Full range of droplet amplification. Both upper and lower bounds are shown, but difference is too miniscule to resolve on this scale. (C) Upper bound of 95% confidence interval when 13 of 1000 droplets amplifies for various total blood volumes analyzed, indicating the impact of total sample volume on LLQ.

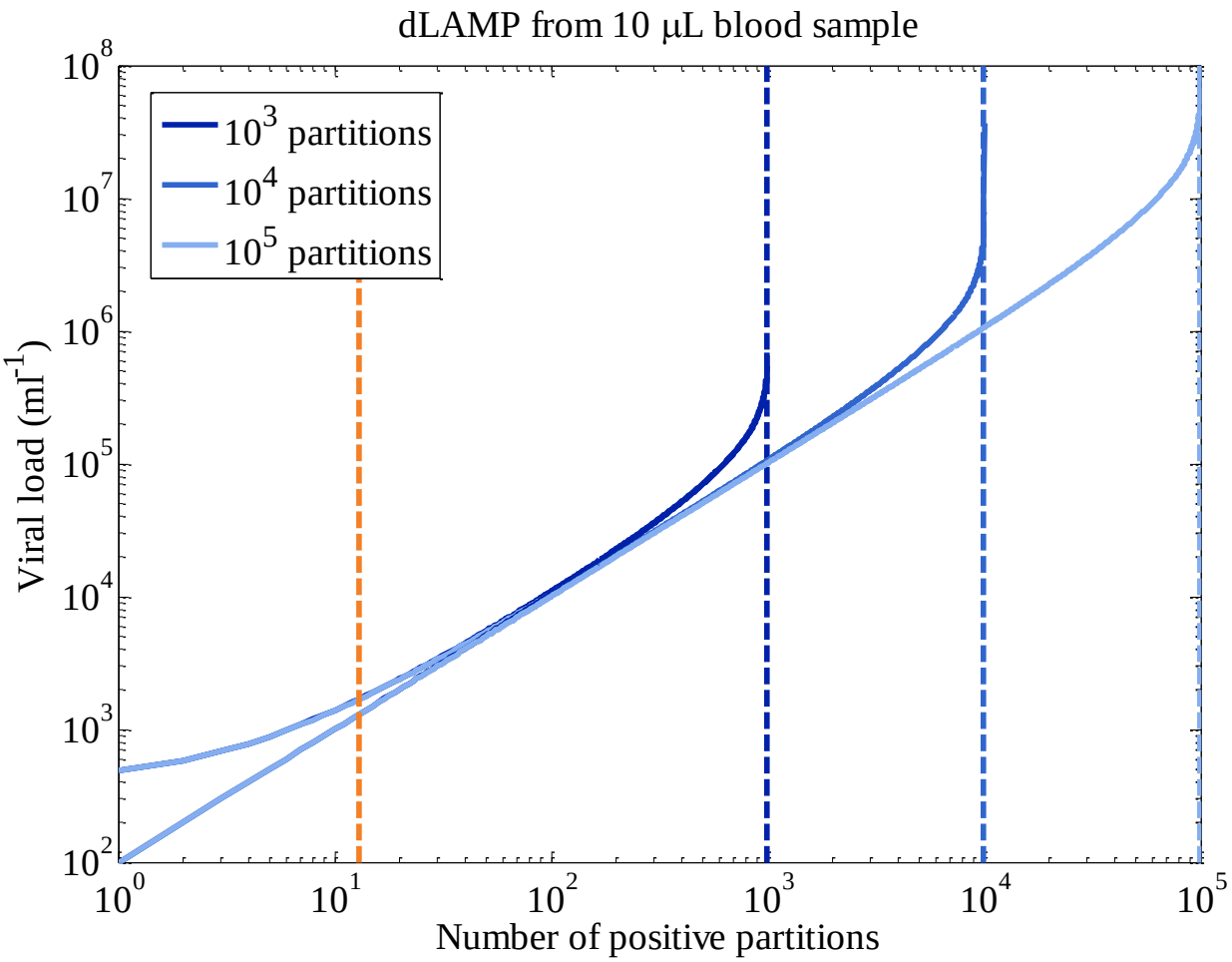

Figure 6.3. Upper and lower bounds of the dLAMP measurement for a 10 μL blood sample divided into 1E3, 1E4, or 1E5 partitions. The vertical orange line corresponds to 13 positive partitions, the Kreutz, *et al*. definition for LLQ and the dotted vertical lines correspond to N-3 positive partitions, the ULQ [255].

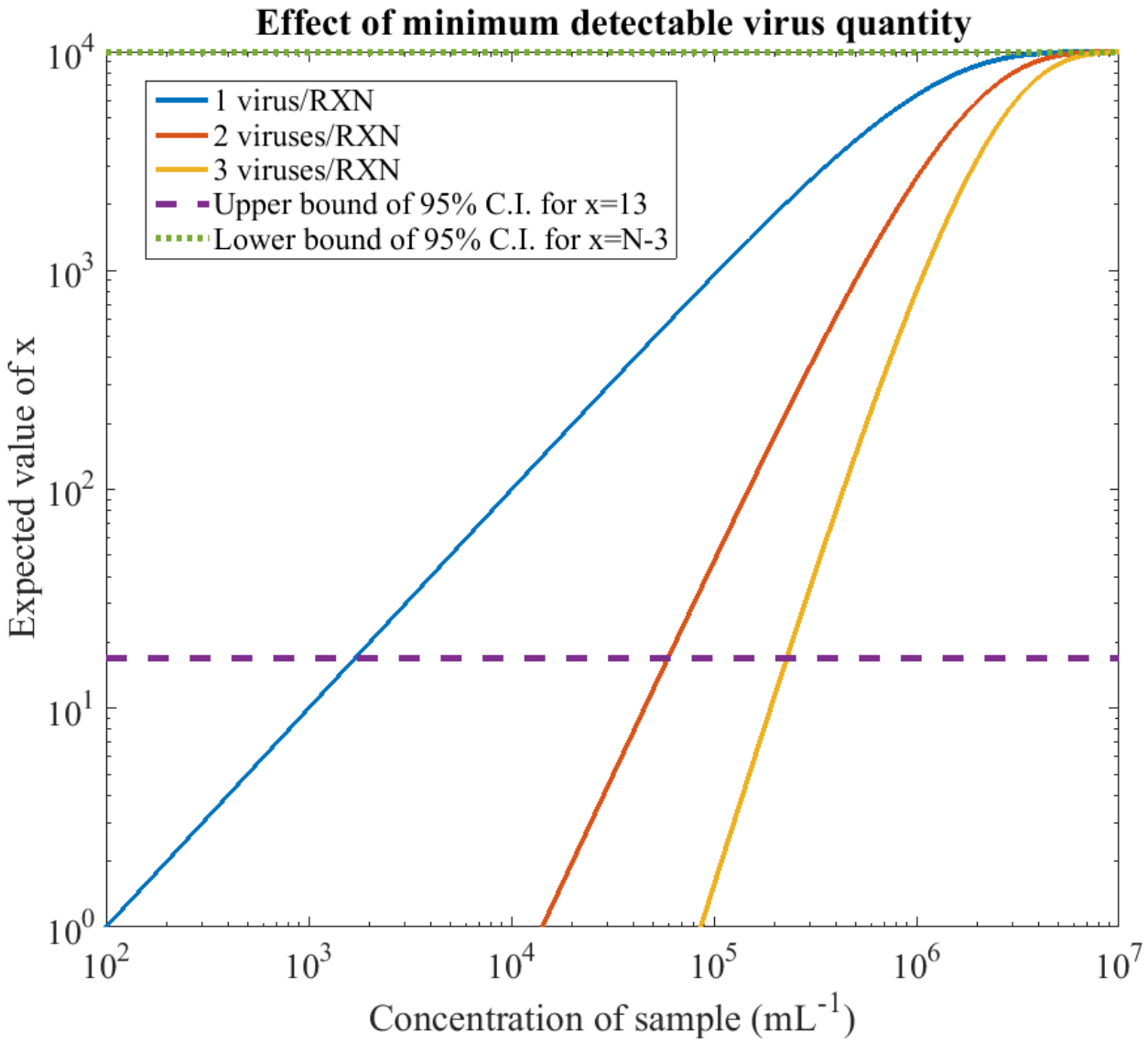

Figure 6.4. Effects of more-than single virus sensitivity. We plot the expected value, x, for the conditions $N = 10{,}000$ and $v = 1\ nL$ (total sample of $10\ \mu L$) versus the actual viral load. The upper bound of the 95% confidence interval is represented by the dashed line. Its intersection with each curve represents the lower limit of detection. The intersection with the dotted line represents the upper limit of the dynamic range.

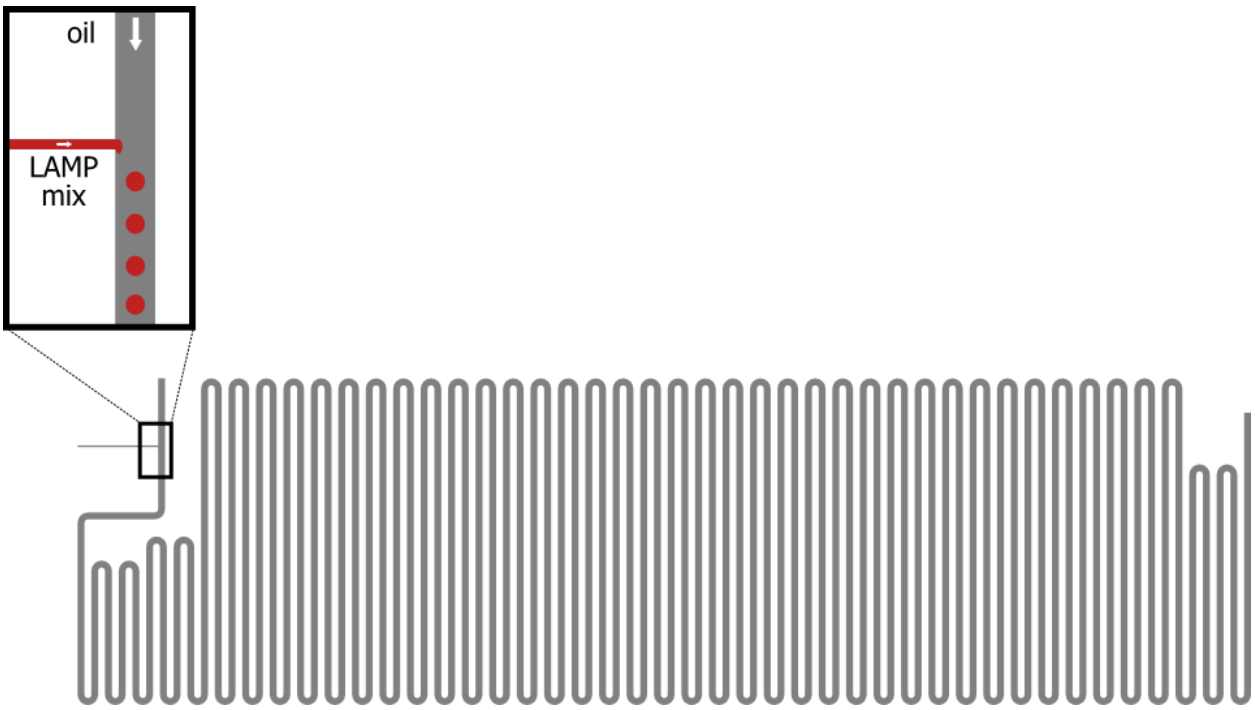

Figure 6.5. Schematic of T-junction and reaction serpentine channel.

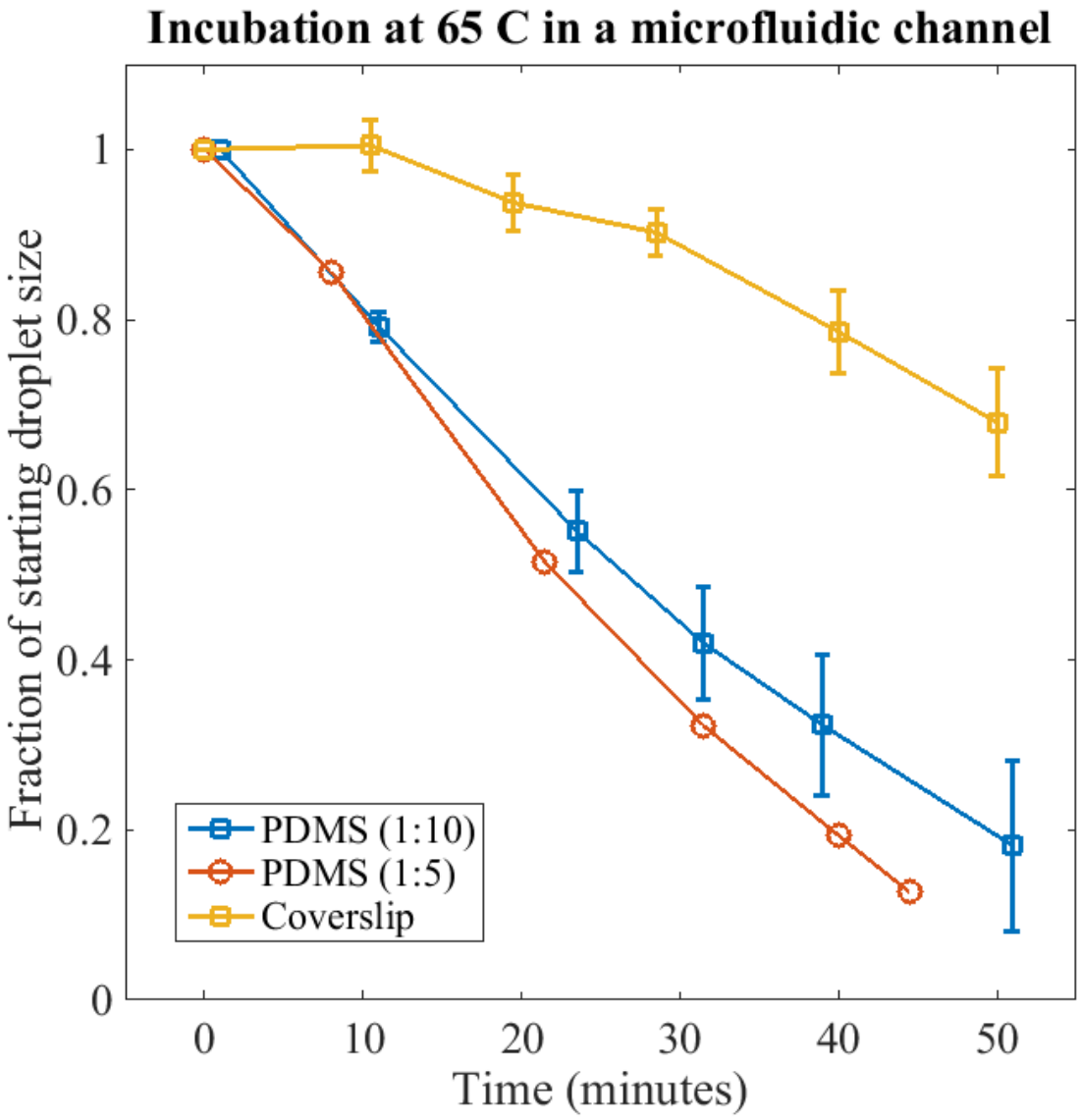

Figure 6.6. Droplet evaporation in classic PDMS and modified PDMS channels. The slowest evaporation rates were observed in PDMS channels with an added coverslip to decrease vapor permeability of the channel materials.

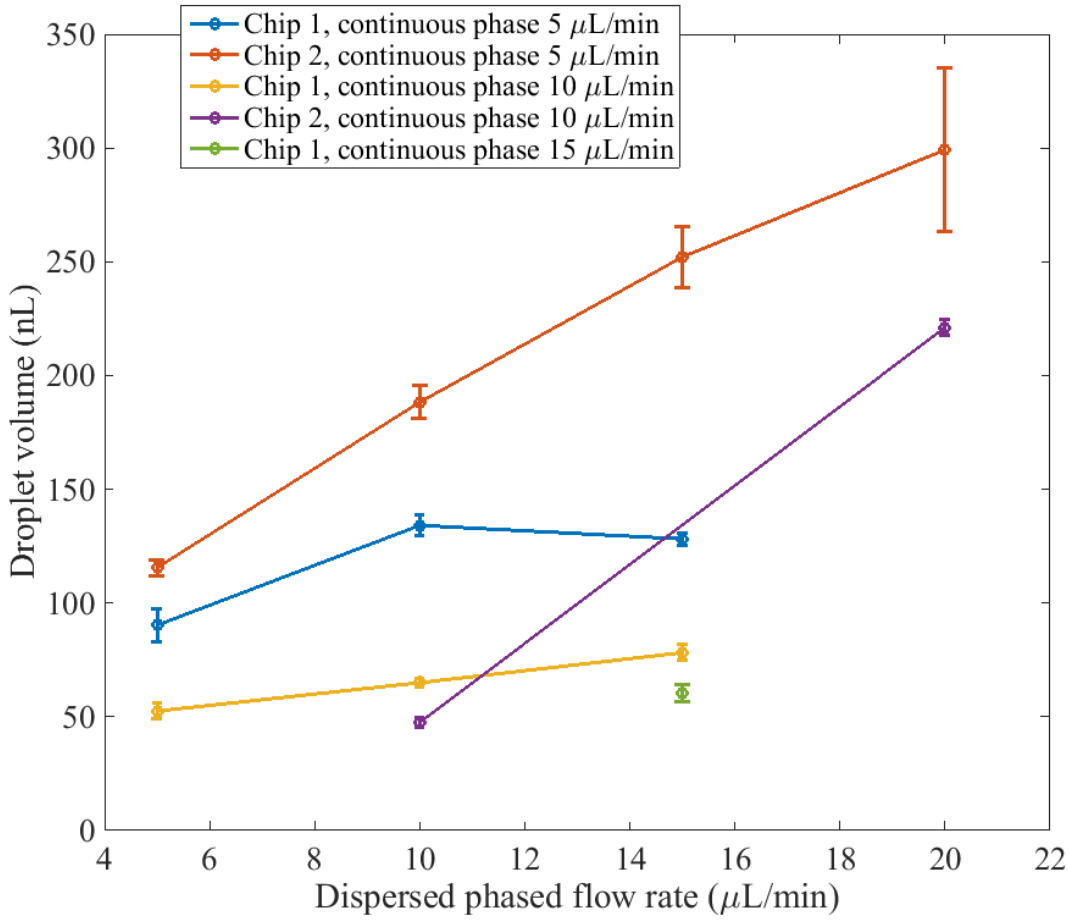

Figure 6.7. Droplet formation in the simple microfluidic T-junction.

CHAPTER 7: CONCLUSIONS AND FUTURE WORK

CONCLUSION

Access to the appropriate diagnostic technologies continues to be an immense problem for people living with HIV/AIDS around the world. The core markers of disease progression and efficacy of therapy, CD4 count and viral load, traditionally require large instruments in advanced laboratories with complicated protocols. Micro- and nanotechnologies are the tools which may bring these measurements to the point-of-care, making life-altering differences for millions of people worldwide.

An antigen-based approach to viral load detection which we developed incorporated an ion-filled liposome as the novel component of an impedance spectroscopy-based immunoassay. Viruses in solution were immobilized on a glass substrate by capture with a primary antibody to gp-120, followed by tagging with liposomes functionalized with Protein A, also anchoring gp-120. We showed qualitative detection of virus and also demonstrated the capacity for the measurement to be quantitative. We attempted to establish a basis for analysis of whole blood with a magnetic micro-particle based virus separation method incorporating novel virus-recognition components. Ultimately, however, we turned to a different strategy for more sensitive detection of virus by analyzing whole blood for viral RNA.

Our nucleic acid-based approach targeted a viral RNA sequence which was amplified by RT-LAMP and implemented in a silicon microchip in nanoliter-scale droplets. We integrated this measurement with a mobile smartphone device and 3-D printed platform, demonstrating significant potential toward application of the approach in a low-cost mobile device. We further demonstrated that in a high-throughput digital amplification approach, clinically significant measurements can be achieved.

FUTURE WORK IN ION-RELEASE IMPEDANCE SPECTROSCOPY

While we found the nucleic acid approach to be more promising toward a truly applicable viral load test, the antigen detection approach based on ion-filled liposomes is not without its merits. Next steps

require improvement in the synthesis of liposomes, ideally through a highly-uniform and automated process such as those microfluidic methods which have been demonstrated by our collaborators [218], [219]. Additionally, improvements in the design of the sensing microchannel could allow for detection of fewer analytes and achieve a lower limit of detection provided that a concentration step could be incorporated.

Overall, future work with antigen-based detection of viruses by ion-release impedance spectroscopy will target the p24 protein from the viral capsid as the primary analyte for liposome tagging. A variety of options exist, including magnetic capture and separation of whole viruses or inertial-microfluidic techniques which can be employed to separate viruses from whole blood with subsequent lysis to release p24 followed by liposome tagging and sensing.

FUTURE WORK IN DIGITAL RT-LAMP DETECTION

Primary objectives of future work in the nucleic acid-based approach center on analysis of a sample based on the digital RT-LAMP approach. This can be achieved with the automatic droplet-forming T-junction described in Chapter 6. Further work is required to demonstrate repeatability and uniformity of this approach. Ultimately, a device material other than PDMS is desired. Devices may be prototyped in silicon by etching channels with one surface of the channel composed of glass coupled by anodic bonding, or purchased from an off-the-shelf microfluidics vendor.

Upon demonstrating a reliable assay with spiked samples, we will obtain blood samples with detectable viral load from HIV-positive patients at the Carle Foundation Hospital in Urbana, IL. These will be discarded tissue samples which were drawn as part of routine testing and a viral load measurement in the clinical laboratory, also performed as part of routine care, will be used as the control.

APPENDIX A: FABRICATION RUN SHEETS

DOUBLE-RESIST METAL LIFT-OFF PROTOCOL

1. Perform piranha clean (Sulfuric Acid:Hydrogen Peroxide::1:1) of 100 mm glass wafer for 15 minutes; rinse 10 minutes with deionized water; blow nitrogen dry.
2. Dehydration bake @ 110 C, 5 minutes minimum; 5 minutes cool-off.
3. Spin LOR 3A (put on enough LOR 3A to cover entire wafer before spinning; this helps chip yield greatly).
    a. 0 to 500 rpm in 1 s (acceleration setting).
    b. hold at 500 rpm for 2 s.
    c. 500 to 3000 rpm in 2 s (acceleration setting).
    d. hold at 3000 rpm for 35 s.
4. Soft bake: 5 min. @ 183 C (directly on hotplate, not with metal holders); 5 minutes cool off.
5. Spin S1805 (put on enough S1805 to cover entire wafer, not just 4 mL).
    a. 0 to 500 rpm in 1 s (acceleration setting).
    b. hold at 500 rpm for 5 s.
    c. 500 to 4000 rpm in 3 s (acceleration setting).
    d. hold at 4000 rpm for 40 s.
6. Soft bake, 90 s @ 110 C; 5 minutes cool off (important before exposure to prevent wafer from sticking to mask).
7. Exposure energy: 28 mJ/cm2:
    a. 3.7 s exposure time with MNTL's Quintel (currently 7.5 mW/cm2 power output).
    b. 2.6 s exposure time with MNMS' Mask Aligner (currently 21.4 mW/cm2 power output).
8. Post Exposure Bake: 60 s @ 110 C (wafer directly on hotplate).
9. Develop in CD-26 for 18 s (CD-26 underneath developer hood, on right).

10. Simply let wafer sit in developer (no agitation, swirling, etc.; this can cause features to break off of wafer).
11. Rinse in DI water for 2 minutes in a dish with DI water gently flowing into it or simply swirling the wafer gently in a static dish of DI water.
12. Examine wafer under microscope.
13. Perform 20 s oxygen plasma on wafer(s) before placing in CHA for metal deposition.
14. Evaporation: 250 Angstroms of titanium + 750 Angstroms of gold per wafer.
15. Metal lift-off (do this in the biolab).
    a. Place wafers in Remover PG at 70 C for 1 hour+.
    b. Dump liquid into non-halogenated solvent waste container.
    c. Wipe gently with a cleanroom wipe to remove any stubborn metal.
16. Examine wafer for adequate lift-off.
17. Spin protective layer of photoresist.
18. Dice wafer using dicing saw and appropriate blade.
19. Remove protective photoresist with appropriate developer or solvent.

SU-8 PHOTOLITHOGRAPHY FOR RAPID PROTOTYPING OF MICROFLUIDIC DEVICES

1. Piranha clean Si wafer (1:1::sulfuric acid:hydrogen peroxide)
2. Nitrogen dry and dehydration bake for 5 minutes at 110 °C
3. Using appropriate SU8 for the desired height, pour on dry wafer and spin according to the provided recipe.
4. Softbake according to recipe.
5. Allow wafer to cool.
6. Expose wafer according to recipe and instrument intensity.
7. Post exposure bake according to recipe.

8. Develop in SU8 developer until pattern has fully developed. Do not over-develop.
9. Place wafer in a glass dish, secure gently with double-sided tape.
10. In a fume hood, pipet 1 mL of T2492-KH (Tridecafluoro-1,1,2,2-tetrahydro octyl)-1-trichlorosilane) into a scintillation vial and place in a dessicator without a cap. Place the dish containing the wafer next to it without a lid. Close the dessicator and degas for 5 minutes.
11. Close the vacuum line and let the dessicator sit for 30 mintes.
12. Vent the chamber and cap the silane.
13. Mix PDMS 1:10 curing agent to elastomer and mix well. Pour over mold.
14. Degas in dessicator.
15. Cure at 60 C overnight or for several hours.

APPENDIX B: CELL AND VIRUS CULTURE PROTOCOLS

OVERVIEW

VSV-G pseudotype lentivirus will be used as a model virus for HIV viral detection as it has a similar size to HIV (~100nm) and contains the p24 capsid protein which can be used to quantify the virus via p24 ELISAs. VSV-G virus is made by transfecting 293T cells with 4 plasmids containing the essential viral synthesis genes: PHDLglp (contains viral structural proteins), Rev (for reverse transcription), VSV-G (coating), GRR (packaged product, contains GFP). Viruses are harvested after transfection of 293T cell and kept freezed in -40˚C till use.

Protocol for culture of VSV-G pseudotype lentivirus. Provided by G. Chen, April 5, 2011 and modified by G. Damhorst with advice from L. Millet.

Genes

- PHDLglp
- Rev
- VSV-G
- GRR

Plasmids

- pRSV-Rev (gene: Rev)
- pMDLg/pRRE (gene: HIV-1 GAG/POL)
- pVSV-G (gene: VSV-G)
- pVPR-GFP (gene: VPR)
- pLenti-luc (gene: Firefly Luciferase)

Safety precautions to be observed throughout viral culture

All cell and virus handling must be performed under a ventilated cell culture hood. The working area must observe BL2 safety standards.

No sharps are to be used or be in the vicinity when performing cell or viral handling. Sharps include all glassware, needles, and metal syringe tips.

Personal protective equipment required are: lab coat, nitrile gloves, goggles, close toed shoes.

CULTURE OF BACTERIA FOR PLASMID EXTRACTION

1. Begin with media broth, LB or HTB + Prolim (4x as effective). Take 4 conical flasks (with ridges on bottom) and add 50ml of broth to each. Use a Bunsen to flame the mouth of each flask and mouth of the media flask before media transfer.
2. Take a tube of Carbencillin (antibiotic derived from Amoxycillin) from the –20 freezer (found in box marked antibiotics, tubes are labeled with 'C'). Defrost in water bath, and add 1:1000 to the media (50uL antibiotic to 50mL media)
3. Get small batch of dry ice (down corridor on left hand side, found in a box behind a freezer). Take 1 tube each of the 4 bacterial stocks from the –80 freezer (in box marked Yoni) and put on the dry ice.
4. Take rod with wire loop on end, heat up wire loop on Bunsen, then allow to cool a little before dipping inside the frozen bacteria tubes. Dip wire inside the culture flasks, introducing one type of bacteria to each flask. Flame the wire in between each change of bacteria type. Return bacteria stocks to –80 freezer.
5. Seal culture flasks and place inside Innova 4300 incubater, set to 250rpm, Hrs = OFF, temp=37 degrees.
6. Leave 16-20 hours (overnight)

7. Check the flasks for turbidity. If flasks are still clear, redo the inoculation. If flasks turbid, transfer contents to 50ml plastic centrifuge tubes.
8. Centrifuge at 3000 RPM for 15mins. Collect supernatant in a plastic tub, add a squirt of Wex-cide, shake for 1-2mins, then discard down sink
9. Freeze the tubes with the pellets in –20 freezer and use when needed. This will keep indefinitely.

Lysis of bacteria

1. Suspend bacteria pellet in 3 ml Cell Resuspension Solution (make sure not to make to much air bubbles while pipetting the fluid back and forward when dissolving the bacteria).
2. Transfer the suspension to the 50 ml centrifuge plastic tubes.
3. Add 3 ml Cell Lysis Solution and mix by gently inverting the tube 3-5 times. Incubate for 3 minutes.
4. Add 10 ml Neutralixation Solution to the lysed cells. Mix by mixing vigorously 3 to 5 times.
5. Centrifuge (fixed rotor) at 14000g for 30 minutes at 4˚C.
6. Place a white (PureYield) Binding Column, and a blue column on top, onto the vacuum manifold, pour lysate into the Binding Column and apply vacuum. Release the vacuum gently, else the membrane will detach.

Wash (after removing the blue column)

1. Add 5 ml of Endotoxin Removal Wash to the column and allow the vacuum to pull the solution through.
2. Add 20 ml Column Wash Solution to the column and allow the vacuum to draw the solution through.
3. Dry the membrane by applying a vacuum for 30 seconds. Remove the Binding Column, tap the tip of the column on a paper towel to remove excess ethanol and wipe excess ethanol from the outside and inside of the tube. Place the column into a new 50 ml disposable plastic tube.

Elute

1. Elute the DNA from the column by adding 800 ul Nuclease-Free Water (spreading it over the whole membrande).
2. Centrifuge (in the swing rotor centrifuge) at 3000 x g for 5 minutes.
3. Collect the filtrate from the 50 ml tube and transfer to a 1.5 ml tube.

Quantify

1. Measure the concentration of the DNA.
2. First measure 2 times blanco with Demi-water (on top of the shelf, above the computer), then put 4ul and measure the sample.

HUMAN EMBRYONIC KIDNEY 293 CELLS

Preparation of cell culture media for 293T cells (makes 1 L)

Materials

- 1 packet Dulbecco's Modified Eagle Medium
- 1 L DI Water
    - g Sodium Bicarbonate
- 50 mL Heat Inactivated FBS
- 10 mL PenStrep

Equipment

- Magnetic Stirrer
- Water Bath (optional)
- 0.22 µm filter (yellow)
- 500 mL glass bottle (2)

- Vacuum extractor
- 4 C refrigeratir

Procedure

1. Add 1 packet DMEM (Dulbecco's Modified Eagle Medium) to 1 L DI water. Add 3.9 g Sodium Bicarbonate. Mix on magnetic stirrer for a few minutes. Check that the solution is colored red.
2. Thaw out 50 mL HI (heat inactivated) FBS and 10 mL PenStrep. Ideally thaw overnight at 4 degrees, otherwise thaw in the water bath for ~20 minutes, tipping the tube every 5 minutes.
3. Take a 0.22 μm filter (yellow), place on top of a 500 mL glass bottle (no cracks on bottle mouth), and hook onto vacuum extractor. Pour 500ml media into each bottle through the filter. Label and store one of the bottles at 4 degrees.
4. To the other bottle, add the FBS and PenStrep. Do this under a hood to ensure sterile medium.

Culture of 293T cells from cryogenic storage

Materials

- 50 mL medium
- Dry ice

Equipment

- 37 C water bath
- T75 flask
- 5 mL pipet

Procedure

Larry's Modified Day 0 Protocol:

1. Thaw cells from liquid N2 in your hand
2. Pipet cells to centrifuge tube from cryogenic storage tube and add 5 ml medium
3. Spin at 300 rcf for 5 min at 24 C
4. Remove tube, careful not to dislodge pellet. Aspirate liquid.

5. Flick 5-6 times to dislodge pellet. Add 2 mL media. Pipet up and down 2 times to mix.
6. Remove 20 µL from this culture and add to a 1 mL tube.
7. Pipet 20 µL Trypan Blue into cap.
8. Add cells to cap and mix. Add to hemacytometer and count.
9. Count four corner quadrants and sum
10. Multiply sum by 5; this is cells/µL
11. Add 666 µL of culture to each of 3 T25 flask.
12. Add 8 mL of media to each T25 flask. Pipet up and down to mix.
13. Label flasks and incubate at 37 C, 5% CO2.

Larry's Splitting Protocol (1:3):

1. Thaw out trypsin in the 37 C water bath. Need 3 mL of trypsin per T25 flask.
2. Warm up media in the 37 C water bath.
3. Spray everything with 70% EtOH before placing them in the hood.
4. Aspirate the media from each flask. Use the same aspirating tip.
5. Add 3 mL of trypsin in to each flask using the micropipettor.
6. Cap each flask and observe under the microscope. Look for cells beginning to detach from the plate.
7. Obtain 3 T75 flasks. These will be used for the 1:3 split of each T25.
8. Gently pipet the cells and trypsin to ensure all cells are losely attached. Pipet up and down in order to break up the sheets of cells.
9. Add 10 mL of media to the T25 flasks to dilute the trypsin. Pipet the media up and down.
10. Remove ~8 mL (whatever fits in the 5 mL pipet) from the T25 flasks and place them into the T75 flasks. Try to spread the cells evenly across the surface.
11. Add enough media to reach about 20 mL of total media into each T75.
12. Label flasks and incubate at 37 C, 5% CO2.
13. Note: Did not necessarily keep A to A, B to B, and C to C.

Mitch's Splitting Protocol (1:20)

1. Aspirate media (tip flask upside down and tip media to corner).
2. Add ~2 mL trypsin and aspirate.
3. Add 5 mL trypsin. Incubate for 2-3 min.
4. Add 5 mL media to inactivate trypsin. Pipet up and down to mix.
5. Add 0.5 mL cells to new flask.
6. Add 10 mL fresh media. Pipet up and down to mix.

Day 0:

1. Warm up 50 mL tube of medium in 37º water bath for ~15 mins.
2. Remove cells from liquid nitrogen. Place immediately either on dry ice or in 37 degree water bath (just let it float in there).
3. While cells are thawing, add 9 mL medium to a T75 flask.
4. Once cells have thawed completely (~5-10 minutes), SLOWLY pipet them out of their vial (using 5 mL pipet) and into the prepared media in the flask.
5. Gently mix by rocking flask back and forth to ensure equal coverage of the bottom face of the flask. Be sure to maintain sterile technique throughout, and spray everything that goes into the hood with isopropanol.

Day 1:

- The following day, be sure to come in in the morning and switch to fresh media, as the DMSO carried over in the cryostock is toxic to cells.

Day 2:

- Split cells 1:3

Day 3:

- Change media.

Day 4:

- Transfect with viral plasmids (see transfection protocol).
- Split cells again for stocks.

Day 5:

- Change media.

Day 6 & 7:

- Make cryostocks on day 6-7.
- Collect virus on Days 6 and 7.

VSV-G PSEUDOTYPED LENTIVIRUS CULTURE

Plasmid and DNA transfection

Materials

- DMEM-media
- Heat Inactivated FBS
- PenStrep
- 30μg DNA for transfection
- Opti-Mem I REduced Serum Medium (see below)
- Lipofectamine 2000

Equipment

- T75 Flask
- CO2 Incubator

Procedure

1. One day before transfection plate cells in a T75 flask with 10 ml of DMEM-media (Dulbecco's Modified Eagle Medium + HI (heat inactivated) FBS + PenStrep). Start with transfection when cell are 70-75% confluent.

2. Dilute (in total) 30µg DNA (four plasmid in specific ratio's, see excel sheet of Yoni -- attached) in 1.9 ml Opti-Mem I Reduced Serum Medium (mix gently).
3. Mix Lipofectamine 2000 gently before use, then dilute 15µl in 1.9ml of Opti-MEM I Reduced Serum Medium. Incubate for 5 minutes at room temperature.
4. Mix diluted DNA and Lipofectamine gently and incubate for 20 minutes at room temperature (complexes are stable for 6 hours at room temperature).
5. Wash flask with cell: remove media, wash with PBS, wash with OptiMEM. By rotating the flask when aspirating the media you reduce the risk of aspirating the cells (which are not very sticky).
6. Add 10 ml of OptiMem and complexes to each flask. (Flask should be upside down when adding the media omitting the chance of detaching the cells when adding the media).
7. Mix gently by rocking the plate back and forth.
8. Incubate at 37˚C in a CO2 incubator and change media next day.
9. When cells are 90-95% confluent one can start with harvesting.
10. Opti-Mem I Reduced Serum Medium components: modification of Eagle's Minimum Essential Media, buffered with HEPES and sodium bicarbonate and supplemented with hypoxanthine, thymidine, sodium pyruvate, L-glutamine, trace elements and growth factors. Suggested for transfection using Lipofectamine 2000. (Invitrogen)

Harvest viruses

1. When cells are 90-95% confluent one can start with harvesting.
2. If cell are 90-95% confluent the day after transfection one changes the media. (The time at which the media is changed is the time at which one will harvest the viruses the next day.)
3. 24 hours after changing the media one pipettes out the media with the viruses and distributes this in several vials of 1ml. (10 vials per flask) Only use plastic pipettes.
4. One will harvest only two times. After use, clean flasks and used materials carefully with Wexcide (leave in Wexcide for at least 15 minutes), and dispose in biohazard boxes.

5. The vials with viruses are stored in the -40˚C freezer.

Greg's modified harvesting protocol

1. Pipet out the media from the T75 flasks into a 15 mL tube. Label which flask the media came from.
2. Bleach the flasks after harvesting for the second time.
3. Centrifuge the 15 mL tube at 250g for 5 minutes to centrifuge out dead cells/cellular debris.
4. Using the pipettor, place ~1 mL of media into the Cryotubes. Be sure to not pipet up the pellet.

BIBLIOGRAPHY

[1] J. Kates, A. Wexler, and Kaiser Family Foundation, "Financing the Response Response to HIV in Low- and and Middle-Income Countries," 2014.

[2] WHO, UNAIDS, and UNICEF, "Global HIV/AIDS Response: Epidemic update and health sector progress towards Universal Access," 2011.

[3] N. N. Watkins, U. Hassan, G. Damhorst, H. Ni, A. Vaid, W. Rodriguez, and R. Bashir, "Microfluidic CD4+ and CD8+ T Lymphocyte Counters for Point-of-Care HIV Diagnostics Using Whole Blood.," *Sci. Transl. Med.*, vol. 5, no. 214, p. 214ra170, Dec. 2013.

[4] G. L. Damhorst, C. E. Smith, E. M. Salm, M. M. Sobieraj, H. Ni, H. Kong, and R. Bashir, "A liposome-based ion release impedance sensor for biological detection.," *Biomed. Microdevices*, vol. 15, no. 5, pp. 895–905, Oct. 2013.

[5] G. L. Damhorst, C. Duarte-Guevara, W. Chen, T. Ghonge, B. T. Cunningham, and R. Bashir, "Smartphone-imaged HIV-1 reverse transcription loop-mediated isothermal amplification (RT-LAMP) on a chip from whole blood," *Engineering*, vol. 1, no. 3, 2015.

[6] C. for D. Control, "Morbidity and Mortality Weekly Report, June 5, 1981," no. 21, pp. 249–264, 1981.

[7] Centers for Disease Control, "Pneumocystis pneumonia," *cdc.gov*, 2014. .

[8] L. K. Altman, "RARE CANCER SEEN IN 41 HOMOSEXUALS: Outbreak Occurs Among Men in New York and California," *New York Times*, p. A20, 03-Jul-1981.

[9] "Cancer Linked to Gays," *The Washington Post*, p. A10, 04-Jul-1981.

[10] L. J. Rose, "Kaposi Sarcoma," *Medscape Reference*, 2015. [Online]. Available: http://emedicine.medscape.com/article/279734-overview. [Accessed: 27-Jun-2015].

[11] World Health Organization, "HIV/AIDS Fact Sheet," 2015. [Online]. Available: http://www.who.int/mediacentre/factsheets/fs360/en/#.

[12] F. Barre-Sinoussi, J. Chermann, F. Rey, M. Nugeyre, S. Chamaret, J. Gruest, C. Dauguet, C. Axler-Blin, F. Vezinet-Brun, C. Rouzioux, W. Rozenbaum, and L. Montagnier, "Isolation of a T-lymphotropic retrovirus from a patient at risk for acquired immune deficiency syndrome (AIDS)," *Science (80-.).*, vol. 220, no. 4599, pp. 868–871, May 1983.

[13] R. Gallo, P. Sarin, and E. Gelmann, “Isolation of human T-cell leukemia virus in acquired immune deficiency syndrome (AIDS),” *Science (80-.).*, 1983.

[14] Aids.gov, “30 YEARS OF HIV / AIDS TIMELINE,” no. Cdc, pp. 1–13, 2011.

[15] M. T. P. Gilbert, A. Rambaut, G. Wlasiuk, T. J. Spira, A. E. Pitchenik, and M. Worobey, “The emergence of HIV/AIDS in the Americas and beyond.,” *Proc. Natl. Acad. Sci. U. S. A.*, vol. 104, no. 47, pp. 18566–70, Nov. 2007.

[16] F. Clavel, D. Guetard, and F. Brun-Vezinet, “Isolation of a new human retrovirus from West African patients with AIDS,” *Science (80-.).*, vol. 248, no. 1976, 1986.

[17] P. M. Sharp and B. H. Hahn, “Origins of HIV and the AIDS pandemic.,” *Cold Spring Harb. Perspect. Med.*, vol. 1, no. 1, p. a006841, Sep. 2011.

[18] B. F. Keele, F. Van Heuverswyn, Y. Li, E. Bailes, J. Takehisa, M. L. Santiago, F. Bibollet-Ruche, Y. Chen, L. V Wain, F. Liegeois, S. Loul, E. M. Ngole, Y. Bienvenue, E. Delaporte, J. F. Y. Brookfield, P. M. Sharp, G. M. Shaw, M. Peeters, and B. H. Hahn, “Chimpanzee reservoirs of pandemic and nonpandemic HIV-1.,” *Science*, vol. 313, no. 5786, pp. 523–6, Jul. 2006.

[19] N. R. Faria, a. Rambaut, M. a. Suchard, G. Baele, T. Bedford, M. J. Ward, a. J. Tatem, J. D. Sousa, N. Arinaminpathy, J. Pepin, D. Posada, M. Peeters, O. G. Pybus, and P. Lemey, “The early spread and epidemic ignition of HIV-1 in human populations,” *Science (80-.).*, vol. 346, no. 6205, pp. 56–61, Oct. 2014.

[20] U.S. Food and Drug Administration, “Antiretroviral drugs used in the treatment of HIV infection,” *fda.gov*, 2014. [Online]. Available: http://www.fda.gov/ForPatients/Illness/HIVAIDS/Treatment/ucm118915.htm. [Accessed: 01-Jan-2015].

[21] World Health Organization, “Global update on HIV treatment 2013: results, impact and opportunities,” 2013.

[22] J. a Aberg, J. E. Gallant, K. G. Ghanem, P. Emmanuel, B. S. Zingman, M. a Horberg, and Infectious Diseases Society of America, “Primary care guidelines for the management of persons infected with HIV: 2013 update by the HIV medicine association of the Infectious Diseases Society of America.,” *Clin. Infect. Dis.*, vol. 58, no. 1, pp. e1–34, Jan. 2014.

[23] J. a Aberg, J. E. Kaplan, H. Libman, P. Emmanuel, J. R. Anderson, V. E. Stone, J. M. Oleske, J. S. Currier, and J. E. Gallant, “Primary care guidelines for the management of persons infected with human immunodeficiency virus: 2009 update by the HIV medicine Association of the Infectious Diseases Society of America.,” *Clin. Infect. Dis.*, vol. 49, no. 5, pp. 651–81, Sep. 2009.

[24] W. H. O. (WHO), “Consolidated guidelines on the use of antiretroviral drugs for treating and preventing HIV infection,” no. June, 2013.

[25] U.S. Department of Health and Human Services, “Guide for HIV/AIDS Clinical Care,” no. January. U.S. Department of Health and Human Services, 2011.

[26] United Nations, “The Millennium Development Goals Report 2014,” New York, NY, 2014.

[27] World Health Organization, “Global tuberculosis report 2013,” Geneva, Switzerland, 2013.

[28] World Health Organization, “World Health Statistics 2014,” 2014.

[29] World Health Organization, “Roll Back Malaria Partnership: A Decade of Partnership and Results,” Geneva, Switzerland, 2011.

[30] A. N. Abou Tayoun, P. R. Burchard, I. Malik, A. Scherer, and G. J. Tsongalis, “Democratizing molecular diagnostics for the developing world.,” *Am. J. Clin. Pathol.*, vol. 141, no. 1, pp. 17–24, Jan. 2014.

[31] RAND Corporation, “Estimating the Global Health Impact of Improved Diagnostic Tools for the Developing World,” 2007.

[32] C. F. Rowley, “Developments in CD4 and viral load monitoring in resource-limited settings.,” *Clin. Infect. Dis.*, vol. 58, no. 3, pp. 407–12, Mar. 2014.

[33] World Health Organization, “Malaria World Report 2013,” *World Heal. Organ.*, Aug. 2013.

[34] World Health Organization, “Global Health Observatory (GHO): HIV/AIDS,” 2012. [Online]. Available: http://www.who.int/gho/hiv/en/.

[35] W. H. Organization, “Automated real-time nucleic acid amplification technology for rapid and simultaneous detection of tuberculosis and rifampicin resistance: Xpert MTB/RIF,” 2011.

[36] K. Dheda, M. Ruhwald, G. Theron, J. Peter, and W. C. Yam, “Point-of-care diagnosis of tuberculosis: past, present and future.,” *Respirology*, vol. 18, no. 2, pp. 217–32, Mar. 2013.

[37] World Health Organization, “TB diagnostics and laboratory strengthening,” 2014. [Online]. Available: http://who.int/tb/laboratory/mtbrifrollout/en/. [Accessed: 08-Dec-2014].

[38] Foundation for Innovative New Diagnostics, “Price for Xpert MTB/RIF and FIND country list,”

2013. [Online]. Available: http://www.finddiagnostics.org/about/what_we_do/successes/find-negotiated-prices/xpert_mtb_rif.html. [Accessed: 08-Dec-2014].

[39] C. Toumazou, L. M. Shepherd, S. C. Reed, G. I. Chen, A. Patel, D. M. Garner, C.-J. a Wang, C.-P. Ou, K. Amin-Desai, P. Athanasiou, H. Bai, I. M. Q. Brizido, B. Caldwell, D. Coomber-Alford, P. Georgiou, K. S. Jordan, J. C. Joyce, M. La Mura, D. Morley, S. Sathyavruthan, S. Temelso, R. E. Thomas, and L. Zhang, "Simultaneous DNA amplification and detection using a pH-sensing semiconductor system.," *Nat. Methods*, vol. 10, no. 7, pp. 641–6, Jul. 2013.

[40] M. T. Glynn, D. J. Kinahan, and J. Ducrée, "CD4 counting technologies for HIV therapy monitoring in resource-poor settings - state-of-the-art and emerging microtechnologies," *Lab Chip*, vol. 13, no. 14, pp. 2731–48, Jul. 2013.

[41] J. a Davis, D. W. Inglis, K. J. Morton, D. a Lawrence, L. R. Huang, S. Y. Chou, J. C. Sturm, and R. H. Austin, "Deterministic hydrodynamics: taking blood apart.," *Proc. Natl. Acad. Sci. U. S. A.*, vol. 103, no. 40, pp. 14779–84, Oct. 2006.

[42] S. Nagrath, L. V Sequist, S. Maheswaran, D. W. Bell, D. Irimia, L. Ulkus, M. R. Smith, E. L. Kwak, S. Digumarthy, A. Muzikansky, P. Ryan, U. J. Balis, R. G. Tompkins, D. a Haber, and M. Toner, "Isolation of rare circulating tumour cells in cancer patients by microchip technology.," *Nature*, vol. 450, no. 7173, pp. 1235–9, Dec. 2007.

[43] C. Liu, M. Mauk, R. Gross, F. D. Bushman, P. H. Edelstein, R. G. Collman, and H. H. Bau, "Membrane-based, sedimentation-assisted plasma separator for point-of-care applications.," *Anal. Chem.*, vol. 85, no. 21, pp. 10463–70, Nov. 2013.

[44] Z. T. F. Yu, K. M. Aw Yong, and J. Fu, "Microfluidic blood cell sorting: now and beyond," *Small*, vol. 10, no. 9, pp. 1687–703, May 2014.

[45] W. Tian and E. Finehout, "Microfluidic Diagnostic Systems for the Rapid Detection and Quantification of Pathogens," *Microfluid. Biol. Appl.*, pp. 1–52, 2009.

[46] L. Lafleur, D. Stevens, K. McKenzie, S. Ramachandran, P. Spicar-Mihalic, M. Singhal, A. Arjyal, J. Osborn, P. Kauffman, P. Yager, and B. Lutz, "Progress toward multiplexed sample-to-result detection in low resource settings using microfluidic immunoassay cards," *Lab Chip*, vol. 12, no. 6, pp. 1119–27, Mar. 2012.

[47] N. Watkins, B. M. Venkatesan, M. Toner, W. Rodriguez, and R. Bashir, "A robust electrical microcytometer with 3-dimensional hydrofocusing.," *Lab Chip*, vol. 9, no. 22, pp. 3177–84, Nov. 2009.

[48] S. Yang, A. Undar, and J. D. Zahn, "A microfluidic device for continuous, real time blood plasma separation.," *Lab Chip*, vol. 6, no. 7, pp. 871–80, Jul. 2006.

[49] E. Ozkumur, A. M. Shah, J. C. Ciciliano, B. L. Emmink, D. T. Miyamoto, E. Brachtel, M. Yu, P. Chen, B. Morgan, J. Trautwein, A. Kimura, S. Sengupta, S. L. Stott, N. M. Karabacak, T. a Barber, J. R. Walsh, K. Smith, P. S. Spuhler, J. P. Sullivan, R. J. Lee, D. T. Ting, X. Luo, A. T. Shaw, A. Bardia, L. V Sequist, D. N. Louis, S. Maheswaran, R. Kapur, D. a Haber, and M. Toner, "Inertial focusing for tumor antigen-dependent and -independent sorting of rare circulating tumor cells.," *Sci. Transl. Med.*, vol. 5, no. 179, p. 179ra47, Apr. 2013.

[50] P. Sethu, L. L. Moldawer, M. N. Mindrinos, P. O. Scumpia, C. L. Tannahill, J. Wilhelmy, P. a Efron, B. H. Brownstein, R. G. Tompkins, and M. Toner, "Microfluidic isolation of leukocytes from whole blood for phenotype and gene expression analysis.," *Anal. Chem.*, vol. 78, no. 15, pp. 5453–61, Aug. 2006.

[51] P. Sethu, M. Anahtar, L. L. Moldawer, R. G. Tompkins, and M. Toner, "Continuous flow microfluidic device for rapid erythrocyte lysis.," *Anal. Chem.*, vol. 76, no. 21, pp. 6247–53, Nov. 2004.

[52] X. Cheng, Y. Liu, D. Irimia, U. Demirci, L. Yang, L. Zamir, W. R. Rodríguez, M. Toner, and R. Bashir, "Cell detection and counting through cell lysate impedance spectroscopy in microfluidic devices," *Lab Chip*, vol. 7, no. 6, pp. 746–55, Jun. 2007.

[53] N. N. Watkins, S. Sridhar, X. Cheng, G. D. Chen, M. Toner, W. Rodriguez, and R. Bashir, "A microfabricated electrical differential counter for the selective enumeration of CD4+ T lymphocytes," *Lab Chip*, vol. 11, no. 8, pp. 1437–47, Apr. 2011.

[54] S. Wang, M. Esfahani, U. a Gurkan, F. Inci, D. R. Kuritzkes, and U. Demirci, "Efficient on-chip isolation of HIV subtypes.," *Lab Chip*, vol. 12, no. 8, pp. 1508–15, Mar. 2012.

[55] G. Chen, C. J. Alberts, W. Rodriguez, and M. Toner, "Concentration and purification of human immunodeficiency virus type 1 virions by microfluidic separation of superparamagnetic nanoparticles.," *Anal. Chem.*, vol. 82, no. 2, pp. 723–8, Jan. 2010.

[56] E. Kim, J. Stanton, and B. Korber, "Detection of HIV-1 p24 Gag in plasma by a nanoparticle-based bio-barcode-amplification method," *Nanomedicine*, vol. 3, no. 3, 2008.

[57] M. Liong, A. N. Hoang, J. Chung, N. Gural, C. B. Ford, C. Min, R. R. Shah, R. Ahmad, M. Fernandez-Suarez, S. M. Fortune, M. Toner, H. Lee, and R. Weissleder, "Magnetic barcode assay for genetic detection of pathogens.," *Nat. Commun.*, vol. 4, p. 1752, Jan. 2013.

[58] P. Gascoyne, C. Mahidol, M. Ruchirawat, J. Satayavivad, P. Watcharasit, and F. F. Becker, "Microsample preparation by dielectrophoresis: isolation of malaria.," *Lab Chip*, vol. 2, no. 2, pp. 70–5, May 2002.

[59] K.-H. Han and a. Bruno Frazier, “Continuous magnetophoretic separation of blood cells in microdevice format,” *J. Appl. Phys.*, vol. 96, no. 10, p. 5797, 2004.

[60] B. Kuswandi, Nuriman, J. Huskens, and W. Verboom, “Optical sensing systems for microfluidic devices: a review.,” *Anal. Chim. Acta*, vol. 601, no. 2, pp. 141–55, Oct. 2007.

[61] W. H. Organization, “Fluorescent light-emitting diode (LED) microscopy for diagnosis of tuberculosis: policy statement,” 2011.

[62] J.-H. Kim, W.-H. Yeo, Z. Shu, S. D. Soelberg, S. Inoue, D. Kalyanasundaram, J. Ludwig, C. E. Furlong, J. J. Riley, K. M. Weigel, G. a Cangelosi, K. Oh, K.-H. Lee, D. Gao, and J.-H. Chung, “Immunosensor towards low-cost, rapid diagnosis of tuberculosis.,” *Lab Chip*, vol. 12, no. 8, pp. 1437–40, Apr. 2012.

[63] E. Liandris, M. Gazouli, M. Andreadou, L. a Sechi, V. Rosu, and J. Ikonomopoulos, “Detection of pathogenic mycobacteria based on functionalized quantum dots coupled with immunomagnetic separation,” *PLoS One*, vol. 6, no. 5, p. e20026, Jan. 2011.

[64] F. Shen, B. Sun, J. E. Kreutz, E. K. Davydova, W. Du, P. L. Reddy, L. J. Joseph, and R. F. Ismagilov, “Multiplexed quantification of nucleic acids with large dynamic range using multivolume digital RT-PCR on a rotational SlipChip tested with HIV and hepatitis C viral load.,” *J. Am. Chem. Soc.*, vol. 133, no. 44, pp. 17705–12, Nov. 2011.

[65] P. V Baptista, M. Koziol-Montewka, J. Paluch-Oles, G. Doria, and R. Franco, “Gold-nanoparticle-probe-based assay for rapid and direct detection of Mycobacterium tuberculosis DNA in clinical samples,” *Clin. Chem.*, vol. 52, no. 7, pp. 1433–4, Jul. 2006.

[66] L. B. Silva, B. Veigas, G. Doria, P. Costa, J. Inácio, R. Martins, E. Fortunato, and P. V Baptista, “Portable optoelectronic biosensing platform for identification of mycobacteria from the Mycobacterium tuberculosis complex,” *Biosens. Bioelectron.*, vol. 26, no. 5, pp. 2012–7, Jan. 2011.

[67] B. Veigas, J. M. Jacob, M. N. Costa, D. S. Santos, M. Viveiros, J. Inácio, R. Martins, P. Barquinha, E. Fortunato, and P. V. Baptista, “Gold on paper-paper platform for Au-nanoprobe TB detection,” *Lab Chip*, vol. 12, no. 22, pp. 4802–8, Nov. 2012.

[68] S. Wang, S. Tasoglu, P. Z. Chen, M. Chen, R. Akbas, S. Wach, C. I. Ozdemir, U. A. Gurkan, F. F. Giguel, D. R. Kuritzkes, and U. Demirci, “Micro-a-fluidics ELISA for rapid CD4 cell count at the point-of-care.,” *Sci. Rep.*, vol. 4, p. 3796, Jan. 2014.

[69] Z. Gorocs and A. Ozcan, “On-chip biomedical imaging,” *IEEE Rev. Biomed. Eng.*, no. c, pp. 29–46, 2013.

[70] S. Moon, H. O. Keles, A. Ozcan, A. Khademhosseini, E. Haeggstrom, D. Kuritzkes, and U. Demirci, "Integrating microfluidics and lensless imaging for point-of-care testing.," *Biosens. Bioelectron.*, vol. 24, no. 11, pp. 3208–14, Jul. 2009.

[71] F. Inci, O. Tokel, S. Wang, U. A. Gurkan, S. Tasoglu, D. R. Kuritzkes, and U. Demirci, "Nanoplasmonic Quantitative Detection of Intact Viruses from Unprocessed Whole Blood," *ACS Nano*, no. Xx, May 2013.

[72] H. Shafiee, E. a Lidstone, M. Jahangir, F. Inci, E. Hanhauser, T. J. Henrich, D. R. Kuritzkes, B. T. Cunningham, and U. Demirci, "Nanostructured optical photonic crystal biosensor for HIV viral load measurement.," *Sci. Rep.*, vol. 4, p. 4116, Jan. 2014.

[73] D. Holmes, D. Pettigrew, C. H. C. H. Reccius, J. D. Gwyer, C. van Berkel, J. Holloway, D. E. Davies, H. Morgan, C. Van Berkel, and D. Morganti, "Leukocyte analysis and differentiation using high speed microfluidic single cell impedance cytometry," *Lab Chip*, vol. 9, no. 20, pp. 2881–9, Oct. 2009.

[74] E. Du, S. Ha, M. Diez-Silva, M. Dao, S. Suresh, and A. P. Chandrakasan, "Electric impedance microflow cytometry for characterization of cell disease states.," *Lab Chip*, vol. 13, no. 19, pp. 3903–9, Oct. 2013.

[75] S. Ha, M. Diez-Silva, E. Du, S. Kim, and J. Han, "Microfluidic Electric Impedance Spectroscopy for Malaria Diagnosis," *Miniaturized Syst. Chem. Life Sci.*, pp. 1960–1962, 2012.

[76] Y. Liu, T. Kwa, and A. Revzin, "Simultaneous detection of cell-secreted TNF-α and IFN-γ using micropatterned aptamer-modified electrodes," *Biomaterials*, vol. 33, no. 30, pp. 7347–55, Oct. 2012.

[77] Y. Liu, N. Tuleouva, E. Ramanculov, and A. Revzin, "Aptamer-based electrochemical biosensor for interferon gamma detection.," *Anal. Chem.*, vol. 82, no. 19, pp. 8131–6, Oct. 2010.

[78] M. De Souza Castilho and T. Laube, "Magneto immunoassays for Plasmodium falciparum histidine-rich protein 2 related to malaria based on magnetic nanoparticles," *Anal. Chem.*, pp. 5570–5577, 2011.

[79] M. K. Sharma, V. K. Rao, S. Merwyn, G. S. Agarwal, S. Upadhyay, and R. Vijayaraghavan, "A novel piezoelectric immunosensor for the detection of malarial Plasmodium falciparum histidine rich protein-2 antigen," *Talanta*, vol. 85, no. 4, pp. 1812–7, Sep. 2011.

[80] Q. Guo, S. J. Reiling, P. Rohrbach, and H. Ma, "Microfluidic biomechanical assay for red blood cells parasitized by Plasmodium falciparum.," *Lab Chip*, Feb. 2012.

[81] D. Gao, H. Liu, Y. Jiang, and J.-M. Lin, “Recent advances in microfluidics combined with mass spectrometry: technologies and applications.,” *Lab Chip*, vol. 13, no. 17, pp. 3309–22, Sep. 2013.

[82] G. Pantaleo, C. Graziosi, and A. S. Fauci, “The immunopathogenesis of human immunodeficiency virus infection,” *N. Engl. J. Med.*, vol. 328, no. 5, pp. 327–335, Feb. 1993.

[83] National Institute of Allergy and Infectious Diseases, “The Relationship Between the Human Immunodeficiency Virus and the Acquired Immunodeficiency Syndrome,” *HIV/AIDS*, 2010. [Online]. Available: http://www.niaid.nih.gov/topics/hivaids/understanding/howhivcausesaids/pages/relationshiphivaids.aspx. [Accessed: 12-Apr-2012].

[84] W. H. Organization, “Antiretroviral therapy for HIV infection in adults and adolescents,” 2010.

[85] E. M. Krantz, K. H. Hullsiek, J. F. Okulicz, A. C. Weintrob, B. K. Agan, N. F. Crum-Cianflone, A. Ganesan, T. M. Ferguson, and B. R. Hale, “Elevated CD8 counts during HAART are associated with HIV virologic treatment failure.,” *JAIDS J. Acquir. Immune Defic. Syndr.*, vol. 57, no. 5, pp. 396–403, Aug. 2011.

[86] N. L. Michael, T. Mo, A. Merzouki, M. O. Shaughnessy, C. Oster, D. S. Burke, R. R. Redfield, and D. L. Birx, “Human Immunodeficiency Virus Type 1 Cellular RNA Load and Splicing Patterns Predict Disease Progression in a Longitudinally Studied Cohort,” *J. Virol.*, vol. 69, no. 3, pp. 1868–1877, 1995.

[87] K. Saksela, C. Stevens, and P. Rubinstein, “HIV-1 messenger RNA in peripheral blood mononuclear cells as an early marker of risk for progression to AIDS,” *Ann. Intern. Med.*, vol. 123, no. 9, 1995.

[88] A. O. Pasternak, S. Jurriaans, M. Bakker, B. Berkhout, and V. V Lukashov, “Steady increase in cellular HIV-1 load during the asymptomatic phase of untreated infection despite stable plasma viremia.,” *AIDS*, vol. 24, no. 11, pp. 1641–9, Jul. 2010.

[89] M. R. Furtado and L. A. Kingsley, “Changes in the viral mRNA expression pattern correlate with a rapid rate of CD4 + T-cell number decline in human immunodeficiency virus type 1-infected individuals . Changes in the Viral mRNA Expression Pattern Correlate with a Rapid Rate of CD4 ♀ T-Cell ,” 1995.

[90] A. O. Pasternak, S. Jurriaans, M. Bakker, J. M. Prins, B. Berkhout, and V. V Lukashov, “Cellular levels of HIV unspliced RNA from patients on combination antiretroviral therapy with undetectable plasma viremia predict the therapy outcome.,” *PLoS One*, vol. 4, no. 12, p. e8490, Dec. 2009.

[91] M. Zanchetta, S. Walker, N. Burighel, D. Bellanova, O. Rampon, C. Giaquinto, and A. De Rossi,

"Long-Term Decay of the HIV-1 Reservoir in HIV-1 – Infected Children Treated with Highly Active Antiretroviral Therapy," vol. 193, 2006.

[92] A. O. Pasternak, K. W. Adema, M. Bakker, S. Jurriaans, B. Berkhout, M. Cornelissen, and V. V Lukashov, "Highly sensitive methods based on seminested real-time reverse transcription-PCR for quantitation of human immunodeficiency virus type 1 unspliced and multiply spliced RNA and proviral DNA.," *J. Clin. Microbiol.*, vol. 46, no. 7, pp. 2206–11, Jul. 2008.

[93] R. S. Soares, P. Matoso, M. Calado, and A. E. Sousa, "Strategies to quantify unspliced and multiply spliced mRNA expression in HIV-2 infection," *J. Virol. Methods*, vol. 175, no. 1, pp. 38–45, Jul. 2011.

[94] S. H. Vermund, "Chapter 1: HIV Epidemic," in *Challenges in Infectious Diseases*, I. W. Fong, Ed. New York, NY: Springer New York, 2013, pp. 3–46.

[95] U.S. Food and Drug Administration, "Complete List of Donor Screening Assays for Infectious Agents and HIV Diagnostic Assays," *Approved Products*, 2013. .

[96] U.S. Food and Drug Administration, "Vaccines , Blood & Biologics Approved Products: HIV-1," 2010. [Online]. Available: http://www.fda.gov/BiologicsBloodVaccines/BloodBloodProducts/ApprovedProducts/LicensedProductsBLAs/BloodDonorScreening/InfectiousDisease/ucm126582.htm.

[97] T. Peterson and M. Stuart, "PCR HIV Test," *Medscape Reference*, 2011. [Online]. Available: http://emedicine.medscape.com/article/1983649-overview.

[98] U.S. Food and Drug Administration and R. Klein, "Three new HIV assays approved," 2007.

[99] C. Garrido, N. Zahonero, A. Corral, M. Arredondo, V. Soriano, and C. de Mendoza, "Correlation between human immunodeficiency virus type 1 (HIV-1) RNA measurements obtained with dried blood spots and those obtained with plasma by use of Nuclisens EasyQ HIV-1 and Abbott RealTime HIV load tests.," *J. Clin. Microbiol.*, vol. 47, no. 4, pp. 1031–6, Apr. 2009.

[100] A. Johannessen and C. Garrido, "Dried blood spots perform well in viral load monitoring of patients who receive antiretroviral treatment in rural Tanzania," *Clin. Infect. Dis.*, vol. 49, 2009.

[101] S. Cassol, M. Gill, and R. Pilon, "Quantification of human immunodeficiency virus type 1 RNA from dried plasma spots collected on filter paper.," *J. Clin. Microbiol.*, 1997.

[102] P. Mwaba, S. Cassol, A. Nunn, and R. Pilon, "Whole blood versus plasma spots for measurement of HIV-1 viral load in HIV-infected African patients," *Lancet*, vol. 362, no. 9401, pp. 2067–2068, Dec. 2003.

[103] R. de la Rica and M. M. Stevens, “Plasmonic ELISA for the ultrasensitive detection of disease biomarkers with the naked eye,” *Nat. Nanotechnol.*, no. October, pp. 2–5, Oct. 2012.

[104] C. Jennings and S. Fiscus, “Comparison of two human immunodeficiency virus (HIV) RNA surrogate assays to the standard HIV RNA assay,” *J. Clin. Microbiol.*, 2005.

[105] G. Stevens and N. Rekhviashvili, “Evaluation of Two Commercially Available, Inexpensive Alternative Assays Used for Assessing Viral Load in a Cohort of Human Immunodeficiency Virus Type 1 Subtype C-Infected Patients from South Africa,” *J. Clin. Microbiol.*, vol. 43, no. 2, pp. 857–861, Feb. 2005.

[106] S. a Fiscus, J. Wiener, E. J. Abrams, M. Bulterys, A. Cachafeiro, and R. a Respess, “Ultrasensitive p24 antigen assay for diagnosis of perinatal human immunodeficiency virus type 1 infection.,” *J. Clin. Microbiol.*, vol. 45, no. 7, pp. 2274–7, Jul. 2007.

[107] R. Respess and A. Cachafeiro, “Evaluation of an ultrasensitive p24 antigen assay as a potential alternative to human immunodeficiency virus type 1 RNA viral load assay in resource-limited settings,” *J. Clin. Microbiol.*, 2005.

[108] D. Bonard, F. Rouet, T. Toni, and A. Minga, “Field evaluation of an improved assay using a heat-dissociated p24 antigen for adults mainly infected with HIV-1 CRF02_AG strains in Cote d’Ivoire, West Africa.,” *JAIDS J. Acquir. Immune Defic. Syndr.*, 2003.

[109] K. Steegen, S. Luchters, N. De Cabooter, J. Reynaerts, K. Mandaliya, J. Plum, W. Jaoko, C. Verhofstede, and M. Temmerman, “Evaluation of two commercially available alternatives for HIV-1 viral load testing in resource-limited settings.,” *J. Virol. Methods*, vol. 146, no. 1–2, pp. 178–87, Dec. 2007.

[110] K.-B. Lee, E.-Y. Kim, C. a. Mirkin, and S. M. Wolinsky, “The Use of Nanoarrays for Highly Sensitive and Selective Detection of Human Immunodeficiency Virus Type 1 in Plasma,” *Nano Lett.*, vol. 4, no. 10, pp. 1869–1872, Oct. 2004.

[111] Z. a Parpia, R. Elghanian, A. Nabatiyan, D. R. Hardie, and D. M. Kelso, “p24 antigen rapid test for diagnosis of acute pediatric HIV infection.,” *JAIDS J. Acquir. Immune Defic. Syndr.*, vol. 55, no. 4, pp. 413–9, Dec. 2010.

[112] S. Tang, J. Zhao, and J. Storhoff, “Nanoparticle-based biobarcode amplification assay (BCA) for sensitive and early detection of human immunodeficiency type 1 capsid (p24) antigen,” *JAIDS J. Acquir. Immune Defic. Syndr.*, vol. 46, no. 2, pp. 231–237, Oct. 2007.

[113] S. Tang and I. Hewlett, “Nanoparticle-based immunoassays for sensitive and early detection of

HIV-1 capsid (p24) antigen.," *J. Infect. Dis.*, vol. 201 Suppl, no. Suppl 1, pp. S59–64, Apr. 2010.

[114] J. Nam, C. Thaxton, and C. Mirkin, "Nanoparticle-based bio-bar codes for the ultrasensitive detection of proteins," *Science (80-.).*, vol. 301, no. 5641, pp. 1884–1886, Sep. 2003.

[115] D. H. Ekstrand, R. J. Awad, C. F. Källander, and J. S. Gronowitz, "A sensitive assay for the quantification of reverse transcriptase activity based on the use of carrier-bound template and non-radioactive-product detection, with special reference to human-immunodeficiency-virus isolation.," *Biotechnol. Appl. Biochem.*, vol. 23 (Pt 2), pp. 95–105, Apr. 1996.

[116] A. Malmsten, X.-W. Shao, K. Aperia, G. E. Corrigan, E. Sandström, C. F. R. Källander, T. Leitner, and J. S. Gronowitz, "HIV-1 viral load determination based on reverse transcriptase activity recovered from human plasma.," *J. Med. Virol.*, vol. 71, no. 3, pp. 347–59, Nov. 2003.

[117] A. Malmsten, X.-W. Shao, S. Sjödahl, E.-L. Fredriksson, I. Pettersson, T. Leitner, C. F. R. Källander, E. Sandström, and J. S. Gronowitz, "Improved HIV-1 viral load determination based on reverse transcriptase activity recovered from human plasma.," *J. Med. Virol.*, vol. 76, no. 3, pp. 291–6, Jul. 2005.

[118] J. Lombart, M. Vray, and A. Kafando, "Plasma virion reverse transcriptase activity and heat dissociation-boosted p24 assay for HIV load in Burkina Faso, West Africa," *Aids*, no. April, pp. 1273–1277, 2005.

[119] M. Mine, K. Bedi, T. Maruta, D. Madziva, M. Tau, T. Zana, T. Gaolathe, S. Moyo, K. Seipone, N. Ndwapi, M. Essex, and R. Marlink, "Quantitation of human immunodeficiency virus type 1 viral load in plasma using reverse transcriptase activity assay at a district hospital laboratory in Botswana: a decentralization pilot study.," *J. Virol. Methods*, vol. 159, no. 1, pp. 93–7, Jul. 2009.

[120] V. Greengrass, B. Lohman, L. Morris, M. Plate, P. M. Steele, J. L. Walson, and S. M. Crowe, "Assessment of the low-cost Cavidi ExaVir Load assay for monitoring HIV viral load in pediatric and adult patients.," *JAIDS J. Acquir. Immune Defic. Syndr.*, vol. 52, no. 3, pp. 387–90, Nov. 2009.

[121] J. Braun, J.-C. Plantier, M.-F. Hellot, E. Tuaillon, M. Gueudin, F. Damond, A. Malmsten, G. E. Corrigan, and F. Simon, "A new quantitative HIV load assay based on plasma virion reverse transcriptase activity for the different types, groups and subtypes.," *AIDS*, vol. 17, no. 3, pp. 331–6, Feb. 2003.

[122] S. Sivapalasingam and S. Essajee, "Human immunodeficiency virus (HIV) reverse transcriptase activity correlates with HIV RNA load: implications for resource-limited settings," *J. Clin. Microbiol.*, 2005.

[123] H. S. Iqbal, P. Balakrishnan, A. J. Cecelia, S. Solomon, N. Kumarasamy, V. Madhavan, K. G.

Murugavel, A. K. Ganesh, S. S. Solomon, K. H. Mayer, and S. M. Crowe, “Use of an HIV-1 reverse-transcriptase enzyme-activity assay to measure HIV-1 viral load as a potential alternative to nucleic acid-based assay for monitoring antiretroviral therapy in resource-limited settings,” *J. Med. Microbiol.*, vol. 56, no. 12, pp. 1611–4, Dec. 2007.

[124] V. L. Greengrass, M. M. Plate, P. M. Steele, J. T. Denholm, C. L. Cherry, L. M. Morris, A. Hearps, and S. M. Crowe, “Evaluation of the Cavidi ExaVir Load assay (version 3) for plasma human immunodeficiency virus type 1 load monitoring.,” *J. Clin. Microbiol.*, vol. 47, no. 9, pp. 3011–3, Sep. 2009.

[125] W. Labbett, A. Garcia-Diaz, Z. Fox, G. S. Clewley, T. Fernandez, M. Johnson, and A. M. Geretti, “Comparative evaluation of the ExaVir Load version 3 reverse transcriptase assay for measurement of human immunodeficiency virus type 1 plasma load.,” *J. Clin. Microbiol.*, vol. 47, no. 10, pp. 3266–70, Oct. 2009.

[126] P. Stewart, A. Cachafeiro, S. Napravnik, J. J. Eron, I. Frank, C. van der Horst, R. J. Bosch, D. Bettendorf, P. Bohlin, and S. a Fiscus, “Performance characteristics of the Cavidi ExaVir viral load assay and the ultra-sensitive P24 assay relative to the Roche Monitor HIV-1 RNA assay.,” *J. Clin. Virol.*, vol. 49, no. 3, pp. 198–204, Nov. 2010.

[127] W. Tang, W. H. a Chow, Y. Li, H. Kong, Y.-W. Tang, and B. Lemieux, “Nucleic acid assay system for tier II laboratories and moderately complex clinics to detect HIV in low-resource settings.,” *J. Infect. Dis.*, vol. 201 Suppl, no. Suppl 1, pp. S46–51, Apr. 2010.

[128] H. H. Lee, M. a Dineva, Y. L. Chua, A. V Ritchie, I. Ushiro-Lumb, and C. a Wisniewski, “Simple amplification-based assay: a nucleic acid-based point-of-care platform for HIV-1 testing.,” *J. Infect. Dis.*, vol. 201 Suppl, no. Suppl 1, pp. S65–72, Apr. 2010.

[129] S. H. Lee, S.-W. Kim, J. Y. Kang, and C. H. Ahn, “A polymer lab-on-a-chip for reverse transcription (RT)-PCR based point-of-care clinical diagnostics.,” *Lab Chip*, vol. 8, no. 12, pp. 2121–7, Dec. 2008.

[130] B. A. Rohrman, V. Leautaud, E. Molyneux, and R. R. Richards-Kortum, “A Lateral Flow Assay for Quantitative Detection of Amplified HIV-1 RNA,” *PLoS One*, vol. 7, no. 9, pp. e45611–e45611, Sep. 2012.

[131] S. Tanriverdi, L. Chen, and S. Chen, “A rapid and automated sample-to-result HIV load test for near-patient application,” *J. Infect. Dis.*, vol. 201 Suppl, no. s1, pp. S52–8, Apr. 2010.

[132] Y.-G. Kim, S. Moon, D. R. Kuritzkes, and U. Demirci, “Quantum dot-based HIV capture and imaging in a microfluidic channel.,” *Biosens. Bioelectron.*, vol. 25, no. 1, pp. 253–8, Sep. 2009.

[133] S. Wang, A. Ip, F. Xu, F. F. Giguel, S. Moon, A. Akay, D. R. Kuritzkes, and U. Demirci,

"Development of a microfluidic system for measuring HIV-1 viral load," *Sensors, Command. Control. Commun. Intell. Technol. Homel. Secur. Homel. Def. IX*, vol. 7666, p. 76661H–76661H–6, Apr. 2010.

[134] S. Cassol, A. Butcher, and S. Kinard, "Rapid screening for early detection of mother-to-child transmission of human immunodeficiency virus type 1.," *J. Clin. Microbiol.*, pp. 1–6, 1994.

[135] J. Weidner, U. Cassens, W. Göhde, W. Sibrowski, G. Odaibo, D. Olaleye, D. Reichelt, and B. Greve, "An improved PCR method for detection of HIV-1 proviral DNA of a wide range of subtypes and recombinant forms circulating globally," *J. Virol. Methods*, vol. 172, no. 1–2, pp. 22–26, Mar. 2011.

[136] T. E. Schutzbank and J. Smith, "Detection of human immunodeficiency virus type 1 proviral DNA by PCR using an electrochemiluminescence-tagged probe.," *J. Clin. Microbiol.*, vol. 33, no. 8, pp. 2036–41, Aug. 1995.

[137] D. Zella, A. Cavicchini, and E. Cattaneo, "Utilization of a DNA enzyme immunoassay for the detection of proviral DNA of human immunodeficiency virus type 1 by polymerase chain reaction," *Clin. Diagn. Virol.*, vol. 3, no. 2, pp. 155–164, Feb. 1995.

[138] K. L. Barlow, J. H. C. Tosswill, J. V Parry, and J. P. Clewley, "Performance of the Amplicor Human Immunodeficiency Virus Type 1 PCR and Analysis of Specimens with False-Negative Results," vol. 35, no. 11, pp. 2846–2853, 1997.

[139] J. W. Bremer, J. F. Lew, E. Cooper, G. V Hillyer, J. Pitt, E. Handelsman, D. Brambilla, J. Moye, and R. Haft, "Diagnosis of infection with human immunodeficiency virus type 1 by a DNA polymerase chain reaction assay among infants enrolled in the Women and Infants ' Transmission Study," 1996.

[140] C. Delamare, M. Burgard, and M. Mayaux, "HIV-1 RNA detection in plasma for the diagnosis of infection in neonates," *JAIDS J.*, vol. 15, no. 2, pp. 121–125, 1997.

[141] CDC, "HIV Testing Basics for Consumers," *HIV Testing Basics for Consumers*, 2010. [Online]. Available: http://www.cdc.gov/hiv/topics/testing/resources/qa/index.htm.

[142] C. Christopherson, Y. Kidane, B. Conway, H. Sheppard, S. Kwok, and J. Krowka, "PCR-Based Assay To Quantify Human Immunodeficiency Virus Type 1 DNA in Peripheral Blood Mononuclear Cells These include : PCR-Based Assay To Quantify Human Immunodeficiency Virus Type 1 DNA in Peripheral Blood Mononuclear Cells," 2000.

[143] N. Désiré and A. Dehée, "Quantification of human immunodeficiency virus type 1 proviral load by a TaqMan real-time PCR assay," *J. Clin. ...*, 2001.

[144] L. G. Kostrikis, G. Touloumi, R. Karanicolas, N. Pantazis, C. Anastassopoulou, J. J. Goedert, A. Hatzakis, and A. Karafoulidou, "Quantitation of Human Immunodeficiency Virus Type 1 DNA Forms with the Second Template Switch in Peripheral Blood Cells Predicts Disease Progression Independently of Plasma RNA Load Quantitation of Human Immunodeficiency Virus Type 1 DNA Forms with the Se," 2002.

[145] A. E. Hatzakis, G. Touloumi, N. Pantazis, C. G. Anastassopoulou, O. Katsarou, A. Karafoulidou, J. J. Goedert, and L. G. Kostrikis, "Cellular HIV-1 DNA load predicts HIV-RNA rebound and the outcome of highly active antiretroviral therapy," no. September, 2004.

[146] D. Gibellini, M. Borderi, E. De Crignis, R. Cicola, L. Cimatti, F. Vitone, F. Chiodo, and M. C. Re, "HIV-1 DNA load analysis in peripheral blood lymphocytes and monocytes from naïve and HAART-treated individuals.," *J. Infect.*, vol. 56, no. 3, pp. 219–25, Mar. 2008.

[147] M. C. Re, F. Vitone, C. Biagetti, P. Schiavone, F. Alessandrini, I. Bon, E. de Crignis, and D. Gibellini, "HIV-1 DNA proviral load in treated and untreated HIV-1 seropositive patients.," *Clin. Microbiol. Infect.*, vol. 16, no. 6, pp. 640–6, Jun. 2010.

[148] S. M. Moroney, L. C. Heller, and R. H. Widen, "Evaluation of two TaqMan PCR assays for the detection of HIV-1 proviral DNA in blood samples," *J. Microbiol. Methods*, vol. 65, no. 2, pp. 350–353, May 2006.

[149] M. S. Malnati, G. Scarlatti, F. Gatto, F. Salvatori, G. Cassina, T. Rutigliano, R. Volpi, and P. Lusso, "A universal real-time PCR assay for the quantification of group-M HIV-1 proviral load.," *Nat. Protoc.*, vol. 3, no. 7, pp. 1240–8, Jul. 2008.

[150] A. De Rossi, M. Zanchetta, F. Vitone, G. Antonelli, P. Bagnarelli, L. Buonaguro, M. R. Capobianchi, M. Clementi, I. Abbate, F. Canducci, A. Monachetti, E. Riva, G. Rozera, C. Scagnolari, M. Tagliamonte, M. Carla, and I. Society, "Quantitative HIV-1 proviral DNA detection : a multicentre analysis," pp. 293–302, 2010.

[151] S. R. Jangam, D. H. Yamada, S. M. McFall, and D. M. Kelso, "Rapid, point-of-care extraction of human immunodeficiency virus type 1 proviral DNA from whole blood for detection by real-time PCR.," *J. Clin. Microbiol.*, vol. 47, no. 8, pp. 2363–8, Aug. 2009.

[152] S. R. Jangam, A. K. Agarwal, K. Sur, and D. M. Kelso, "A point-of-care PCR test for HIV-1 detection in resource-limited settings.," *Biosens. Bioelectron.*, vol. 42, pp. 69–75, Apr. 2013.

[153] J.-H. Wang, L. Cheng, C.-H. Wang, W.-S. Ling, S.-W. Wang, and G.-B. Lee, "An integrated chip capable of performing sample pretreatment and nucleic acid amplification for HIV-1 detection," *Biosens. Bioelectron.*, Sep. 2012.

[154] S. Y. Bae, H. C. Park, J. S. Oh, S.-Y. Yoon, D. W. Park, I. K. Choi, H. J. Kim, J. H. Oh, D. S. Hur,

C. Chung, J. K. Chang, J. P. Robinson, and C. S. Lim, “Absolute CD4 cell count using a plastic microchip and a microscopic cell counter.,” *Cytometry*, vol. 76B, no. 5, pp. 345–53, Sep. 2009.

[155] W. R. Rodriguez, N. Christodoulides, P. N. Floriano, S. Graham, S. Mohanty, M. Dixon, M. Hsiang, T. Peter, S. Zavahir, I. Thior, D. Romanovicz, B. Bernard, A. P. Goodey, B. D. Walker, and J. T. McDevitt, “A microchip CD4 counting method for HIV monitoring in resource-poor settings.,” *PLoS Med.*, vol. 2, no. 7, p. e182, Jul. 2005.

[156] M. a Alyassin, S. Moon, H. O. Keles, F. Manzur, R. L. Lin, E. Hæggstrom, D. R. Kuritzkes, and U. Demirci, “Rapid automated cell quantification on HIV microfluidic devices.,” *Lab Chip*, vol. 9, no. 23, pp. 3364–9, Dec. 2009.

[157] S. Thorslund, R. Larsson, F. Nikolajeff, J. Bergquist, and J. Sanchez, “Bioactivated PDMS microchannel evaluated as sensor for human CD4+ cells—The concept of a point-of-care method for HIV monitoring,” *Sensors Actuators B Chem.*, vol. 123, no. 2, pp. 847–855, May 2007.

[158] S. Thorslund, R. Larsson, J. Bergquist, F. Nikolajeff, and J. Sanchez, “A PDMS-based disposable microfluidic sensor for CD4+ lymphocyte counting,” *Biomed. Microdevices*, vol. 10, no. 6, pp. 851–7, Dec. 2008.

[159] J. V Jokerst, P. N. Floriano, N. Christodoulides, G. W. Simmons, and J. T. McDevitt, “Integration of semiconductor quantum dots into nano-bio-chip systems for enumeration of CD4+ T cell counts at the point-of-need.,” *Lab Chip*, vol. 8, no. 12, pp. 2079–90, Dec. 2008.

[160] J. V Jokerst, J. W. Jacobson, B. D. Bhagwandin, P. N. Floriano, N. Christodoulides, and J. T. McDevitt, “Programmable nano-bio-chip sensors: analytical meets clinical.,” *Anal. Chem.*, vol. 82, no. 5, pp. 1571–9, Mar. 2010.

[161] X. Li, A. Ymeti, B. Lunter, C. Breukers, A. G. J. Tibbe, L. W. M. M. Terstappen, and J. Greve, “CD4+ T lymphocytes enumeration by an easy-to-use single platform image cytometer for HIV monitoring in resource-constrained settings,” *Cytometry*, vol. 72B, no. 5, pp. 397–407, Sep. 2007.

[162] A. Ymeti, X. Li, B. Lunter, and C. Breukers, “A single platform image cytometer for resource-poor settings to monitor disease progression in HIV infection,” *Cytometry*, vol. 71A, no. 3, pp. 132–142, Mar. 2007.

[163] X. Li, A. G. J. Tibbe, E. Droog, L. W. M. M. Terstappen, and J. Greve, “An immunomagnetic single-platform image cytometer for cell enumeration based on antibody specificity.,” *Clin. Vaccine Immunol.*, vol. 14, no. 4, pp. 412–9, Apr. 2007.

[164] X. Cheng, D. Irimia, M. Dixon, K. Sekine, U. Demirci, L. Zamir, R. G. Tompkins, W. Rodriguez, and M. Toner, “A microfluidic device for practical label-free CD4(+) T cell counting of HIV-infected subjects.,” *Lab Chip*, vol. 7, no. 2, pp. 170–8, Feb. 2007.

[165] X. Cheng, D. Irimia, M. Dixon, J. C. Ziperstein, U. Demirci, L. Zamir, R. G. Tompkins, M. Toner, and W. R. Rodriguez, "A microchip approach for practical label-free CD4+ T-cell counting of HIV-infected subjects in resource-poor settings," *JAIDS J. Acquir. Immune Defic. Syndr.*, vol. 45, no. 3, p. 257, 2007.

[166] X. Cheng, A. Gupta, C. Chen, R. G. Tompkins, W. Rodriguez, and M. Toner, "Enhancing the performance of a point-of-care CD4+ T-cell counting microchip through monocyte depletion for HIV/AIDS diagnostics.," *Lab Chip*, vol. 9, no. 10, pp. 1357–64, May 2009.

[167] M. Beck, S. Brockhuis, N. van der Velde, C. Breukers, J. Greve, and L. W. M. M. Terstappen, "On-chip sample preparation by controlled release of antibodies for simple CD4 counting.," *Lab Chip*, vol. 12, no. 1, pp. 167–73, Jan. 2012.

[168] C. D. Chin, V. Linder, and S. K. Sia, "Commercialization of microfluidic point-of-care diagnostic devices," *Lab Chip*, vol. 12, no. 12, pp. 2118–34, Jun. 2012.

[169] S. Mtapuri-Zinyowera, M. Chideme, D. Mangwanya, O. Mugurungi, S. Gudukeya, K. Hatzold, A. Mangwiro, G. Bhattacharya, J. Lehe, and T. Peter, "Evaluation of the PIMA point-of-care CD4 analyzer in VCT clinics in Zimbabwe.," *JAIDS J. Acquir. Immune Defic. Syndr.*, vol. 55, no. 1, pp. 1–7, Sep. 2010.

[170] I. V Jani, N. E. Sitoe, P. L. Chongo, E. R. Alfai, J. I. Quevedo, O. Tobaiwa, J. D. Lehe, and T. F. Peter, "Accurate CD4 T-cell enumeration and antiretroviral drug toxicity monitoring in primary healthcare clinics using point-of-care testing.," *AIDS*, vol. 25, no. 6, pp. 807–12, Mar. 2011.

[171] B. Larson, K. Schnippel, B. Ndibongo, L. Long, M. P. Fox, and S. Rosen, "How to Estimate the Cost of Point-of-Care CD4 Testing in Program Settings: An Example Using the Alere Pima Analyzer in South Africa," *PLoS One*, vol. 7, no. 4, p. e35444, Apr. 2012.

[172] Y. C. Manabe, Y. Wang, A. Elbireer, B. Auerbach, and B. Castelnuovo, "Evaluation of portable point-of-care CD4 counter with high sensitivity for detecting patients eligible for antiretroviral therapy," *PLoS One*, vol. 7, no. 4, p. e34319, Apr. 2012.

[173] S. Herbert, S. Edwards, G. Carrick, A. Copas, C. Sandford, M. Amphlett, and P. Benn, "Evaluation of PIMA point-of-care CD4 testing in a large UK HIV service.," *Sex. Transm. Infect.*, vol. 88, no. 6, pp. 413–7, Oct. 2012.

[174] I. Jani, N. Sitoe, J. Quevedo, J. Lehe, and T. Peter, "Cost comparison of point-of-care and laboratory CD4 testing in resource-limited settings," in *6th IAS Conference on HIV Pathogenesis, Treatment and Prevention*, 2011.

[175] J. T. Gohring and X. Fan, “Label free detection of CD4+ and CD8+ T cells using the optofluidic ring resonator.,” *Sensors*, vol. 10, no. 6, pp. 5798–808, Jun. 2010.

[176] A. Ozcan and U. Demirci, “Ultra wide-field lens-free monitoring of cells on-chip.,” *Lab Chip*, vol. 8, no. 1, pp. 98–106, Jan. 2008.

[177] Z. Wang, S. Chin, C. Chin, and J. Sarik, “Microfluidic CD4+ T-cell counting device using chemiluminescence-based detection,” *Anal. Chem.*, vol. 82, no. 1, pp. 36–40, Jan. 2010.

[178] S. Moon, U. A. Gurkan, J. Blander, W. W. Fawzi, S. Aboud, F. Mugusi, D. R. Kuritzkes, and U. Demirci, “Enumeration of CD4+ T-cells using a portable microchip count platform in Tanzanian HIV-infected patients,” *PLoS One*, vol. 6, no. 7, p. e21409, Jul. 2011.

[179] N. N. Mishra, S. Retterer, T. J. Zieziulewicz, M. Isaacson, D. Szarowski, D. E. Mousseau, D. a Lawrence, and J. N. Turner, “On-chip micro-biosensor for the detection of human CD4+ cells based on AC impedance and optical analysis,” *Biosens. Bioelectron.*, vol. 21, no. 5, pp. 696–704, Nov. 2005.

[180] N. Mishra and S. Retterer, “Bio-impedance sensing device (BISD) for detection of human CD4+ cells,” ... *Proc. ...*, pp. 228–231, 2004.

[181] X. Jiang and M. G. Spencer, “Electrochemical impedance biosensor with electrode pixels for precise counting of CD4+ cells: a microchip for quantitative diagnosis of HIV infection status of AIDS patients.,” *Biosens. Bioelectron.*, vol. 25, no. 7, pp. 1622–8, Mar. 2010.

[182] P. Kiesel, M. Beck, and N. Johnson, “Monitoring CD4 in whole blood with an opto-fluidic detector based on spatially modulated fluorescence emission.,” *Cytometry*, vol. 79A, no. 4, pp. 317–24, Apr. 2011.

[183] J.-H. Wang, C.-H. Wang, C.-C. Lin, H.-Y. Lei, and G.-B. Lee, “An integrated microfluidic system for counting of CD4+/CD8+ T lymphocytes,” *Microfluid. Nanofluidics*, vol. 10, no. 3, pp. 531–541, Mar. 2011.

[184] H. Yun, H. Bang, J. Min, C. Chung, J. K. Chang, and D.-C. Han, “Simultaneous counting of two subsets of leukocytes using fluorescent silica nanoparticles in a sheathless microchip flow cytometer.,” *Lab Chip*, vol. 10, no. 23, pp. 3243–54, Dec. 2010.

[185] X. Mao, S.-C. S. Lin, C. Dong, and T. J. Huang, “Single-layer planar on-chip flow cytometer using microfluidic drifting based three-dimensional (3D) hydrodynamic focusing.,” *Lab Chip*, vol. 9, no. 11, pp. 1583–9, Jun. 2009.

[186] Y.-N. Wang, Y. Kang, D. Xu, C. H. Chon, L. Barnett, S. a Kalams, D. Li, and D. Li, “On-chip

counting the number and the percentage of CD4+ T lymphocytes.," *Lab Chip*, vol. 8, no. 2, pp. 309–15, Feb. 2008.

[187] X. Wu, Y. Kang, Y.-N. Wang, D. Xu, D. Li, and D. Li, "Microfluidic differential resistive pulse sensors.," *Electrophoresis*, vol. 29, no. 13, pp. 2754–9, Jul. 2008.

[188] X. Wu, C. H. Chon, Y.-N. Wang, Y. Kang, and D. Li, "Simultaneous particle counting and detecting on a chip.," *Lab Chip*, vol. 8, no. 11, pp. 1943–9, Nov. 2008.

[189] C. van Berkel, J. D. Gwyer, S. Deane, N. G. Green, J. Holloway, V. Hollis, and H. Morgan, "Integrated systems for rapid point of care (PoC) blood cell analysis," *Lab Chip*, vol. 11, no. 7, pp. 1249–55, Apr. 2011.

[190] D. Holmes and H. Morgan, "Single cell impedance cytometry for identification and counting of CD4 T-cells in human blood using impedance labels.," *Anal. Chem.*, vol. 82, no. 4, pp. 1455–61, Feb. 2010.

[191] H. Zhu, J. Yan, and A. Revzin, "Catch and release cell sorting: electrochemical desorption of T-cells from antibody-modified microelectrodes.," *Colloids Surfaces B Biointerfaces*, vol. 64, no. 2, pp. 260–8, Jul. 2008.

[192] J. Robertus, W. R. Browne, and B. L. Feringa, "Dynamic control over cell adhesive properties using molecular-based surface engineering strategies.," *Chem. Soc. Rev.*, vol. 39, no. 1, pp. 354–78, Jan. 2010.

[193] U. A. Gurkan, T. Anand, H. Tas, D. Elkan, A. Akay, H. O. Keles, and U. Demirci, "Controlled viable release of selectively captured label-free cells in microchannels," *Lab Chip*, vol. 11, no. 23, pp. 3979–3989, Dec. 2011.

[194] C. Willyard, "Simpler tests for immune cells could transform AIDS care in Africa.," *Nat. Med.*, vol. 13, no. 10, p. 1131, Oct. 2007.

[195] D. S. Boyle, K. R. Hawkins, M. S. Steele, M. Singhal, and X. Cheng, "Emerging technologies for point-of-care CD4 T-lymphocyte counting.," *Trends Biotechnol.*, vol. 30, no. 1, pp. 45–54, Jan. 2012.

[196] R. Zachariah, S. D. Reid, P. Chaillet, M. Massaquoi, E. J. Schouten, and a D. Harries, "Viewpoint: Why do we need a point-of-care CD4 test for low-income countries?," *Trop. Med. Int. Health*, vol. 16, no. 1, pp. 37–41, Jan. 2011.

[197] UNAIDS, "UNAIDS World AIDS Day Report," 2012.

[198] T. Quinn and M. Wawer, “Viral load and heterosexual transmission of human immunodeficiency virus type 1,” *N. Engl. J. Med.*, vol. 342, no. 13, pp. 921–929, Mar. 2000.

[199] World Health Organization, “Global Health Observatory Data Repository,” 2013. [Online]. Available: http://apps.who.int/gho/data/.

[200] D. D. Ho, “Viral counts count in HIV infection,” *Science (80-.).*, vol. 272, no. 5265, p. 1124, 1996.

[201] G. L. Damhorst, N. N. Watkins, and R. Bashir, “Micro- and Nanotechnology for HIV/AIDS Diagnostics in Resource-Limited Settings.,” *IEEE Trans. Biomed. Eng.*, vol. 60, no. 3, pp. 715–26, Mar. 2013.

[202] R. Gómez-sjöberg, D. T. Morisette, R. Bashir, and S. Member, “Impedance Microbiology-on-a-Chip : Microfluidic Bioprocessor for Rapid Detection of Bacterial Metabolism,” *J. Microelectromechanical Syst.*, vol. 14, no. 4, pp. 829–838, 2005.

[203] R. Gómez, R. Bashir, and A. Bhunia, “Microscale electronic detection of bacterial metabolism,” *Sensors Actuators B Chem.*, vol. 86, pp. 198–208, 2002.

[204] F. Lisdat and D. Schäfer, “The use of electrochemical impedance spectroscopy for biosensing.,” *Anal. Bioanal. Chem.*, vol. 391, no. 5, pp. 1555–67, Jul. 2008.

[205] H. Shafiee, M. Jahangir, F. Inci, S. Wang, R. B. M. Willenbrecht, F. F. Giguel, A. M. N. Tsibris, D. R. Kuritzkes, and U. Demirci, “Acute On-Chip HIV Detection Through Label-Free Electrical Sensing of Viral Nano-Lysate.,” *Small*, pp. 1–11, Feb. 2013.

[206] J. T. Connelly, S. Kondapalli, M. Skoupi, J. S. L. Parker, B. J. Kirby, and A. J. Baeumner, “Micro-total analysis system for virus detection: microfluidic pre-concentration coupled to liposome-based detection.,” *Anal. Bioanal. Chem.*, vol. 402, no. 1, pp. 315–23, Jan. 2012.

[207] S. Kwakye, V. N. Goral, and A. J. Baeumner, “Electrochemical microfluidic biosensor for nucleic acid detection with integrated minipotentiostat.,” *Biosens. Bioelectron.*, vol. 21, no. 12, pp. 2217–23, Jun. 2006.

[208] K. a Edwards, O. R. Bolduc, and A. J. Baeumner, “Miniaturized bioanalytical systems: enhanced performance through liposomes.,” *Curr. Opin. Chem. Biol.*, vol. 16, pp. 1–9, Jun. 2012.

[209] S. R. Nugen, P. J. Asiello, J. T. Connelly, and A. J. Baeumner, “PMMA biosensor for nucleic acids with integrated mixer and electrochemical detection.,” *Biosens. Bioelectron.*, vol. 24, no. 8, pp. 2428–33, Apr. 2009.

[210] Q. Liu and B. J. Boyd, “Liposomes in biosensors,” *Analyst*, vol. 138, no. 2, pp. 391–409, Jan. 2013.

[211] N. V Zaytseva, V. N. Goral, R. a Montagna, and A. J. Baeumner, “Development of a microfluidic biosensor module for pathogen detection.,” *Lab Chip*, vol. 5, no. 8, pp. 805–11, Aug. 2005.

[212] N. V Zaytseva, R. a Montagna, and A. J. Baeumner, “Microfluidic biosensor for the serotype-specific detection of dengue virus RNA.,” *Anal. Chem.*, vol. 77, no. 23, pp. 7520–7, Dec. 2005.

[213] Omega Engineering, “Technical Conductivity and Resistivity,” *Omega Engineering, Inc.*, 2013. [Online]. Available: http://www.omega.com/techref/ph-2.html.

[214] Woongjin Chemical Co Ltd, “CSM Technical Manual,” Seoul, Republic of Korea, 2010.

[215] S. a Kim and J. S. Peacock, “The use of palmitate-conjugated protein A for coating cells with artificial receptors which facilitate intercellular interactions.,” *J. Immunol. Methods*, vol. 158, no. 1, pp. 57–65, Jan. 1993.

[216] T. Chen, D. McIntosh, Y. He, J. Kim, D. a Tirrell, P. Scherrer, D. B. Fenske, A. P. Sandhu, and P. R. Cullis, “Alkylated derivatives of poly(ethylacrylic acid) can be inserted into preformed liposomes and trigger pH-dependent intracellular delivery of liposomal contents.,” *Mol. Membr. Biol.*, vol. 21, no. 6, pp. 385–93, 2004.

[217] M. Hwang, R. Prud’homme, J. Kohn, and J. Thomas, “Stabilization of phosphatidylserine/phosphatidylethanolamine liposomes with hydrophilic polymers having multiple ‘Sticky Feet,’” *Langmuir*, vol. 17, no. 25, 2001.

[218] S.-Y. Teh, R. Khnouf, H. Fan, and A. P. Lee, “Stable, biocompatible lipid vesicle generation by solvent extraction-based droplet microfluidics.,” *Biomicrofluidics*, vol. 5, no. 4, pp. 44113–4411312, Dec. 2011.

[219] A. deMello and D. van Swaay, “Microfluidic methods for forming liposomes,” *Lab Chip*, vol. 13, pp. 752–767, 2012.

[220] J. Zhang, S. Yan, W. Li, G. Alici, and N.-T. Nguyen, “High throughput extraction of plasma using a secondary flow-aided inertial microfluidic device,” *RSC Adv.*, vol. 4, no. 63, p. 33149, Jul. 2014.

[221] a. a S. Bhagat, S. S. Kuntaegowdanahalli, and I. Papautsky, “Inertial microfluidics for continuous particle filtration and extraction,” *Microfluid. Nanofluidics*, vol. 7, pp. 217–226, 2009.

[222] J. Zhang, W. Li, M. Li, G. Alici, and N. T. Nguyen, “Particle inertial focusing and its mechanism in a serpentine microchannel,” *Microfluid. Nanofluidics*, vol. 17, pp. 305–316, 2014.

[223] J. Zhang, S. Yan, R. Sluyter, W. Li, G. Alici, and N.-T. Nguyen, "Inertial particle separation by differential equilibrium positions in a symmetrical serpentine micro-channel.," *Sci. Rep.*, vol. 4, no. ii, p. 4527, Jan. 2014.

[224] Zeptometrix, "HIV-1 p24 Antigen ELISA 2.0," pp. 1–4.

[225] Alere, "Alere Pima CD4," *alerehiv.com*, 2012. [Online]. Available: http://alerehiv.com/hiv-monitoring/alere-pima-cd4/. [Accessed: 05-May-2015].

[226] Daktari Diagnostics, "Our Products," *Our Products*, 2013. [Online]. Available: http://www.daktaridx.com/products/. [Accessed: 05-May-2015].

[227] X. Zhang, S. B. Lowe, and J. J. Gooding, "Brief review of monitoring methods for loop-mediated isothermal amplification (LAMP).," *Biosens. Bioelectron.*, vol. 61C, pp. 491–499, 2014.

[228] T. Notomi, H. Okayama, H. Masubuchi, T. Yonekawa, K. Watanabe, N. Amino, and T. Hase, "Loop-mediated isothermal amplification of DNA.," *Nucleic Acids Res.*, vol. 28, no. 12, p. E63, Jun. 2000.

[229] M. P. De Baar, E. C. Timmermans, E. De Rooij, and B. Van Gemen, "One-tube real-time isothermal amplification assay to identify and distinguish human immunodeficiency virus type 1 subtypes A, B, and C and circulating recombinant forms AE and AG," *J. Clin. Microbiol.*, 2001.

[230] M. P. De Baar, M. W. Van Dooren, E. De Rooij, M. Bakker, B. van Gemen, J. Foudsmit, and A. de Ronde, "Single Rapid Real-Time Monitored Isothermal RNA Amplification Assay for Quantification of Human Immunodeficiency Virus Type 1 Isolates from Groups M , N , and O," *J. Clin. Microbiol.*, vol. 39, no. 4, pp. 1378–1384, 2001.

[231] K. a Curtis, D. L. Rudolph, and S. M. Owen, "Rapid detection of HIV-1 by reverse-transcription, loop-mediated isothermal amplification (RT-LAMP).," *J. Virol. Methods*, vol. 151, no. 2, pp. 264–70, Aug. 2008.

[232] C. Liu, E. Geva, M. Mauk, X. Qiu, W. R. Abrams, D. Malamud, K. Curtis, S. M. Owen, and H. H. Bau, "An isothermal amplification reactor with an integrated isolation membrane for point-of-care detection of infectious diseases.," *Analyst*, vol. 136, no. 10, pp. 2069–76, May 2011.

[233] K. a Curtis, D. L. Rudolph, I. Nejad, J. Singleton, A. Beddoe, B. Weigl, P. LaBarre, and S. M. Owen, "Isothermal amplification using a chemical heating device for point-of-care detection of HIV-1.," *PLoS One*, vol. 7, no. 2, p. e31432, Jan. 2012.

[234] K. a Curtis, P. L. Niedzwiedz, A. S. Youngpairoj, D. L. Rudolph, and S. M. Owen, "Real-Time

Detection of HIV-2 by Reverse Transcription-Loop-Mediated Isothermal Amplification.," *J. Clin. Microbiol.*, vol. 52, no. 7, pp. 2674–6, Jul. 2014.

[235] F. B. Myers, R. H. Henrikson, J. M. Bone, J. Bone, and L. P. Lee, "A handheld point-of-care genomic diagnostic system.," *PLoS One*, vol. 8, no. 8, p. e70266, Jan. 2013.

[236] B. Sun, F. Shen, S. E. McCalla, J. E. Kreutz, M. a Karymov, and R. F. Ismagilov, "Mechanistic evaluation of the pros and cons of digital RT-LAMP for HIV-1 viral load quantification on a microfluidic device and improved efficiency via a two-step digital protocol.," *Anal. Chem.*, vol. 85, no. 3, pp. 1540–6, Feb. 2013.

[237] C. Duarte, E. Salm, B. Dorvel, B. Reddy, and R. Bashir, "On-chip parallel detection of foodborne pathogens using loop-mediated isothermal amplification.," *Biomed. Microdevices*, vol. 15, no. 5, pp. 821–30, Oct. 2013.

[238] P. Khlebovich, "IP Webcam." 2015.

[239] G. L. Damhorst, M. Murtagh, W. R. Rodriguez, and R. Bashir, "Microfluidics and Nanotechnology for Detection of Global Infectious Diseases," *Proc. IEEE*, vol. 103, no. 2, pp. 150–160, 2015.

[240] J. M. Walker, *Microfluidic Diagnostics*. 2013.

[241] S.-Y. Teh, R. Lin, L.-H. Hung, and A. P. Lee, "Droplet microfluidics.," *Lab Chip*, vol. 8, no. 2, pp. 198–220, 2008.

[242] The World Bank, "Mobile Phone Access Reaches Three Quarters of Planet's Population," *worldbank.org*, 2012. [Online]. Available: http://www.worldbank.org/en/news/press-release/2012/07/17/mobile-phone-access-reaches-three-quarters-planets-population. [Accessed: 22-May-2015].

[243] A. S. F. Lok and B. J. McMahon, *Chronic hepatitis B: Update 2009*, vol. 50. 2009.

[244] M. Baker, "Digital PCR hits its stride," *Nat. Methods*, vol. 9, no. 6, pp. 541–544, 2012.

[245] Y. Chander, J. Koelbl, J. Puckett, M. J. Moser, A. J. Klingele, M. R. Liles, A. Carrias, D. a. Mead, and T. W. Schoenfeld, "A novel thermostable polymerase for RNA and DNA loop-mediated isothermal amplification (LAMP)," *Front. Microbiol.*, vol. 5, no. AUG, pp. 1–11, 2014.

[246] C. C. Boehme, P. Nabeta, G. Henostroza, R. Raqib, Z. Rahim, M. Gerhardt, E. Sanga, M. Hoelscher, T. Notomi, T. Hase, and M. D. Perkins, "Operational feasibility of using loop-mediated isothermal amplification for diagnosis of pulmonary tuberculosis in microscopy centers of

developing countries," *J. Clin. Microbiol.*, vol. 45, no. 6, pp. 1936–1940, 2007.

[247] A. C. Hatch, J. S. Fisher, A. R. Tovar, A. T. Hsieh, R. Lin, S. L. Pentoney, D. L. Yang, and A. P. Lee, "1-Million droplet array with wide-field fluorescence imaging for digital PCR.," *Lab Chip*, vol. 11, no. 22, pp. 3838–45, Nov. 2011.

[248] R. H. Sedlak and K. R. Jerome, "Viral diagnostics in the era of digital polymerase chain reaction," *Diagn. Microbiol. Infect. Dis.*, vol. 75, no. 1, pp. 1–4, Nov. 2012.

[249] K. a Heyries, C. Tropini, M. Vaninsberghe, C. Doolin, O. I. Petriv, A. Singhal, K. Leung, C. B. Hughesman, and C. L. Hansen, "Megapixel digital PCR.," *Nat. Methods*, vol. 8, no. 8, pp. 649–51, Aug. 2011.

[250] C. M. Hindson, J. R. Chevillet, H. a Briggs, E. N. Gallichotte, I. K. Ruf, B. J. Hindson, R. L. Vessella, and M. Tewari, "Absolute quantification by droplet digital PCR versus analog real-time PCR.," *Nat. Methods*, vol. 10, no. 10, pp. 1003–5, Oct. 2013.

[251] R. A. White, S. R. Quake, and K. Curr, "Digital PCR provides absolute quantitation of viral load for an occult RNA virus.," *J. Virol. Methods*, vol. 179, no. 1, pp. 45–50, Jan. 2012.

[252] F. Shen, W. Du, J. E. Kreutz, A. Fok, and R. F. Ismagilov, "Digital PCR on a SlipChip.," *Lab Chip*, vol. 10, no. 20, pp. 2666–2672, 2010.

[253] M. Pai, M. Ghiasi, and N. P. Pai, "Point-of-Care Diagnostic Testing in Global Health : What Is the Point ?," *Microbe*, vol. 10, no. 3, pp. 103–107, 2015.

[254] K. Curtis, D. Rudolph, and S. Owen, "Sequence-specific detection method for reverse transcription, loop-mediated isothermal amplification of HIV-1," *J. Med. Virol.*, vol. 972, pp. 966–972, 2009.

[255] J. Kreutz, T. Munson, T. Huyunh, F. Shen, W. Du, and R. F. Ismagilov, "Theoretical Design and Analysis of Multivolume Digital Assays with Wide Dynamic Range Validated Experimentally with Microfluidic Digital PCR," *J. Am. Chem. Soc.*, vol. 83, no. 83, pp. 8158–8168, 2011.

[256] R. Luo, M. J. Piovoso, and R. Zurakowski, "Modeling uncertainty in single-copy assays for HIV," *J. Clin. Microbiol.*, vol. 50, no. 10, pp. 3381–3382, 2012.

[257] Ross Haynes, "Principles of Digital PCR and Measurement Issues," *Digital PCR Applications and Advances*. National Institute of Standards and Technology, San Diego, CA, 2012.

[258] R. Biassoni and A. Raso, *Quantitative Real-Time PCR*. 2014.

[259] E. van Pelt-Verkuil, A. van Belkum, and J. P. Hays, *Principles and Technical Aspects of PCR Amplification*. 2008.

[260] Y. Dodge, *The Concise Encyclopedia of Statistics*. 2008.

[261] M. C. Strain, S. M. Lada, T. Luong, S. E. Rought, S. Gianella, V. H. Terry, C. a. Spina, C. H. Woelk, and D. D. Richman, "Highly Precise Measurement of HIV DNA by Droplet Digital PCR," *PLoS One*, vol. 8, no. 4, pp. 2–9, 2013.

[262] S. Dube, J. Qin, and R. Ramakrishnan, "Mathematical analysis of copy number variation in a DNA sample using digital PCR on a nanofluidic device," *PLoS One*, vol. 3, no. 8, pp. 1–9, 2008.

[263] T. Nisisako, T. Torii, and T. Higuchi, "Droplet formation in a microchannel network.," *Lab Chip*, vol. 2, no. 1, pp. 24–26, 2002.

[264] A. M. Foudeh, T. F. Didar, T. Veresa, and M. Tabriziana, "Microfluidic Designs and Techniques Using Lab-on-a-Chip Devices for Pathogen Detection for Point-of-Care Diagnostics," *Lab Chip*, no. 207890, 2012.